



**HAL**  
open science

# Development of an anti-cancer strategy for adrenocortical carcinoma by nanovectorization of microRNAs via Lipidots®

Soha Reda El Sayed

► **To cite this version:**

Soha Reda El Sayed. Development of an anti-cancer strategy for adrenocortical carcinoma by nanovectorization of microRNAs via Lipidots®. Cellular Biology. Université Grenoble Alpes [2020-..], 2022. English. NNT : 2022GRALV019 . tel-04576999

**HAL Id: tel-04576999**

**<https://theses.hal.science/tel-04576999>**

Submitted on 15 May 2024

**HAL** is a multi-disciplinary open access archive for the deposit and dissemination of scientific research documents, whether they are published or not. The documents may come from teaching and research institutions in France or abroad, or from public or private research centers.

L'archive ouverte pluridisciplinaire **HAL**, est destinée au dépôt et à la diffusion de documents scientifiques de niveau recherche, publiés ou non, émanant des établissements d'enseignement et de recherche français ou étrangers, des laboratoires publics ou privés.

## THÈSE

Pour obtenir le grade de

**DOCTEUR DE L'UNIVERSITE GRENOBLE ALPES**

Spécialité : **Biologie cellulaire**

Arrêté ministériel : 25 mai 2016

Présentée par

**Soha REDA EL SAYED**

Thèse dirigée par **Nadia CHERRADI, DR INSERM**

préparée au sein du **Laboratoire Biosanté/ INSERM UMR1292/ CEA/UGA**  
dans **l'École Doctorale Chimie et Sciences du Vivant**

Développement d'une stratégie  
anticancéreuse pour le carcinome  
corticosurrénalien par nanovectorisation de  
microARNs via les Lipidots®

Thèse soutenue publiquement le **25 mars 2022**,  
devant le jury composé de :

**M. Walid RACHIDI**

Professeur d'université, Université Grenoble Alpes, Président

**M. Antoine MARTINEZ**

Directeur de recherche, Université Clermont Auvergne, Rapporteur

**M. Bernard MARI**

Directeur de recherche, Université Cote d'Azur, Rapporteur

**Mme. Isabelle TEXIER**

Ingénieure de recherche, CEA-LETI, Examinatrice

**Mme. Estelle Louiset**

Chargée de recherche, Université Rouen, Examinatrice

**Mme. Nadia CHERRADI**

Directrice de recherche, Université Grenoble Alpes, Directrice de thèse

et du membre invité

**M. Fabrice NAVARRO**

Chargé de projet, CEA-LETI





*"Everybody wants to reach the top of the mountain, but there is no growth at the peak. It is in the valley that we slog through the lush grass and rich soil, learning and becoming what enables us to summit life's next peak."*



*À maman, papa,  
Sarah, Malak et Mira,*



# ACKNOWLEDGEMENTS

---





*~ En toute chose, il faut considérer la fin~*

*Jean de La Fontaine*

Me voici à la fin de quatre agréables années au CEA Grenoble entre mon Master 2 et la Thèse... C'est avec beaucoup d'émotions que je tourne la page d'un chapitre de ma vie, qui a cumulé tant de travail assidu en vue d'atteindre les sommets. Si je devais résumer cette aventure, je dirais un parcours de vallées et de collines ensoleillées par de belles amitiés et rencontres.

~ ~ ~

Avant tout, j'adresse mes sincères remerciements aux membres de mon jury de thèse pour avoir accepté d'évaluer mon travail :

Dr. **Bernard Mari** et Dr. **Antoine Martinez** en tant que rapporteurs, Dr **Isabelle Texier** et Dr **Estelle Louiset**, en tant qu'examinatrices.

Dr. **Walid Rachidi**, merci d'avoir accepté de faire partie de mon jury de thèse. Je tiens également à vous remercier à titre personnel pour m'avoir admise dans le master Ingénierie de la santé grâce auquel j'ai poursuivi en doctorat, mais aussi pour tout le soutien que vous apportez aux étudiants libanais à Grenoble.

Dr. **Fabrice Navarro**, notre membre invité/collaborateur, merci pour votre intérêt et le temps que vous nous avez accordé pendant ces 3 années, pour suivre les grandes lignes de ce projet.

Je remercie aussi les membres de mon comité de suivi individuel Dr. **Marie-Odile Fauvarque**, Dr. **Pierre Val** et Dr. **Béatrice Eymin** pour leurs commentaires constructifs.

~ ~ ~

Mon plus grand merci à toi **Nadia**, pour ta confiance, ta disponibilité et ta douceur. Mon éveil au monde de la recherche a commencé avec toi, et je t'en suis pleinement reconnaissante. Merci d'avoir partagé ton expérience et tes connaissances et de m'avoir guidée tout au long de ces quatre années. J'ai surtout apprécié de travailler avec toi pour ta rigueur et ton enthousiasme pour la recherche, mais aussi pour ton exigence qui m'a incitée à m'investir au mieux dans ce projet innovant. Je tiens également à te remercier pour ton soutien et ta veille à faire une science de qualité, même si celle-ci coûte cher! Je te souhaite une vie épanouie, riche en découvertes et en projets aussi passionnants!

~ ~ ~

Pour faire de la bonne science, il faut de la bonne ambiance.

Merci à tous les membres de BCI qui ont créé un environnement convivial malgré les contraintes sanitaires.

Je pense particulièrement à

**Jean-Jacques Feige, Sabine Bailly et Catherine Picart** merci de m'avoir accueillie dans le laboratoire BCI et de m'avoir aidée administrativement.

La plus aimable, **Josiane Denis**, merci de m'avoir formée en tant que jeune stagiaire ne sachant même pas tenir une pipette. Ma voisine de paillasse, ta bonne humeur a certainement égayé mes jours de manip. Tu as non seulement veillé à la sécurité de tous, mais aussi tu étais toujours disponible pour donner un coup de main et garder mes bébés cellules/souris avec grand plaisir.

**Laurent Guyon**, merci de m'avoir hébergée dans ton bureau pendant mes longues journées de rédaction, au cours desquelles j'ai un peu découvert la vie assise d'un bioinformaticien. Chapeaux bas! Merci pour toutes les discussions et commentaires critiques. Et bien évidemment, je n'oublierai surtout pas de te remercier pour tout le temps et réflexions pour mes analyses de données.

**Nadia Alfaidy**, merci pour ta tendresse et les conseils dont tu m'as fait part. Les pauses repas étaient un vrai plaisir à ton côté avec **Mohamed**. Je n'oublierai pas notre aventure Grenoble-Chambéry, où j'ai apprécié ta douceur et ton humanité.

**Odile Filhol-Cochet**, merci pour ton amabilité et ton partage de savoir-faire et de réactifs au cours de ces 4 années. Tes suggestions, ainsi que celles de **Claude** étaient de grande valeur pour moi. Votre passion de la recherche m'inspire pleinement.

**Christophe Battail**, merci pour toutes les discussions enrichissantes au cours de la découverte du Jupyter de la bioinformatique ! J'espère que tu as oublié notre mésaventure sur les routes montagnardes de notre belle région... haha.

**Christine Cogne, Catherine Pillet, Fred Sergent, Agnès Castan, Emmanuelle Tillet** et surtout les deux Nicolas, **N. Lemaitre** et **N. Chaumontel**, merci pour votre générosité, et votre aptitude à aider avec un grand sourire.

**Isabelle Zanotti**, merci de m'avoir aidée dans toutes mes procédures administratives, avec une gentillesse infinie. L'équipe IMAC est chanceuse d'avoir une gestionnaire comme toi.

**Iza Bama, Charlène Magallon et Hervé Pointu**, la super team de l'animalerie. Merci de m'avoir formée à aimer mes petites copines. Merci aussi pour vos soins pour assurer le bien-être animal, grâce à vous nos souris séjournent dans un hôtel 5 étoiles, musique comprise !

**Véronique Collin-Faure**, merci pour ta patience et ton aide sur la plateforme de FACS.

Je remercie également mes collègues du LETI, **Adrien Nougarede**, **Séverine Escaich** et **Laeticia Kurzawa**. J'ai vraiment apprécié les manips dans les locaux du 40.20.

~ ~ ~

Et qui de mieux pour comprendre un doctorant, qu'un autre doctorant ?

Mes pensées à..

Ma première collègue de bureau, à l'époque de luxe pré-COVID, **Constance Collet**. Je ne pourrais pas imaginer mes longues journées au labo sans te voir et discuter avec toi science et vie. Tu m'as connue à mes moments émus, merci pour ta gentillesse et ton écoute (pas de larmes, tu m'as promis). Pour moi, tu es bien plus qu'une collègue, j'espère que nos parcours se croiseront un jour et que notre amitié perdurera quand on se lancera dans la vraie vie hors CEA !

**Justine Cristante**, la vraie Dr parmi nous ! Merci de m'avoir suivie médicalement quand mes migraines se faisaient sentir. Avec ton dynamisme et ta bonne humeur, j'ai passé les plus belles journées ensoleillées du 213A, discutant avec toi, de tout et de rien. Te voici maintenant reine des PCR, mais aussi de la langue arabe... Je te laisse mes bébés NCI, mes pipettes, ma paillasse... et Nadia. On gardera nos contacts, j'espère.

À **Mohammad Al Tarras**, **Tala Al Tabosh**, **Hadi Younes** et notre « papa » **Roland Abi Nahed**, les Libanais à BCI, merci pour les échanges et le soutien partagé pour nourrir notre amour envers notre pays natal. En ces moments difficiles, être libanais, apporte encore plus de complexité que la recherche en soi, vous êtes les super chercheurs, bon courage ! Merci pour votre amitié !

~ ~ ~

Friends come and go, but the ones that stay are the ones that glow.

Mille mercis...

À **Khadija El Achi**, ma lyonnaise, et oui tu te connais bien, ma « sousé ». Ce fut une sacrée aventure que je n'aurais absolument pas pu achever sans tes conseils aussi personnels que professionnels. Balayant le film de mes souvenirs, je te retrouve partout! Avec toi, j'ai partagé les cours de l'Université Libanaise, les soirées de dortoir, le premier vol, des trajets de trains (ratés ou pas). Nous avons partagé des astuces, des recettes, et surtout nous avons partagé des rêves. Thank you bestie!

À **Fatima Danash**, ma meilleure, one and only « girl next-door », merci pour tous les moments de folie, pour les plans innovants, pour ta présence à mes jours de bonheur et ta veille à mes jours de maladie. Je n'oublierai jamais nos échanges de conseils (et de téléphones haha) ainsi que ton soutien pour bien mener à fin ce manuscrit. Avec toi, j'ai appris que c'est dans les nuits les plus obscures que l'on identifie ses étoiles. Merci « maman » Fatima!

À **Ghina Basharoush**, le 3<sup>ème</sup> membre du gang à trois grenobloises... Merci pour les fous rires, pour ta bonne humeur qui a certainement animé nos soirées weekend, pour toutes les raclettes

qu'on a partagées « avec nos mains ». Tu es et resteras notre référence d'épanouissement culturel, documentaire, linguistique, et éthique... merci sœur ;)

À mes cousins **Hussein** et **Rida Bouzeid**, votre présence sur Grenoble m'a certainement soulagée dans mes moments nostalgiques. Vous êtes les frères que je n'ai jamais eus...

À mes amies au Liban,

**Sanaa Zohbi**, merci de m'avoir entendue et soutenue au quotidien avec foi et tendresse. Comme tu as pu remarquer, ces années furent des stations d'humeur twistée, qui seraient impossibles à franchir à pieds sans notre « van ». À plus d'années d'amitié, d'enthousiasme et de rencontres !

À **Hiba Khalifeh**, ma « twinnie », merci de ton bon cœur, ton soutien et tes conseils. Je n'oublierai jamais nos escapades et nos fous rires qui ont égayé nos jours de confinement. Bien que ton séjour grenoblois était succinct, je suis heureuse de t'avoir connue pendant ce parcours.

À **Hiam Hammoud** et **Zeinab Moussawi** merci pour votre amitié et la tendresse que vous m'avez témoignée au fil des années, malgré les distances.

~ ~ ~

Le plus dur de ce chemin, c'était de devoir quitter ses proches en étant conscient que certains d'entre eux ne seront plus là...

À mon **grand-père**, qui était toujours fier de moi « docteur de la famille », à ma tante **Mona** qui a perdu sa bataille pour le cancer. C'est de telles souffrances qui incitent la recherche fondamentale à avancer. Que leurs âmes reposent en paix !

~ ~ ~

Là où la vie commence et l'amour ne finit jamais, ma famille...

Je dédie ce travail

À papa **Ali** et maman **Najwa**

Si je suis à ce stade, c'est forcément grâce à vous, à vos dévouements, motivation et foi. Vous êtes ma force, mais aussi ma faiblesse, ne vous voir que derrière un écran durant cette quête a été éprouvant. Mon unique souhait c'est de vous rendre fiers, en hommage à vos sacrifices au fil des années. Je me rappelle de mon premier jour d'université, il y a 8 ans déjà, vous m'avez dit « Le voyage de mille lieues commence par un pas », me voici atteignant mon dernier pas du voyage grâce à la confiance que vous m'avez octroyée. Que votre bénédiction m'accompagne dans mes pas à venir !

Vous avez toujours apprécié mon âme de poète, je vous adresse un humble verset qui ne saurait assez illustrer ma gratitude envers vous.

ولا تسعني الدنيا فخراً  
حينما بكما يقترن اسمي،  
دمتما لي في الرشد ذخراً،  
ودمتما لعيشي تمام النعم.

À mes sœurs / support system / forever best friends / life coaches, **Sarah, Malak, Mira**, merci d'être toujours à l'écoute, surtout dans mes moments de nostalgie. Votre manuel de « survie » m'a été de grande utilité pendant ce parcours, avec vos mots motivants qui connaissent parfaitement le chemin vers mon cœur. You raise me up, so I can stand on mountains.

~ ~ ~

À mes montagnes, je suis infiniment reconnaissante pour le bien-être que mon séjour Grenoblois m'a procuré en votre sein. A bientôt, j'espère.

Et finalement, merci Dieu  
*Alhamdulillah*



## Preamble

This thesis comprises a bibliographic introduction, composed of four chapters. The first chapter describes the pathology on which lies this thesis, **adrenocortical cancer**. In a second chapter are explained the therapeutic molecules used in this work, **MicroRNAs**. Basic principles in nanomedicine are then presented in Chapter III leading to a final chapter dealing with the vectors employed in this thesis, **Lipidots**.

Then are exposed the thesis objectives, followed by the thesis work and results in article format. A discussion is presented afterwards to sum up by a conclusion.





## Résumé

Le carcinome corticosurrénalien (CCS) est une tumeur endocrine rare et agressive, qui est associée à un mauvais pronostic. Ce cancer est réfractaire aux thérapies conventionnelles telles que la chimiothérapie ou la radiothérapie ainsi qu'aux thérapies ciblées. Face à ces échecs thérapeutiques, une meilleure connaissance des mécanismes moléculaires de la tumorigenèse corticosurrénalienne est nécessaire pour la conception de thérapies alternatives. Les microARNs (miRs) sont de petits ARN non-codants d'une vingtaine de nucléotides qui répriment l'expression des gènes au niveau post-transcriptionnel. Ils exercent un rôle de régulation majeur de l'ensemble du génome. Des altérations du profil d'expression des miRs (surexpression de miRs oncogènes ou répression de miRs suppresseurs de tumeur) ont été identifiées dans toutes les étapes du développement cancéreux telles que l'initiation, la progression et le développement de métastases. Sur la base de ces découvertes, l'inhibition de miRs oncogènes ou la restitution de miRs suppresseurs de tumeurs ont été proposées comme des stratégies thérapeutiques pertinentes pour le cancer. Cependant, le défi majeur de ces approches reste l'adressage spécifique et sécurisé de ces traitements au foyer tumoral. Le laboratoire LETI/DTBS du CEA a développé et breveté des nanoparticules lipidiques biocompatibles et biodégradables ou Lipidots® (LNP) dont les composants sont approuvés par la FDA et qui présentent un tropisme puissant pour le cortex surrénal. L'étude du miRnome du CCS par notre équipe a révélé que deux microARN, miR-139-5p et miR-483-5p sont surexprimés dans les tumeurs agressives et associés à un mauvais pronostic. L'objectif de ce travail était d'évaluer miR-139-5p et miR-483-5p comme cibles thérapeutiques dans le CCS par nanovectorisation de leurs antimirs respectifs. Dans un premier travail, nous montrons que la transfection simultanée d'antimiR-139-5p et d'antimiR-483-5p nus dans la lignée de CCS humain NCI H295R diminue l'expression de protéines associées au cancer, la phosphorylation des MAP-kinases p38 et AKT et module négativement la voie de signalisation Wnt/ $\beta$ -caténine. Ces résultats indiquant l'implication des deux miRs dans la signalisation oncogénique nous ont amenés dans un deuxième temps à générer des LNP complexés à un mélange d'antimiR-139-5p et antimiR-483-5p et à caractériser ces nanoparticules. Nous avons mis en évidence l'internalisation de ces complexes par les cellules NCI H295R en culture et démontré leur efficacité dans l'inhibition simultanée de l'expression de miR-483-5p et miR-139-5p endogènes. De plus, les antimirs-LNP inhibent la migration et l'invasion des cellules NCI H295R en culture. Enfin, dans une troisième partie, nous montrons que l'injection systémique des antimirs-LNP chez la souris immunodéficiente *scid/CB17* induit une accumulation préférentielle des nanoparticules dans les surrénales et les ovaires sans toxicité apparente. Nous rapportons dans des expériences préliminaires de xénogreffe sous-cutanée de cellules NCI H295R que l'administration des antimirs-LNP inhibe la croissance tumorale. Ce travail décrit la première utilisation des Lipidots pour vectoriser des miRs à visée thérapeutique et suggère que le ciblage des miRs est une stratégie pertinente pour le traitement du CCS. Bien que les mécanismes moléculaires mis en jeu par miR-139-5p et miR-483-5p dans le CCS ne soient encore pas élucidés dans le détail, ces données ouvrent des perspectives prometteuses pour orienter le développement de thérapies innovantes pour le carcinome corticosurrénalien.

## Abstract

Adrenocortical carcinoma (ACC) is a rare and aggressive endocrine tumor, which is associated with poor prognosis. This cancer is refractory to conventional therapies such as chemotherapy or radiotherapy as well as to targeted therapies. In light of these therapeutic failures, understanding the molecular mechanisms of adrenocortical tumorigenesis will be pivotal for the development of alternative therapies. MicroRNAs (miRNAs) are small non-coding RNAs of around 20 nucleotides-long that repress gene expression at the post-transcriptional level. They play a major regulatory role of the entire genome. Alterations in the expression profile of miRNAs (overexpression of oncogenic miRNAs or repression of tumor suppressor miRNAs) have been identified in all stages of cancer development such as initiation, progression and metastasis. Based on these findings, inhibition of oncogenic miRNAs or restoration of tumor suppressor miRNAs were suggested as relevant therapeutic strategies for cancer. However, the major challenge of these approaches remains the specific and safe delivery of these treatments at the tumor site. The CEA LETI/DTBS laboratory has developed and patented biocompatible and biodegradable solid lipid nanoparticles or Lipidots® (LNP), the components of which are approved by the FDA. Remarkably, these nanoparticles exhibit a marked tropism for the adrenal cortex. Previous studies of our team on miRNA landscape in ACC revealed that two miRNAs, miR-139-5p and miR-483-5p, are overexpressed in aggressive tumors and associated with poor prognosis. The aim of this work was to evaluate miR-139-5p and miR-483-5p as therapeutic targets in ACC, using nanovectorization of their respective antimiRs. In the first part of this study, we show that simultaneous transfection of naked antimiR-139-5p and antimiR-483-5p in the human ACC cell line NCI H295R decreases the expression of several cancer-related proteins, reduces the phosphorylation level of p38 MAP kinase and AKT and negatively modulates the Wnt/ $\beta$ -catenin signaling pathway. These results suggesting an involvement of miR-139-5p and miR-483-5p in oncogenic signaling pathways led us in a second part of this work to generate and to characterize antimiRs-LNPs complexes using a combination of antimiR-139-5p and antimiR-483-5p. We subsequently show a massive internalization of these complexes in NCI H295R cells, which is accompanied by an efficient and simultaneous inhibition of endogenous miR-483-5p and miR-139-5p expression. In addition, the antimiRs-LNP impede the migration and invasion of NCI H295R cells in culture. Finally, in a third part, we show that the systemic injection of antimiRs-LNP in immunodeficient *scid/CB17* mice induces a preferential accumulation of these complexes in the adrenals and ovaries without apparent toxicity. We report in preliminary experiments using subcutaneous xenograft of NCI H295R cells that systemic administration of antimiRs-LNP inhibits tumor growth. This work describes the first use of Lipidots® to vectorize miRNAs for therapeutic purposes and suggests that targeting miRNAs deregulations is a relevant strategy for the treatment of ACC. Although the molecular mechanisms involved in miR-139-5p- and miR-483-5p-mediated adrenocortical tumorigenesis remain to be fully elucidated, these data open new perspectives for the development of innovative therapies for adrenocortical carcinoma

## Table of content

Résumé .....	17
Abstract .....	18
List of figures .....	24
List of Tables.....	25
List of abbreviations.....	26
<b>1- INTRODUCTION .....</b>	<b>31</b>
<b>Chapter I. Adrenocortical cancer, a rare but aggressive malignancy .....</b>	<b>33</b>
<b>I.A. The adrenal glands .....</b>	<b>34</b>
I.A. 1. Overview .....	34
I.A. 2. Anatomy and histology .....	34
I.A. 2.a. The capsule.....	35
I.A. 2.b. The adrenal cortex .....	35
Zona glomerulosa .....	37
Zona fasciculata .....	38
Zona reticularis.....	40
I.A. 2.c. The medulla .....	40
I.A. 3. Adrenal gland development.....	41
<b>I.B. Adrenal disorders .....</b>	<b>44</b>
I.B. 1. Primary adrenal insufficiency: Addison’s disease .....	44
I.B. 2. Secondary adrenal insufficiency.....	44
I.B. 3. Congenital adrenal hyperplasia.....	45
I.B. 4. Hypercortisolism: Cushing syndrome.....	45
I.B. 5. Hyperaldosteronism: Conn’s syndrome .....	46
<b>I.C. Benign adrenal tumors.....</b>	<b>46</b>
I.C. 1. Tumors of the medulla: Pheochromocytoma .....	46
I.C. 2. Tumors of the cortex .....	47
I.C. 2.a. Adenomas.....	47
I.C. 2.b. Hyperplasia.....	47
<b>I.D. Adrenocortical cancer.....</b>	<b>48</b>
I.D. 1. Epidemiology.....	48
I.D. 2. Clinical presentation .....	49
I.D. 3. Pathology and genetic predisposition.....	49
I.D. 3.a. Li-Fraumeni Syndrome .....	49

I.D. 3.b. Beckwith-Wiedemann Syndrome .....	50
I.D. 3.c. Multiple Endocrine Neoplasia Type 1.....	50
I.D. 4. Diagnosis .....	50
I.D. 4.a. Biochemical screening and hormone dosage .....	50
I.D. 4.b. Imaging.....	51
I.D. 4. c. Histopathology .....	51
I.D. 5. Staging.....	52
I.D. 6. Therapy .....	53
I.D. 6.a. Surgical resection .....	53
I.D. 6.b. Adjuvant therapy .....	54
Mitotane.....	54
Chemotherapy.....	55
Radiotherapy .....	55
I.D. 6.c. Targeted therapy.....	56
Targeting EGFR .....	57
Targeting VEGF: .....	59
Targeting IGFR and mTOR .....	59
Targeting Wnt/ $\beta$ -catenin.....	60
Targeting SF-1.....	60
I.D. 6.d. Immunotherapy .....	61
I.D. 7. Patient follow-up.....	61
I.D. 8. Molecular landscape .....	62
I.D. 8.a. Chromosomal alterations.....	62
I.D. 8.b. DNA methylation.....	63
I.D. 8.c. Driver gene mutations.....	63
I.D. 8.d. MicroRNA deregulations.....	64
<b>Chapter II. Post-transcriptional regulation of gene expression by microRNAs, a new level of genome complexity .....</b>	<b>65</b>
<b>II.A. Non-coding RNA.....</b>	<b>66</b>
<b>II.B. RNA interference.....</b>	<b>68</b>
<b>II.C. MicroRNA.....</b>	<b>70</b>
II.C. 1. Nomenclature.....	70
II.C. 2. Genomic origins.....	71
II.C. 3. Canonical biosynthesis .....	72
II.C. 4. Interaction with mRNA.....	73

II.C. 4.a. Target gene identification .....	74
II.C. 4.b. CLIP .....	75
II.C. 4.c. CLASH .....	75
II.C. 4.d. Pulldown .....	76
II.C. 5. Gene silencing by microRNA .....	77
II.C. 6. MicroRNA in cancer pathogenesis .....	78
II.C. 7. MicroRNA expression in ACC .....	79
II.C. 7.a. miR-483-5p .....	82
II.C. 7.b. miR-139-5p .....	84
<b>II.D. MicroRNA-based therapeutics .....</b>	<b>85</b>
II.D. 1. Targeting microRNA .....	85
II.D. 2. miRNA-based therapeutics in ACC .....	86
II.D. 3. Obstacles and drawbacks .....	87
<b>Chapter III. Nanomedicine for cancer, basic principles .....</b>	<b>89</b>
<b>III.A. Etiology and nomenclature .....</b>	<b>90</b>
<b>III.B. Advantages of nanoscale therapies .....</b>	<b>92</b>
<b>III.C. Nanoparticles in the COVID-19 pandemic: The era of mRNA vaccines .....</b>	<b>93</b>
<b>III.D. Nanoparticles in cancer research: The rise of miRNA therapeutics .....</b>	<b>95</b>
III.D. 1. Inorganic nanoparticles for miRNA delivery .....	96
III.D. 1.a. Gold nanoparticles .....	97
III.D. 1.b. Iron nanoparticles .....	98
III.D. 1.c. Mesoporous silica nanoparticles .....	99
III.D. 2. Organic nanoparticles for miRNA delivery .....	99
III.D. 2.a. Polymeric nanoparticles .....	99
Micelles .....	101
Polyethyleneimine .....	101
Dendrimers .....	102
III.D. 2. b. Lipid nanoparticles .....	102
Liposomes .....	102
Solid Lipid nanoparticles .....	103
III.D. 3. Biomimetic nanoplatforms .....	103
III.D. 3.a. Bacterial nanocells .....	104
III.D. 3.b. Engineered exosomes .....	105
<b>III.E. Surface remodeling .....</b>	<b>106</b>

III.E. 1. Passive targeting: The EPR effect .....	108
III.E. 2. Active targeting .....	111
III.F. Cellular internalization and cargo discharge .....	113
<b>III.G. Challenges for miRNA nanotherapeutics .....</b>	<b>117</b>
<b>Chapter IV. Lipidots, novel platforms for nucleic acid delivery .....</b>	<b>125</b>
<b>IV.A. Definition.....</b>	<b>126</b>
<b>IV.B. Constitutive components.....</b>	<b>127</b>
IV.B. 1. Surfactants .....	127
IV.B. 1.a. Lecithin .....	127
IV.B. 1.b. Polyethylene glycol .....	127
IV.B. 2. Lipid core .....	128
IV.B. 2.a. Soybean oil .....	128
IV.B. 2.b. Suppocire wax.....	129
<b>IV.C. Formulation method .....</b>	<b>129</b>
<b>IV.D. Physico-chemical characterization of lipidots .....</b>	<b>131</b>
IV.D. 1. Morphology and hydrodynamic diameter.....	132
IV.D. 2. Polydispersity index .....	132
IV.D. 3. Zeta potential.....	133
IV.D. 4. LNP quantification in formulation .....	134
<b>IV.E. Fluorophore encapsulation .....</b>	<b>134</b>
<b>IV.F. Nucleic acid encapsulation .....</b>	<b>137</b>
IV.F. 1. The N/P ratio .....	138
IV.F. 2. Complexation and nucleic acids payload .....	139
<b>IV.G. In vivo behavior of Lipidots .....</b>	<b>140</b>
IV.G. 1. Absorption .....	141
IV.G. 2. Distribution .....	141
IV.G. 3. Metabolization.....	143
IV.G. 4. Elimination.....	143
<b>IV.H. Current applications of lipidots.....</b>	<b>144</b>
<b>Conclusion .....</b>	<b>145</b>
<b>2- THESIS OBJECTIVES .....</b>	<b>147</b>
<b>3- RESULTS .....</b>	<b>151</b>

<b>ARTICLE 1: MicroRNA therapeutics in adrenocortical carcinoma: A lipid nanoparticle-based approach to suppress the oncogenic activity of microRNAs .....</b>	<b>153</b>
Abstract .....	156
Introduction.....	157
Materials and methods .....	158
Results .....	170
Conclusion .....	186
Funding.....	186
Conflicts of Interest .....	187
Figures .....	188
References.....	195
Supplementary Figures and Tables .....	198
<b>4- CONCLUSION AND PERSPECTIVES.....</b>	<b>209</b>
<b>5- ANNEX.....</b>	<b>217</b>
<b>ARTICLE 2: MicroRNA Therapeutics in Cancer: Current Advances and Challenges .....</b>	<b>219</b>
<b>Scientific production.....</b>	<b>221</b>
<b>6- REFERENCES .....</b>	<b>223</b>



## List of figures

Figure 1: Adrenal gland anatomy and histology.....	35
Figure 2: Steroid hormones biosynthesis.....	36
Figure 3: Renin-angiotensin axis for aldosterone biosynthesis by Zona Glomerulosa. ....	38
Figure 4: Hypothalamo-pituitary axis for cortisol biosynthesis by Zona Fasciculata. ....	39
Figure 5: Adrenal gland development and zonation. ....	42
Figure 6: Therapies targeting key signaling cascades in ACC. ....	56
Figure 7: Genomic landscapes in ACC. ....	62
Figure 8: Different types of RNA. ....	66
Figure 9: The RNA interference pathways.....	69
Figure 10: The miRNA-host gene relationship .....	72
Figure 11: Representation of interactions between the miRNA seed region and the 3'UTR of target mRNA.....	74
Figure 12: Molecular mechanisms for miRNA-mediated gene silencing. ....	78
Figure 13: miRNA deregulations in cancer. ....	79
Figure 14: miRNA expression patterns in ACC, according to Assié et al. 2014. ....	80
Figure 15: miR-483 genomic localization and sequence.....	83
Figure 16: miR-139 genomic localization and sequence. ....	84
Figure 17: The very first nanotechnologies. ....	90
Figure 18: Size comparison of living and non-living matter in nanometric scale.....	91
Figure 19: How the COVID-19 mRNA vaccines work.....	94
Figure 20: Surface modification of gold NPs with thiol derivatives. ....	98
Figure 21: Schematic representation of emerging nanoplatforms for miRNA delivery.....	100
Figure 22: A proposed model of miR-7 replacement via EDVs in adrenocortical carcinoma. ....	105
Figure 23: Evolution of nanoparticles, an example of liposomes. ....	107
Figure 24: Simplified representation of the EPR effect.....	109
Figure 25: Characteristics of the tumor microenvironment behind the EPR effect in humans.....	110
Figure 26: Active targeting of cancer cells or tumor vessels via surface-functionalized nanoparticles. ....	111
Figure 27: Surface engineering strategies for liposome active targeting. ....	112
Figure 28: Possible routes for miRNA nanoparticles cellular uptake. ....	115
Figure 29: Mechanisms of endosomal escape. ....	116
Figure 30: Translating miRNA biology from bench to bedside in cancer. ....	118
Figure 31: Schematic representation of oil-in-water nanoemulsions, Lipidots. ....	128
Figure 32: Formulation process of cationic lipidots as oil-in-water nanoemulsions.....	130
Figure 33: Physical characterization of neutral and cationic Lipidots. ....	131
Figure 34: Representation of a particle's zeta potential according to the Gouy-Stern model. ....	133
Figure 35: Cyanines encapsulation in LNP core.....	136
Figure 36: Lipidots-nucleic acids complex in blood.....	138
Figure 37: Definition of the N/P ratio.....	139
Figure 38: In vivo distribution of LNP fluorescence. ....	142

## List of Tables

Table 1: The Weiss scoring system.....	52
Table 2: Staging of ACC according to ENSAT guidelines.....	53
Table 3: Current clinical trials for ACC.....	58
Table 4: Different types of non-coding RNAs according to their function.....	68
Table 5: Two members of the RNAi family, siRNA and miRNA. ....	69
Table 6: Studies reporting miRNA deregulations in ACC tissues vs NAC and ACA.....	81
Table 7: Some of the reported siRNA-based clinical trials.....	120
Table 8: Reported miRNA-based compounds in clinical trials .....	120
Table 9: Composition of soybean oil.....	129
Table 10: Fatty acids composition of Suppocire® NC.....	129
Table 11: Physico-chemical properties of the used LNP formulations after synthesis.....	132
Table 12: Optical properties of LNP-loaded dyes.....	137

## List of abbreviations

<i>18FDG</i>	<i>18F-fluorodeoxyglucose</i>
<i>3'UTR</i>	3' untranslated region
<i>4-SU / 6-SG</i>	4-thiouridine / 6-thioguanosine
<i>AAP</i>	Adrenal androgen precursors
<i>ACA</i>	Adrenocortical adenomas
<i>ACC</i>	Adrenocortical carcinoma
<i>ACE</i>	Angiotensin-converting enzyme
<i>ACTH</i>	Adrenocorticotrophic hormone
<i>ADME</i>	Absorption, distribution, metabolism, and excretion
<i>Ago2</i>	Argonaute 2
<i>APC</i>	Adenomatous Polyposis Coli
<i>ARMC5</i>	Armadillo repeat containing 5
<i>AT1</i>	Angiotensin II receptor type 1
<i>AVP</i>	Arginine vasopressin
<i>BUB1B</i>	budding uninhibited by benzimidazoles 1 homolog beta
<i>BWS</i>	Beckwith–Wiedemann syndrome
<i>CAH</i>	Congenital adrenal hyperplasia
<i>CDK4</i>	Cyclin-dependent kinase 4
<i>CIMP</i>	CpG island methylator phenotype
<i>Cited2</i>	CBP/p300 Interacting Transactivator with ED-rich tail 2
<i>CLASH</i>	crosslinking, ligation and sequencing of hybrids
<i>CLIP</i>	Cross-linking and immunoprecipitation
<i>CREB</i>	cAMP Response Element Binding protein
<i>CRH</i>	Corticotrophin releasing hormone
<i>CRISPR/Cas9</i>	Clustered Regularly Interspaced Short Palindromic Repeats/CRISPR-associated protein 9
<i>CT</i>	Computerized tomography
<i>CYP11B2, CYP11B1, CYP17</i>	Cytochrome P450 isozymes
<i>DAXX</i>	death-associated protein
<i>DDD</i>	Dichlorodiphenyltrichloroethane
<i>DGCR8</i>	DiGeorge syndrome Critical Region 8
<i>DHEA</i>	Dehydroepiandrosterone
<i>DHEAS</i>	Dehydroepiandrosterone- Sulfate
<i>DLG7</i>	Discs large homolog 7
<i>DLS</i>	Dynamic Light Scattering
<i>DLT</i>	Dose-limiting toxicity
<i>DOPE</i>	dioleoylphosphatidyl ethanolamine
<i>DOTAP</i>	1,2-dioleoyl-3-trimethylammonium-propane
<i>DOTMA</i>	(N-[1-(2,3-dioleoyloxy)propyl]-N,N,N-trimethylammonium chloride
<i>DROSHA</i>	Double-Stranded RNA-Specific Endoribonuclease
<i>dsRNA</i>	Double stranded RNA
<i>ECM</i>	Extracellular matrix
<i>EDV</i>	EnGeneIC Dream Vectors
<i>EGF</i>	Epithelial growth factor

<i>EGFR</i>	Epithelial growth factor receptor
<i>EIF4E</i>	Eucaryotic initiation factor 4E
<i>EMT</i>	Epithelial to mesenchymal transition
<i>ENS@T</i>	European Network for the Study of Adrenal Tumors
<i>EpCAM</i>	Epithelial cell adhesion molecule
<i>EPR</i>	Enhanced Permeability and Retention
<i>ERR<math>\alpha</math></i>	Estrogen-Related Receptor alpha
<i>ESE</i>	European Society for Endocrinology
<i>EZH2</i>	Enhancer of zeste homolog 2
<i>FAP</i>	Familial adenomatous polyposis
<i>FDA</i>	Food and drug administration
<i>FIRM-ACT</i>	First International Randomized Trial in Locally Advanced and Metastatic Adrenocortical Carcinoma Treatment
<i>FZ</i>	Fetal zone
<i>Fzd</i>	Frizzled
<i>Gli1</i>	Glioma-Associated Oncogene Homolog 1
<i>GRAS</i>	Generally Recognized As Safe
<i>HDL</i>	High Density Lipoprotein
<i>HE</i>	Hematoxylin-eosin
<i>HIF-1<math>\alpha</math></i>	Hypoxia Inducible Factor1 alpha
<i>HITS-CLIP</i>	High throughput sequencing is termed
<i>HPA</i>	Hypothalamic–pituitary axis
<i>hsa</i>	Homo sapiens
<i>HSD11B2</i>	Hydroxysteroid 11-Beta Dehydrogenase 2
<i>HU</i>	Hounsfield units
<i>IGF1/2</i>	Insulin growth factor type 1/2
<i>IGF-2</i>	Insulin-like Growth Factor 2
<i>IGFR</i>	Insulin growth factor receptor
<i>IMPACT-seq</i>	Identification of MREs by pull-down and alignment of captive transcripts—sequencing
<i>IP3</i>	Inositol Triphosphate
<i>IR</i>	Insulin receptor
<i>LDL</i>	Low Density Lipoprotein
<i>LFS</i>	Li-Fraumeni syndrome
<i>LNA</i>	Locked nucleic acids
<i>lncRNA</i>	Long non-coding RNA
<i>LNP</i>	Lipid nanoparticle
<i>LOH</i>	Loss of heterozygosity
<i>m7G</i>	7-methylguanosine triphosphate
<i>MAPK</i>	Mitogen-activated protein kinase
<i>MC2R</i>	Melanocortin receptor 2
<i>MDR-1</i>	Multidrug resistance gene
<i>M-EDP</i>	Mitotane- etoposide- doxorubicin-cisplatin
<i>MEN1</i>	Multiple Endocrine Neoplasia Type 1
<i>MEN1</i>	Multiple endocrine neoplasia type 1
<i>miRNA, miR</i>	MicroRNA
<i>MMP</i>	Metalloproteinases

<i>MRE</i>	miRNA recognition elements
<i>MRI</i>	magnetic resonance imaging
<i>MSN</i>	Mesoporous silica nanoparticles
<i>MT1-MMP</i>	Membrane type 1 matrix metalloproteinase
<i>NAC</i>	Normal adrenal cortex
<i>ncRNA</i>	Non-coding RNA
<i>NDRG2</i>	N-myc downstream-regulated gene 2
<i>NDRG4</i>	N-myc downstream-regulated gene 4
<i>NIR</i>	Near infrared
<i>NLC</i>	Nanostructured lipid carrier
<i>NPs</i>	Nanoparticles
<i>NSCLC</i>	Non-small cell lung cancer
<i>ORR</i>	Overall response rate
<i>OS</i>	Overall survival
<i>PABP</i>	Poly-A Binding Protein
<i>PAR-CLIP</i>	Photoactivatable ribonucleoside-enhanced CLIP
<i>PBMAH</i>	Primary Bilateral Macronodular Adrenal Hyperplasia
<i>PBR/TSPO</i>	Peripheral Benzodiazepin Receptor/ Translocator protein
<i>PCC</i>	Pheochromocytomas
<i>PD-1</i>	Programmed Death 1
<i>PDE2A</i>	Phosphodiesterases 2A
<i>PDGF</i>	Platelet derived growth factor
<i>PDI</i>	Polydispersity index
<i>PD-L1</i>	Programmed Death ligand 1
<i>PEG</i>	Polyethylene glycol
<i>PEI</i>	Polyethyleneimine
<i>PET scan</i>	Positron emission tomography scan
<i>PFS</i>	Progression free survival
<i>PGF2<math>\alpha</math></i>	Prostaglandin F2 alpha
<i>PI3K-AKT</i>	phosphoinositol-3-kinase
<i>PINK1</i>	PTEN induced putative kinase 1
<i>piRNA</i>	Piwi-interacting RNA
<i>PKA</i>	Protein kinase A
<i>PKA</i>	Protein Kinase A
<i>PLC</i>	Phospholipase C
<i>PNMT</i>	Phenylethanolamine-N-methyltransferase
<i>PORC</i>	Porcupine
<i>PPNAD</i>	Primary Pigmented Nodular Adrenocortical disease
<i>pre-miR</i>	Precursor microRNA
<i>Pri-miR</i>	Primary microRNA
<i>PRKAR1A</i>	Protein kinase cAMP-dependent regulatory type I alpha
<i>QD</i>	Quantum dots
<i>RBC</i>	Red blood cell
<i>RES</i>	Reticuloendothelial system
<i>RFS</i>	Recurrence free survival
<i>RISC</i>	RNA-induced silencing complex
<i>RISC</i>	RNA-Induced Silencing Complex

<i>RNA</i>	Ribonucleic acid
<i>RNAi</i>	RNA interference
<i>rRNA</i>	Ribosomal RNA
<i>SEER</i>	Surveillance, Epidemiology, and End Results
<i>SF1</i>	Steroidogenic factor 1
<i>SHH</i>	Sonic Hedgehog
<i>siRNA</i>	Small interfering RNA
<i>SLN</i>	Solid lipid nanoparticles
<i>snoRNA</i>	Small nucleolar RNA
<i>snRNA</i>	Small nuclear RNA
<i>SO-miRs</i>	Site-overlapping microRNAs
<i>SPION</i>	SuperParamagnetic Iron Oxide
<i>StAR</i>	Steroidogenic Acute Regulatory Protein
<i>TCF/LEF</i>	T cell factor/lymphoid enhancer factor
<i>TCGA</i>	The Cancer Genome Atlas
<i>TE</i>	Transposon elements
<i>TEM</i>	Transmission electron microscopy
<i>TGF-<math>\beta</math></i>	Transforming Growth Factor $\beta$
<i>TKI</i>	Tyrosine kinase inhibitors
<i>TLDA</i>	TaqMan Low-density Arrays
<i>TME</i>	Tumor microenvironment
<i>TMTME</i>	Too many targets for miRNA effect
<i>TNF-<math>\alpha</math></i>	Tumor necrosis factor- $\alpha$
<i>TNM</i>	Tumor, Nodes and Metastasis
<i>TRBP</i>	HIV-1 transactivating response RNA-binding protein
<i>tRNA</i>	Transfer RNA
<i>USF1</i>	Upstream transcription factor
<i>USPION</i>	Ultra small SuperParamagnetic Iron Oxide
<i>VEGF</i>	Vascular endothelial growth factor
<i>VEGFR</i>	Vascular endothelial growth factor receptor
<i>WGD</i>	Whole genome doubling
<i>WT1</i>	Wilms Tumor 1
<i>ZNRF3</i>	Zinc and ring finger 3
<i>ZNRF3</i>	Zinc and Ring Finger 3
<i>PDEs</i>	Phosphodiesterases



# 1-INTRODUCTION

---





## **Chapter I. Adrenocortical cancer, a rare but aggressive malignancy**

The aim of this chapter is to discuss different aspects of adrenocortical cancer, the pathology on which relies this thesis. We first provide a synopsis of the adrenal gland's functions and potential gland-risen pathologies, with focus on tumorigenesis. We then expose clinical aspects of adrenocortical cancer and address the insufficiency of current therapies. We believe that deciphering the molecular landscape of this cancer may provide new venues for therapy.

## **I.A. The adrenal glands**

### **I.A. 1. Overview**

The adrenals are a pair of endocrine glands initially described as kidney accessory tissue due to their localization in the suprarenal region. They are known to control vital physiological functions mainly through releasing hormones (1). Overall, adrenal hormones include immunosuppressors, stress regulators, metabolism modulators and androgens.

### **I.A. 2. Anatomy and histology**

The adrenal glands are ductless glands settled in the retroperitoneum within the posterior abdominal wall, just above each kidney. They are easily recognized thanks to their suprarenal localization with a pyramidal shape for the right gland and a crescent form for its left counterpart (Figure 1A). The adrenals confer a yellowish cap to the kidneys from which they are separated by a septum of connective tissue within the renal fascia. Size wise, human adrenals account for 3 cm in width and 5 cm in height with a combined weight of around 7-10 grams for adults (2). Despite their small dimensions, the adrenals are highly vascularized structures in agreement with their endocrine functionalities. The arterial supply is ensured by three vessels: the inferior phrenic artery, the aorta and the renal artery; all arborizing in up to 50 arterial branches at the adrenal hilum. Each gland drains through a central vein: the inferior vena cava for the right adrenal gland, and the left renal vein via the inferior phrenic vein for the left gland (3). Histologically, the adrenal gland is a zonated entity: it is outlined by a fatty capsule surrounding an outer cortex and an inner medulla, each characterized by a panel of secreted hormones (Figure 1).

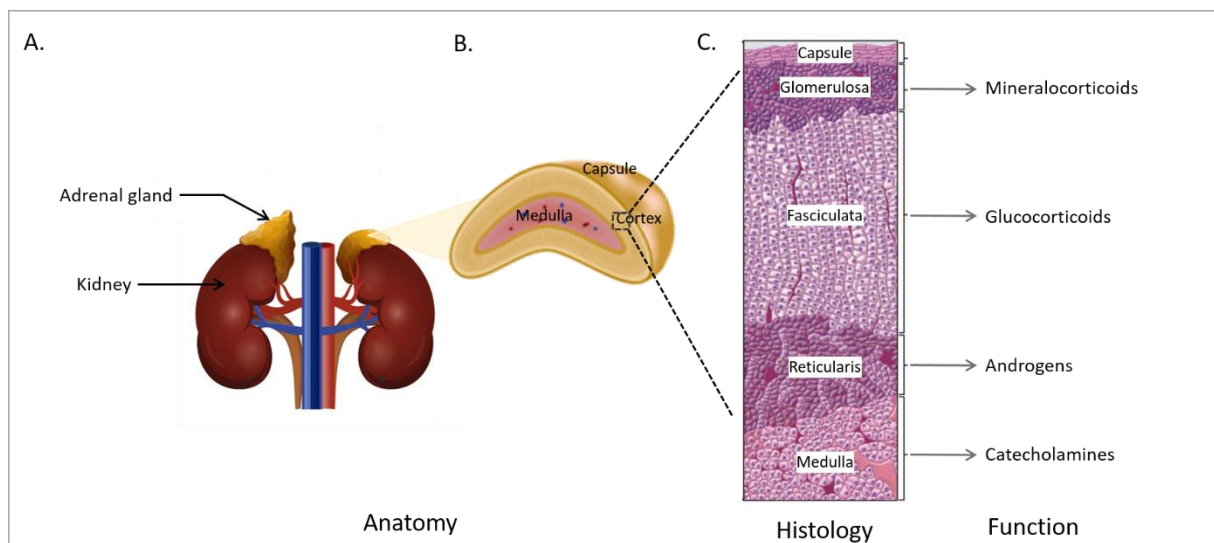


**Figure 1: Adrenal gland anatomy and histology.**

(A) The adrenal glands are yellowish glands located on top of the kidneys. The cross section (B) of an adrenal gland reveals three main zones: an outer capsule, an intermediate cortex and an inner medulla. In terms of histology (C), the cortex is subdivided into three zones: Zona glomerulosa secreting mineralocorticoids (i.e. aldosterone), Zona fasciculata releasing glucocorticoids (i.e. cortisol), Zona reticularis secreting adrenal androgens (i.e. DHEA, DHEAS). In the core of the gland, the medulla produces catecholamines (i.e. adrenaline).

### I.A. 2.a. The capsule

The capsule is a thin layer of flattened mesenchymal cells, which envelop the adrenal gland. It arises by the 8<sup>th</sup>- 9<sup>th</sup> week of gestation, where mesenchymal cells migrate and condensate to encapsulate the fetal adrenal gland (4). This capsule emits trabeculae of blood vessels and nerves into the adjacent tissue, thus providing structural support. Moreover, it is implicated in cortex homeostasis and development as supported by adrenal enucleation experiments (5). Along with fetal precursors, the capsule and subcapsular region are potential reservoirs for adrenocortical progenitor cells, since gland repopulation occurs by cell displacement inwards towards the medulla (5, 6)

### I.A. 2.b. The adrenal cortex

The cortex is the most prominent part of the gland mass (90%). In addition to the gonads, the adrenal cortex constitutes the main niche for steroid hormone synthesis. Cholesterol is the precursor of steroids (Figure 2); its conversion in the cortex into intermediate or mature hormones requires a series of hydroxylations and shuttling between mitochondria and

endoplasmic reticulum (7, 8). Briefly, cholesterol is either imported into the adrenocortical cells by plasma lipoproteins (LDL and HDL) or synthesized de novo within the endoplasmic

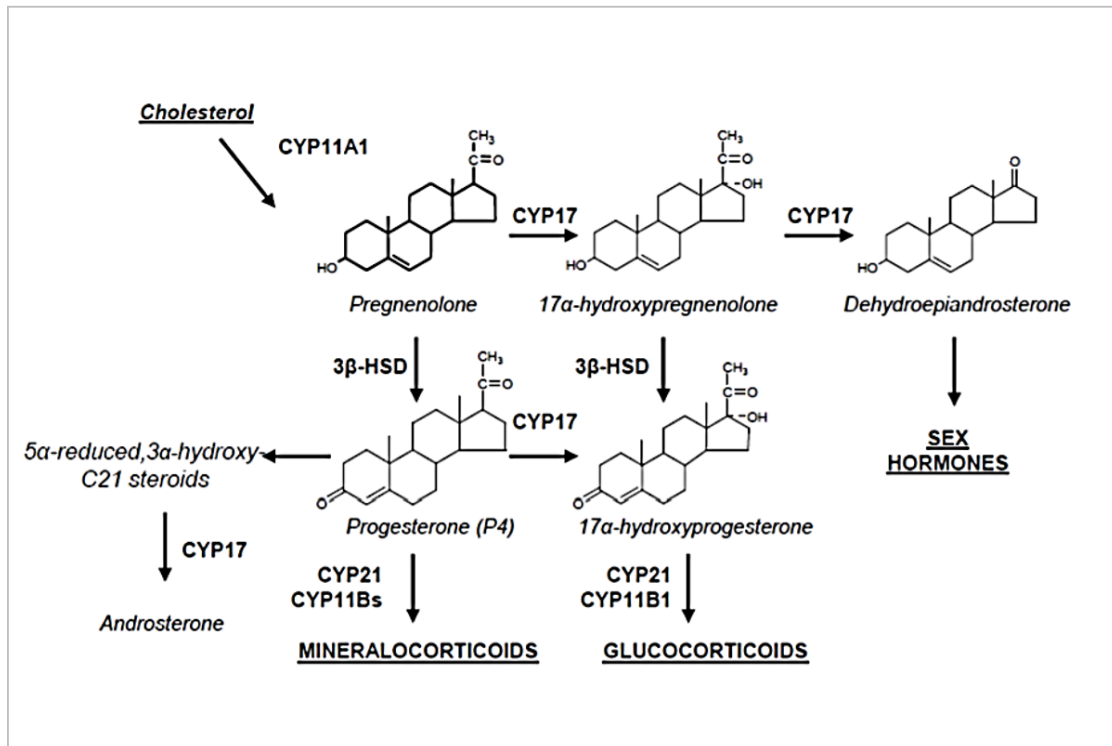


**Figure 2: Steroid hormones biosynthesis.**

Adrenal steroids originate from cholesterol as precursor, after its cleavage into pregnenolone. The biosynthesis engages various enzymes, some of which act at the mitochondrial level (CYP11A1, CYP11B1, CYP11B2), others at the level of the endoplasmic reticulum (CYP17, 3βHSD, CYP21). Aldosterone is the main mineralocorticoid produced within the Zona Glomerulosa, cortisol is the main glucocorticoid produced in humans by the Zona Fasciculata (corticosterone in rodents). Androgen precursors are synthesized in the Zona Reticularis. Adapted from Sushko et al. 2014.

reticulum. Once in steroidogenic cells, cholesterol is transported to the mitochondria; the first step of steroidogenesis takes place in the inner membrane of this organelle where cholesterol is cleaved into pregnenolone by the P450 side chain cleavage enzyme CYP11A1. The transfer of cholesterol into the mitochondria is the limiting step in steroidogenesis and involves several proteins like StAR (Steroidogenic Acute Regulatory) and PBR (Peripheral Benzodiazepine Receptor). Following conformational changes, StAR protein is translocated to the mitochondrial matrix through the inner membrane, thus favoring intramitochondrial cholesterol transport (9). This activity can be directly stimulated via its phosphorylation by PKA (Protein kinase A). Another protein, PBR or TSPO (Translocator Protein) has been considered as a mitochondrial carrier of cholesterol (10). Remarkably, adrenocortical cells harbor dense

mitochondrial network and abundant smooth endoplasmic reticulum and Golgi system. The cortex itself is segmented into three concentric zones each featuring distinct morphologies and functionalities. The adrenal cortex zonation relies, among others, on differential expression of two cytochrome P450 isozymes namely CYP11B2 and CYP11B1, which are respectively essential for aldosterone and cortisol synthesis (11).

### Zona glomerulosa

Zona glomerulosa is the outer zone of the adrenal cortex lying beneath the capsule. It occupies 15% of the cortex and comprises mineralocorticoid-secreting cells arranged in round clusters (7). Besides their distinguished mitochondria with lamellar cristae, glomerulosa cells exclusively express the aldosterone synthase CYP11B2 gene, which is crucial for their endocrine activity (11). Indeed, aldosterone is the key mineralocorticoid regulating hydromineral balance and blood pressure. In response to increased potassium and Angiotensin II levels, cells of the zona glomerulosa produce aldosterone as part of the renin-angiotensin axis (Figure 3).

Briefly, the kidney enzyme renin cleaves the liver-derived precursor angiotensinogen into angiotensin I, which is subsequently converted to angiotensin II by an angiotensin-converting enzyme (ACE) in the lungs. Angiotensin II is a crucial stimulator of CYP11B2 gene expression; it binds to its cellular G protein-coupled receptors (AT1R) in the zona glomerulosa. This activates the phospholipase C (PLC) signaling, allowing the production of inositol Triphosphate (IP3) and diacylglycerol (DAG). IP3 stimulates the outflow of calcium from the endoplasmic reticulum, whereas DAG inhibits potassium channels (12). This leads to membrane depolarization and entry of Ca<sup>2+</sup> into the cell. The increase in calcium concentration activates calmodulin and therefore CaMKs (Calmodulin dependent kinases) which phosphorylate CREB, thus activating the expression of StAR (acute response), CYP11B2 and AT1R (chronic response) (13). CYP11B2 triggers aldosterone release by the glomerulosa cells. Aldosterone acts on the distal tubules of kidney nephrons in order to favor potassium excretion conversely to sodium reabsorption and water retention. In concordance with the centripetal adrenal repopulation, cells of the zona glomerulosa are able to migrate and differentiate into cells of the zona fasciculata, thus maintaining cortex integrity (14, 15). Recent studies have further demonstrated that boosted Wnt/ $\beta$ -catenin signaling in zona

glomerulosa is critical for adrenal cortex zonation, as it positively regulates glomerulosa signature genes, i.e. CYP11B2, and negatively regulates fasciculata genes i.e. CYP11B1 (16, 17)

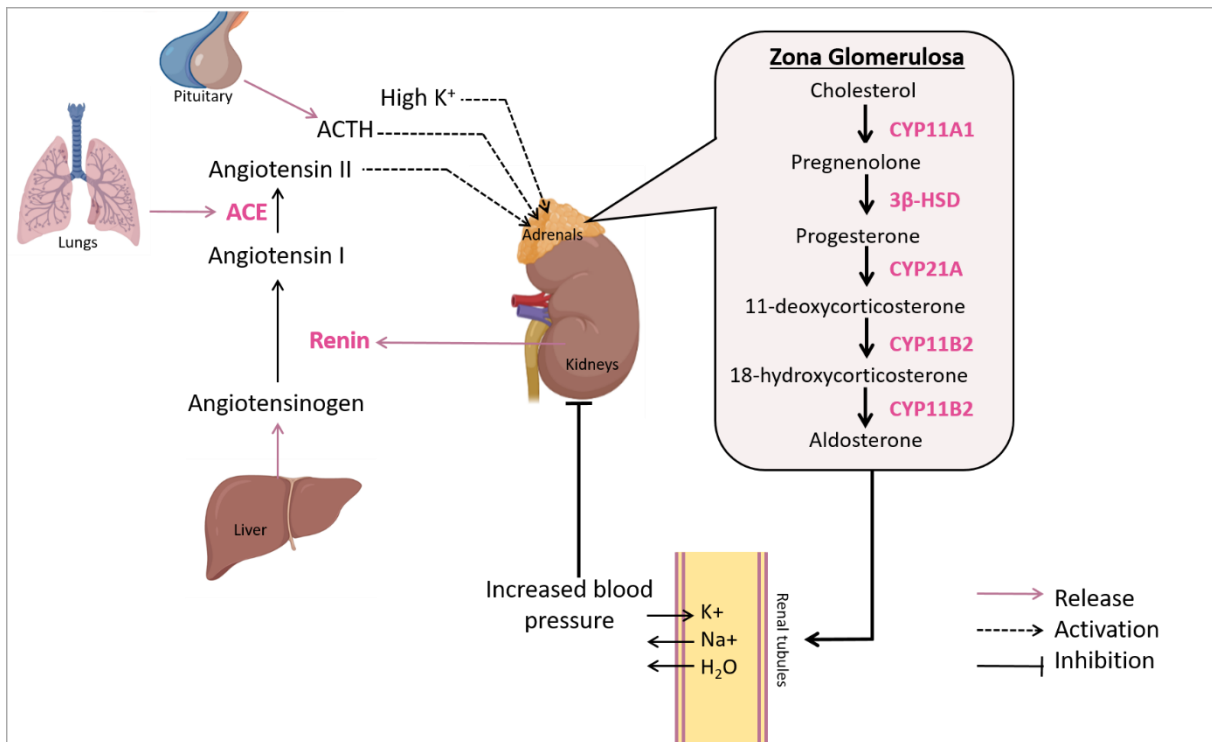


**Figure 3: Renin-angiotensin axis for aldosterone biosynthesis by Zona Glomerulosa.**

Low blood pressure, hypovolaemia, or decreased plasma concentration of  $\text{Na}^+$  stimulates the secretion of renin by the kidney. Angiotensinogen produced by the liver is transformed into angiotensin I, which is cleaved into angiotensin II by angiotensin-converting enzyme (ACE), produced in the lung epithelium. Angiotensin II in addition to pituitary ACTH stimulate Zona Glomerulosa cells to produce aldosterone from cholesterol through successive catalytic reactions, of which the last step is catalyzed by CYP11B2. Aldosterone induces reabsorption of  $\text{H}_2\text{O}$  and  $\text{Na}^+$  in the nephron, thus increasing blood pressure, and inhibiting the release of renin.

### Zona fasciculata

Zona fasciculata is the cortical layer inwardly adjacent to the zona glomerulosa. It accounts for 70% of the adrenal cortex with a population of polygonal cells organized into radial columns within the cortex-medulla axis (1). These cells display tubulovesicular cristae in their mitochondria. This layer is the secretion site of glucocorticoids i.e. cortisol for humans and corticosterone for rodents. This species-specific hormonal production is due to an exclusive expression, in humans, of the CYP17 enzyme, which is required for cortisol synthesis. Glucocorticoids are released during response to stress. They regulate a variety of biological processes such the immune response, metabolism and inflammation. Their release is controlled by the hypothalamic–pituitary axis (HPA) (7). Upon nervous stimuli, the

hypothalamus produces corticotrophin releasing hormone (CRH) and arginine vasopressin (AVP). CRH/AVP then trigger synthesis and discharge of adrenocorticotrophic hormone (ACTH) from the pituitary towards the adrenal glands. ACTH binds to its transmembrane G protein-coupled receptor (melanocortin receptor 2 MC2R) on the fasciculata cells, thus activating adenylate cyclase, which produces cAMP from ATP. Cytoplasmic levels of cAMP are controlled by the hydrolytic enzymes phosphodiesterases (PDEs). cAMP binding to the regulatory subunits of PKA induces their dissociation from the catalytic subunits, thus allowing them to phosphorylate different transcription factors such as CREB, which will activate the transcription of genes involved in the production of glucocorticoids (18).

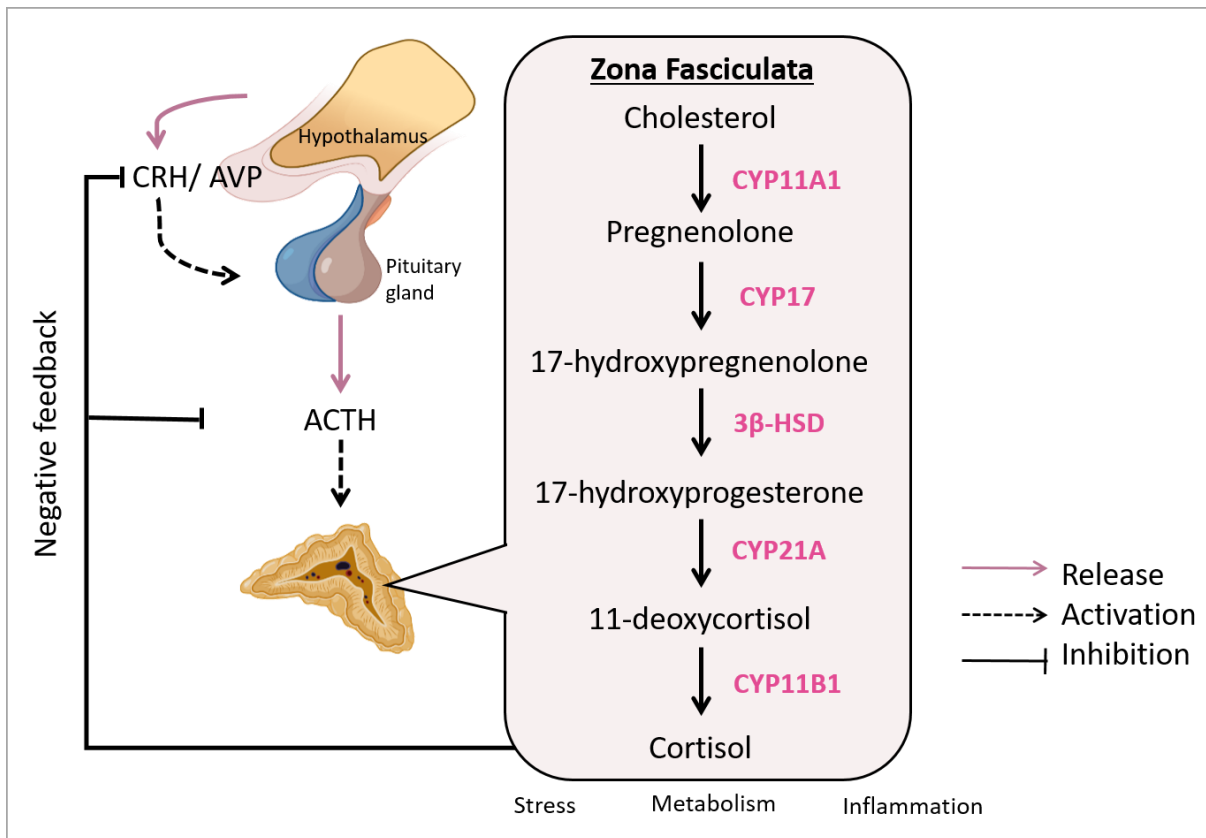


**Figure 4: Hypothalamo-pituitary axis for cortisol biosynthesis by Zona Fasciculata.**

The release of glucocorticoids is regulated by the hypothalamic-pituitary-adrenal axis. In response to nervous stimuli, the hypothalamus secretes CRH (Corticotrophin Releasing Hormone) and AVP (Arginine VasoPressin) which induce secretion of ACTH by the pituitary gland. ACTH released into the blood stimulates glucocorticoids production by Zona fasciculata, in a series of reactions of which the last step is catalyzed by CYP11B1. Cortisol is known to regulate metabolism, inflammation and stress. Cortisol exerts a negative feedback loop on the hypothalamus in order to stop the secretion of CRH, thus allowing fine regulation of cortisol levels in the blood.



Fine-tuning of cortisol levels is ensured by cortisol itself; when adequately accumulated, circulating cortisol shuts off secretion of CRH, thus inhibiting ACTH production and its subsequent cortisol release (Figure 4). Cortisol secretion has a circadian rhythm following the pulsatile secretion of ACTH, with a peak at early morning upon waking (19).

### Zona reticularis

The innermost zone of the adrenal cortex is zona reticularis. Composed of polyhedral cells with prominent lysosomes and tubulovesicular mitochondria, zona reticularis is distinguished by the biosynthesis of adrenal androgen precursors (AAP) such as dehydroepiandrosterone (DHEA) and its sulfate conjugate DHEAS in humans and primates (20). Of note, AAP conversion to testosterone mainly occurs in the testis, whereas the adrenal cortex is the only source of androgens in woman. In mice, lineage tracing experiments show remnants of fetal cortex, namely X-zone, in the innermost zone of the cortex rather than a distinct functional reticularis. The X-Zone regresses after puberty in male mice and after pregnancy in females (21).

### I.A. 2.c. The medulla

The medulla is the core of the adrenal gland. It is the main stress and metabolism regulator with regards to the catecholamines it releases (22). Consisting of neuroendocrine cells, namely chromaffin cells -also known as the body's main source of adrenaline, noradrenaline and less commonly dopamine- the adrenal medulla is considered as a unique ganglion of the sympathetic nervous system. In fact, chromaffin cells are modified neurons which have lost their axons and dendrites, yet they still receive innervation via the splanchnic nerve (23). The specific discharge of acetylcholine and its binding to its medullar receptors activate chromaffin cells not only to release catecholamines in the adjacent bloodstream, but also to emit paracrine signals. Adrenaline accounts for 85% of the medullar catecholamines, whereas noradrenaline constitutes the other 15%. Major roles of these hormones include reactions of the fight-or-flight response such as increasing heart rate, blood pressure, liver glycogenolysis and lipolysis (24).

As predicted by their name, catecholamines are medullar hormones structurally holding a catechol and an amine group. An interesting feature of catecholamines is that they act as neurotransmitters in the central nervous system and as hormones in the bloodstream where

high levels are detected in stress conditions. Their metabolism in the medulla involves a first conversion of tyrosine into L-DOPA via the tyrosine hydroxylase enzyme (25). Sequential enzymatic reactions convert L-DOPA into dopamine and eventually noradrenaline. Further metabolic modification by the phenylethanolamine-N-methyltransferase (PNMT) transforms noradrenaline into adrenaline, which is stored in the granules of medullar chromaffin cells. Functional interactions are well described between adrenal zones. Of note, glucocorticoids of the adrenal cortex trigger the catecholamine synthesis by increasing the enzymatic levels of tyrosine hydroxylase and PNMT (1). However, in acute stress, the adrenal cortex inhibits catecholamine discharge from the medulla through paracrine release of prostaglandin F2 alpha (PGF2 $\alpha$ ) (26).

### **I.A. 3. Adrenal gland development**

The development of the adrenal gland is regulated by the sequential expression of transcriptional regulators. Because of the homology with human processes, murine models are well adapted for comprehending the signaling pathways and components involved in adrenocortical development (27). Embryologically, the adrenal glands originate from two distinct tissues: the adrenal cortex arises from a mesothelial proliferation between the root of the dorsal mesentery and the gonadal ridge, whereas the adrenal medulla originates from cells of the neural crest, which migrate into the forming adrenal cortex (Figure 5). These primary structures assemble into an adrenogonadal primordium whose emergence is marked by the expression of steroidogenic factor 1 (SF1) at day 28 of gestation (Embryonic day 9 in mice). SF1 expression is controlled by the transcription factor WT1 (Wilms Tumor 1) and its cofactor Cited2 (CBP/p300 Interacting Transactivator with ED-rich tail 2). SF1 is an essential transcription factor capable of regulating several genes encoding for key steroidogenesis enzymes. Most importantly, SF1 depletion is lethal for mice, hence recalling the vital role of adrenal glands. SF1 positive cells within the adrenogonadal primordium delaminate from the epithelium, and penetrate the intermediate mesoderm's underlying mesenchyme, where they migrate dorsally to form the adrenal fetal zone. Neural crest cells move from the dorsal midline immediately lateral to the neural tube to the region where the embryonic adrenal is growing at around day 48 post-conception in humans (E11.5-E13.5 in mice). These cells remain as distinct islands dispersed in the fetal adrenal until birth, when they merge and develop into

catecholamine-producing chromaffin cells of the adrenal medulla (28). Herein, the adrenal gland begins to individualize from the surrounding mesenchyme and acquires a fibrous capsule by day 52 (E14.5 in mice).

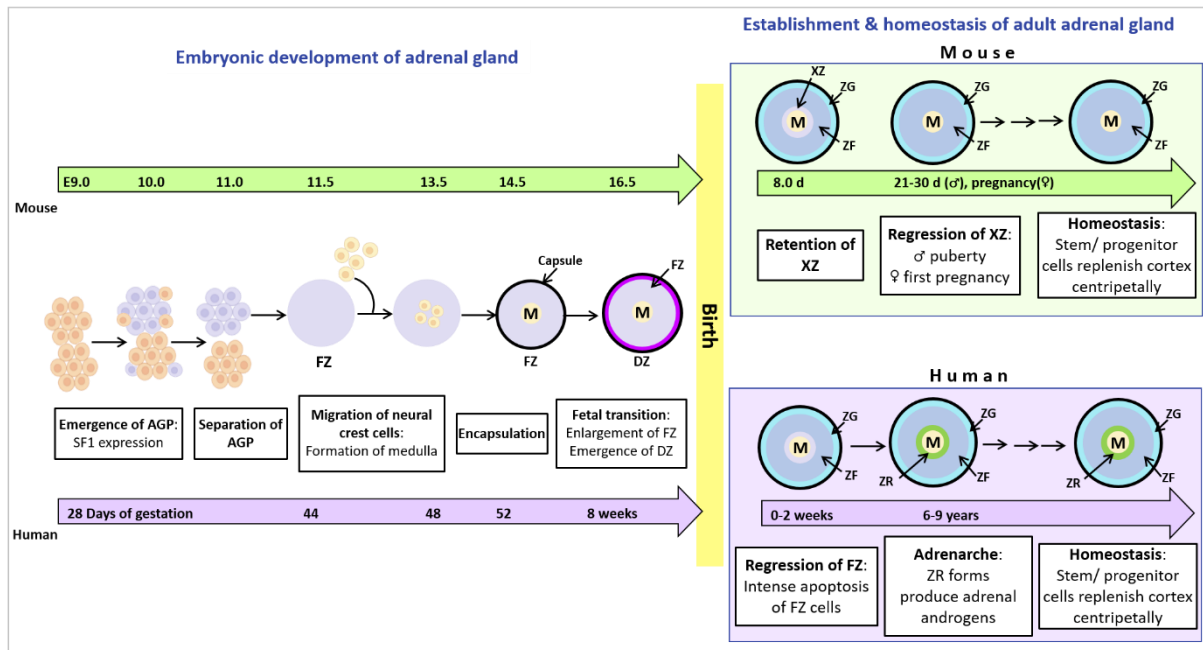


**Figure 5: Adrenal gland development and zonation.**

The WT1 transcription factor, in association with Cited2, initiates the expression of SF1, allowing the differentiation of adrenogonadal primordium (AGP). After separation of the adrenal and gonadal forms, there is a loss of Wt1 whose role in activating SF1 expression is replaced by the fetal enhancer FAdE. Cells derived from the neural crest migrate and then invade the embryonic adrenal gland to eventually form the medulla. Meanwhile, gland encapsulation by cells of various origins occurs, some of which express Wt1. As development progresses, the fetal zone (FZ) is replaced by cells from the definitive zone (DZ). Clear cortex zonation takes place after birth, with only two zones glomerulosa and fasciculata surrounding the human medulla; an internal X zone is reported in mice as remnant of the fetal cortex. The definitive adrenal gland is acquired at adrenarche in humans with an additional reticularis layer at the core of the cortex. In mice, the definitive cortex is marked by regression of X zone. Homeostasis of the gland is maintained by centripetal differentiation.

The capsular cells may originate from mesenchymal or adrenal progenitor cells, which have lost part of their WT1 expression in favor of Gli1 (Glioma-Associated Oncogene Homolog 1), a downstream activator of the hedgehog SHH pathway. The embryonic adrenal cortex quickly grows after encapsulation. In fact, the fetal cortex is established by the proliferation and differentiation of Gli1/Wt1 positive cells, which will gradually replace the cells of the fetal cortex. At this stage, the adrenal gland is a large entity occupying 0.2% of the total fetal weight, just the size of a kidney. Fetal cortex (or fetal zone FZ) itself accounts for 80% of the adrenal mass. The steroidogenic cells of the FZ have a prominent cytoplasm and highly express cytochrome P450 17 alpha-hydroxylase (CYP17), an enzyme that transforms pregnenolone to

dehydroepiandrosterone (DHEA) via its 17,20-lyase activity. DHEA are androgen precursors much produced by FZ and subsequently metabolized by the placenta into estrogens to maintain pregnancy. Besides androgen precursors, the fetal adrenal gland synthesizes glucocorticoids such as cortisol. One of the physiological functions of these glucocorticoids is to promote the maturation of fetal organs such as the liver, intestine and lungs in which they induce the synthesis of surfactant, which is essential for extra-uterine life (29). However, while the human fetal cortex plays an essential endocrine role for fetal survival, it is only transient and regresses to allow the establishment of the final cortex. Atrophy of this fetal structure in humans is the consequence of a massive wave of apoptosis triggered by parturition in a TGF- $\beta$  (Transforming Growth Factor  $\beta$ )- involving signalling. Activins and inhibins are peptide hormones belonging to the TGF- $\beta$  family, produced and secreted mainly by the adrenals and gonads (30).

Shortly after birth, the outermost zone develops into zona glomerulosa and zona fasciculata, whereas the inner fetal zone undergoes significant involution, resulting in a drop in adrenal androgen levels. Approaching puberty at 6-8 years of age is marked by adrenarche and androgene restoration, upon formation of zone reticularis at the fasciculo-medullary junction. In mice, the kinetics of definitive cortex onset and fetal cortex regression are different from those in humans. The final cortex begins to fall into place from E14.5. After birth, the adrenal cortex is made up of three distinct cell populations forming the glomerulosa zone, the fasciculata zone and an X zone, located between the fasciculate and the medulla (15). This X zone is indeed derived from fetal cortical cells expressing the SF1 enhancer FAdE and therefore corresponds to a remnant of the fetal murine cortex. The regression of the X zone follows a sexual dimorphism since its involution begins, in male, at puberty (approximately 28 days postpartum), and at the first gestation in female. This sexual dimorphism strongly indicates the involvement of sex hormones in the X zone dynamics.

Once the adrenal cortex is formed, its maintenance, renewal and differentiation are modulated by hormonal signals. In order to sustain gland size and function, the adrenal cortex is constantly replenished with steroidogenic cells to reconstitute the lost cells at the cortico-medullary junction. Capsular stem cells and subcapsular/zona glomerulosa progenitors are responsible for homeostatic renewal via RSPO/WNT/-catenin and SHH signaling pathways. This mechanism leads to the differentiation of progenitors into glomerulosa cells, which are

then shifted centripetally and converted into zona fasciculata cells. WNT and PKA signaling pathways have critical and complementary roles in zonation of the adult cortex (27). RSPO/WNT/ $\beta$ -catenin signaling promotes zona glomerulosa identity, represses zona fasciculata phenotype, and possesses tumorigenic potentials when constitutively activated. Conversely, cAMP/PKA signaling was demonstrated to inhibit zona glomerulosa fate, to maintain zona fasciculata identity, and to prevent  $\beta$ -catenin-induced carcinogenesis (31).

## **I.B. Adrenal disorders**

Hypo or hyperfunction of the adrenal glands can induce more or less severe pathologies. Hormonal imbalances are usually caused by abnormalities in the adrenal or pituitary functions.

### **I.B. 1. Primary adrenal insufficiency: Addison's disease**

Also known as, hypocortisolism or primary adrenal insufficiency, Addison's disease is a rare endocrine pathology in which the adrenals fail to produce sufficient glucocorticoids and mineralocorticoids (32). A characteristic symptom of Addison's disease is skin hyperpigmentation for which the disorder owes its name "bronze skin disease". The emergence of this pathology lies on autoimmune or infectious adrenalitis; genetic disorders may also contribute to adrenal insufficiency. Mechanistically, continuous discharge of pituitary ACTH towards the adrenal gland without appropriate hormone response results in the loss of cortisol-mediated negative feedback. ACTH accumulation persists additionally to enhanced secretion of proopiomelanocortin peptides, therefore triggering hyperpigmentation through their melanocyte-stimulating activity (33). Treatment of Addison's disease involves hormonal intake in order to normalize ACTH levels.

### **I.B. 2. Secondary adrenal insufficiency**

This disorder arises secondary to pituitary dysfunction, which is generally a tumor of the hypothalamus or the pituitary, usually associated with hypopituitarism, thus insufficient ACTH production (34). Mineralocorticoid secretion by zona glomerulosa is not altered as it is controlled by the renin-angiotensin axis. The typical cause of secondary adrenal insufficiency

is chronic administration of glucocorticoid therapeutics as it promotes atrophy of pituitary cells (33). Hypothalamo-pituitary disruptions are generally assessed using the insulin tolerance test since low blood glucose rapidly activates this axis in physiological contexts. When adrenal insufficiency shows up suddenly and not gradually over time, one can talk of adrenal crisis or acute adrenal failure (35).

### **I.B. 3. Congenital adrenal hyperplasia**

Genetic forms of adrenal insufficiency are known as congenital adrenal hyperplasia (CAH). Inherited in an autosomal recessive manner, CAH patients exhibit impaired steroidogenesis due to mutations in the enzymes involved in steroidogenesis. The most common cause of CAH is the absence of the enzyme 21-hydroxylase (95% of all cases). Other much rarer forms of CAH include deficiencies in CYP21A2, CYP11B1, CYP17A1 or the cholesterol-binding protein STAR (36). Patients usually develop symptoms related to cortisol/ aldosterone deficiencies and androgens overproduction and require chronic steroid therapy to compensate low hormone levels (37, 38) (38, 24).

### **I.B. 4. Hypercortisolism: Cushing syndrome**

Cushing syndrome is the most investigated disorder of overactive adrenals. It emerges because of excessive cortisol release from the adrenal gland. This endogenous hypercortisolism is mainly due to an overproduction of ACTH by a functional pituitary adenoma, a condition called "Cushing disease" (39). Interestingly, ACTH has been found to be abnormally produced in adrenal neoplasms in which the hormone acts as an autocrine/paracrine factor to activate steroid secretion, thus inducing Cushing syndrome (40). Another cause for Cushing syndrome is chronic consumption of exogenous steroids (i.e. dexamethasone and prednisone) for the treatment of several inflammatory and autoimmune diseases. Rarely, excess of ACTH can be produced by a tumor elsewhere in the body, which is referred to as "ectopic" production of ACTH (41). Finally, Cushing's syndrome can also be caused by excessive production of cortisol by benign or malignant adrenal tumors. Though with rare prevalence (40 cases/million/year), Cushing syndrome recalls various comorbidities such as cardiovascular diseases, respiratory problems, weight gain, osteoporosis (42). Besides

clinical signs highlighted by weight gain in a “moon face” or “buffalo hump”, imaging of ACTH-secreting pituitary (Computational Tomography or Magnetic Resonance) can discriminate underlying macro adenomas. In addition, cortisol diurnal pattern is flattened in patients with Cushing disease, thus it can be useful for diagnosis (19). High cortisol dosage after dexamethasone administration is also indicative of this disease. The gold standard treatment is pituitary ablation, which can be supported by radiotherapy and inhibition of adrenal steroidogenesis using preoperative medication (i.e. Mitotane, Metopirone, ketoconazole..) (42).

### **I.B. 5. Hyperaldosteronism: Conn’s syndrome**

Overproduction of aldosterone by one or both adrenal glands is termed hyperaldosteronism. While most cases are sporadic, 6% of patients carry familial forms of the disease. Mechanistically, defects in genes encoding ion channels (KCNJ5, ATP1A1, ATP2B3, CACNA1D, CACNA1H, and CLCN2) lead to aberrant cytosolic trafficking of calcium in zona glomerulosa cells, which triggers CYP11B2 expression and abundant aldosterone production. Increased volemia, hypokalemia, hypertension as well as cardiovascular issues are commonly reported in hyperaldosteronism (43). Recommended treatment involve surgical adrenalectomy for unilateral aldosteronism or administration of mineralocorticoid antagonists when both glands are affected (44).

## **I.C. Benign adrenal tumors**

### **I.C. 1. Tumors of the medulla: Pheochromocytoma**

The medulla is a neuroendocrine entity harboring catecholamine-secreting chromaffin cells co-localized with neurons, which govern adrenalin/noradrenalin release. Pheochromocytomas (PCC) are rare neuroendocrine tumors (one case/300 000/year) arising from chromaffin cells in the adrenal medulla or from extra-adrenal gangliomas, where they are called paragangliomas (45). While most PCC are benign, high morbidity and death rates were linked to excessive catecholamine production, which causes arrhythmia, hypertension, and stroke. PCC are benign, but can become cancerous, as indicated by distant metastases to non-chromaffin tissues (46). These neoplasms are strongly influenced by genetics as 40% of patients harbor germinal mutations in predisposing genes like VHL, SDHB, NF1, SDHD, and

RET (47). The remaining 60% cases mostly carry somatic mutations in at least one susceptibility gene.

## **I.C. 2. Tumors of the cortex**

Adrenocortical tumors can be benign or malignant. Unilateral or bilateral adrenal tumors affect 7,3% of the population and are often incidentally detected during imaging performed for indications other than adrenal disease (48). Benign tumors of the cortex cover adenomas and hyperplasia.

### **I.C. 2.a. Adenomas**

Most adrenal lesions are not cancerous and designated as adrenocortical adenomas (ACA) with focalized proliferations. ACA can be diagnosed via abdominal imaging or autopsy followed by meticulous histopathology (49). Depending on their lipid content, six centimeter-sized ACA nodules appear yellow (high lipids) or brown (low lipids); they are well delimited, but lacking a defined capsule. Tumors' secretory profile allowed their classification into aldosterone-secreting, cortisol-secreting or non-functional ACA (50). On this basis, patients with ACA are either asymptomatic or manifest hormone-related clinical signs resulting from adrenal corticosteroid hypersecretion, most often Cushing's syndrome, but also primary hyperaldosteronism and, rarely, virilization or feminization. ACA are generally sporadic, but exome-sequencing revealed somatic mutations in driver genes such as CTNNB1 for 70% of non-functional ACA (51). Moreover, activating mutations in Protein Kinase A (PKA) catalytic subunit (PRKACA) are encountered in functional ACA (52). It is obvious that benign ACA will not expand in metastases; the long-term prognosis of patients with ACA is very good and unilateral ablation ensures limited morbidity. Though benign transformation towards adrenal cancer is very rare, understanding and managing ACA are crucial, given their high incidence rate and potential morbidity due to hormonal excess.

### **I.C. 2.b. Hyperplasia**

Adrenocortical hyperplasia is characterized by bilateral diffuse enlargement of the adrenals and is often associated with Cushing syndrome. Micronodular hyperplasia, also known as Primary Pigmented Nodular Adrenocortical disease (PPNAD), is an ACTH-independent



hyperplasia and is a rare cause of Cushing syndrome, which occurs sporadically or in the context of the Carney complex multi-neoplastic syndrome (50). PPNAD holds germinal inactivating mutations in PRKAR1A gene (Protein kinase cAMP-dependent regulatory type I alpha regulatory subunit). Mutations in phosphodiesterases 11A and 8B (PDE11A, PDE8B) were additionally described (53). Large nodules (>1 cm) are indicative of Primary Bilateral Macronodular Adrenal Hyperplasia (PBMAH) which is also associated to hypercortisolism. In addition to adrenal enlargement, local ACTH production has been demonstrated in PBMAH. Fifty percent of patients present germline mutations in the putative tumor suppressor Armadillo repeat containing 5 (ARMC5) (54). Silencing ARMC5 led to reduced expression of steroidogenic enzymes with decreased cortisol production while its overexpression promoted cell death (54).

## **I.D. Adrenocortical cancer**

Adrenocortical carcinoma (ACC) is a rare endocrine malignancy with pejorative prognosis. To date, surgical resection is the ultimate treatment option for early stage tumors, whereas cytotoxic chemotherapy is adopted for advanced cases. As targeted therapies were rather disappointing, the clinical management of ACC still requires multidisciplinary approaches in order to better understand the disease pathogenesis.

### **I.D. 1. Epidemiology**

The yearly incidence of ACC is 0.5-2 cases per million, thus accounting for 0.2% of cancer-related deaths (50). The age categories of ACC patients show two peaks: a first spike at early childhood (before five years of age) and a second one between the third and fifth decade (55). In infants, ACC occurs at an incidence of 0.2-0.3 cases per million per year; this rate is 15 times higher in children of South Brazil where germinal mutations in the TP53 gene seem frequent (56). Epidemiological studies revealed that women are more affected by ACC compared to men with a ratio of 1.5-2.5:1. Mice genetic models suggested that this over-representation of adrenocortical tumors in women may be attributed to a higher potential for cortical cell renewal in female adrenals (57, 58).

## **I.D. 2. Clinical presentation**

Clinical manifestations of ACC are related either to excessive hormone secretion or to enlarged adrenal mass. The most common clinical presentation is Cushing's syndrome with or without virilization in women (59). Instead of classical tumor symptoms, ACC patients present typical hypercortisolism features such as hypertension, diabetes mellitus, visceral obesity, hypokalemia and osteoporosis (60). Because of increased cortisol release in ACC, the renal Hydroxysteroid 11-Beta Dehydrogenase 2 (HSD11B2) system responsible of cortisol-cortisone conversion is saturated, thus resulting in mineralocorticoid receptor activation in a glucocorticoid-mediated manner. Adrenal androgens are also produced in 40-60% of patients; this is followed by acquisition of male pilosity patterns, baldness and menstrual irregularities in women. Additional symptoms related to enlarged tumors include flank pain, abdominal discomfort, nausea and back pain. Abdominal imaging have confirmed that most ACCs are indeed asymptomatic incidentalomas, which explains their delayed diagnosis.

## **I.D. 3. Pathology and genetic predisposition**

While most ACC cases occur sporadically, several genetic disorders seem to predispose for adrenocortical malignancy, notably in children.

### **I.D. 3.a. Li-Fraumeni Syndrome**

Accounting for 50-80% of pediatric ACC, the Li-Fraumeni syndrome (LFS) results from germline mutations inactivating the TP53 tumor suppressor gene (61). LFS can increase susceptibility to a spectrum of cancers including sarcoma, leukemia, breast cancer, and ACC. Most importantly, about 6,5-10% of LFS patients develop ACC, whereas 16% of ACC patients carry mutated TP53 as shown in a cohort studied by Assié et al. (62). It is worth mentioning that TP53 mutations found in ACC are not strictly inherited, since de novo mutations are acquired in 25% of cases (63). High prevalence of ACC in Brazilian children highlighted a unique germline mutation, namely R377H, harbored in exon 10 of TP53, outside the hot spot regions of conventional TP53 mutations within exons 4-8 (64).

### I.D. 3.b. Beckwith-Wiedemann Syndrome

Another familial disease associated to ACC, is Beckwith–Wiedemann syndrome (BWS), which features genetic or epigenetic alterations within the Insulin-like Growth Factor 2 (IGF-2) at locus 11p15 (65). Consequently, affected children exhibit abnormal overgrowth, congenital malformations and higher incidence of childhood cancers, particularly Wilms' tumor, pancreatoblastoma and hepatoblastoma. ACC accounts for 15% of BWS-related neoplasms.

### I.D. 3.c. Multiple Endocrine Neoplasia Type 1

Multiple Endocrine Neoplasia Type 1 (MEN1) results from an autosomal mutation of the tumor suppressor gene MEN1 within the menin coding locus 11q13 (66). Just as predicted by its name, MEN1 involves several endocrine tumors i.e. parathyroid (90%), endocrine pancreatic tumors (30-70%) and pituitary neoplasms (30-40%). The prevalence of adrenal tumors in MEN1 patients is estimated to 20-55% of which only 14% account for ACC (67). ACC cases were also reported in familial adenomatous polyposis (FAP) with germline mutations in Adenomatous Polyposis Coli (APC) gene, leading to abnormal beta-catenin concentrations (68).

## I.D. 4. Diagnosis

After incidental suspicion of ACC, patients should undergo comprehensive hormonal and radiological inspections. Clinical assessment also involves tracking case history and careful histopathology analysis (69).

### I.D. 4.a. Biochemical screening and hormone dosage

The secretory profile of adrenal lesions holds great value when deciphering ACC from non ACC. Clinical manifestations at initial assumption may guide adequate hormone screening according to guidelines of the European Network for the Study of Adrenal Tumors (ENS@T) (70). For instance, patients with hypertension and hypokalemia are subjected to aldosterone/renin dosing in order to rule out primary aldosteronism. In addition, serum ACTH and dexamethasone suppression test can specifically distinguish Cushing's syndrome from ACC-born hypercortisolism. Advanced metabolomics technologies demonstrated that urine metanephrines (metabolites of catecholamines) are indicative of pheochromocytomas,

whereas plasma methoxytyramine (metabolite of dopamine) is predictive of malignancy (70). Hormone imbalances in ACC include excess in glucocorticoids, mineralocorticoids, androgens and inactive steroid precursors (androstenedione or 17 $\alpha$ -hydroxyprogesterone). However, it is recommended to remain cautious with regards to hormone assessments, because several parameters (i.e. sex, age, daily rhythm, drug interactions) have to be considered in order to set reference non-pathological ranges.

#### I.D. 4.b. Imaging

Medical imaging is the frontline diagnosis tool as it provides insights on the size and appearance of the suspicious adrenal mass. In general, clinicians correlate homogeneous, lipid-rich incidentalomas with benign tumors (69). In contrast, ACCs are large irregular tumors, with hemorrhagic or necrotic lesions expanding to adjacent tissue, notably vena cava. Seventy percent of ACCs measure around 6 cm in computed tomography (CT) scans with a tumor density >10HU and an absolute washout <60% (71). In magnetic resonance imaging (MRI), ACC is typically hypointense on T1-weighted imaging and hyperintense on T2. Small areas of no signal may result from intracytoplasmic lipid droplets. In addition, ACC shows intense uptake of the 18F-fluorodeoxyglucose (18FDG) tracer in positron emission tomography (PET) scans. FDG-PET displays a sensitivity of 95% in discriminating malignant from benign masses, but can also decipher local invasions to inferior vena cava and regional lymph nodes (72). As distant metastasis in ACC include liver, lungs, peritoneum and subsequently bones, high-resolution imaging of abdomen and chest are performed. When the tumor nature is confirmed, it can be classified and staged according to TNM (Tumor, Nodes and Metastasis) features.

#### I.D. 4. c. Histopathology

Along with macroscopic evaluation of tumor weight and hemorrhagic profile, microscopic observations may also guide tumor staging to assess their malignancy and aggressiveness. The gold standard classification criteria rely on a Weiss scoring system (73) which states that recognition of at least 3 out of 9 histopathological features is suggestive of malignancy. These morphologic parameters take into consideration cytological aspects (nuclear atypia, high mitotic index and abnormal mitoses), tumor structure (diffuse architecture, eosinophilic cytoplasm) and invasion (capsular, sinusoidal or venous) (Table 1).

Histological criteria	Weight of criteria	
	0	1
Nuclear grade	1 and 2	3 and 4
Mitoses	≤ 5 for 50 fields x 400	≥ 6 for 50 fields x 400
Atypical mitoses	No	Yes
Clear cells	> 25%	≤ 25%
Diffuse architecture	≤ 33% surface	> 33% surface
Confluent necrosis	No	Yes
Venous invasion	No	Yes
Sinusoidal invasion	No	Yes
Capsular invasion	No	Yes

**Table 1: The Weiss scoring system.**

The presence of three or more criteria correlates with malignancy. Nuclear grades are as follows: (1) round nuclei, small size, no nucleoli, (2) nuclei slightly irregular, prominent nucleoli at x400, (3) irregular large nucleoli at x100, (4) irregular large nucleoli at x100, monstrous cells.

Despite their stringency, these criteria remain subjective, thus misleading for diagnosis in some cases (74). Other approaches like immunohistochemistry can also distinguish ACC from ACA based on a high Ki-67 expression in proliferating cells (75). Besides its diagnosis interest, the Ki-67 index has emerged as a potent negative prognostic factor (76, 77). Similarly, overexpression of cell cycle markers, i.e. cyclin D1 responsible for G1 progression, cyclin E contributing to the G1-S transition, or p27, is correlated to malignancy of adrenal masses. When Hematoxylin-eosin (HE) staining fail to affirm cortex integrity, immunostaining for adrenal markers such as Steroidogenic Factor-1 (SF-1), Melan A, Inhibin-alpha, and calretinin is useful for ACC diagnosis (78). Chromogranin A staining is characteristic for pheochromocytoma and paraganglioma. With this panel of tools supporting the Weiss scoring system, diagnostic performance should be improved for ACC.

## I.D. 5. Staging

The European Network for the Study of Adrenal Tumors (ENSAT) proposed staging ACC according to tumor size, location and metastases status. Stages I and II correspond to local, gland-confined tumors with respective diameters less or greater than 5 cm, whereas stage III

tumors have already invaded adjacent tissue and lymph nodes. Stage IV ACC displays distant metastasis (Table 2). The most common metastatic sites are lung, liver, and bone. Most patients are diagnosed at advanced stages with tumors stage III or stage IV, representing 18%-26% and 21%-46% of ACC at diagnosis, respectively (79). This renders ACC management quite challenging (70).

Stage	Tumor Size	Infiltration to surrounding tissue or invasion of adjacent organs	Infiltration to lymph nodes	Metastasis
Stage I	≤ 5 cm	No	No	No
Stage II	> 5 cm	No	No	No
Stage III	≤ 5 cm or > 5 cm	Infiltration and invasion	No	No
Stage IV	≤ 5 cm or > 5 cm	Infiltration and invasion	Yes/No	Yes

**Table 2: Staging of ACC according to ENSAT guidelines.**

## **I.D. 6. Therapy**

Despite major advances in the molecular profiling for ACC, thanks to the international and European networks for ACC management, our knowledge of the disease pathogenesis is still scarce. It is well known that prior characterization of the tumor biology is crucial for treatment decisions. So far, therapeutic options include surgical resection, radiotherapy and adjuvant chemotherapy with highlights on mitotane. No innovative therapy has yet shown its effectiveness.

### **I.D. 6.a. Surgical resection**

For low grade ACC, complete surgical resection (R0) is the ultimate curative modality; the R0 status correlates with better outcome and prognosis than incomplete resection statuses R1 and R2. Given their burden, such interventions should be conducted by surgeons with high qualifications in visceral oncology (>10 adrenalectomies/year) (80). Moreover, preoperative assessments effectively guide the surgical approach to be adopted. Open adrenalectomy is the gold standard treatment mainly for infiltrating tumors, whereas noninvasive laparoscopic adrenalectomy may be carried out when tumor size is smaller than 5 cm (81). No matter the

method, the main goal is to avoid disrupting the capsule thus limiting local spread. Further lymph node dissection was shown to reduce tumor recurrence. In addition, some surgeons perform laparoscopy to exclude intraperitoneal invasion of the adrenal gland into adjacent sites. If such is the case, complete R0 resection may require in depth intervention within the surrounding organs i.e. kidneys, liver, vena cava or stomach (82).

#### I.D. 6.b. Adjuvant therapy

High recurrence rates are still observed in 19-34% of ACC patients despite seemingly complete adrenalectomy (81). This highlights the difficulty of surgical excision when it comes to setting the incision margins. Adjuvant therapies such as mitotane, chemotherapy and radiotherapy are routinely implemented after surgery in attempt to reduce relapse risks. Whether these adjuvants are indeed beneficial for ACC outcomes remains controversial.

#### Mitotane

Mitotane (o,p'-DDD or 1,1-(o,p'-dichlorodiphenyl-2,2-dichloroethane) is an adrenolytic drug that is derived from the insecticide dichlorodiphenyltrichloroethane (DDD) first proved effective in dogs in 1948 (83). Though mitotane is the only approved drug for systemic treatment of ACC, it was also shown to exhibit adrenolytic and cytostatic effects on normal adrenocortical cells. It is established that mitotane can interfere with steroidogenesis through inhibiting major enzymes involved in cholesterol cleavage such as CYP11A1 and CYP11B1 (84). Nonetheless, the adrenolytic mechanism of mitotane is still partly understood and is probably associated to blockage of mitochondrial respiration and subsequent oxidative damage. Another hypothesis is that mitotane induces necrosis and consequent inflammatory infiltration in the adrenal glands. Current guidelines by the ENSAT and the European Society for Endocrinology (ESE) recommend mitotane for patients at high risk of relapse as predicted by an advanced stage III, a R1-Rx resection status or a Ki67>10% (69). In their retrospective study involving 177 patients treated with mitotane after complete surgery, Terzolo et al. demonstrated that recurrence-free survival (RFS) was extended to 42 months in the mitotane group as compared to controls (10-25 months). In addition, patients sustaining adjuvant mitotane show better overall survival (OS) (85). Conversely, mitotane did not enhance RFS/OS in an American meta-analysis (86). For that, the risk/ benefit balance is still debated before

proceeding to adjuvant administration. A first prospective analysis, namely the ADIUVO trial (ClinicalTrials.gov identifier, NCT00777244), evaluated efficacy of adjuvant mitotane in prolonging RFS of patients with low-moderate risks of relapse (87, 88). As mitotane has a narrow therapeutic window (14-20 mg/l), yet a broad cytotoxic potential, administered doses and mitotane should be constantly monitored (89). Mitotane-related adverse effects include dizziness, drowsiness, gastro-intestinal discomfort, and central nervous system disturbances. Most importantly, all patients develop adrenal insufficiency due to the adrenolytic action of mitotane. This is palliated by glucocorticoid intake (90).

### Chemotherapy

For metastatic ACC, cytotoxic chemotherapy is the mainstay treatment to alleviate tumor burden. However, chemotherapy regimens still pose limited effectiveness and acute toxicity (77). The multidrug resistance gene (MDR-1) encoding for the p-glycoprotein pump is highly expressed in ACC (91), which may justify chemotherapy failure. Interestingly, mitotane was shown to reverse multidrug resistance by hindering drug efflux through blockage of (MDR-1) (92). These findings paved the way for the use of mitotane in combination with chemotherapeutic drugs. The phase III trial FIRM-ACT (First International Randomized Trial in Locally Advanced and Metastatic Adrenocortical Carcinoma Treatment, ClinicalTrials.gov identifier NCT00094497) established the combination of mitotane with etoposide-doxorubicin-cisplatin (M-EDP) as first-line therapy for advanced cases (93, 94). According to the protocol, a first round of mitotane monotherapy is initiated 7 days prior to cytotoxic administration. The primary endpoint was OS; response rate and progression free survival (PFS) were subsequently evaluated. More recently, retrospective meta-analyses demonstrated that associating etoposide (inhibitor of topoisomerase), doxorubicine (DNA intercalating agent) and cisplatin (cell death inducer via DNA alkylation) improved response rates in non-resectable ACC (90).

### Radiotherapy

The implementation of radiotherapy in ACC treatment remains ambiguous; it is rather considered in adjuvant or palliative contexts. In their retrospective analyses using the german ACC registry, Fassnacht et al. highlighted benefits of adjuvant radiotherapy on local relapse



post-resection, but not on OS (95). On this basis, the 2018 guidelines of the European Society of Endocrinology do not recommend adjuvant radiation (77). Conversely, a recent revision of the SEER (Surveillance, Epidemiology, and End Results) database showed that radiotherapy remarkably improved OS especially in node-free-stage III patients, as compared to surgery alone (96). Another analysis from the chinese ACC registry showed that adjuvant radiotherapy also enhanced OS in addition to recurrence-free survival (97). As observations continue to fluctuate, collaborative multivariate analyses require unifying algorithms as well as data collection methods with regards to patient staging, molecular patterns and administered therapy. By doing so, retrospective studies shall not bypass discrete patient groups, which may benefit from a certain therapy.

I.D. 6.c. Targeted therapy

Molecular targeted therapies are a trendy option in cancer treatment. Given the unmet clinical needs in ACC, multiple tyrosine kinase inhibitors (TKI) have been tested in patients. These therapies aim to shut down key pathways and growth factors to which potential clinical value has been attributed. Such molecules may impair phosphorylation, thus activation of kinases, or may simply compete with extracellular ligands in order to prevent subsequent signaling cascades (Figure 6).

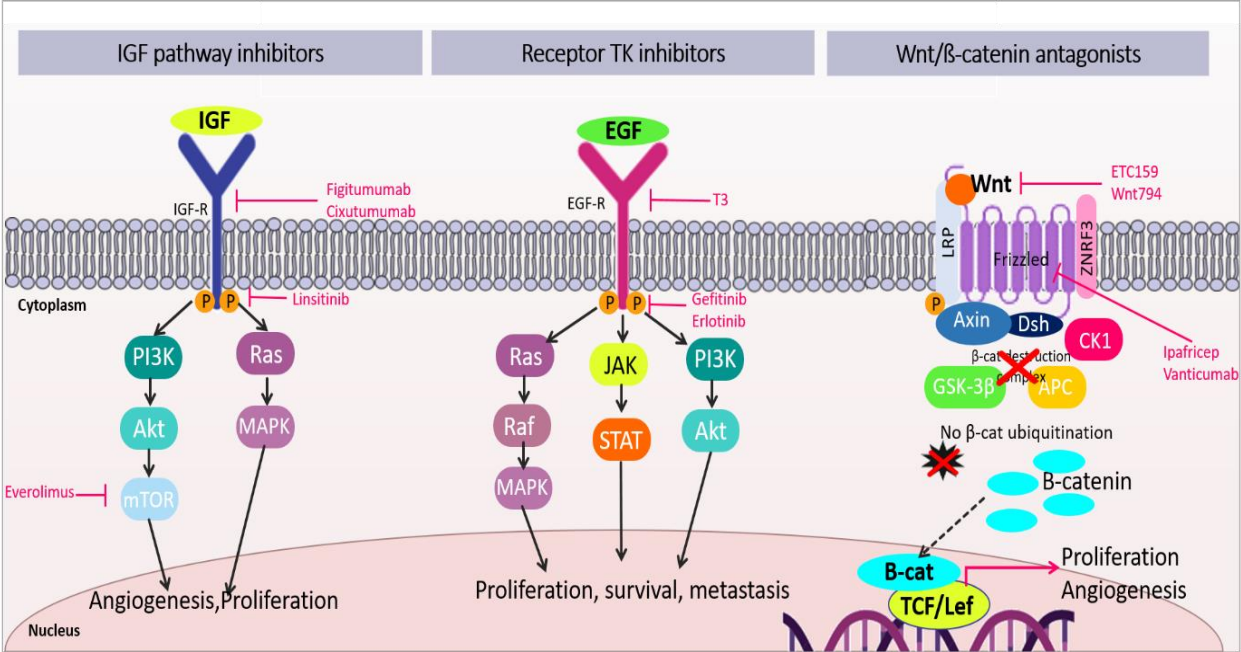


Figure 6: Therapies targeting key signaling cascades in ACC.

A subset of clinical trials with molecular targets are shown in table 3.

### Targeting EGFR

Epithelial growth factor receptor family (EGFR or ERBB) are typical receptor tyrosine kinases with an EGF binding extracellular domain. EGFR has a ubiquitous expression in nearly 90% of tumors. Most importantly, EGFR staining holds valuable diagnostic value in discriminating ACC from ACA (98). Although EGF displays low tumoral expression, EGFR signaling is ensured by other growth factors such as TGF $\alpha$ , which is highly expressed in ACC (99). EGFR signaling favors tumor growth through secretion of angiogenic growth factors, which suggests that reversing EGFR cascades is relevant for therapy. In a small trial of ten ACC patients, EGFR inhibitor Erlotinib combined to the cytotoxic agent Gemcitabine did not show convincing activity; this regimen even provoked cerebral seizure and disease progression (100).

Drug	Clinical trials ID	Study design	Phase	Molecular target	Patients enrolled	ACC stage	Endpoint
Cabazitaxel	NCT03257891	Single arm, Open-label	II	Chemotherapy	25	Advanced, progressing after previous chemotherapies	Clinical benefit after 4 months
Cabozantinib	NCT03612232	Single arm, Open-label	II	TK c-MET	37	Advanced unresectable	PFS at 4 months
Relacorilant Pembrolizumab	NCT04373265	Single arm, Open-label	I	Glucocorticoid receptor	20	Advanced with glucocorticoid excess	ORR, DLT
Cisplatin /Sodium thiosulfate	NCT03127774	Single arm, Open-label	II	Surgery and Heated Intraperitoneal Chemotherapy	30	Unresectable, metastatic	PFS
ADIUVO-2 Trial: Cisplatin + Etoposide +/- Mitotane	NCT03583710	Open-label, Randomized	III	Chemotherapy	240	I- II- III with high recurrence risk	RFS
Nivolumab/ipilimumab	NCT02834013	Single arm, Non-randomized	II	Combination with immunotherapy	818	Locally advanced or metastatic ACC and rare cancers	ORR Up to 10 years
Therapeutic Vaccine (EO2401)	NCT04187404	Open-label	I-II	Immunotherapy using oncomimics for Tumor Associated Antigens and microbiome-derived peptides	60	Locally advanced / metastatic ACC (also including pheochromocytoma/ paraganglioma)	Safety
Ipilimumab Nivolumab	NCT03333616	Open-label	II	Anti-PD1 Immunotherapy	100	Advanced Rare Genitourinary Tumors	ORR

**Table 3: Current clinical trials for ACC.**

PFS: Progression free survival, RFS: Recurrence free survival, ORR: Overall response rate, DLT: Dose-limiting Toxicity. Data are reported for Clinicaltrials.gov <adrenocortical carcinoma> and <adrenal cancer> and <recruiting> and <interventional>.

### Targeting VEGF:

Angiogenesis is mainly promoted via the vascular endothelial growth factor (VEGF) pathway and its receptors VEGFR1 (Flt1), VEGFR2 (Flk1/KDR), and VEGFR3 (Flt4). The anti-VEGFR monoclonal antibody bevacizumab is already in clinics for solid cancers (101). Moreover, multikinase inhibitors namely sorafenib and sunitinib have also been deployed. Anti-angiogenic agents were also tested in ACC considering the increased VEGF/VEGFR expression (102). In their prospective phase II trial, Berruti et al. assessed sorafenib as a second line treatment after mitotane combinatorial chemotherapy. Serious adverse events including tumor progression have been observed and led to the interruption of the trial (103). Since these strategies are proposed as salvage therapy, therapeutic failure was explained by an anti-correlation between mitotane and plasmatic drug concentrations. One probable reason is an enhanced drug metabolism due to CYP3A4 induction by mitotane (82).

### Targeting IGFR and mTOR

Insulin growth factor type 1 and 2 are mitogenic polypeptides with structural similarities to human insulin. IGF1 and IGF2 exert their effects through binding to their receptors IGF-1R or insulin receptor (IR), therefore triggering downstream signaling via mitogen-activated protein kinase (MAPK) and phosphoinositol-3-kinase (PI3K-AKT). The overall impact of such cascade is increased proliferation and survival. It is well established that IGF pathway plays pivotal role in ACC pathogenesis. Also, IGF2 and IGF-1R are significantly overexpressed in ACC, which renders their targeting appealing for novel therapies (104). Phase III trials involving the IGF-1R/IR inhibitor linsitinib, in mitotane-treated patients, mimicked placebo in terms of OS and PFS. Authors assured that mitotane did not affect linsitinib pharmacokinetics in this study, though particular attention should be paid to patients' genetic profiles (105). A recombinant monoclonal antibody, cixutumumab targeting IGF-R1, in combination with mitotane, was assessed as first-line therapy for unresectable ACC. Disease stability was achieved in 7 out of 20 patients with a limited efficacy of 6 weeks PFS only, thus prompting study abortion (106). As mTOR is a downstream effector of IGF signaling, rapamycin analogs i.e. everolimus were also evaluated as monotherapy for ACC. Patient outcomes were not clinically convincing, maybe because of mitotane cross-signaling interactions (107). Moreover, De Martino et al.

evidenced that adding mTOR inhibitors may potentiate linsitinib's antiproliferative effects in vitro (108).

### Targeting Wnt/ $\beta$ -catenin

Wnt/ $\beta$ -catenin is a central pathway in cancer as it governs cell fate, proliferation and migration. Multiple tumor analyses pinpointed frequent mutations in the  $\beta$ -catenin-encoding gene CTNNB1, resulting in aberrant pro-cancer signaling. Over the last years, efforts were shifted towards developing Wnt/ $\beta$ -catenin pathway-inactivating compounds, mainly for colon cancer. A relevant strategy is to prevent Wnt secretion using small molecular inhibitors of porcupine PORC, a membrane protein required for production of Wnt ligands (109). Though limited responses were obtained in the Wnt974 phase I trial, this anti-PORC compound may boost immune recruitment to the tumor niche and is currently tested in combination with anti-PD1 treatments in solid tumors (110). ETC159 is another PORC inhibitor which entered phase II clinical trials based on its encouraging preclinical behavior (82). Other approaches involve blocking the canonical Wnt signaling via Wnt competitors, or targeting the Frizzled (Fzd) receptors using chimeric anti-Frizzled antibodies (111). Fzd monoclonal antibodies ipafricep and vanticumab displayed effective anti-tumor capacities in addition to outstanding synergistic effects with taxanes. Moreover, Fischer et al. showed that taxane-resistant cancer cells were sensitized to paclitaxel upon administration of ipafricep/vanticumab (112). Agents that repress downstream effectors include  $\beta$ -catenin degrading-drugs i.e. CWP232291, which proceeded to phase I trials for leukemia. As most of these advancements were observed in solid cancers, the Wnt/ $\beta$ -catenin pathway is still open for investigation in ACC therapeutics.

### Targeting SF-1

Further molecules like SF-1 are worth exploring for novel ACC therapies. The transcription factor SF-1 is ubiquitously expressed in adrenocortical cells and is implicated in adrenal development, steroidogenesis and proliferation (113). Beyond adrenal function, SF-1 was identified as a functional repressor of Wnt/ $\beta$ -catenin signaling as demonstrated in ACC cell lines harboring SF-1 knockdown (114). SF-1 targeting molecules have not yet reached the clinics.

### I.D. 6.d. Immunotherapy

In the last decade, immuno-oncology has revolutionized the dogma of cancer therapy through boosting host's immune system in order to destroy cancerous cells. Immune checkpoints are critical for self-tolerance, hence tumor escape (115). Checkpoint inhibitors are broadly assayed in malignancies like melanoma, renal cell carcinoma, non-small-cell lung cancers, and others. Recently, two clinical trials using the PD-1 inhibitor pembrolizumab have been reported as monotherapy for ACC. Though enrolled patients did not show PD-L1 staining or severe safety concerns, modest outcomes (27 weeks vs. 2.1 months) were scored when considering PFS (116, 117). On the other side, avelumab was tested in advanced ACC as anti-PD-L1 immunotherapy (ClinicalTrials.gov Identifier: NCT01772004); 42% of patients were responsive with a scarce PFS of 2.6 months (118). In fact, resistance to immunotherapy is not surprising since only 11% of ACCs express PD-L1, not to forget the low T cell infiltration in the tumor microenvironment (TME). Most importantly, hypersecretion of adrenal glucocorticoids in a subset of ACC generate an immunosuppressive TME, thus treatment with glucocorticoid inhibitors might enhance immunotherapy (119). Other mechanisms of immunoevasion in ACC are conferred by Wnt/ $\beta$  catenin pathway alterations, which modulate the CD8+ population in the TME. TP53 inactivation can also impair the cytokine cascades required for effector cells invasion (120). Other strategies combining checkpoint inhibitors and molecular targeted therapies seem promising. Given the so far limited effectiveness of immunotherapy, it seems essential to screen patients who could potentially benefit from this treatment by looking at their TME immune content.

### I.D. 7. Patient follow-up

After first-line therapy, ACC patients should undergo medical surveillance every 3 months for two years, then every 6 months for the rest of their lives. Routine checkups include tumor markers, steroid hormone dosages and of course clinical examinations via CT scanning. Such follow-up regimen aims to detect local recurrence or distant metastases, as well as therapeutic biases.

## I.D. 8. Molecular landscape

Choosing the appropriate treatment regimen can rely on a multitude of molecular evidences relative to the tumor biology. Over the last decades, breakthroughs in the fields of molecular biology and next generation sequencing thanks to major technological developments have enhanced our knowledge of ACC pathogenesis. Although transcriptome profiling and mutational status of ACC have been studied since the early 2000s, the first pan-genomic characterization of ACC molecular landscape was only published in 2014 by Assié et al. (62)(Figure 7). This study revealed many molecular alterations that have been expanded by the TCGA consortium (121).

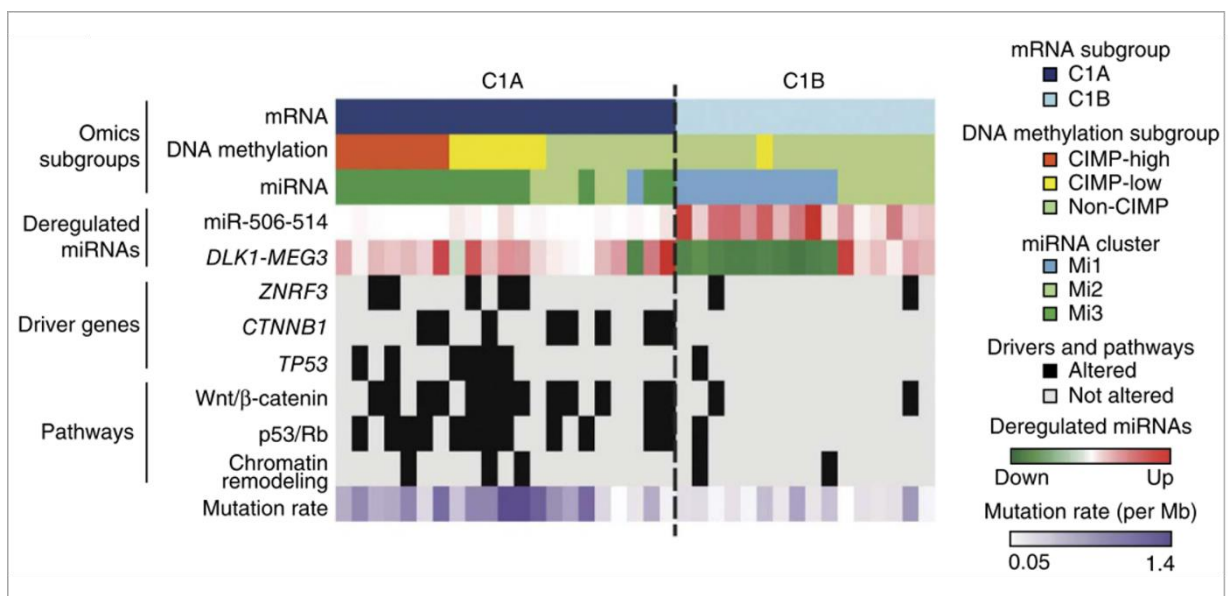


**Figure 7: Genomic landscapes in ACC.**

ACCs are clustered into two molecular subtypes C1A and C1B according to their mRNA expression, DNA methylation and miRNA expression. C1A comprises tumors with bad prognosis; C1B regroups good prognosis tumors. CpG island methylator phenotyping revealed CIMP-high and CIMP-low ACCs in the C1A group. Three miRNA clusters have been identified Mi1, Mi2 and Mi3, among which Mi3 tumors were the most aggressive. Taken from Assié et al. 2014.

### I.D. 8.a. Chromosomal alterations

ACC genomics were mainly investigated by Assié et al (62) and later on by Zheng et al. (121). These studies revealed copy number alterations within critical cancer loci i.e. oncogenes or tumor suppressor genes. Chromosomal amplifications were reported in multiple genomic regions harboring the cyclin-dependent kinase 4 (CDK4 12q14) and telomerase reverse transcriptase (TERT 5p15.33) genes, whereas deletions were frequently encountered within

the zinc and ring finger 3 (ZNF3 22q12.1), cyclin-dependent kinase inhibitor 2A (CDKN2A 9p21.3) and RB transcriptional corepressor 1 (RB1 13q14) genes. Loss of heterozygosity (LOH) is recurrent in nearly 30% of ACCs with a common LOH (in 80% of ACCs) of the 11p15 imprinted locus containing IGF2, therefore leading to upregulation of IGF2 expression and overactivation of the IGF2/IGF1R axis. Widely associated to tumor aggressiveness, whole genome doubling (WGD) occurs after LOH and is considered as a hallmark of disease progression.

#### I.D. 8.b. DNA methylation

Methylation is the main arm of epigenetics, in which a methyl group is added to a DNA nucleotide mainly cytosine or adenine within the CpG sequences. It is well known that DNA methylation profile governs gene expression, and that methylation is a mechanism for gene silencing (122). ACCs are globally hypomethylated in intergenic regions as compared to ACAs (123). However genome-wide methylation analysis showed hypermethylated CpG islands correlated to downregulation of tumor suppressor genes. In their assessment of the methylome of 15 ACCs, Fonseca et al. found hypermethylations in genes involved in apoptosis and cell cycle arrest like CDKN2A, GATA4, and HDAC10. Clustering DNA methylation patterns identified high CpG island methylator phenotype (CIMP-high ACCs) and CIMP-low ACCs (124). Most importantly, whole exome sequencing by Assié et al. revealed a subgroup of patients namely C1A with CIMP-high tumors and poor prognosis (62).

#### I.D. 8.c. Driver gene mutations

Transcriptomic analyses established a robust molecular signature for ACC diagnosis. Several genes are differentially expressed in ACC versus ACA and are clustered into functional pathways. Overall, ACC features downregulated steroidogenesis-related genes like the ACTH receptor MC2R, in addition to a steroidogenesis cluster of 14 genes i.e. STAR, CYP11A2, CYP11A1... (125)(126). MC2R LOH was also reported in ACC but not in cortisol-secreting ACA. Conversely, cell cycle regulators such as cyclins, G1-S and G2-M transition factors are drastically upregulated in ACC, contributing to its aggressiveness. These upregulations were strictly found in the poor prognosis group C1A (5-years survival of 20%) and not in the good prognosis group C1B (5-years survival of 91%) (62).



IGF2 is the most overexpressed gene in 90% of ACC, and its expression level is indicative of malignancy. Upregulated IGF2 sustains tumor proliferation in a paracrine manner through binding to its receptor IGF1R.

In terms of activated pathways, Wnt/ $\beta$ -catenin is on top of the list (activated in 39% of ACC) as determined by comprehensive integrated genomic analysis and whole exome sequencing led by Assié et al. However, these activations are not restricted to ACC and can occur in ACA. Briefly, canonic signaling is initiated when Wnt binds to its receptor Frizzled, mediating dissociation of the  $\beta$ -catenin destruction complex (axin-APC-GSK3 $\beta$ ), thus nuclear translocation of  $\beta$ -catenin. Interaction of  $\beta$ -catenin with the TCF/LEF (T cell factor/lymphoid enhancer factor) family of transcription factors triggers expression of  $\beta$ -catenin target genes.  $\beta$ -catenin (CTNNB1) gain of function mutations are mutually exclusive with the frequently altered tumor suppressive gene ZNRF3 (Zinc and Ring Finger 3), an E3 ubiquitin-protein ligase known to arrest Wnt signaling by promoting the turnover of Wnt receptors. Other driver genes of ACC tumorigenesis have been reported in the largest genome sequencing study of 91 ACC samples by The Cancer Genome Atlas consortium (TCGA) (121). Additional mutations inactivating the TP53 gene as well as chromatin remodeling genes like MEN1 (multiple endocrine neoplasia type 1), DAXX (death-associated protein) were reported. Nonetheless, the combined expression of two cell cycle regulating genes DLG7 (discs large homolog 7) or BUB1B (budding uninhibited by benzimidazoles 1 homolog beta) with PINK1 (PTEN induced putative kinase 1) -implicated in mitochondrial homeostasis- is highly predictive of disease-free survival or overall survival, respectively (127).

#### I.D. 8.d. MicroRNA deregulations

Extensive alterations in microRNA expression profile has been reported in ACC. The ACC miRnome is described in details in section II.C. 7.

## **Chapter II. Post-transcriptional regulation of gene expression by microRNAs, a new level of genome complexity**

The complexity of the human genome relies on an orchestrated molecular framework for gene expression regulation. Besides epigenetics, gene expression is finely controlled during transcription, mRNA maturation as well as mRNA turnover and translation. Messenger RNAs are subjected to post-transcriptional regulation by RNA-binding proteins (128) and non-coding RNA (ncRNA) (129). In this thesis, we propose to develop a novel therapeutic strategy targeting a specific ncRNA subtype, namely microRNA. The aim of this chapter is to describe microRNAs in terms of biogenesis and biological activity. We expose the current approaches for target gene identification and explore their potencies in cancer therapy, with emphasis on ACC.

## II.A. Non-coding RNA

Deciphering the components of the human genome was the central dogma of molecular biology. With 100,000 protein-coding genes predicted at the start of the Human Genome Project in the late 1990s, this prediction has steadily declined throughout the years, until completion of the human genome sequencing project in 2004. The number of genes encoding for proteins was reduced to 20–25,000 (130). A recent update of these data is described in the GENCODE dataset (version 38) which provides sequencing-based mapping of the human genome (131)(Figure 8A). According to this project, the number of genes encoding for protein was 19,982, accounting for only 33% of the human genome. Most importantly, the GENCODE

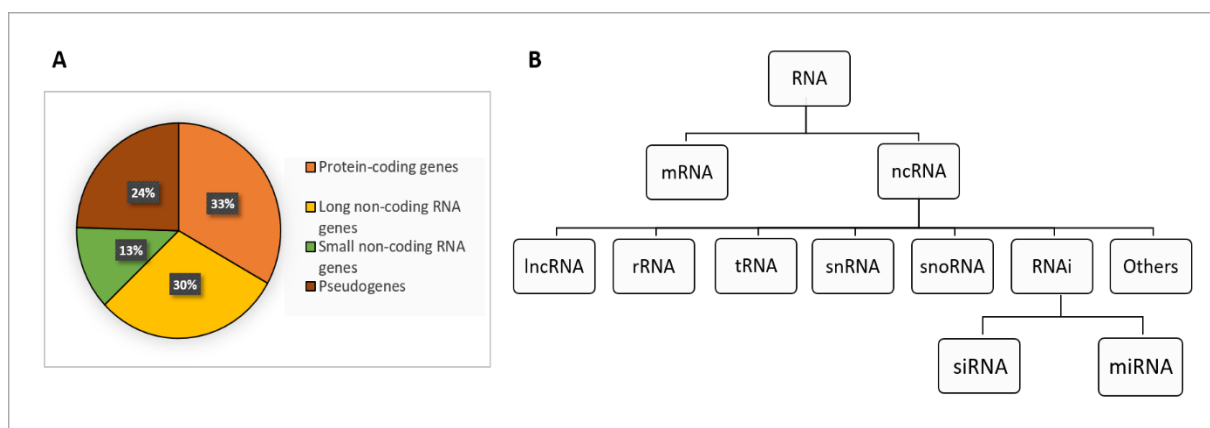


**Figure 8: Different types of RNA.**

(A) Percentage of non-coding RNA genes in the whole genome according to the GENCODE database. (B) Different types of RNA consist of protein-coding (mRNA) and non-coding RNAs. Non-coding RNAs include small and long RNAs.

dataset provided a detailed landscape of the non-coding transcriptome and allowed better annotation of non-coding RNAs in public databases such as miRbase and NONCODE. Many ncRNA can regulate physiological, developmental or even pathological events. In plants, they are well characterized as stress response regulators (132). As shown in Figure 8B, ncRNA include ribosomal RNA (rRNA), transfer RNA (tRNA), long non-coding RNA (lncRNA) as well as small nuclear RNA (snRNA), small nucleolar RNA (snoRNA), microRNA (miRNA), small interfering RNA (siRNA) and piwi-interacting RNA (piRNA). RNA species are identified according to their size, their cellular localization as well as the genomic region they derive from (Table 4). In terms of function, some ncRNA are regulatory molecules modulating gene expression at epigenetic, transcriptional or post-transcriptional levels, while others are simply ‘housekeeping’ elements that are ubiquitously expressed in cells and exert basic structural and catalytic roles.

Type	ncRNA	Full name	Genomic transcription origin	Size (nucleotide)	Cellular location	Function
<b>Regulatory ncRNA</b>	miRNA	microRNA	Introns / intergenic regions	21 - 23	Nucleus and cytoplasm	Act within the RNAi pathway Translational repression or mRNA degradation
	siRNA	Small interfering RNA	- Exogenous dsRNA (exo-siRNA) -Endogenous genomic locus mainly transposons elements (endo-sRNA)	20 - 25	Cytoplasm	Act within the RNAi pathway mRNA cleavage
	piRNA	Piwi-interactingRNA	Intergenic regions	26 - 32	Nucleus and cytoplasm	Repress transposon activity Genome stability
	eRNA	Enhancer RNA	Enhancers	50 - 2000	Nucleus	Stimulate transcription by modeling DNA looping between promoter and enhancer Histone modifications Chromatin remodeling

	circRNA	Circular RNA	Exons	100 - 10 000	Cytoplasm	Bind to sponges, Interaction with RNA-binding proteins
	lncRNA	Long non-coding RNA	Exons	> 200	Nucleus, cytoplasm and mitochondria	Unclear, gene regulation, developmental processes
<b>Housekeeping ncRNA</b>	rRNA	Ribosomal RNA	Specific genes	120 - 4500	Ribosome	Major components of ribosomes, role in binding to mRNA and recruitment of tRNA
	tRNA	Transfer RNA	Specific genes	76 - 90	Cytoplasm	Translation, transfers amino acids to the ribosome according to the mRNA code
	snRNA	Small nucleolar RNA	Introns	60 - 400	Nucleole	Chemical modifications of other RNAs
	snRNA	Small nuclear RNA	Specific genes	100 – 300	Nucleus	RNA splicing

**Table 4: Different types of non-coding RNAs according to their function.**

## II.B. RNA interference

The RNA interference (RNAi) pathway regulates gene expression in eukaryotic cells through two small ncRNA: siRNA and miRNA (Table 5). Since its discovery in *Caenorhabditis elegans* in 1998, RNAi has revolutionized the dogma of gene regulation in plants and higher species (133). In fact, these entities are capable of specific mRNA knockdown based on sequence complementarity following a Watson-Crick basis.

Properties	siRNA	miRNA
Size (nucleotides)	~21-24	~22
Processing enzymes	Dicer	Drosha and Dicer
Effector proteins	AGO	AGO
Mechanism of action	mRNA cleavage	mRNA degradation Translational repression

Function	Regulation of protein-coding genes and transposons Antiviral defense	Regulation of protein-coding genes
----------	---	------------------------------------

**Table 5: Two members of the RNAi family, siRNA and miRNA.**

siRNAs are a class of double stranded (ds)RNA widely used for gene silencing. Structurally, siRNAs account for 21-22 base pairs and two-nucleotide overhangs at the 3' end enabling RNAi pathway activation. Depending on their origin, siRNAs are exogenous nucleic acids (exo-siRNA) resulting from viral infections or endogenous molecules (endo-siRNAs) transcribed

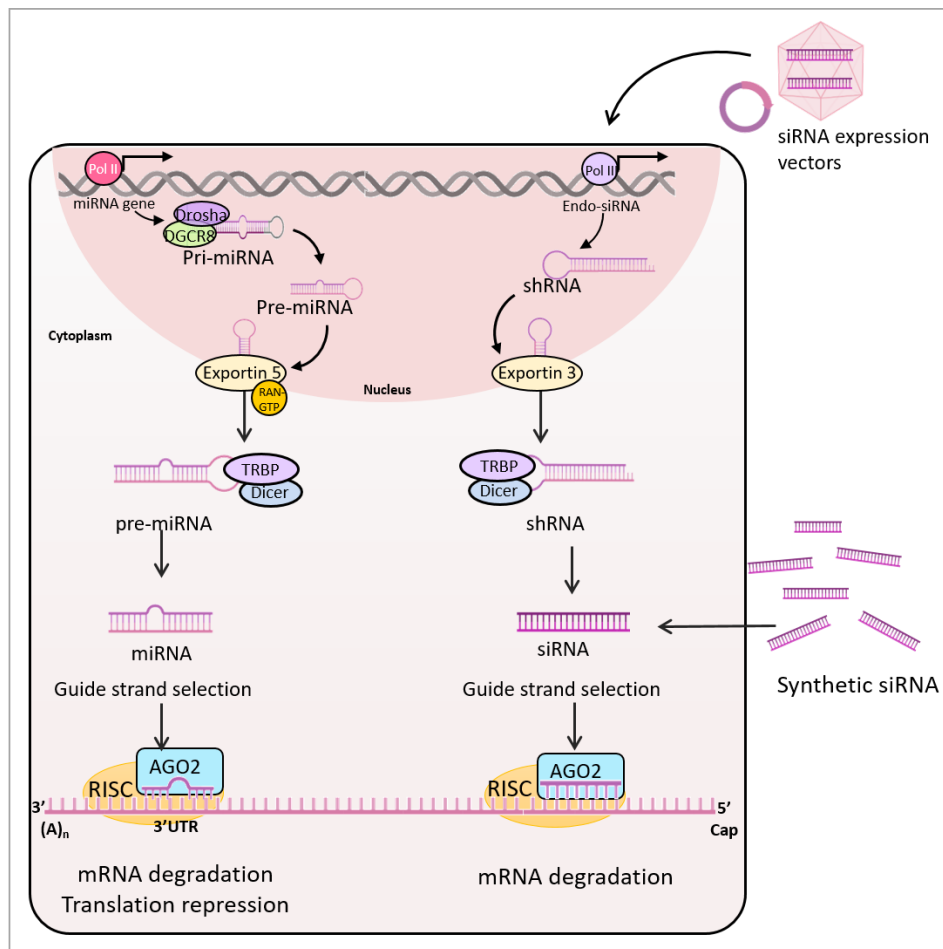


**Figure 9: The RNA interference pathways.**

The RNAi process is schematized into two steps, each involving a ribonuclease enzyme. The triggering RNA (either exogenous siRNA or miRNA), is first processed by the RNase II enzymes Drosha and/or Dicer into siRNA or miRNA. In the second stage, the siRNA or miRNA are loaded into the RNA-induced silencing complex effector complex (RISC). During RISC assembly, the siRNA or miRNA is unwound, and the single-stranded RNA hybridizes with the mRNA target. Perfect base-pairing between siRNA and mRNA favors endonucleolytic cleavage by the RNase H-related enzyme Argonaute 2 (Ago2 Slicer activity). mRNA fragments are further degraded by major cellular exonucleases. In the presence of mismatches in the miRNA/mRNA duplex, Ago2-miRNA binding to the mRNA leads to gene silencing through translation repression and mRNA degradation.

from repeated transposon elements (TE) (132). Conversely, miRNAs are transcribed in the nucleus from double stranded precursors. They are further processed and exported into the cytoplasm, where they can exert their effects.

RNAi machinery is triggered by the ribonuclease Dicer, which recognizes and cleaves dsRNA precursors into 21-24 nucleotide-sized double-stranded fragments (134) (Figure 9).

After removal of the passenger strand, the guide strand binds to Argonaute 2 (Ago2) which along with other proteins forms the RNA-induced silencing complex (RISC). Guide strand selection is facilitated by structural asymmetry within the siRNA nucleotides, such as the siRNA strand whose 5'-end is more weakly paired to its complementary sequence is more prone to enter RISC (135). The whole siRNA sequence guides RISC to recognize and cleave their target mRNA thus specifically inhibiting its expression (136), whereas the seed region of miRNAs pairs with mRNA most likely at its 3' untranslated region (3'UTR). The degree of homology dictates transcript fate: perfect base pairing most likely induces mRNA degradation, whereas imperfect matching preferentially mediates translation arrest (137). The potencies of RNAi therapeutics are extensively investigated as highlighted by 70 studies registered in Clinicaltrials.gov under the terms siRNA or small interfering RNA. Recently, the FDA approval of patisiran for treatment of liver disease marked a new milestone in the field of siRNA-based drugs (138).

## II.C. MicroRNA

As key players of the RNAi pathway, microRNAs (miRNAs or miRs) are small non-coding RNAs that regulate gene expression through imperfect base pairing with the 3' untranslated region (3'UTR) of target mRNA (139). Lin-4 was the first miRNA discovered in 1993 in nematodes *Caenorhabditis elegans* and associated to severe structural and developmental defects (140). In fact, Lin-4 repressed translation of the protein Lin-14 through complementary base pairing to its mRNA. Then have emerged numerous miRNA families, found to be conserved between species, further highlighting their significance in gene regulation (141).

### II.C. 1. Nomenclature

To date, about 1917 human precursors and 2654 mature miRNAs have been described in miRBase (<http://www.mirbase.org/>). Since its first publishing in 2002, the miRbase registry

has grown exponentially to group thousands of experimentally validated miRNAs, with unique information on their location and sequence. As these data are retrieved by the miRNA name, rigorous naming guidelines are required for easier access to available and new entries (142). Firstly, stringent criteria must be met in order to classify a RNA sequence as miRNA: A size of 21-22 nucleotides, presence of a hairpin precursor, phylogenetic conservation... In terms of nomenclature, precursor miRNA is designated “pre-miR” while the “miR” naming refers to the mature miRNA. Moreover, the specie in which the miRNA is found is denoted as a three letters prefix before the miR name i.e. “hsa” for Homo sapiens, “mus” for mus musculus, “ggo” for gorilla... After the word “miR” are provided numbers and letters to distinguish miRs, as well as members of the same family. When two identical miRNAs are obtained from two different loci, an additional number is given; for example, hsa-miR-24-1 and hsa-miR-24-2 refer to the same mature miRNA: hsa-miR-24. For evolutionary related miRNAs differing only by few nucleotides at their 3’ end, a letter is added to the gene number, for example hsa-miR-451a and hsa-miR-451b. It is also common to indicate the RNA strand from which the mature miRNA originates. For example, hsa-miR-139-5p is derived from the 5’ -arm of the pre-miRNA while hsa-miR-139-3p is obtained from the 3’-arm of the precursor. The first detected miRNAs (lin-4 and let-7) escaped these rules. Though some nomenclature rules may demand revision for further standardization, it is essential to follow these naming guidelines especially for the entry of newly discovered miRNAs.

## **II.C. 2. Genomic origins**

There are different patterns for genomic organization of miRNA (Figure 10A): 28% of canonical miRNAs are intergenic, thus located between two genes as independent transcriptional units. However, the majority of human miRNAs are intragenic with 85% of them embedded within the introns of host genes. miRNAs can also emerge from exons or exon-intron junctions (site-overlapping SO-miRs) of both protein-coding and non-coding genes (143). In general, intragenic miRNAs are co-transcribed with their host gene, thus releasing hairpin precursors upon splicing. The amount of synthesized miRNAs is often correlated with the expression magnitude of its harboring gene. Moreover, the miRNA concentrations in a cell can rapidly change in response to extracellular stimuli (144). miRNAs and their host genes can be functionally related through conferring self-regulation capacities (145). Some of these



miRNAs can exert direct negative feedback on the mRNA of their hosts. Others are capable of regulating downstream effectors or diverse genes belonging to the same pathway as their host (Figure 10B).

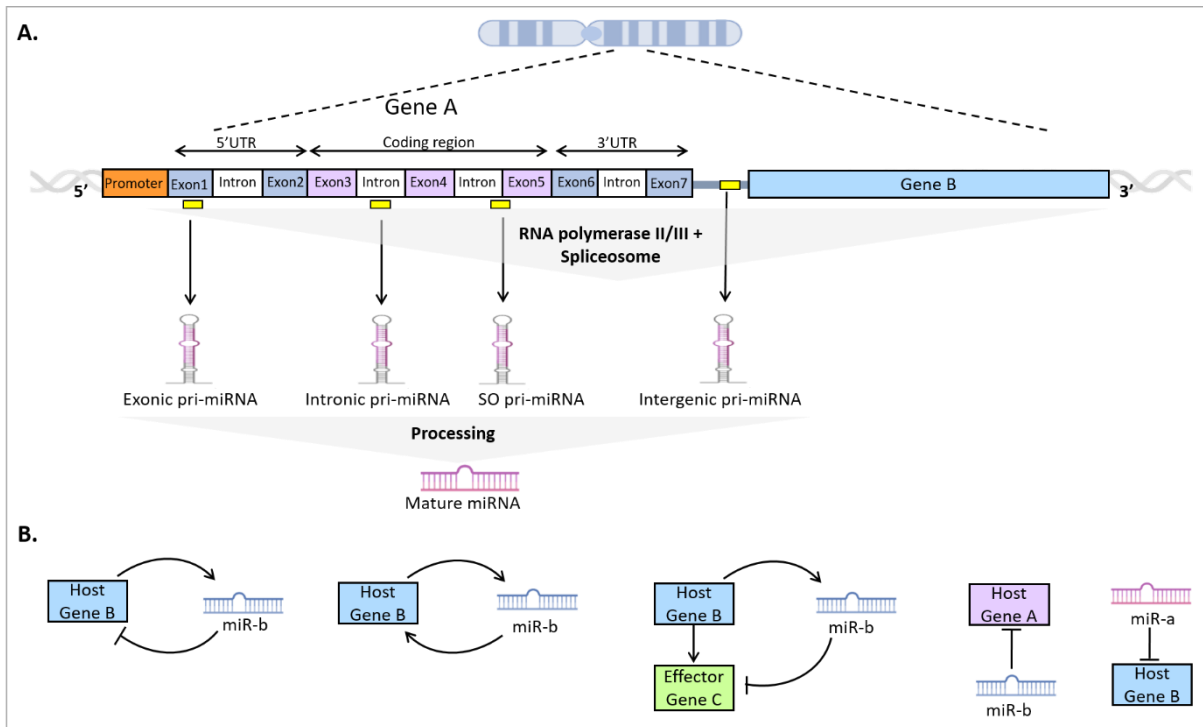


**Figure 10: The miRNA-host gene relationship**

(A) The vast majority of miRNA genes are intragenic, thus embedded within exons, introns or at splice site overlaps of their host genes. miRNA host genes can be protein-coding or lncRNA genes. A small fraction of miRNAs may also emerge from distinct genomic sites within intergenic regions. miRNAs are transcribed first into pri-miRNA then undergo sequential maturation through several steps. (B) Some genes are directly auto-regulated by the miRNAs they harbor in negative or positive feedback loops. Other miRNAs can regulate the expression of their hosts' downstream effectors. A pair of genes can also regulate each other through their intragenic miRNAs.

### II.C. 3. Canonical biosynthesis

The biogenesis of mature miRNAs involves several cleaving and processing of the primary miRNA (pri-miRNA) into small 21-25 nucleotide sized miRNAs (Figure 9). No matter their loci, miRNA genes are transcribed by RNA polymerase II or III into long primary transcripts, pri-miRNA, which present an m7G (7-methylguanosine triphosphate) cap in its 5'-end and a polyadenylated tail at the 3'-end. In the nucleus, the Double-Stranded RNA-Specific Endoribonuclease DROSHA (RNase III) and its cofactor DiGeorge syndrome Critical Region 8 (DGCR8) crop the pri-miRNA stem loop into 65 nucleotide-hairpin pre-miRNA. Pre-miRNAs are then exported into the cytoplasm by an Exportin-5 RanGTP complex to undergo further

processing. The RNase III dicer, in association with TRBP (HIV-1 transactivating response (TAR) RNA-binding protein) cleaves the pre-miRNA into small (~20 nucleotides) imperfect-pairing dsRNA consisting of complementary mature miRNA strands. This miRNA duplex is then loaded into an AGO effector protein, which recruits other proteins to form the RNA-Induced Silencing Complex (RISC). Formation of AGO2-miRNA complex depends on the respective recognition of the miRNA 3'- and 5'-ends by PAZ and MID domains of the AGO2 protein. Herein, the guide strand is selected by AGO2 in order to regulate gene expression (146). Globally, a perfect miRNA-mRNA complementarity allows mRNA transcript degradation, whereas imperfect pairing leads to translation blockade (147). Perfect complementarity covers a small part of the miRNA sequence at its 5'-domain which is the "seed" sequence that spans between nucleotide positions 2 and 8 of the miRNA. Of note, the redundant action of miRNAs relies on this imperfect miRNA-mRNA binding. In other terms, a single miRNA can target hundreds of transcripts (139). Besides canonical biogenesis, small RNA sequencing from cells depleted in Drosha, DGCR8 or Dicer, revealed an unconventional miRNA production independently of the microprocessor complex or Dicer. In this case, nuclear processing by Drosha is skipped and miRNA precursors may be obtained through refolding after splicing of the host mRNA (147). The assessment of pre-miR-451a by Yang et al. revealed that Drosha-processed pre-miRNA is loaded and cleaved by AGO2 then packaged to form the RISC complex. This demonstrated that miR-451 is indeed trimmed by Drosha, but Dicer is not crucial for its maturation (148). It is noteworthy that the majority of miRNAs still follow the canonical biogenesis route; non-conventional miRNAs are also poorly conserved and non-abundant.

#### **II.C. 4. Interaction with mRNA**

The specificity of miRNA-mRNA interactions is governed by the configuration through which the miRNA seed sequence pairs with its target. There are several types of pairing between a miRNA and its target mRNA according to its nucleotide composition (Figure 11):

- The 7mer-A1 configuration features perfect complementarity of the seed sequence with mRNA, which presents a conserved adenine facing base 1 of the miRNA sequence. This 1A is recognized by RISC and may improve miRNA-mediated silencing.
- The 7mer-m8 site shows additional Watson-Crick pairing at position 8 beyond the seed sequence.

- The 8mer disposition is characterized by a fusion of the above configurations.
- The 6mer model exhibits perfect seed region pairing, with no other site recognition element, thus leading to lower specificity.
- The 3' supplementary and compensatory pairing types include additional pairing of the 3' region of the miRNA to enhance the interaction with the target or compensate for a mismatch in the 5' sequence, respectively (149).

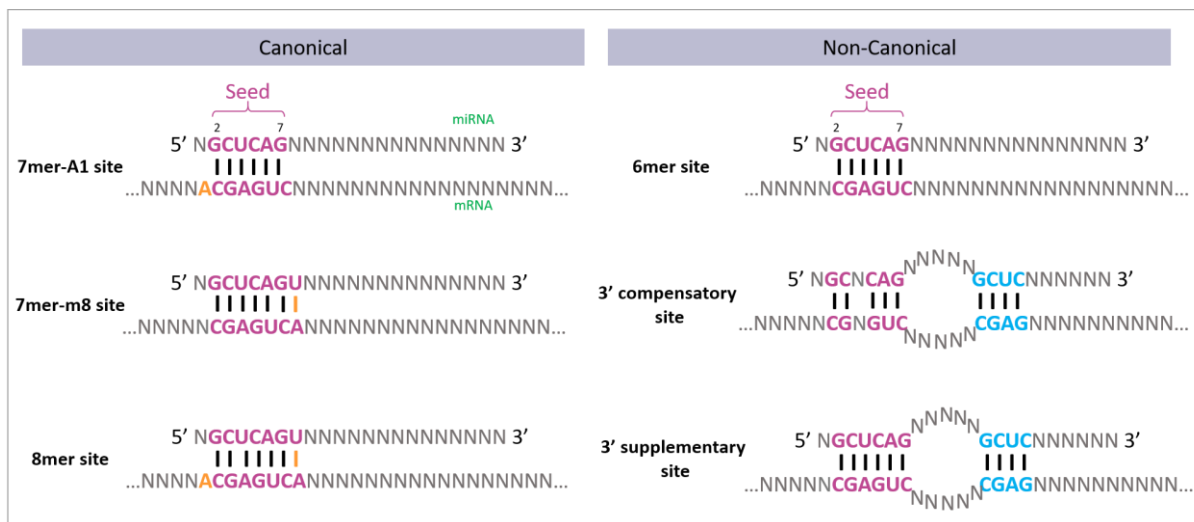


**Figure 11: Representation of interactions between the miRNA seed region and the 3'UTR of target mRNA.** miRNA seed region span from nucleotides 2 to 7 at the miRNA 5'-end. Canonical matching involves perfect pairing in the seed region. 7mer-A1 features an exact matching to the seed with an 'A' facing the miRNA start at the 5'-end. 7mer-m8 involves additional base-pairing at position 8. This is the most abundant type of binding sites for conserved miRNAs. 8mer configuration combines presence of Adenine facing miRNA position1 and an additional Watson-crick matching at position 8. 6mer interaction is weak, slightly above noise and only holding perfect seed matching. 3'-compensatory sites involve an imperfect seed match compensated by additional 3' pairing which bulges the middle mismatches to form a loop. Additional base pairing at position 13-16 near the 3' end of miRNA may also be present. Seed sequence is in purple. Additional adenine at position 1 is in orange. Blue sequences represent matching at 3'end.

#### II.C. 4.a. Target gene identification

miRNA functionalities rely on the transcripts they regulate. For that, bioinformatic prediction of potential targets is crucial before further investigation. Besides seed match configuration, target prediction tools consider conservation, folding, site accessibility and thermodynamic energy (150). These softwares use algorithms to align the miRNA seed sequence with transcript sequences reported in databases, in order to provide lists of putative targets with corresponding prediction scores. Among these tools, we can cite TargetScan, miRanda, DIANA, miRwalk. However, these programs still suffer from a lack of sensitivity and accuracy with an

estimated 70% of computational false positives (151). Many experimentally validated miRNA-mRNA interactions do not follow in silico rules, since para-3'UTR regulation, as well as imperfect seed match between miRNA and its target mRNA should not be neglected.

#### II.C. 4.b. CLIP

More complex methods like UV cross-linking and immunoprecipitation (CLIP) are employed to map miRNA-mRNA footprints. Briefly, upon exposure to UV radiations, covalent bonds are created between mRNA and proximal proteins of the RISC complex i.e. AGO2. The RNA-binding protein of interest is purified by immunoprecipitation as part of protein-RNA complexes. Further proteinase K digestion allows discarding proteins from the complexes in order to specifically analyze their bound RNA (152). Subsequent sequencing of the RNAs (miRNA and target mRNA) associated with the immunoprecipitated Argonaute proteins makes it possible to identify functional interactions between miRs and their target mRNAs. This method, combining CLIP with high throughput sequencing is termed HITS-CLIP. For instance, Ago HITS-CLIP confirmed a panel of previously validated targets of miR-124, thus demonstrating the approach sensitivity (153). Several variants have emerged to the CLIP protocol for better optimization. Photoactivatable ribonucleoside-enhanced CLIP (PAR-CLIP) relies on the incorporation of photoreactive ribonucleoside analogs such as 4-thiouridine (4-SU) and 6-thioguanosine (6-SG) into nascent RNA transcripts. This allowed mapping of direct crosslinking sites (154). Since CLIP-precipitated complexes show different RNA compartments more or less bound to the eluted protein, two-leveled sequencing is required for miRNAs and mRNAs, separately. Subsequent bioinformatic alignments is expected to pair each miRNA to its mRNA (155).

#### II.C. 4.c. CLASH

Inspired by the HITS-CLIP approach, the miRNA-mRNA interactome is also mapped by crosslinking, ligation and sequencing of hybrids (CLASH). Basically, CLASH introduces a ligation step after AGO immunoprecipitation. First, cells expressing tagged AGO proteins are UV irradiated to crosslink RNA binding proteins. AGO proteins are purified using tag-specific dynabeads or via conventional immunoprecipitation. Eluted RNA molecules are partially hydrolyzed, then those within the AGO-miRNA-mRNA duplexes are ligated together (156). In

other terms, miRNA and mRNA bound to the same AGO molecule are joined by their ends to form a single hybrid RNA molecule. After reverse transcription, cDNA is subjected to Illumina sequencing. miRNA-target pairs are reported as chimeric hybrids for deep sequencing or as single reads similarly to HITS-CLIP in case of ligation insufficiency. Compared to CLIP, the implementation of ligation steps in CLASH provides higher detection confidence since sequencing hybrids directly indicates the miRNAs bound to a specific mRNA fragment. There is no need for misleading bioinformatics interpretations to identify the miRNA binding sites on mRNA (155). For example, CLASH was validated upon retrieving the targets of miR-92a obtained via luciferase assays and other approaches. However, inefficient crosslinking, low RNA yields after sample processing and insufficient intermolecular ligation are common limitations for CLASH.

#### II.C. 4.d. Pulldown

Affinity purification is another experimental approach based on transfecting synthetic miRNA mimics typically biotinylated at the 3' end of their guide strand. The introduced biotinylated miRNA incorporates into cellular RISC to form miRNA-mRNA duplexes. After cell lysis, tagged miRNAs (and their direct targets) are eluted on streptavidin beads followed by RNA purification and sequencing (157). As many doubts were raised regarding masking AGO2 recognition sites by biotin, the miRNA-RISC loading was validated by AGO2 immunoprecipitation prior to affinity pulldown. Strategy credibility was also supported by luciferase reporter assays, which demonstrated that biotinylated miRNAs do not lose their gene silencing capacities. Moreover, comparing transcriptomic profiles upon miR-34a overexpression or miR-34a pulldown showed that the number of common mimics-downregulated transcripts and pulldown-enriched targets is only 22 targets (158). This poor overlapping is likely due either to miRNA altering protein synthesis rather than binding mRNA directly, or to different computational processing of sequencing data. Interestingly, this analysis provides insights on miRNA direct and indirect targets (159). For more specificity, it is also possible to strictly collect miRNA recognition elements (MRE) through a procedure named IMPACT-seq (identification of MREs by pull-down and alignment of captive transcripts sequencing). IMPACT-seq introduces an additional RNase treatment to the pulldown-isolated miRNA-RNA complexes. Thereafter, only MRE are retrieved for sequencing (160). These

experiments are simple to carry out from a small cellular input while avoiding crosslinking and target assumption biases. In addition, compared to CLIP, pulldown approaches allow assessment of a single miRNA's interactome regardless of the AGO proteins (159). It is well established that miRNAs can regulate numerous transcripts of a given pathway through modulating transcription factors expression. By combining promoter analysis and gene ontology tools, Tan et al. generated a robust pipeline for miR-522 functionalities in epithelial to mesenchymal transition (EMT).

### **II.C. 5. Gene silencing by microRNA**

It is now clear that miRNAs exert their silencing effects through mRNA destabilization or translation repression (161). However, the exact molecular mechanisms for this gene regulation are still partly elucidated. A miRNA-loaded Argonaute, in addition to its protein partner GW182, occupy the core of the RISC. By base pair complementarity, miRNA dictates the sequence of the transcript to be targeted by the miRISC (miRNA + RISC). However, it is the protein component of the miRISC that actually executes the mRNA silencing, mainly through protein-protein interactions (162). The structural architecture of RISC proteins is well adapted and features silencing and deadenylation- promoting domains. miRNAs can induce target decay through mRNA deadenylation and decapping. This is ensured by interaction of GW182 domains with the CCR4-NOT and PAN2-PAN3 deadenylase complexes. After discarding the poly(A) tail at the 3'-end of the mRNA, the 5'-terminal m7G is decapped by the DCP1-DCP2 complex. At translation level, miRISC disturbs recognition of the translation initiation factor eIF4 by the mRNA cap, thus disrupting ribosome recruitment to the translation site (Figure 12). Other studies proposed that GW182 could bind to PABP (Poly-A Binding Protein) thus affecting its translation initiation capacities and favoring miRNA-mediated deadenylation (163). miRISC can also prevent 80S ribosome complex formation and might interfere with ribosome elongation steps. Although both events yield similar repressive outcomes, it is worth mentioning that translation arrest and target decay are not necessarily sequential. Such was the case of lin-4, which inhibited lin-14 translation without destabilizing its RNA. Closer investigations are still required in order to understand whether these events are mechanistically coupled (162).

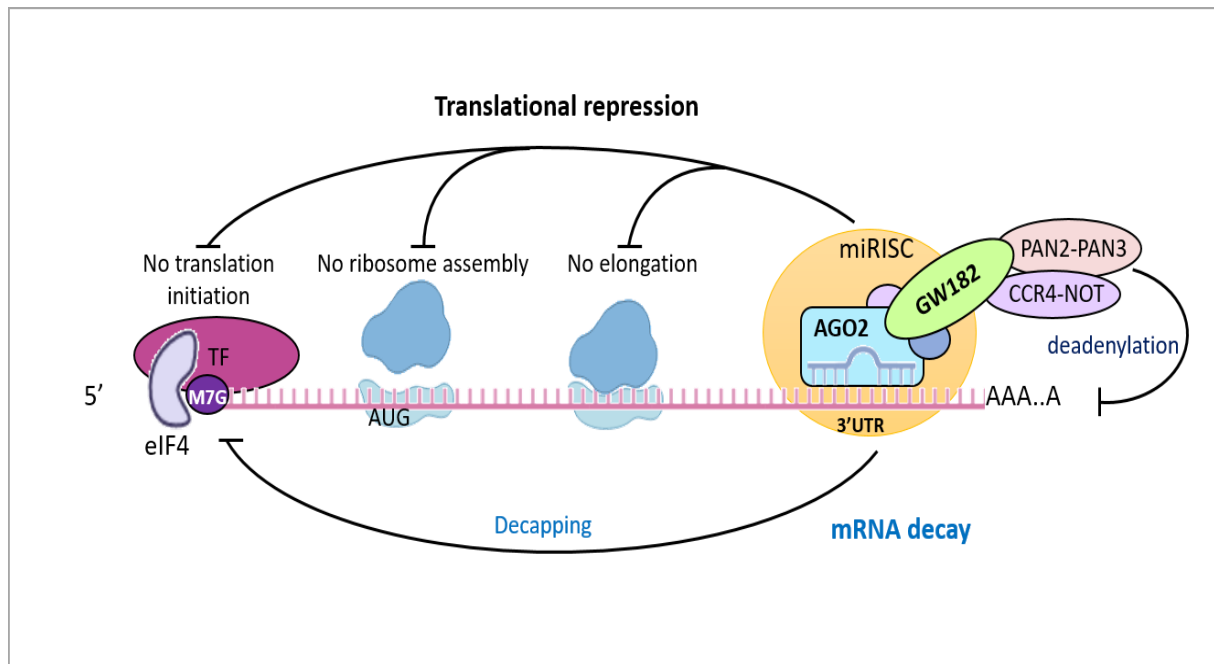


**Figure 12: Molecular mechanisms for miRNA-mediated gene silencing.**

miRNAs bound to the AGO2 protein within the mi-RISC complexes detect their mRNA targets by base-pairing to partly complementary binding sites, which are mostly found in the mRNA's 3'-untranslated region. AGO proteins interact with the GW182 protein, which associates with the cytoplasmic deadenylase complexes PAN2–PAN3 and CCR4–NOT, therefore catalyzing mRNA deadenylation. Deadenylated mRNAs are depleted of their M7G cap and quickly degraded by 5'-to-3' exoribonuclease 1. The exact molecular interplay for miRNA-mediated translation inhibition is still unclear. MiRNAs are thought to interfere at different stages of translation; they can impede translation initiation by interrupting the function and/or assembly of the eukaryotic initiation factor 4 (eIF4) complex. eIF4 acts as a scaffold for protein–protein interactions, which are required for the recruitment of the ribosomes and the initiation of translation. miRNAs can also disrupt assembly of ribosomal subunits or even block translation elongation.

## II.C. 6. MicroRNA in cancer pathogenesis

miRNAs, by virtue to their target variety and broad spectrum of activity, can efficiently regulate cancer hallmarks (Figure 13A). Their involvement in cancer was first demonstrated in 2002, when miR-15 and miR-16-1 were found downregulated in Chronic Lymphocytic Leukemia (164). Ever since, mapping miRNA profiles in cancer defined cancer-specific signatures, not only useful for diagnosis, but also for therapy and prognosis (165). Imbalanced miRNA expressions in normal versus tumor contexts are mainly explained by the localization of miRNA genes within fragile genomic regions. In general, miRNAs embedded in cancer-amplified loci i.e. miR-17-92 cluster, act as oncogenes (or oncomiRs) whereas miRNAs within cancer-deleted regions i.e. miR-15a-miR-16-1 cluster, function as tumor suppressors (166). Besides genetic alterations such as mutations, deletions and amplifications, epigenetic alterations as well as defects in the miRNA machinery strongly affect miRNA expression. For

instance, downregulation of several miRNAs was linked to a Drosha failure. This observation was consistent with frequent p53 mutations in cancer, since p53 may favor the Drosha-mediated processing of several growth suppressive miRNAs (167). Tumor hypoxia can also modulate miRNA profiles as shown by a decreased miR-34a upon Hypoxia-Inducible-Factor1 alpha (HIF-1 $\alpha$ ) stimulation (168). Globally, overexpressed miRNAs are oncomiRs that trigger pro-cancer signaling. Such was the case of miR-203, which in prostate cancer is associated with tumor proliferation and invasion (169). miRNAs that silence oncogenes are commonly downregulated in cancer (Figure 13B); miR-34a is the best described tumor suppressor miR (159).

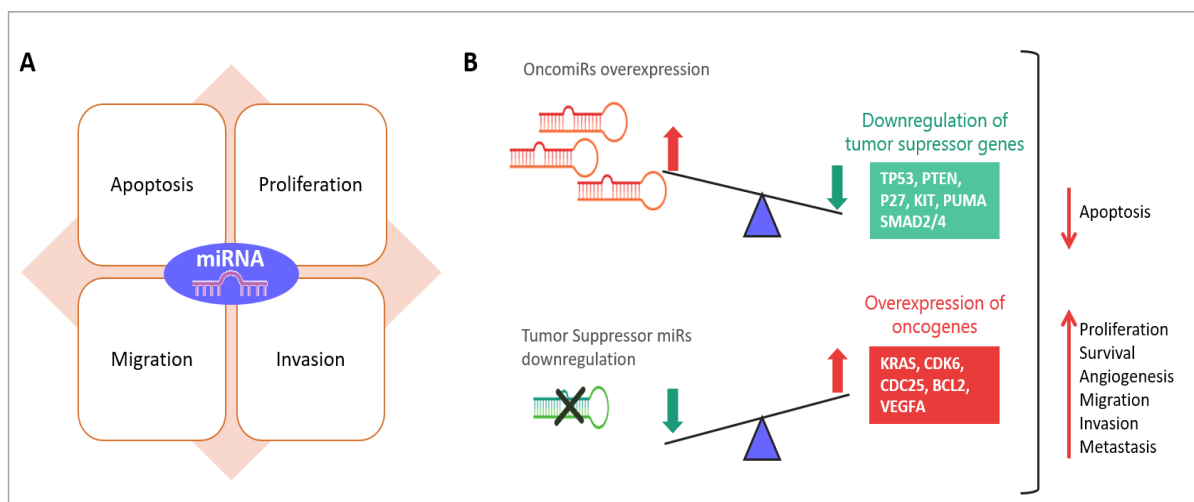


**Figure 13: miRNA deregulations in cancer.**

(A) miRNAs interfere with key cancer hallmarks to promote or not apoptosis, proliferation, migration and invasion, according to their deregulation pattern. (B) OncomiRs are miRNAs that repress tumor suppressor genes, whereas tumor suppressor miRs silence oncogenes. In cancer, oncomiRs are overexpressed so that their tumor suppressor targets are downregulated. Conversely, the cancer-driven repression of tumor suppressor miRs leads to an upregulation of their oncogene targets, hence cancer growth and aggressiveness.

## II.C. 7. MicroRNA expression in ACC

Despite the disease rarity, ACC miRnome was extensively analyzed in patient cohorts (Table 6). In their genomic analysis of 45 ACCs, Assié et al. identified three clusters of deregulated miRNAs as compared to normal tissue (Figure 14). Though the Mi1 subgroup exhibited great differences to normal tissue with an upregulation of 11 miRNAs of the miR-506-514 cluster and a downregulation of 38 miRNAs belonging to the DLK1-MEG3 cluster, this subgroup in addition to the Mi2 cluster were found in good prognosis tumors (C1B). Conversely, Mi3 tumors were included in the bad prognosis group (C1A) because of their consistency with driver genes' alterations (62).



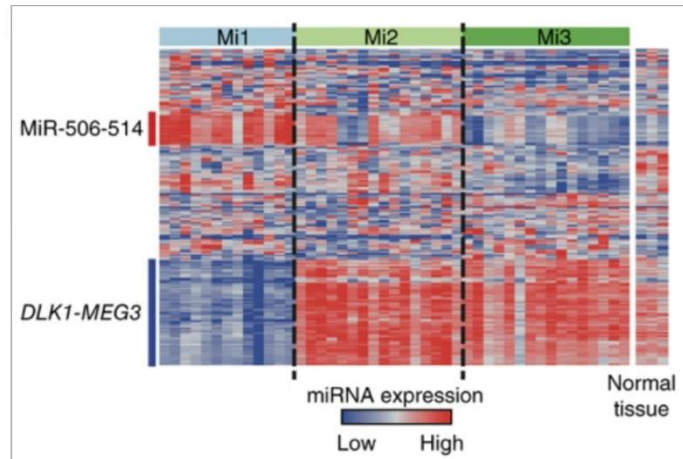


Figure 14: miRNA expression patterns in ACC, according to Assié et al.

Differential miRNA expression in ACC versus ACA or normal cortices was profiled in pioneer as well subsequent studies using quantitative PCR, microarrays, TaqMan Low-density Arrays (TLDA) and deep sequencing (Table 6). Common upregulated miRNAs comprise miR-483, miR-184, miR-503, miR-139 and miR-210. On the other hand, miR-195, miR-497, miR-335 were among the most investigated underexpressed miRNAs in ACC (49); (170) (171). Various studies associated such imbalance to overall and recurrence-free survival. Deregulated miRNA expression may be explained, at least in part, by disruptions in miRNA machinery. For example, overexpression of Tarbp2, Dicer1 and Drosha were reported in ACC but not in ACA. Of note, Dicer1 and Tarbp2 are validated targets of two miRNAs downregulated in ACC (miR-195 and miR-497), thus demonstrating the auto-regulation capacities of miRNAs (172).

Year of publication	Reference	Methodology	Tissue sample	Upregulated miRNA	Downregulated miRNA
2009	(173)	TLDA	7 ACC, 19 ACA, 10 NAC	miR-184 miR-210 miR-503	miR-214 miR-511 miR-375
2009	(174)	Microarray VC: RT-q-PCR	22 ACC, 27 ACA, 6 NAC VC (10 ACC, 9 ACA)	miR-483-5p miR-503	miR-7 miR-195 miR-335
2011	(175)	Microarray VC: RT-q-PCR	25 ACC, 43 ACA, 10 NAC	miR-483-3p miR-483-5p miR-210 miR-21	miR-195 miR-497
2011	(176)	Microarray VC: RT-q-PCR	10 ACC, 26 ACA VC (31 ACC, 35 ACA, 21 NAC)	miR-483-5p	miR-195 miR-125b miR-100

2011	(177)	TLDA VC: RT-q-PCR	7 ACC, 9 ACA, 4 NAC VC (16 ACC)	miR-139-5p	miR-139-3p miR-675 miR-335
2013	(178)	Microarray	12 ACC, 6 NAC VC (18 ACC, 10 ACA, 3 NAC)	miR-483-5p miR-503 miR-210 miR-542-5p miR-320a miR-93 miR-148b	miR-195 miR-335 miR-497 miR-199a-5p miR-199a-3p
2014	(179)	RT-q-PCR	51 ACC, 47 ACA	miR-483-3p miR-483-5p miR-210	miR-195
2014	(62)	RNA sequencing	45 ACC, 3 NAC	miR-34b-5p miR-410 miR-483-3p miR-483-5p miR-503 miR-506-3p miR-506-5p miR-508-3p miR-508-5p miR-510	miR-511 miR-214-3p miR-485-3p miR-497 miR-195
2015	(180)	Microarray VC: RT-q-PCR	8 ACC, 25 ACA VC (11 ACC, 4 ACA)	miR-503	miR-34a miR-497
2016	(121)	RNA sequencing	79 ACC, 120 NAC	miR-10-5p miR-483-5p miR-22-3p miR-508-3p miR-509-3p miR-509-5p miR-340 miR-146a miR-21-3p miR-21-5p	-
2017	(181)	RNA sequencing	7 ACC, 8 ACA, 8 NAC VC (8 ACC, 10 ACA, 10 NAC)	miR-503-5p miR-450a-5p miR-542-5p miR-483-3p miR-542-3p miR-450b-5p miR-210 miR-483-5p miR-421 miR-424-3p miR-424-5p miR-598 miR-148b-3p miR-184 miR-128	-

Table 6: Studies reporting miRNA deregulations in ACC tissues vs NAC and ACA.

NAC, normal adrenal cortex; ACC, adrenocortical carcinoma; ACA, adrenal adenoma; TLDA, TaqMan Low Density Array; VC, Validation Cohort; RT-qPCR, real time quantitative polymerase chain reaction. Adapted from Chehade et al.2020.

Importantly, it is possible to explore circulating miRNAs in patient sera. This provides insights on the potencies of miRNAs as non-invasive biomarkers of malignancy or recurrence. Supporting this feature is the outstanding miRNA stability in body fluids especially when released within tumor-derived microvesicles or when bound to protein complexes (171). Indeed, Chabre et al. demonstrated that circulating miR-483-5p is predictive of ACC aggressiveness (AUC 0.929) (178). At post-operative stages, Oreglia et al. recently reported that high levels of miR-483-5p in patient sera are associated to recurrence and bad prognosis (182). However, no miRNA biomarker has yet translated to clinics despite the body of knowledge supporting their diagnostic/prognostic value. This is mainly due to the lack of specificity of a single miRNA to distinguish between diverse cancers; notably miR-483-5p is explored as biomarker for hepatocellular and head and neck cancers in addition to ACC (183). Another argument concerns sample collection and standardization methods in terms of miRNA calibrations and measurements. Spiking-in an exogenous non-human RNA is an accepted solution to bypass normalization obstacles. Many studies suggested that combining several deregulated miRNA for diagnostic purposes greatly improves the diagnostic accuracy and specificity. Throughout this thesis, we focus on two oncomiRs in ACC, miR-483-5p and miR-139-5p.

### II.C. 7.a. miR-483-5p

miR-483-5p was found upregulated in eight of eleven cohorts, and is foremost associated with poor prognosis in ACC (Table 6). Besides ACC, miR-483 is overexpressed in Wilms' tumors and a handful of common cancers such as colorectal, liver and breast cancer (184). As shown in figure 15, the miR-483 gene, from which emerge the 5p and 3p strands, is embedded within the second intron of IGF2 gene at chromosome 11 (171).

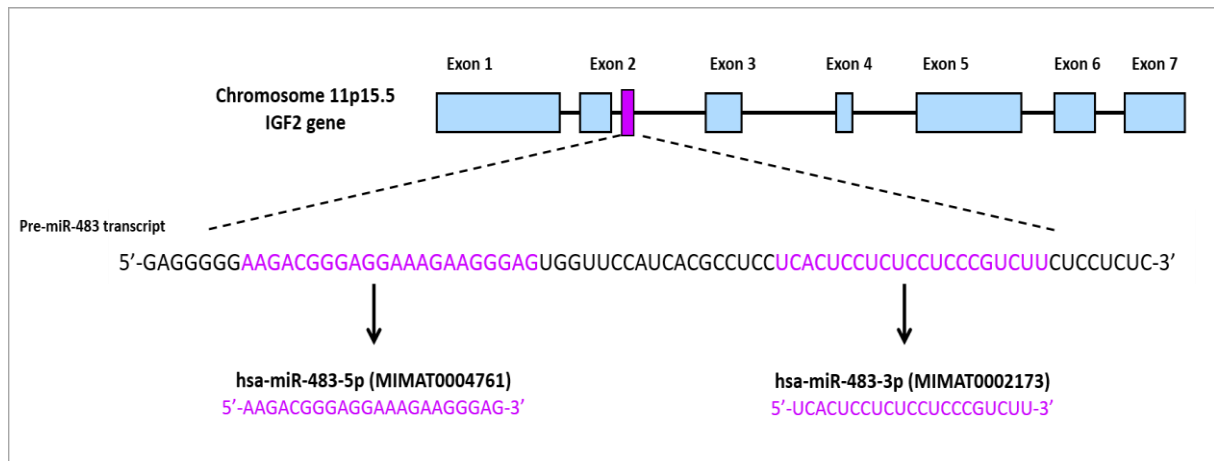


**Figure 15: miR-483 genomic localization and sequence.**

In ACC, one can rapidly correlate miR-483-5p upregulation to IGF2 overexpression. However, other host-independent mechanisms suggest that beta-catenin may transcriptionally induce miR-483 expression through interacting with the upstream transcription factor USF1 (184). Vice versa, miR-483-5p overexpression could trigger Wnt/ $\beta$ -catenin signaling as demonstrated in gastric cancer, thus promoting growth and survival of gastric cancer cell lines (185). Circulating miR-483-5p also serves as powerful biomarker for gastric cancer diagnosis (186). Concerning its oncogenic activity, miR-483-3p overexpression was linked to apoptosis arrest via the BBC3/PUMA axis in common cancers and neuroblastoma (187, 188). Along the same line, Ozata et al. observed reduced proliferation upon silencing miR-483-3p and miR-483-5p in the human ACC cell line NCI H295R. Apoptosis was only restored after inhibiting miR-483-3p and not its 5p counterpart, again highlighting the specific PUMA targeting by miR-483-3p. (175). Moreover, miR-483 was useful for treatment follow-up; tissue biopsy revealed that high miR-483-5p levels are indicative of chemoresistance in ovarian cancer (189). Of note, miR-483 is not strictly oncogenic, for example, miR-483-3p suppresses proliferation and progression of MDA-MB breast cancer cell lines by targeting HDAC8 (190). In ACC, tumor tissue and serum levels of miR-483-5p were found across many studies to be considerably upregulated as compared with ACA or healthy cortices (191). In addition, Agosta et al. recently showed that miR-483-5p enhanced ACC cell migration and invasion by silencing N-myc downstream-regulated gene 2 (NDRG2) (192), thus suggesting that miR-483-5p contributes to ACC aggressiveness. While waiting for other mechanisms to be discovered, the upregulation of miR-483-5p in ACC is suggested to be linked to the dramatic overexpression of its host gene

IGF2 in this cancer, hence of the miR-483 locus. These observations make miR-483-5p a kind of hallmark of ACC when considering other cancers.

### II.C. 7.b. miR-139-5p

MiR-139 plays crucial roles in tumorigenesis, yet it is less popular in ACC. It is 23 nucleotide-sized miRNA, nested within the intron 2 of PDE2A at chromosome 11q13.4 (Figure 16). Though amplification of PDE2A at 11q13 arises in several neoplasms including ACC, miR-139 is frequently described as tumor suppressor (49). Epigenetic silencing of miR-139 in pancreatic cancer cell lines is ensured by enhancer of zeste homolog 2 (EZH2), a histone methyltransferase that methylates H3K27 (193). Similarly, epigenetic repression of miR-139 occurs in leukemia. Restoring miR-139 expression delayed leukemia growth in miR-139 depleted mice (194).

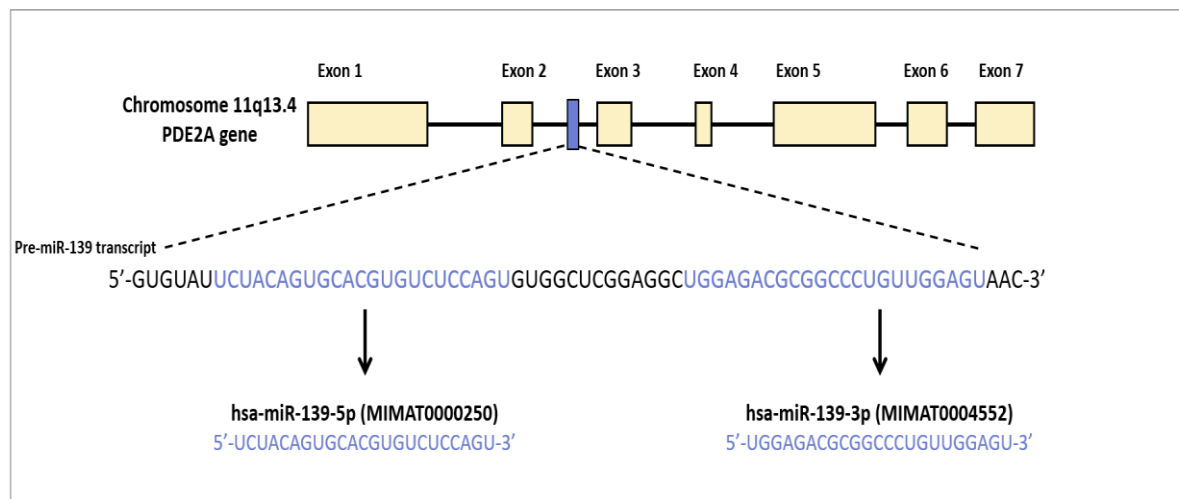


**Figure 16: miR-139 genomic localization and sequence.**

Sequencing of cells derived from these mice showed a panel of upregulated genes mainly involved in cell cycle arrest or apoptosis induction. Most importantly, using luciferase assays, this study validated EIF4G2, PTPRT and HPGD as direct targets of miR-139. These genes are known to tightly modulate the translation machinery, thus cancer progression (195). Other direct or indirect targets of miR-139-5p engage core-signaling pathways such as Wnt/ $\beta$ -catenin, PI3K/AKT/mTORC1, TGF- $\beta$ /SMAD and MAPK signaling (196). Hence, it is relevant to evaluate miR-139 in cancer diagnosis, prognosis, therapy and follow-up. In cervical cancer, Ji et al. demonstrated increased metastasis in patients with low miR-139-5p levels in response

to alleviation of Wnt/ $\beta$ -catenin silencing upon miR-139-5p repression (197). Similarly, miR-139-5p expression is inversely correlated with patients' survival in hepatic cancer. MiR-139-5p diagnostic value is under consideration for stomach adenocarcinoma with 71.7% sensitivity and 87.5% specificity (196). In ACC, higher miR-139-5p expression is associated with worse survival rates. Mechanistically, miR-139-5p exerts its oncogenic effects at least by downregulating N-myc downstream-regulated gene 4 (NDRG4) (192). Unexpectedly, ACCs displayed significantly lower expression of miR-139-3p, the 3'-arm of miR-139, than ACAs or normal cortices. This study suggested no significance of miR-139-3p in predicting the clinical behavior of adrenocortical lesions (177). In terms of therapy, nanovectorizing miR-139-5p in liposomal nanoparticles conjugated with surface epithelial cell adhesion molecule (EpCAM) exhibited remarkable anti-cancer effects on colorectal cancer mice models, basically through Notch1 regulation (198). The contradictory findings above mentioned emphasize the tissue-specific functionalities of miRNAs as well as the distinct roles of miRNA-5p and -3p species.

## **II.D. MicroRNA-based therapeutics**

### **II.D. 1. Targeting microRNA**

MiRNA expression patterns can be modulated to abolish or restore miRNA biological function. To inhibit oncogenes or restore tumor suppressors, one anti-cancer strategy consists of silencing the overexpressed oncomiRs or replacing the downregulated tumor suppressor miRNAs (199). There are three approaches to achieve miRNA loss of function: miRNA sponges, antisense oligonucleotides (antagomiRs, antimiRs), and genetic knockouts based on the application of Clustered Regularly Interspaced Short Palindromic Repeats/CRISPR-associated protein 9 (CRISPR/Cas9) genome-editing technologies (200, 201). Synthetic miRNA sponge vectors express transcripts with miRNA binding sites that mimic those found in natural mRNAs and complementary to the targeted miRNA (202). This system sequesters endogenous intracellular miRNAs, thus preventing their binding availability for the target mRNAs (203). By transducing a retroviral miRNA sponge to inhibit miR-9, Ma et al. demonstrated that metastasis was significantly reduced in a syngeneic mouse model of breast cancer (204). High affinity-inhibition is also feasible via chemically modified oligonucleotides such as locked nucleic acids (LNA). As a part of the cell endogenous DNA repair machinery, the CRISPR/Cas9

system has been reported recently as a potent genetic engineering tool for miRNA-based therapeutic intervention. Yoshino and colleagues targeted miR-210-3p and miR-210-5p using the CRISPR/Cas9 system in renal cell carcinoma cell lines and demonstrated that deletion of miR-210-3p increased tumorigenesis, both in vitro and in vivo (205). Another growing field in miRNA therapeutics is miRNA replacement therapy, which aims at restoring miRNAs which are downregulated or deleted in cancer cells. With the recurrence of downregulated tumor suppressor miRNAs in human malignancies, mainly miR-34 and let-7, administration of miRNA mimics can re-establish miRNA levels to their basal non-pathological states. Indeed, a decrease of let-7 promotes expression of a number of oncogenic factors, including RAS, Myc, cyclins, and cyclin-dependent kinases (206). In cultured lung cancer cells as well as in pre-clinical models of lung cancer, re-introduction of let-7 mimics impedes cell proliferation and reduces growth of lung tumors. MiR-34a is markedly under-expressed in most human cancer types. Re-expression of miR-34a induces growth arrest and apoptosis, by silencing pro-proliferative and anti-apoptotic genes (207). Integrating miRNA targeting agents within unique vectors has broadened the spectra of miRNA-based therapeutics, as discussed in chapter III of this manuscript.

## **II.D. 2. miRNA-based therapeutics in ACC**

MiRNA-based therapeutic approaches for ACC are still scarce as most studies focused on the biomarker potential of tumor or circulating miRNAs (171). A first preclinical approach was performed using the genetically modified bacterial nanocells (EDVs) to deliver systemically the tumor suppressor miR-7 into a human ACC mouse model (208). Specific tumor homing was ensured by using EGFR-tailored EDVs. MiR-7-loaded nanoparticles could effectively reduce ACC xenograft growth arising from both an ACC cell line and patient-derived xenografts, without any evidence of off-target effects. As miR-7 replacement therapy acted synergistically with Erlotinib therapy in head and neck cancer (209), it is crucial to assess whether combination of miR-7 and mitotane would have similar effects in ACC. Such was the case of miR-431, which efficiently sensitized ACC cell lines to mitotane and doxorubicin. In fact, miR-431 was 100-fold underexpressed in patients who were resistant to adjuvant therapy, when compared to sensitive ones. Following transfection of the ACC cell line H295R with miR-431 mimics followed by treatment with doxorubicin or mitotane, H295R cells showed reduced

proliferation and increased apoptosis. Restoring miR-431 expression could reverse the EMT phenotype as shown by ZEB1 (Zinc finger E-box-binding homeobox 1) transcription factor repression (210). These findings support a great potential of miRNA therapeutics for ACC alongside clinical trials based on combined chemotherapy. Jung et al. proposed an experimental setup with liposome-encapsulated chemotherapeutics (L-EDP-M etoposide (E), doxorubicin (D), cisplatin (P), and mitotane (M)) in order to minimize unintended targeting (211). Treatment of the ACC cell line SW-13-derived xenografts in mice induced necrosis and reduction in tumor size. Interestingly, the research group reported an increased expression of circulating miR-210 in the L-EDP-M-responsive animals. Since miR-210 is a frequently described as an oncomiR in ACC, its release from the tumor to the circulation may be valuable for monitoring response to therapy.

### **II.D .3. Obstacles and drawbacks**

Improvement of miRNA mimics or antimiRs stability and development of safe and efficient delivery systems are critical steps to bring miRNA therapies from bench to bedside. Indeed, synthetic miRNA mimics or antimiR oligonucleotides have short half-life and are immediately degraded in biological fluids by nucleases (212). To overcome this hurdle, several strategies have been devised, including chemical modifications such as phosphodiester and phosphorothioate internucleotide linkages, addition of a 2'-O-methyl group or synthesis of locked nucleic acids in which the ribose ring is constrained by a methylene linkage between the 2-oxygen and the 4-carbon. In addition to chemical modifications, entrapment of therapeutic miRNAs within functionalized nanoparticles allowed further improvement in their protection from degradation, decreased the immune response and enhanced the circulation time. Finally, conjugation of nanoparticles with targeting ligands such as proteins, peptides, and antibodies improved cellular uptake and specific targeting of the tumor site. Several viral and non-viral miRNA delivery systems have been used successfully in vitro and in vivo. Nevertheless, whether based on chemically modified oligonucleotides, miRNA sponges or miRNA mimics, developing therapeutic approaches still present clearance, accessibility, tissue-specific targeting and safety issues (213). The exponential growth in nanotechnology research is expected to help to overcome these barriers: oligonucleotides can be encapsulated into complex nanoparticles (NPs) capable of efficient and targeted drug delivery. Besides



improved endosomal escape, these nanocarriers achieve tumor-selective accumulation through the Enhanced Permeability and Retention (EPR) effect, a central paradigm in cancer nanomedicine (214). This passive targeting mechanism results from the extravasation of long-circulating nanoparticles (diameter < 100 nm) through the leaky tumor microvasculature into the tumor interstitium. Subsequent nanoparticle cellular uptake and intracellular fate are strongly influenced by their size, shape and surface properties (215).

## **Chapter III. Nanomedicine for cancer, basic principles**

The aim of this chapter is to define the position and benefits of nano-objects in oncology. We provide an overview of different classes of nanoformulations, their clinical relevance and possible engineering for personalized medicine. Their miRNA-delivery capacities are then evaluated in cancer context. We provide the principles of nanoparticles delivery to tumor site and the subsequent discharge of their cargo. Finally, particular attention is brought to obstacles still impeding miRNAs' golden era in therapeutic advancement.

### III.A. Etiology and nomenclature

Since ancient times, nanoparticles have been naively handled, definitely without holding this specific terminology. From colored glass to renaissance pottery, going through ceramic

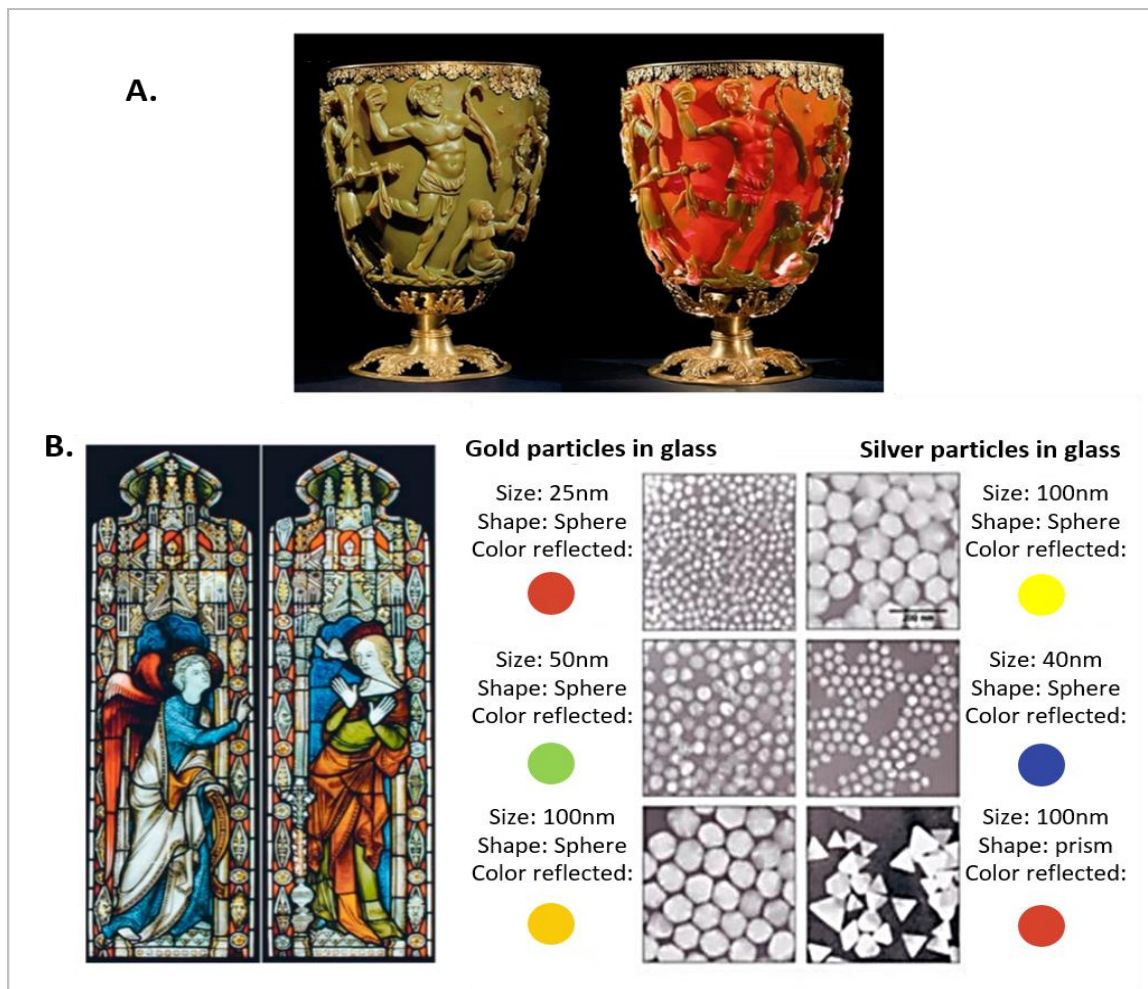


**Figure 17: The very first nanotechnologies.**

(A) The glass of the Lycurgus cup appears green in reflected light (Left panel) and red in transmitted light (Right panel) due to the presence of silver-gold nanoparticles. (B) Adding tiny amounts of silver and gold changed the glass physical properties towards colorful glass staining on cathedrals' windows. Size and shape strongly affect materials characteristics.

lusters, nanomaterials have long fascinated and triggered old populations (Figure 17). The Lycurgus cup best represents nanoparticles' involvement in dichroism phenomenon.

In fact, the color change of this cup following light conditions remained mysterious until the 1990s. Breakthroughs in material chemistry revealed the presence, in this cup, of 50-100nm sized silver-gold nanoparticles (Ag-Au ratio 7:3) with an additional 10% copper, all dispersed in a glass matrix (216). Different size and optical properties of these particles were responsible of the red-green color switch.

Of note, the field of nanomaterials has progressively evolved as scientists began to question matter continuity, or in other words, its divisibility to smaller and smaller particles until reaching an indivisible stage, corresponding today to atoms. The first milestone into nanoparticles world was achieved by the American physicist Richard Feynman back in 1959. "There is plenty of room at the bottom" (217), "why can't we write the entire 24 volumes of the Encyclopedia Britannica on the head of a pin?" Thereafter, have emerged many advancements leading to our current perception of nanoparticles and nanotechnologies.

The word nanoparticle (NP) has been introduced in the 1960s after formulation of liposomes. The prefix "nano" is of Greek origins, meaning dwarf or a tiny object representing one billionth of a meter ( $10^{-9}$ ). Therefore, by definition, a nanoparticle is a nano-object with a three dimensional nanometric scale ranging between 1 and 100nm. Nanotechnology utilizes these structures by modulating their size and shape to exploit their nanoscale properties into

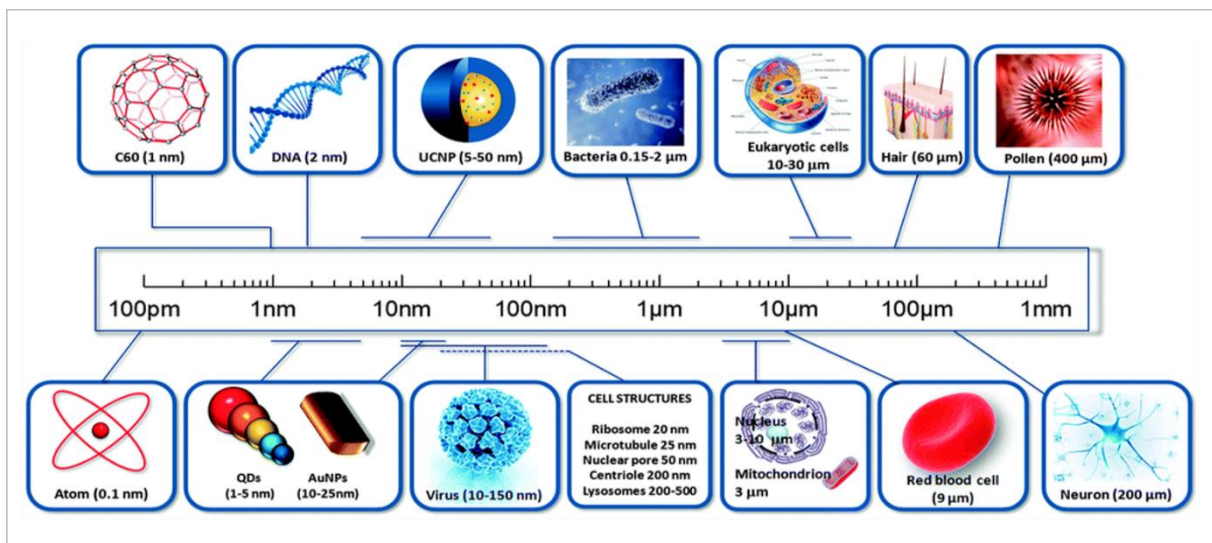


Figure 18: Size comparison of living and non-living matter in nanometric scale.

innovative tools (216). Figure 18 positions nanomaterials on a scale with common microscopic and macroscopic entities.

As of the 2000s, the scope of nanotechnology has expanded to human health through the trendy field of nanomedicine. The ultimate goal of nanomedicine is to develop safe and effective theranostic candidates (218). Indeed, the unique properties of NP have provided breakthroughs in molecular imaging and drug/ gene delivery over the last decade.

### III.B. Advantages of nanoscale therapies

The therapeutic potency of a given molecule is first evaluated through its physicochemical properties, i.e. molecular weight, shelf-life/ stability, solubility in buffer, surface affinity and eventual coupling with opposite charged entities. Then is assessed the drug pharmacology, which governs its fate upon in vivo administration. Common parameters include stability, biodistribution, bioavailability and clearance (219). Moreover, administration routes dictate the biological barriers to which is exposed a molecule, therefore affecting its pharmacokinetics. Among these barriers, membrane permeability, enzymatic degradation, pH and hydrophobicity should be carefully considered (220). However, the most hazardous property to be checked, is drug cytotoxicity, which emerges either from undesired accumulation in certain organs or from a prolonged journey in the organism before clearance (221). Structural modification of some molecules can reshape their physico-chemical properties in order to enhance in vivo behavior. However, since altering some molecules may disrupt their therapeutic value, another trendy alternative is to encapsulate these compounds in nanometric vectors, which allow optimal control of the therapeutic outcome (218). The relevance of nanoscale therapies is achieved at four levels:

- 1) **Protection:** Nanovectors shield the molecule of interest against biological barriers and external environment which may degrade it, i.e. storage buffers or blood-borne enzymes.
- 2) **Biodistribution:** It is possible to optimize drug biodistribution by remodeling the nanovector's properties, which are more likely manageable than the molecule itself. For example, the kidneys rapidly clear out molecules of small molecular weight. Encapsulating such entities increases their bioavailability before excretion, thus potentiating therapeutic outcomes.

- 3) **Off-target effects:** NP encapsulation ensures safe and targeted homing of the molecule to its therapeutic site without undesired effects on neighboring tissue. In oncology, the nanometric scale of common NPs allows passive targeting to the tumor. Another line of specificity can be added by engrafting guiding ligands on the surface of the vectors.
- 4) **Therapeutic outcome:** Nanovectors confer stability to the molecule of interest while still preserving its original properties. This shall scale down the required dose and minimize its potential toxicity. Moreover, the variety of available nanovectors makes it possible to adapt the administration routes of a single molecule according to the requested pathology or context.

### III.C. Nanoparticles in the COVID-19 pandemic: The era of mRNA vaccines

Not only has the global pandemic caused by the severe acute respiratory syndrome coronavirus-2 (SARS-CoV-2) dislocated healthcare systems and economies all over the world, but also it has clearly shifted efforts of the R&D community towards nanoparticle-based mRNA vaccines (222). As of June 2020, 185 COVID-19 vaccine candidates were in preclinical testing, with another 102, of which 19 mRNA vaccines are already in clinical trials. After a fierce race to the finish line, the two mRNA vaccines from Pfizer-BioNTech and Moderna ranked first and second in the United States, receiving FDA emergency use authorization a week apart in mid-December 2020, just 11 months after the viral genome sequence was publically available (223). The achievement of these rapidly conceived, safe and efficient vaccinations was attributed to nanotechnology.

Briefly, the mRNA vaccines from Pfizer and Moderna consist of a synthetic messenger RNA that encodes the SARS-CoV-2 "spike protein" which is generally located on the surface of coronavirus particles (Figure 19). This mRNA is coated with a combination of synthetic cationic lipids forming a lipid nanoparticle (LNP) structure that protects mRNA throughout its transit inside the body, while also facilitating endocytosis into target cells. Once the vaccine nanoformulation enters a cell, the acidic endosomal environment causes the lipid corona to be stripped off, hence releasing the mRNA into the cytosol. The mRNA then attaches to ribosomes and promotes synthesis of spike protein. The majority of spike protein molecules

are then transferred to the cell surface where B-lymphocytes detect them and start producing spike-neutralizing antibodies. Furthermore, proteases on the cell surface can cleave portions of the spike protein and release it from the cell (224). If this occurs in the circulation, the released fragment, known as S1, might attach to and activate blood platelets, thus directly provoking blood clotting. The aim of this vaccine strategy is to launch an immune response regardless of the spike origin: When initiating a cytotoxic response, the immune system will not discriminate between an actual viral infection and the viral synthesis via mRNA vaccination—as long as the spike protein fragments are presented by the cells for killer cells to destroy. Other protein NP vaccines displaying spike receptor (ACE2) binding domains on their shell are also under construction, but to date mRNA have exhibited enhanced stability (225). Moreover, an interplay between host cell miRNAs and SARS-CoV-2 components has been reported, thus implying that nanoparticle-vehicled miRNAs might be nanoformulated to prevent SARS-CoV-2 infection, in a fashion comparable to current mRNA vaccines (226).

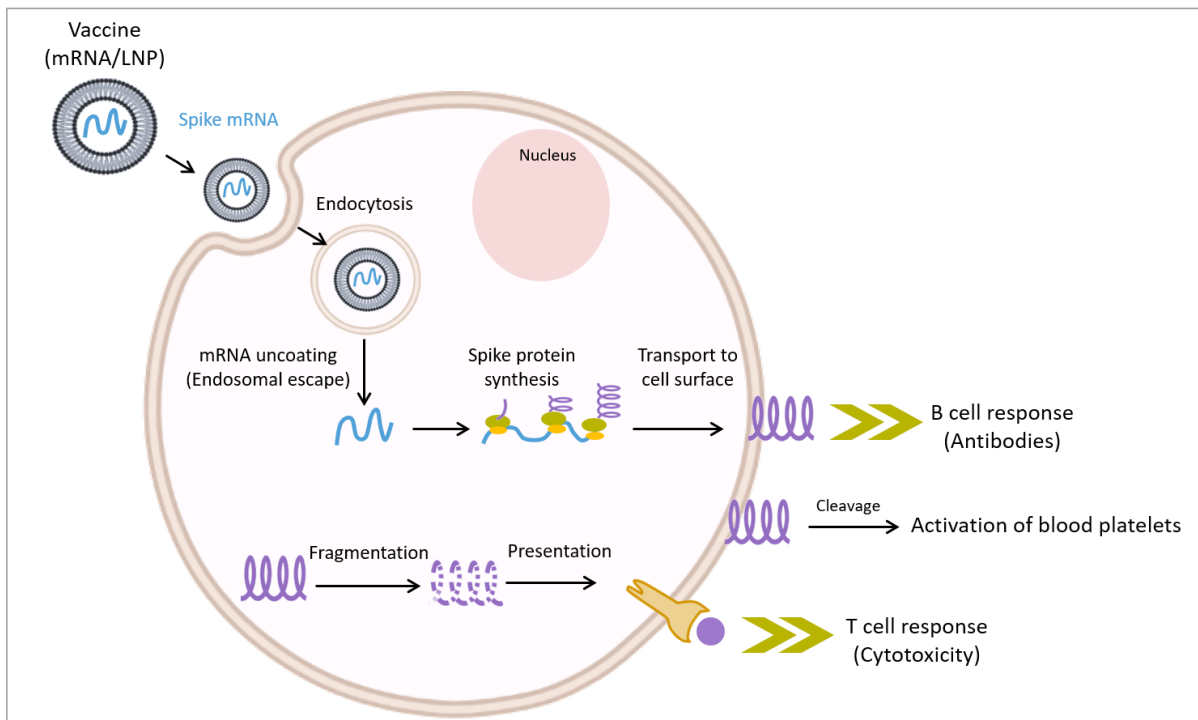


**Figure 19: How the COVID-19 mRNA vaccines work.**

Synthetic spike mRNA is encapsulated in lipid nanoparticle-formulated vaccines. After endocytosis, mRNA is uncoated via endosomal escape. In the host cell cytosol, spike mRNA is translated into spike proteins. Most of the spike proteins are transported to the cell surface where they induce B cells to produce antibodies. Few spike molecules undergo fragmentation to be associated on cell surface with HLA. This induces cytotoxic responses. When surface proteases are present, some spike fragments may directly associate to blood platelets.

Messenger RNA-based therapeutics have significant benefits over other techniques. Firstly, mRNA delivery is safer than whole virus or DNA delivery because it is not infectious and cannot be integrated into the host genome. Unlike DNA, which must be decoded in the nucleus, mRNA is processed directly in the cytosol. The mRNA half-life is short, but can be regulated through molecular design (227). Also, mRNA is immunogenic, which may represent an advantage for vaccine design. Interestingly, unlike conventional vaccines, mRNA bioengineered vaccines may be quickly and cheaply modified to meet mutant antigenic epitopes. Keeping that into mind, the nanotechnology field is expected to remain in constant race to hamper the virus' mutation before its vast evolving. Using a cocktail of nanomedicine technologies, the end of the present epidemic looks genuinely within grasp.

A non-negligible drawback of these formulations is that they require low temperatures for long-term storage, providing logistical challenges to their distribution and administration, particularly in regions of the global south. Our knowledge of the pharmacokinetics of COVID-19 vaccines is still foggy due to officially endorsed haste and systematic rush in their research and approval (223). For example, documented LNP accumulations in the ovaries may raise concerns about vaccination safety and potential long-term reprotoxicity. Apart from the bioactive compound -core of the vaccination strategy-, pejorative attitudes are also fostered by the anti-vaccine communities regarding the hidden hazards of the newborn NP vaccines. Despite all, antiCovid-19 vaccines based on mRNA are a game-changing invention in nanomedicine and a major scientific breakthrough that will surely assist some of the most promising miRNA nanocarriers to reach the market.

### **III.D. Nanoparticles in cancer research: The rise of miRNA therapeutics**

Cancer is a complex multistep disease disrupting cellular homeostasis. Despite the variety of treatment options, multidrug resistance thus therapeutic failure are still problematic. With the rise of nanotechnology, novel screening and anti-cancer avenues are under consideration. These take advantage of the capacities of NPs to overcome biological barriers and specifically accumulate in tumors (228). NPs have successfully marked their relevance in precision oncology for diagnosis, imaging, and drug delivery. Some NPs like liposomes and polymeric



micelles, have already stepped to clinics, notably for conventional cancer treatment i.e. chemotherapy, radiotherapy and immunotherapy, but to less extent for RNAi gene therapy (229). The first liposomal formulation to receive FDA approval in 1995 was a nanotreatment for ovarian cancer and Kaposi's sarcoma, namely Doxil®. Then have emerged numerous trials more or less effective.

Of course, the biomaterial configurations within the NPs strongly affect their stability, encapsulation and targeting properties (218). The core components of NPs consist of organic or inorganic biomaterials, which are engineered to meet clinical needs. NPs are now implicated in a plethora of applications, of which gene therapy has witnessed massive growth in the past years. The pleiotropic activity of miRNAs combined to cancer complexity, rendered miRNAs appealing tools for the creation of anti-cancer gene therapies. As a result, restoring downregulated miRNA by the use of synthetic oligonucleotides or silencing overexpressed miRNAs through artificial antagonists has become a trendy strategy in cancer research. The eventual success of miRNA therapies, however, highly depends on resolving pharmacokinetic hurdles through safely addressing miRNA formulations. The revolution in nanotechnology-based systems offers great potential for improving the cell-specific delivery of miRNA-based therapeutics.

### **III.D. 1. Inorganic nanoparticles for miRNA delivery**

Inorganic NPs mostly involve metal gold Au-NPs and silver Ag-NPs, in addition to metal oxides such as iron oxide ( $\text{Fe}_3\text{O}_4$ ) and copper oxide ( $\text{TiO}_2$ ). Other stiff materials like graphene and silica have also been tested. The majority of magnetic NPs are based on the use of superparamagnetic iron oxides. These particles consist of small particles of maghemite ( $\text{Fe}_2\text{O}_3$ ) or magnetite ( $\text{Fe}_3\text{O}_4$ ), which can be encapsulated in a matrix of silica, polymer or polysaccharide (dextran) (230). These magnetic particles are designated by the term SPION ("SuperParamagnetic Iron Oxide") for those whose size is between 50 and 500 nm, and USPIO ("Ultra small SuperParamagnetic Iron Oxide") if their diameter is less than 50 nm.

The NP implementation to cancer treatment is more and more pronounced with virtue to their stability at high temperature. For instance, iron oxide NPs are already commercialized in Europe for heat-modulated radiotherapy in glioblastoma (231).

In addition, fluorescent semiconductor nanocrystals, better known as Quantum dots are widely assessed as nanoprobes for theranostic applications. These NPs measure between 2 and 10nm in diameter and are composed of a semiconductor crystalline core covered with a zinc sulphide shell in order to passivate the NP surface while stabilizing their optical properties (232).

Apart from conductive, optical and magnetic properties, inorganic NPs present several advantages, including stability, tunable size and surface functionalization. However, concerns regarding their long-term toxicity are still raised, especially with increased oxidative stress upon NP uptake (230). Surface tailoring is one way to relieve this issue. Moreover, nanotechnology has shown fruitful applications in miRNA packaging (165).

In the next sections, we expose few examples of common NPs with emphasis on their contributions to miRNA-based therapeutics in cancer.

#### III.D. 1.a. Gold nanoparticles

Gold NPs (Au-NPs) retain unique optical properties linked to their free electron system called plasma. A variety of techniques has been utilized to functionalize Au-NPs in order to improve their interaction with biological molecules and promote intracellular payload release (233). To improve bonding with miRNA, gold nanoparticles can be functionalized with thiol groups as shown in figure 20 (234). Ekin et al. used this method to successfully deliver miR-145 to prostate PC3 and breast MCF-7 cell lines (235).

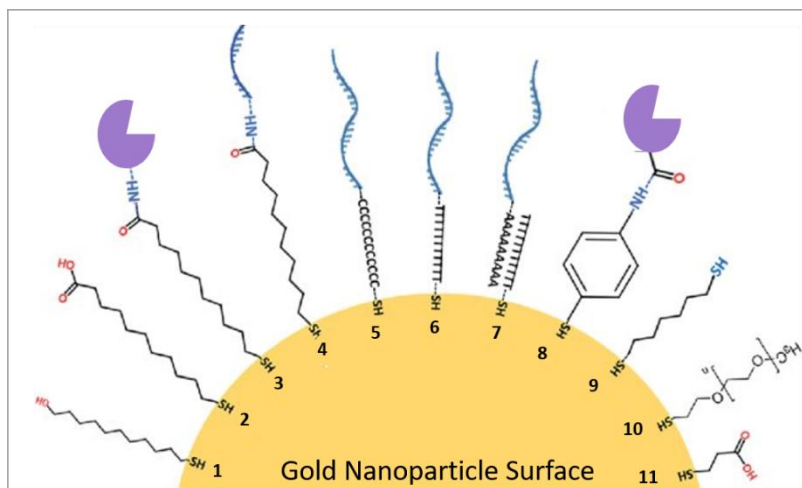


**Figure 20: Surface modification of gold NPs with thiol derivatives.**

To the thiol group can be added: (1) 11-Mercapto-1undecanol, (2) 11-mercaptoundecanoic acid, (3) protein bound to 11-mercaptoundecanoic acid, (4) DNA bound to 11-mercaptoundecanoic acid, (5) DNA directly bound to gold surface via a carbon spacer, (6) DNA directly bound to the surface through a poly A tail, (7) DNA bound to the gold surface via a partially complementary DNA strand with thiol modification, (8) protein bound to gold surface with 4-aminothiophenol, (9) dithiol molecule, (10) thiolated PEG, (11) mercaptopropionic acid. Adapted from Yüce et al.2017

A second polyethylene glycol (PEG) layer was shown to maintain Au-NPs nanoformulations by preventing aggregation and miRNA degradation (236). Furthermore, the binding of Au-NPs to the target site can be enhanced by coating their surface with target-specific ligands. Even though Au-NPs have sparked a lot of interest in recent years, additional research into biocompatibility, cytotoxicity, retention, and clearance time is required to develop conjugated Au-NPs with minimum adverse effects (230).

### III.D. 1.b. Iron nanoparticles

Iron is among the most abundant metals used both in macroscopic and nanoscale industry. The magnetic characteristics of iron NPs makes them suitable as drug nanocarriers and contrast agents in magnetic resonance imaging (230). Thanks to their physical entrapment in polymeric matrix, certain chemotherapy compounds such as doxorubicin, paclitaxel and methotrexate were successfully conjugated in iron NPs, thus manifesting strong affinity to cancer cells (237). The efficacy of dextran-coated iron NPs as miR-29a vehicle in breast cancer was demonstrated by a decreased expression of anti-apoptotic genes after selective uptake by MCF-7 cells (238).

### III.D. 1.c. Mesoporous silica nanoparticles

Mesoporous silica nanoparticles (MSN) are a special group of inorganic NPs that have porosities at the nanoscale. They provide a high surface area, thermal stability, and easy surface modification, with biocompatible and non-toxic properties (228). Their large and active surface allows the attachment of different functional groups for targeted drug delivery. Among the many strategies that are used to functionalize MSNs, chemical modifications within the pores to increase the retention time of loaded molecules, coating with PEG for stabilization and attachment of targeting ligands to target specific cell receptors have been extensively investigated. Tivnan et al. exploited the high expression level of the tumor-associated antigen disialoganglioside (GD2) in neuroblastoma to develop GD2-targeting MSN for the delivery of miR-34 into neuroblastoma murine models (239). However, the synthesis of functionalized MSN requires multiple steps with complex chemical reactions that limited their fabrication at industrial scale.

### III.D. 2. Organic nanoparticles for miRNA delivery

Organic NPs do not hold intrinsic magnetic or optical properties; instead, they are mainly employed as platforms for numerous molecules serving as imaging, diagnostic or therapeutic entities. Compounds simultaneously offering diagnostic and therapeutic benefits are assigned as theranostic agents. The main goal of such nanovectorization is to shift the pharmacology of the encapsulated drug towards safe and controlled release monitored by its shielding carrier. There are two major families of organic NPs: Polymeric and lipid NPs (Figure 21).

#### III.D. 2.a. Polymeric nanoparticles

Different polymers can be nanostructured to form NPs; the most commonly used are poly (lactic acid), poly (glycolic acid) and their copolymer poly (lactide-co-glycolide), respectively abbreviated PLA, PGA and PLGA. These polymers offer high biocompatibility and biodegradability. Thus, they have been used for many years to manufacture medical devices and subcutaneous implants. Polymeric NPs also offer better stability than liposomes, whether in vivo or during storage (240). However, even if polymers have good biocompatibility, they are not devoid of all cytotoxicity. The presence of residual organic solvents within the NPs is

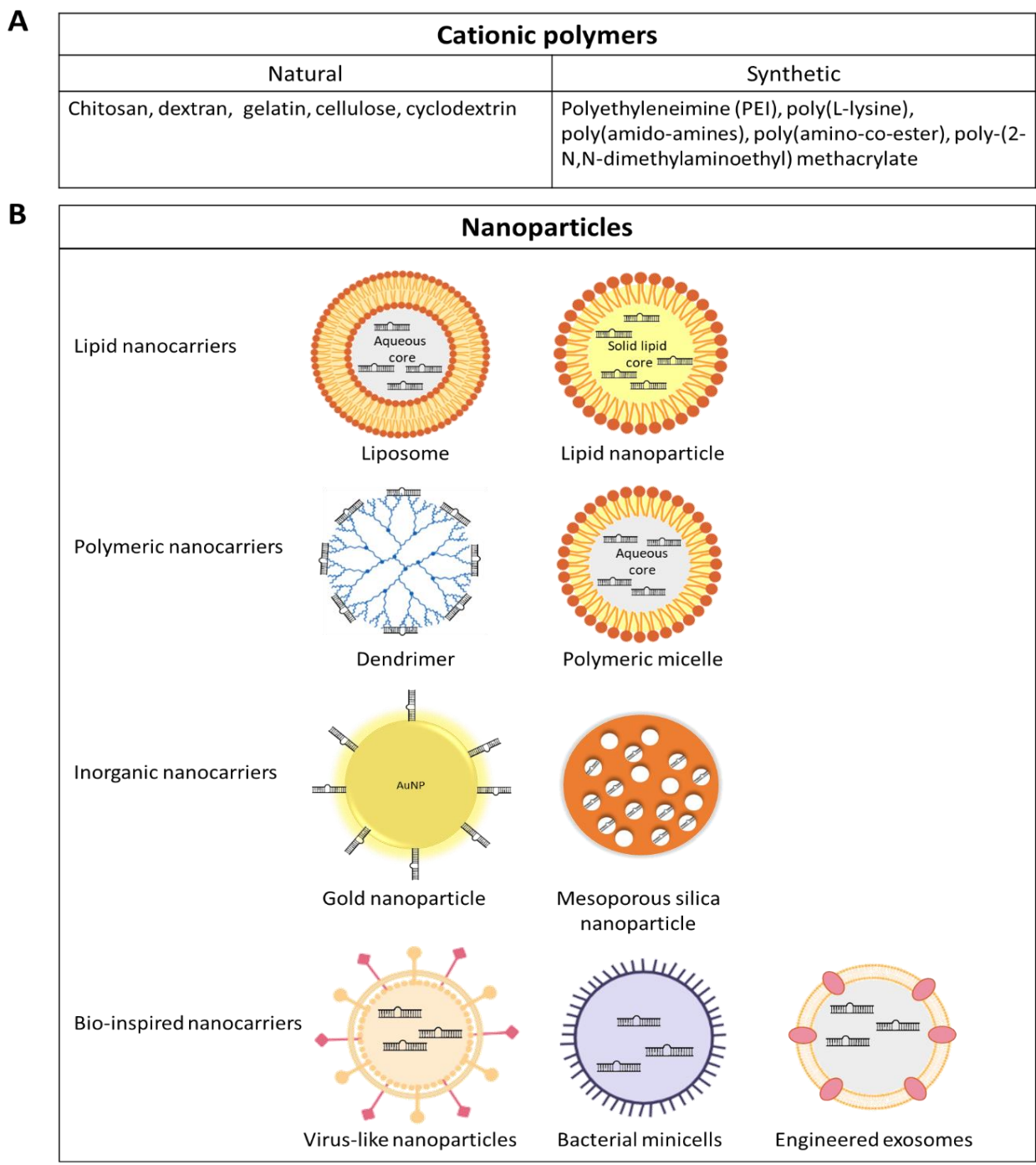


**Figure 21: Schematic representation of emerging nanoplatforms for miRNA delivery.**

(A) Natural and synthetic polymers can form electrostatic complexes with nucleic acids such as miRNAs. (B) Nanoparticle-based platforms are characterized by tunable size, shape, and surface characteristics, which enable them to have compatibility with different administration routes. Specific recognition molecules such as antibodies or peptides can be grafted to target tissues more specifically. Tumor-derived exosomes are being increasingly explored as delivery systems in cancer research since their identification as drivers of organotropic metastatic spread. However, their complex composition and still non-established biological functions led to the development of Exosome-Mimetic Nanosystems that recapitulate natural exosomes structure with a controlled composition.

also problematic. Finally, the production of such NPs is difficult to industrialize and generally results in low particle yield (241). Polymeric NPs can be either natural like micelles, dextran and chitosan NPs, or synthetic such as PLGA or Polyethyleneimine (PEI) NPs or even dendrimers.

### Micelles

Micelles are self-assemblies of amphiphilic molecules, which form structures of the core-shell type in an aqueous environment. Micelles are formed when the concentration of surfactants in the medium exceeds a threshold value called the critical micellar concentration (242). In this case, the amphiphilic molecules self-assemble to group their hydrophobic parts together and expose only their hydrophilic domains on the surface. There exist different types of micelles depending on the surfactants used. We can cite micelles based on phospholipids or PEG-ylated surfactants, but it is those using copolymers that had attracted most of the current research (243). Reported benefits of micelles cover their easy preparation and efficient cellular uptake. However, micelles are prone to dilution in the bloodstream, which limits their systemic administration (244). Incorporating anionic entities such as nucleic acids in the core of cationic micelles may offer enough hydrophobicity to stabilize the formulations in aqueous settings. Mittal et al. designed gemcitabine-conjugated cationic micelles for the co-delivery of gemcitabine and miR-205 in pancreatic cancer (245). Combination formulations efficiently reversed chemoresistance, invasion and migration in gemcitabine-resistant pancreatic cancer cells in vitro, and showed significant growth inhibition in vivo.

### Polyethyleneimine

PEI, an organic macromolecule with a high cationic-charge-density potential, is the most commonly used polymeric gene delivery system (246). The overall positive charge of PEI makes it convenient for condensing large negatively charged molecules such as nucleic acids, resulting in the formation of polyplexes through electrostatic complexation. PEI internalization occurs via proton-sponge effect, a process detailed in section III.F. The large number of preclinical studies assessing its biodistribution, imaging and therapeutic index

reflects the enthusiasm for PEI-based siRNA or miRNA polyplexes. PEI usage in vivo was also spread towards miRNA replacement therapy. For instance, intraperitoneal injection of miR-155-PEI was found to boost anti-cancer immunity and improve survival rates of ovarian cancer bearing mice (247). However, the outstanding biological activity of PEI remains hindered by its higher cytotoxicity with increased molecular weight, branching and particle aggregation (248).

### Dendrimers

Dendrimers are polymeric complexes ranging between 1 and 10nm, which are built by the addition of successive layers of monomers. Though these branched polymeric constructs have a well-controlled structure, their synthesis is delicate (249).

### III.D. 2. b. Lipid nanoparticles

The second subtype of organic NPs regroups lipid NPs (LNPs) which are widely used due to their efficient cellular uptake through the cell membrane. Different types of nanoformulations, such as liposomes and solid lipid nanoparticles (SLNs) proved to be less toxic than other delivery systems such as polymer nanoparticles, owing to their biocompatibility and biodegradability (250). As predicted by their name, phospholipids and fatty acids are the standard components of lipid nanocarriers; meaning that these vectors ideally encapsulate hydrophobic molecules. MiRNA loaded LNPs are usually a cocktail of cationic lipids (N-[1-(2,3-dioleoyloxy)propyl]-N,N,N-trimethylammonium chloride (DOTMA) or 1,2-dioleoyl-3-trimethylammonium-propane (DOTAP), neutral lipids and PEG (251). Helper lipids, i.e., neutral lipids like cholesterol and dioleoylphosphatidyl ethanolamine (DOPE), can be incorporated in LNPs in order to reduce the charge-driven toxicity and to enhance delivery efficiency (252). LNPs increased the therapeutic index of many drugs and offered improved drug targeting and controlled release.

### Liposomes

Liposomes are vesicles made up of one or more concentric double layers of phospholipids and cholesterol molecules encapsulating an aqueous reservoir. The size of the liposomes varies between 30 nm and several micrometers (229).

These particles have been used for many years as tools for biology and medicine as carriers of therapeutic active ingredients or imaging agents. Their non-toxic and biocompatible character make these colloids interesting systems for clinical applications (253). However, liposomes also have some limitations: they have shown a low capacity for encapsulation (especially for lipophilic molecules trapped in the double layer of phospholipids), moderate stability, delicate production, and early release of hydrophilic active ingredients in the blood. In the context of miRNA-based therapy, miR-135a-loaded immunoliposomes coated with anti-EGFR antibodies were shown to inhibit gallbladder carcinoma invasion and metastasis, and to promote apoptosis. The GBC tumor growth rate was 60% lower in xenograft-bearing mice treated with Anti-EGFR-CIL-miR-135a as compared to controls (254).

### Solid Lipid nanoparticles

SLNs offer additional advantages over polymeric NPs and liposomes. Indeed, incorporation of both hydrophilic and hydrophobic drugs is achievable along with controlled release of the drug for up to several weeks (255). Moreover, the lipids used in the preparation of SLNs are biodegradable and safe. SLN formulations are also characterized by a high stability and loading capacity as compared to their lipid counterparts. The core of these particles is made up of a lipid matrix that is solid at room temperature but also at human body temperature. This more or less crystallized matrix is stabilized by a layer of surfactants (253). The lipids used are either highly purified triglycerides, or mixtures of fatty acids and waxes. Cationic lipids facilitate interaction with the cell membrane, improving transfection efficiency. Combining miRNA with chemotherapeutic drugs using SLNs was shown to be a powerful anticancer strategy. Shi et al. demonstrated that co-incorporation of miR-34a and paclitaxel (PTX) in SLNs increases the uptake of these nanoparticles by B16F10-CD44<sup>+</sup> melanoma cells and induces more cell death than single drug-loaded nanoparticles (256). We expose in depth the profile of Lipidots as example of SLNs later in chapter IV.

### **III.D. 3. Biomimetic nanoplatfoms**

Mimicking natural platforms is a powerful approach to engineer NPs for drug and vaccine delivery while guaranteeing biocompatibility. In fact, most supramolecular formulations require a cylindrical assembly of amphiphilic molecules in a bilayer-like manner (257).



Biomimetic NPs recall functional or structural aspects of bacteria, viruses and other entities like exosomes, taking great advantage of the natural phospholipid assembly within their biological membranes. Cell membrane-camouflaged NPs have been fairly exploited for drug delivery because of their enhanced targeting and retention of encapsulated molecules (258). There are three strategies for manufacturing biomimetic platforms: (1) cell membrane-coated NPs, (2) synthetic NPs conjugated to surface protein-mimicking ligands, (3) engineered liposomes with cell membrane proteins. The first line of cell membrane-based NPs featured a shell of red blood cell (RBC) membrane and a core of PLGA in a core-shell structure. RBC membrane-coated NPs were reported as excellent venues for chemotherapeutics administration, as RBC are abundant, easy to isolate, non-nuclear and most importantly, they hold a long half-life of about 120 days in the circulation (259). Besides RBC, all sorts of membranes including platelets, albumin, bacteria and exosomes were explored as drug/miRNA carriers.

#### III.D. 3.a. Bacterial nanocells

A powerful delivery vehicle based on bacteria derived nanocells, called EDV™ (EnGeneIC Dream Vectors) has been developed by EnGeneIC Ltd. (Sydney, Australia) (260). Bacterial nanocells are achromosomal nanoparticles produced by inactivation of the genes that control normal bacterial cell division. They can package a range of anticancer chemotherapeutic drugs (261). Targeted delivery was achieved by using bispecific antibodies, which are capable of binding the EDVs with one arm and the tumor antigen with the other arm. In addition, the bacterial cell wall of the nanocells stimulates key components of the immune system, which are then activated to kill cancer cells. EDVs proved to be safe and well tolerated despite high and repeated doses in different animal models (261, 262). Employing EDVs for miRNA transfer was investigated in several studies. For instance, EDVs or TargomiRs were used as carriers for miR-16 delivery to 26 NSCLC patients in a phase I clinical study (NCT02369198). The targeting moiety of this bacteria derived delivery system was an anti-EGFR bispecific antibody to target EGFR-expressing cancer cells. Tumor growth was impaired after systemic administration of TargomiRs at low dosages. However, dose-dependent toxicities were reported, i.e., anaphylaxis, inflammation as well as cardiac events. Variable response rates were observed (263). Based on these observations, the authors recommended to conduct a new trial

combining TargomiRs with chemotherapy or immunotherapy in larger groups of patients. Interestingly, a first preclinical approach was performed using genetically modified EDVs to deliver systemically the tumor suppressor miR-7 into a human ACC mouse model (208). Specific tumor homing was ensured by using EGFR-tailored EDVs. MiR-7-loaded nanoparticles could effectively reduce ACC xenograft growth arising from both an ACC cell line and patient-derived xenografts, without any evidence of off-target effects. Mechanistically, this phenotype was mediated by repression of RAF1, mTOR, and CDK1 (Figure 22).

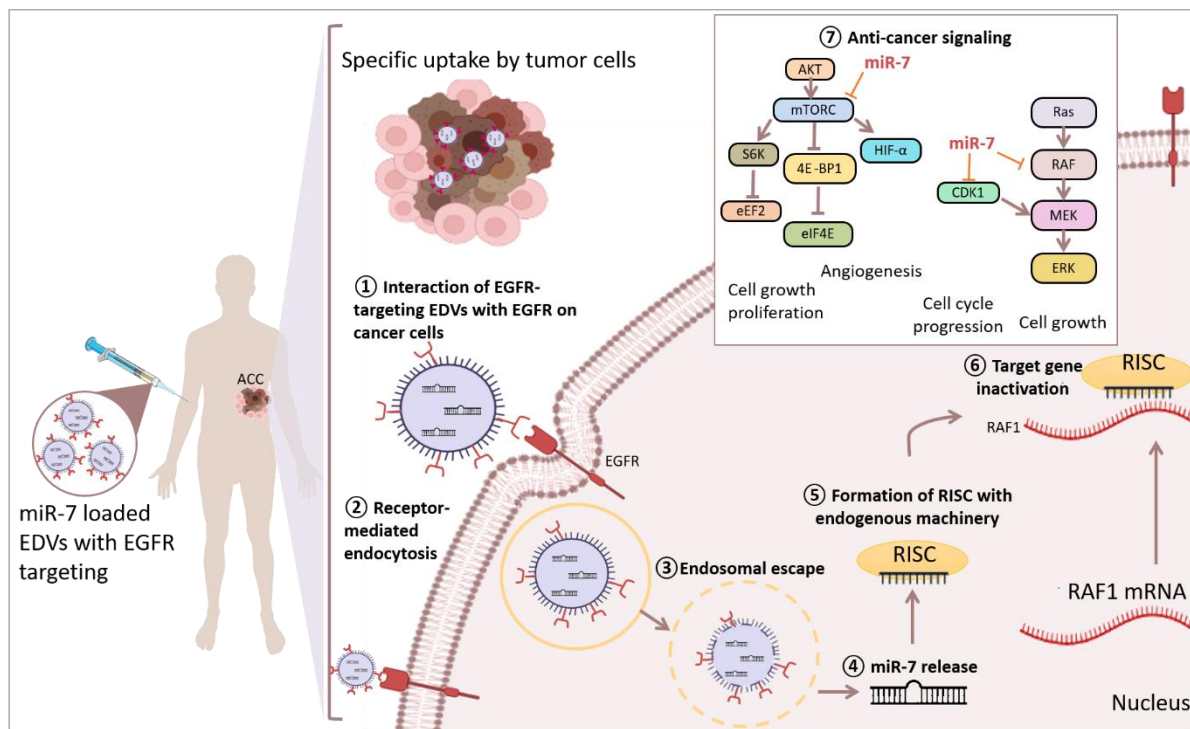


**Figure 22: A proposed model of miR-7 replacement via EDVs in adrenocortical carcinoma.**

Using EnGeneIC Delivery Vehicle miR-7 could inhibit multiple oncogenic pathways including mTOR, MAPK and CDK1 signaling pathways. mTORC: mammalian target of rapamycin Complex; 4EBP1: eukaryotic translation initiation factor 4E- (eIF4E-) binding protein 1; eIF4E: eukaryotic translation initiation factor 4E; S6K: ribosomal protein S6 kinase; eEF2: eukaryotic elongation factor 2; CDK1: cyclin dependent kinase 1.

### III.D. 3.b. Engineered exosomes

Another elegant strategy for drug delivery was inspired by natural exosomes, which shield and convey, among others, miRNAs into the tumor niche. Exosomes are a subtype nanosized extracellular vesicles produced by various cell types. The role of exosomes in intercellular communication via biomaterial transfer without direct cell-to-cell contact has been reported in many studies (258). Exosomes originate from inward budding of multivesicular bodies and

are subsequently released into the extracellular compartment with a plasma membrane encompassing a broad parental cell-derived cargo i.e. nucleic acids, proteins and enzymes. As they innately enter recipient cells with minimal clearance and toxicity, it is worth investing exosomes as vehicles for cancer therapeutics. Recently, Zhou and colleagues customized mesenchymal stem cell-derived exosomes with an englobed Galectine-9 siRNA and an oxaliplatin surface stealth. Injecting these formulations in pancreatic cancer mouse models enhanced immunotherapy outcomes through Immune Cell Death induction (264). Nevertheless, the clinical translation of exosome NPs is still hampered by their complex composition, their modest loading capacity and poor harvesting yields (265). To overcome these issues, Vazquez-Rios et al. took advantage of the existing liposome technology to develop Exosome-Mimetic Nanosystems (EMNs). These nanostructures reproduce cell-derived exosomes structure, physicochemical properties, and loading capacities. In this study, EMNs were engineered with organ specific proteins such as Integrin  $\alpha 6\beta 4$  for the targeted delivery of miR-145 mimics to lung adenocarcinoma cells. In vivo experiments were carried out using intraperitoneal or retro-orbital injection of labeled miR-145-EMNs into nude mice bearing lung tumors. Fluorescence was mainly detected at tumor sites and mild off-target effects were found in the liver and spleen (266).

On the other hand, tumor-derived exosomes are being increasingly explored as delivery systems in cancer research since their identification as drivers of organotropic metastatic spread. Indeed, exosome origins strongly affect cell targeting; thereby exosome-shuttled molecules are selectively captured by certain cell types, but not others (267).

### **III.E. Surface remodeling**

If the choice of a particle's core is essential for drug packaging and release, the control of its surface is just as critical. It is in fact the outer layer of the NP that will allow its interaction with its nurturing environment, hence conveying its cargo to the desired site. In order to improve the biological behavior of nanoparticles, modifications of NP surface properties have been carried out, thus leading to three generations of NPs (Figure 23).

The first generation of NPs consisted of stable colloids in an aqueous medium, such as liposomes. In addition to their intrinsic therapeutic or diagnostic properties, their interest lays mainly in their ability to prevent excretion by the renal system (251).

Indeed, kidney function is based on the filtration through nanometric pores. Thus, the encapsulation of low molecular weight compounds within such vectors makes it possible to avoid renal elimination and to prolong their half-life. However, the size of the NPs should be small enough to evade the finest blood vessels, without sequestration (268).

In fact, longer journey in the blood compartment is still confronted to adsorption of opsonins at NPs surface, resulting in formation of protein corona. Common blood-borne opsonins include immunoglobulins (IgG and IgM), complement (C3, C4, C5) and plasma proteins (albumin, fibronectin), apolipoproteins (269). This surface recognition would trigger phagocytosis by kupffer cells, spleen or lung macrophages, or even circulating macrophages; therefore degrading the NP and its cargo before reaching the target site.

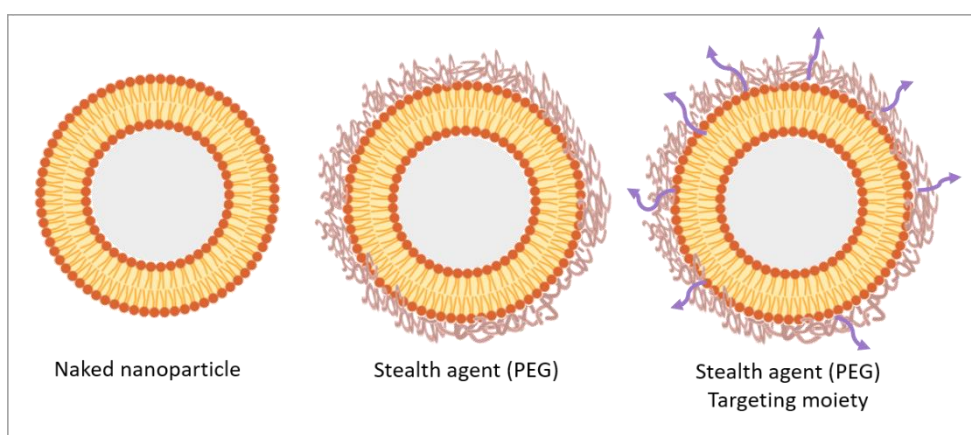


**Figure 23: Evolution of nanoparticles, an example of liposomes.**

(Left) First generation accounts for native naked nanoparticles, which acquired a stealth layer mostly polyethylene glycol in the second generation (middle) for enhanced stability. The third generation (right) is the most complex with targeting agents (i.e. ligands or antibodies) in addition to the pegylated stealth.

Herein has emerged the second line of NPs, which display a protective envelope of polymers such as PEG or dextran. Much work has been done to optimize the percentage of polymers at the surface of NPs, as well as the size and structure of polymer chains. Overall, it has been found that branched chains are more efficient than linear ones, and that a minimal molecular weight of 2000 g/mol is required to clearly improve the blood half-life of NPs (270). Other NPs were designed with biomimetic coatings of “don’t eat me proteins” or leucocyte-derived cell

membranes (271). This surface functionalization prevents phagocytosis of NPs by the reticuloendothelial system, thus increasing the therapeutic index of incorporated drugs. Camouflaged NPs have a bloodstream journey long enough to release their cargo into the blood or to passively accumulate in tissues with discontinued endothelium.

While Enhanced Permeability and Retention is highly appreciated in cancer contexts, the need of specific tissue addressing -without extravasation through the leaky vasculature- gave rise to a third generation of targeted NPs (229). On the stealth polymeric layer are engrafted ligands with known interactions with a given biologic target. Ligands can be antibodies, saccharides, peptides, oligonucleotides or other molecules such as folate (272).

### **III.E. 1. Passive targeting: The EPR effect**

Nanocarriers exhibit tumor-specific accumulation through the Enhanced Permeability and Retention (EPR) effect, a central dogma in cancer nanomedicine. The EPR effect was first described by Maeda in 1986 and was, for the last decades, considered as the “royal gate” for cancer drug delivery (273). Briefly, NPs extravagate from the bloodstream to the tumor via its leaky endothelium holding inter-endothelial gaps reaching 2000nm of size (274) (Figure 24). The rationale of using NPs in oncology relies on their customized engineering and their tunable size to infiltrate through this vascular fenestration (215). In depth understanding of the EPR modality requires knowledge of the tumor pathophysiology and precisely the molecular players involved in neovasculature. During tumorigenesis, cells show anarchic proliferation leading to the formation of a tumor mass, which after reaching 2mm<sup>3</sup>, develops its own network for blood supply via the process of angiogenesis (214). Increased expression of hypoxia inducible factor (HIF) promotes upregulation of pro-angiogenic agents such as platelet-derived growth factor (PDGF), vascular endothelial growth factor (VEGF) or tumor necrosis factor- $\alpha$  (TNF- $\alpha$ ) thus activating endothelial cells towards the angiogenic switch. Subsequently, activated endothelial cells express the transmembrane integrin  $\alpha\beta_3$ , which regulates endothelial cells migration by interacting with extracellular matrix (ECM) proteins fibronectin and vitronectin... In addition, endothelial cells secrete metalloproteinases, which degrade the basement membrane (275). Established tumor vessels are structurally and functionally abnormal in response to imbalanced angiogenic factors. For instance, VEGF and

nitric oxide were shown to increase endothelial gaps in tumor vessels. Also, monitoring metalloproteinases MMP2 and MMP9 is of particular interest as they degrade dense collagen matrix, which may prevent NP penetration to the tumor mass (269).

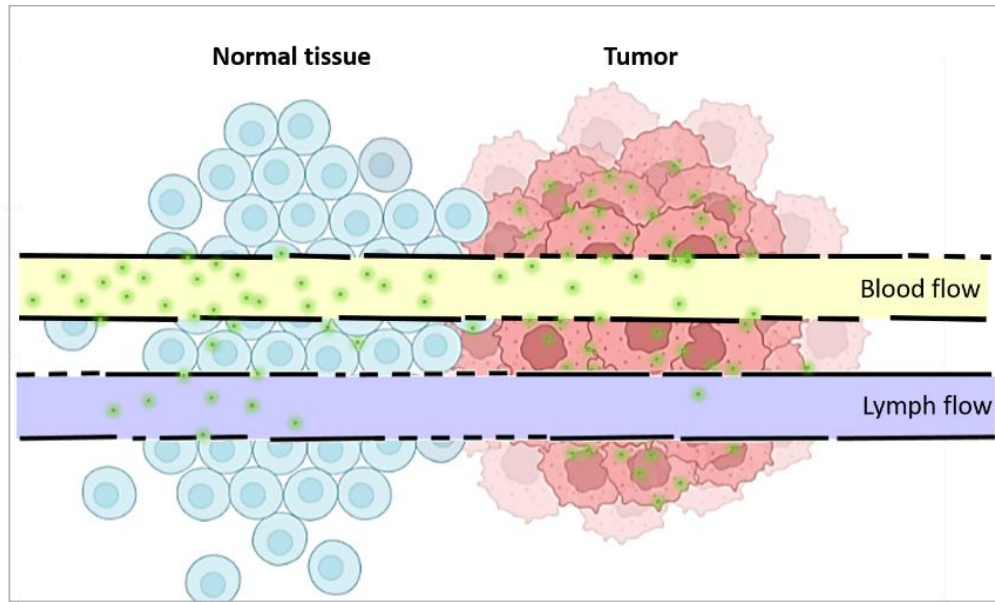


**Figure 24: Simplified representation of the EPR effect.**

In contrast to the tight vasculature of normal tissue, which retains nanoparticles (green dots), the leaky vasculature and defective lymphatics of solid tumors allow for the preferential accumulation and retention of colloidal nanoparticles within the tumor mass.

Moreover, the tumor endothelium shows an unorganized network with a disrupted basal membrane lacking pericytes, thus displaying loose endothelial junctions (276). This vascular loosening enables not only hypoxia and intravasation of tumor cells, but also routing of blood-borne nutrients/compounds towards the tumor. Hyperpermeable vessels, in addition to limited lymphatic drainage, promote permeability and retention of large particles within the tumor mass. This leads to the passive accumulation of NPs in the tumor core (277).

The EPR effect therefore relies on (1) Nanometric size of NPs enabling their escape from the renal system; (2) Prolonged plasmatic half-life of the nanoformulations thanks to surface stealth; (3) Architectural deregulations of tumor vessels; (4) Low lymphatic efflux resulting in NPs retention in the tumor.

Though rising mount of studies claim EPR likeliness, the reliability of the EPR effect in human patients has been recently debated as the extent of nanocarriers accumulation varies profoundly between patients and tumor types (215). The differences in tumor vasculature

between humans and rodents should not be neglected; this may justify the discordance between preclinical success and their non-translation to clinics. Indeed, EPR is the gold standard mode of drug diffusion towards most tumors, but it strongly depends on the tumor vascularization state which is foremost implied by its anatomic site (278); prostate and pancreatic cancers are examples of hypovascularized tumors not reachable by EPR. Along the same line, it has been shown that the tumor microenvironment (pH, multidrug resistance, diffusion/ convection, flow pressure...) tightly influences the EPR effect (Figure 25). The mechanism by which NPs enter solid tumors appears more complex than previously thought and probably involves active trans-endothelial pathways (274). The EPR-dependent drug delivery is compromised by high tumor interstitial fluid pressure and poor blood flow inside human tumors, thus resulting in non-homogeneous uptake of NP in tumors (269). Liver and spleen remain the first accumulation sites for nanoparticles due in part to their fenestrated endothelium. Thus, these organs are major barriers to clinical translation of nanomaterials administered intravenously (279). Understanding the mechanisms behind this accumulation more extensively will help develop new strategies for tumor targeting and liver or spleen escape.

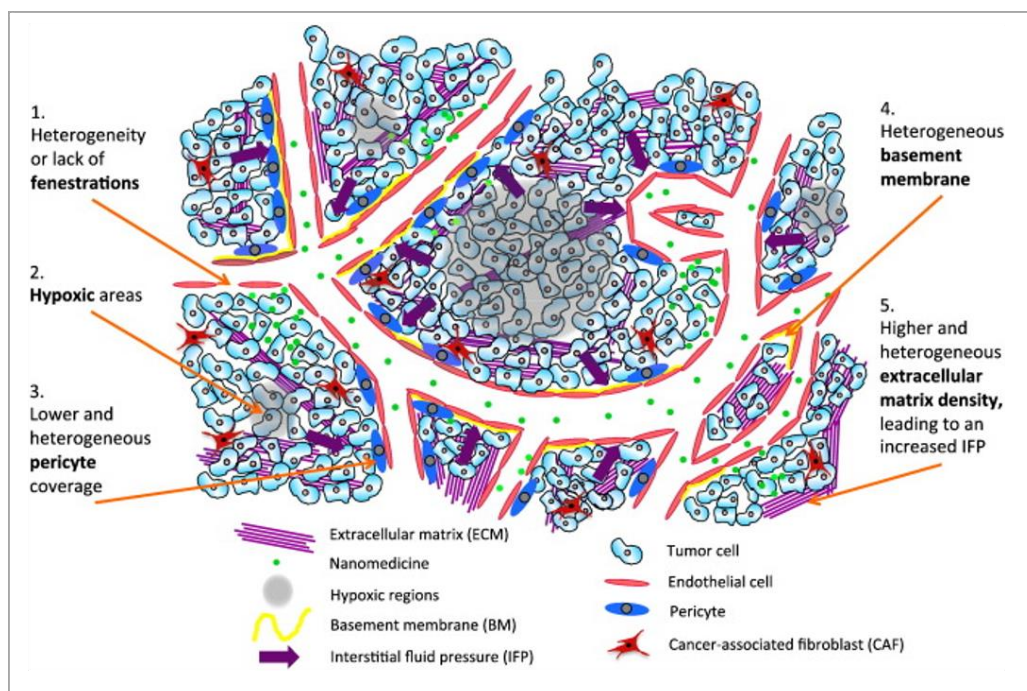
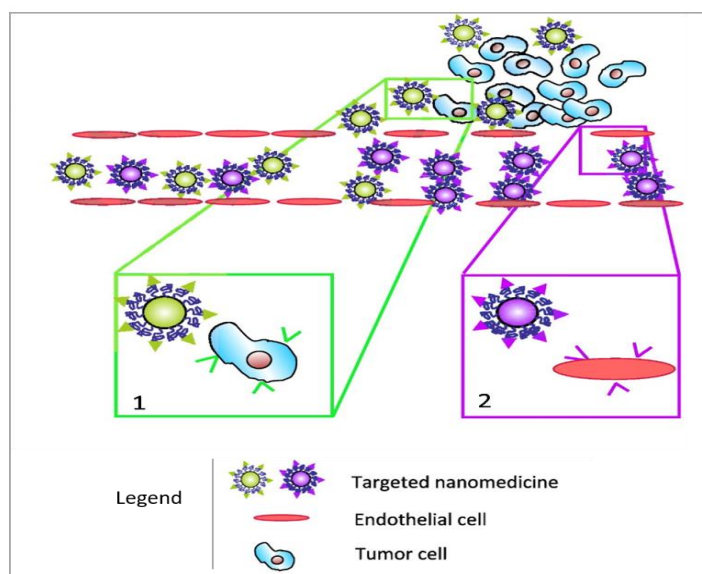


Figure 25: Characteristics of the tumor microenvironment behind the EPR effect in humans. Adapted from Danhier 2016

### III.E. 2. Active targeting

Active targeting involves surface engrafted ligands, which preferentially guide the NP to its target. Peptides, antibodies or saccharides are therefore displayed on NPs surfaces to favor their recognition by cellular receptors, hence their endocytosis and cargo discharge. However, adding these molecules directly to the surface of nanoparticles generally provokes their discarding by macrophages. Hence, it is important to pair targeting moieties with stealth agents i.e. PEG in order to avoid uptake by immune cells. Moreover, the formation of a steric barrier risks masking the ligands, thus rendering active targeting obsolete. To overcome this issue, ligands are separated from the core of the NP via a spacer arm (most often a polyoxyethylene chain) (280). Apart from immune evasion, this linker enhances NPs motility to maximize the likelihood of encountering its target site.

According to the chosen ligand, active targeting is achievable at two cellular levels: cancer cells and tumor endothelium (Figure 26).



**Figure 26: Active targeting of cancer cells or tumor vessels via surface-functionalized nanoparticles.**

Since the EPR effect is not yet achievable in clinics, nanoparticles may be actively guided to (1) cancer cells or (2) tumor vessels via their surface chemistry holding ligands or antibodies, which specifically bind to cancer-overexpressed receptors.

The idea of actively addressing NPs to the tumor is to take advantage of endocytosis-prone receptors specifically overexpressed at the surface of cancer cells, by presenting its ligand at the outer shell of nanocarriers (214). The enhanced internalization of NPs is thus responsible



of the anti-cancer effects regardless of passive accumulation via vascular fenestrations. Figure 27 depicts frequently targeted receptors, which include:

- Epidermal growth factor receptor (EGFR), a member of the tyrosine kinase receptor family ErbB. EGFR is overexpressed in several solid tumors like lung, colorectal, kidney, adrenal, pancreatic cancer where it activates key pro-cancer signaling (281). EGFR targeting was well exploited in miRNA therapeutics; Yang et al. demonstrated that packaging miR-135a within anti-EGFR coated liposomes exhibited a promising anti-cancer efficiency in gallbladder cancer (254).
- Transferrin receptor is a serum glycoprotein involved in iron homeostasis and cell growth. It is about a 100-fold overexpressed in cancer contexts, thus it is an attractive target for cancer therapy. For example, decorating NPs with transferrin ligands was proved efficient to vehiculate drugs through the blood brain barrier (282). In the context of miRNA therapeutics, miR-29b targeting via transferrin-conjugated lipoplexes resulted in longer survival in mice with acute myeloid lymphoma (283).

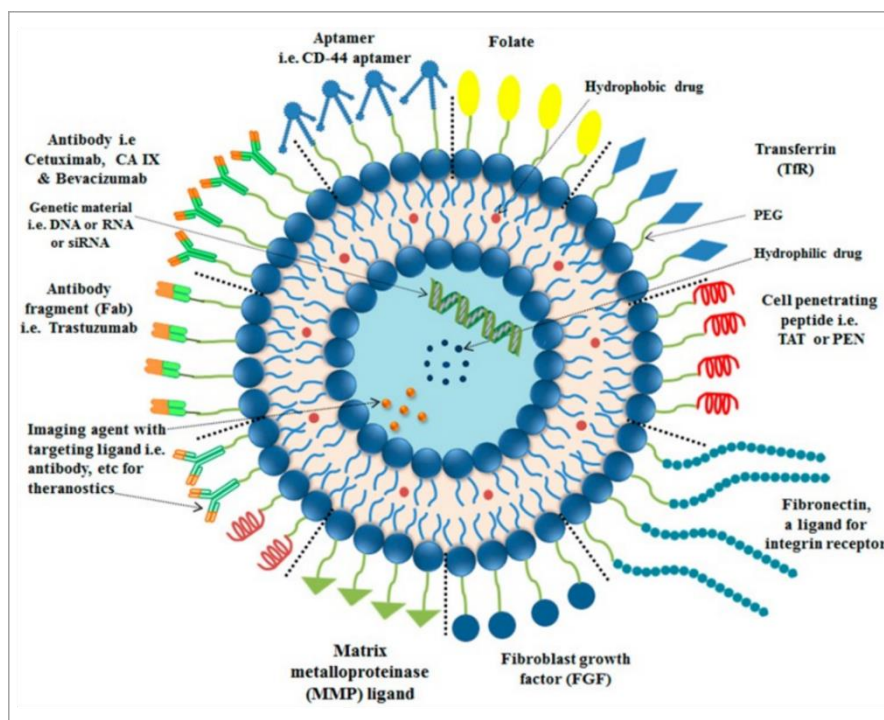


Figure 27: Surface engineering strategies for liposome active targeting.  
Adapted from Riaz et al. 2018

- Folate receptor is a well-known tumor marker expressed in 40% of human cancers. It engulfs folate-coupled NPs to the cellular compartment through receptor-mediated endocytosis. Interestingly, by modifying the miRNA backbone, Orellana et al. generated vehicle-free strategies namely FolamiR, consisting of miR-34a mimics stabilized by folate chains. This formulation was quite impressive in terms of tumor shrinkage in breast and non-small-cell lung cancer models (284).

Another strategy to arrest tumor growth is to cut off its blood supply of oxygen and nutrients. In this approach, ligand-targeted NPs bind then destroy the tumor vascular network (214). Targeting tumor vascularization presents several advantages: (1) It excludes the necessity of NP extravasation to attend the desired site, (2) The in situ systemic injection of active-targeted NPs makes it easier to associate the receptor with its ligand, (3) It is applicable on a large spectrum of tumors, since endothelial markers are ubiquitously expressed, no matter the tumor type. Among the most addressed endothelial receptors, we can cite:

- $\alpha\beta3$  integrin which is strictly expressed by neovessels as a receptor for ECM proteins. It is implicated in endothelial migration in a calcium dependent manner. RGD oligopeptide (Arg-Gly-Asp) binds with high affinity to endothelial integrin  $\alpha\beta3$  (285). RGD gold NP having encapsulated miR-320a-3p showed a dramatic inhibition of growth and proliferation of lung cancer, both in vitro and in vivo (286).
- Vascular endothelial growth factor (VEGFR) and its ligand VEGF are central actors in neovascularization. VEGFR is overexpressed in endothelial cells under hypoxic conditions rendering targeting this receptor appealing for nanotechnology (287). Besides competing with VEGF binding, the aim of VEGFR-targeting NPs is to trigger the endocytic pathway for cargo release (214).
- MMPs are a family of proteinases that degrade ECM and contribute to angiogenesis. Several MMPs particularly Membrane type 1 matrix metalloproteinase (MT1-MMP) are expressed in tumor endothelial cells in response to hypoxia. Anti-MT1-MMP-tailored liposomes enhanced doxorubicin uptake by fibrosarcoma cell lines (285).

### **III.F. Cellular internalization and cargo discharge**

After extravasation, NPs are internalized by their recipient cells, where they exert their therapeutic function upon delivering their content to cytosolic or nuclear targets. While small

hydrophobic drugs can simply cross the lipid cell membrane by passive diffusion, supramolecular nanoformulations often require active convection within interstitial fluids to reach the intracellular compartment. Basically, nanocarriers can be internalized through direct interaction with membrane receptors, or through fusion with the phospholipid bilayer of recipient cells. Electrostatic interactions may also favor NP internalization through pinocytosis within vesicles of extracellular fluid (288).

The mechanisms of cellular uptake tightly depend on the NP itself; surface charge -hence its interaction with plasma membrane- is a major parameter to consider (289). Though charge-mediated internalization occurs in a tissue specific manner, positive nanocarriers were shown to exert better homing to tumor cells than their negative counterparts because of the negatively charged plasma membrane. This lead many groups to adopt a charge-conversion strategy by engineering NPs with zwitterionic biomaterials prone to external stimuli such as pH (290). Briefly, upon blood evasion, low tumor pH discards the stabilizing anionic elements of NPs, therefore leaving a positive surface charge, favoring cell entry (269). Low tumoral pH provokes NP instability, hence release of the entrapped nucleic acids payload.

There are energy-dependent and energy-independent modalities for cell internalization. Active cellular internalization calls out for NP engulfment via endocytosis, which englobes phagocytosis and pinocytosis depending on the size and nature of ingested particles. Phagocytosis strictly concerns immune cells performing their pathogen-discarding function, whereas pinocytosis is a common mechanism allowing cellular ingestion of molecules like NPs. To date, four pinocytic mechanisms were proposed for NP internalization. These differ by the size of the vesicle, its internal coating and fate after molecule internalization (289).

- Macropinocytosis is a non-specific form of endocytosis, the course of which varies according to the cell type. Macropinosomes generally acidify, then shrink and redirect the internalized particles towards degradation via endo-lysosomal routes. Though this endocytic pathway does not display selectivity, it is involved, among others, in the uptake of drug-loaded vectors.
- Clathrin-mediated endocytosis is the classic gateway for NP uptake. This pathway internalizes molecules in clathrin-coated invaginations that eventually detach from the cell membrane in a GTP-dependent mode to form the so-called clathrin vesicles. Herein, these vesicles deliver their cargo to early endosomes, which are then acidified and matured into

late endosomes. The latter fuse to lysosomes and create a harsh environment for the internalized cargo. The main challenge for bioactive molecules is therefore to escape the endo-lysosomal digestion.

- Receptor-mediated endocytosis often calls out for clathrin coated pits. Intake through this pathway is ideal for ligand-tailored nanocarriers, thus enabling their internalization upon receptor endocytosis.
- Caveolae-mediated endocytosis internalizes NPs into caveolin-1-coated endosomes resulting from membrane pinching. Caveolae is a non-acidifying, non-digesting pathway, but it is not exempted from lysosomal control.

Other non-clathrin/caveolae dependent pathways were also proposed. They require cholesterol and a specific lipid composition, but still lack complete knowledge of the exact mechanism of action (291). Figure 28 represents the cellular uptake mechanisms for miRNA encapsulating NPs.

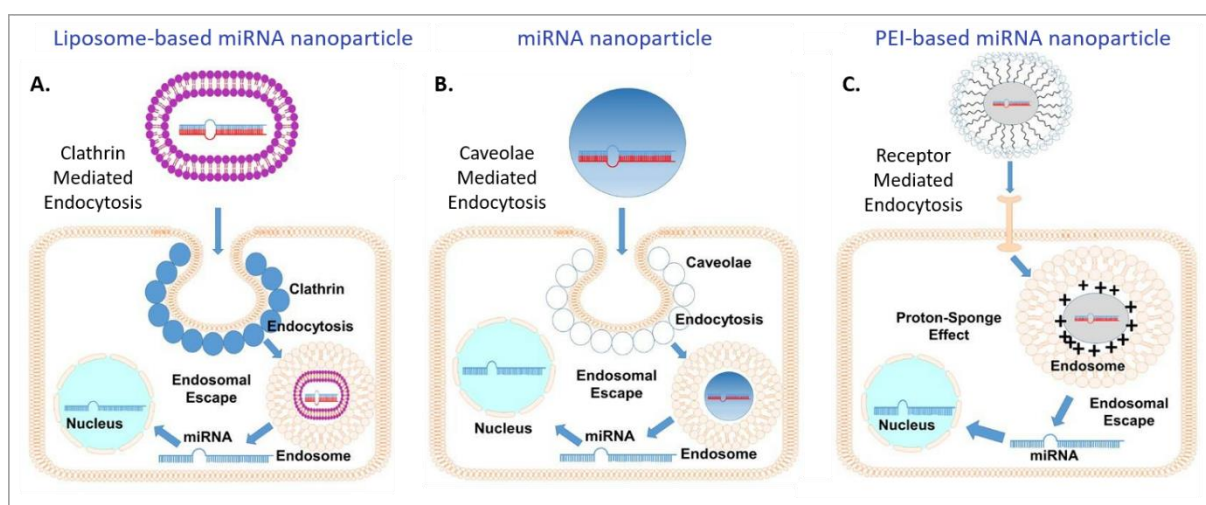


**Figure 28: Possible routes for miRNA nanoparticles cellular uptake.**

Active nanoparticle internalization involves their endocytosis into (A) clathrin or (B) caveolae coated pits which may also be aided by (C) receptor endocytosis if the nanoparticle is functionalized by a specific ligand. Release of miRNA from nanoparticles is promoted by the proton-sponge effect. MiRNAs are delivered to the cytoplasm or nucleus. Adapted from Ganju et al. 2017

Considering the hostile conditions within endo/lysosomes, **endosomal escape**, thus lysosomal avoidance is mandatory for optimal performance of the engulfed biomolecules (i.e. miRNAs). A viable strategy to prompt endosomal escape is to engraft membrane-destabilizing peptides such as GALA and INF7 at the outer of NPs (292). Moreover, introducing cationic polymers like

PEI in NP design outstandingly improved endosomal escape, thus intracellular trafficking of loaded therapeutics (269). Following endocytosis, PEI undergoes protonation of its amine groups within endosomes and thereby exerts a **proton-sponge** effect Figure 29. Proton accumulation, due to endosome acidification, triggers cytosolic water towards the endosomes, leading therefore to osmotic swelling, endosome bursting, and polyplex release into the cytosol (246).

Lipid NPs could evade endosomal traps through the “**flip-flop**” mechanism. Fusion of internalized lipoplexes with the endosomal membrane results in an exchange of negatively charged phospholipids from the cytoplasmic to the inward compartment of endosomes (293). Such local disruptions destabilize endosomal lamellar membrane and provoke the release of nucleic acids into the cytosol (Figure 29 right panel). However, using experimental observations and computational modeling, Gilleron et al. showed that only 2% of siRNA cargo successfully escapes endocytic vesicles, at a time frame where LNPs reside in early or late

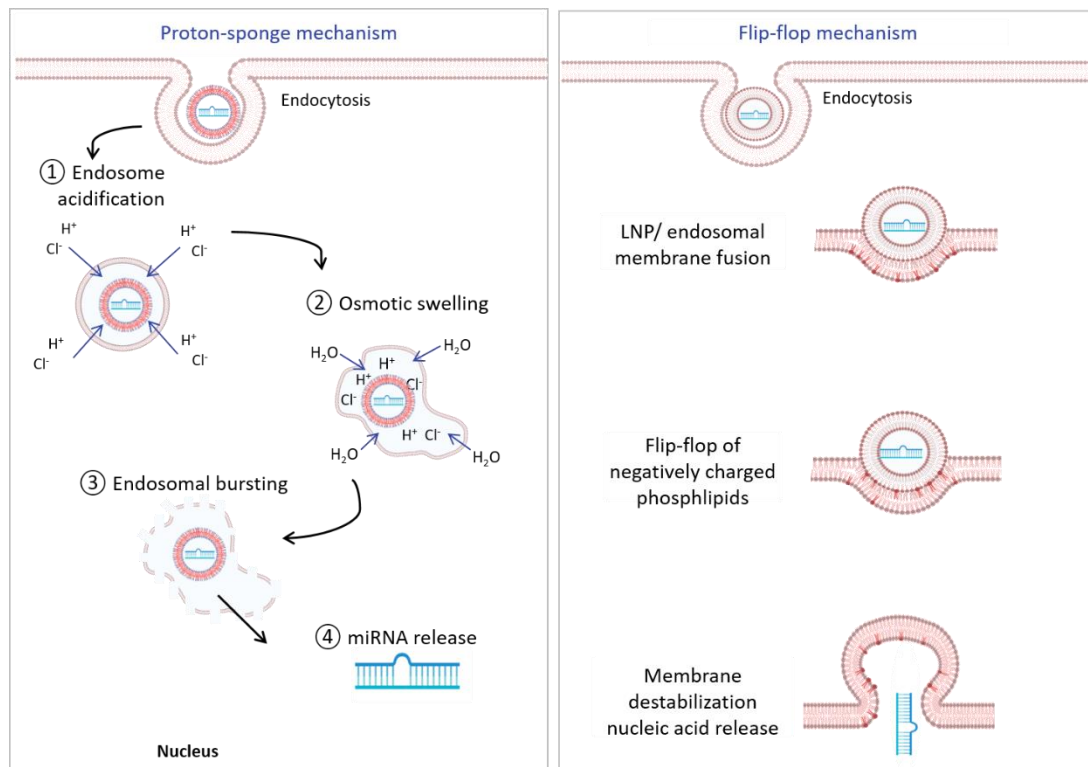


**Figure 29: Mechanisms of endosomal escape.**

Polymeric nanoparticles such as PEI shuttle their cargo to the cellular cytosol by a Proton-sponge manner (Left panel). After endocytosis, acidification of the endosomes causes osmotic swelling by the flux of water, therefore leading to endosomal burst and cargo release. Lipid nanoparticles (LNP) may simply fuse to the endosomal membrane (Right panel) then induce a charge exchange known as the flip-flop mechanism. As a result, membrane instability provokes nucleic acid leakage.

endosomes (294). This low release efficiency suggests that bioactive doses for miRNA therapy are still complex to set, since introducing a non-active dose or a potentially toxic dose is not recommended.

The next step in nucleic acid delivery is their cytosolic trafficking towards the desired intracellular compartment. For nucleic acids with cytoplasmic activity such as siRNA and miRNA, there are no translocation barriers after endosomal escape. Simply, internalized RNAi hybridize to their complementary mRNA in a sequence specific-manner, thereby blocking its translation or favoring its cleavage (295). However, larger molecules such as pDNA are prone to digestion by nucleases because of their reduced cytoplasmic mobility, thus limiting their effective bioavailability. Nuclear activity demands an additional transnuclear passage enabled by membrane disruptions during cell division. For non-dividing cells, exogenous nucleic acids are incorporated via the nuclear pore complex (296).

### **III.G. Challenges for miRNA nanotherapeutics**

Over the last decades, rising mount of studies have shed the light on siRNAs' clinical relevance. The RNAi breakthrough was recently crystallized in therapeutic contexts when Patisiran and Givosiran (Alnylam Pharmaceuticals), two siRNA-based compounds, were approved by the FDA in 2018 and 2019 for respective treatment of hereditary transthyretin-mediated amyloidosis and acute hepatic porphyria (297, 298). Nearly 60 siRNA drugs attained phase I, II, or III of clinical evaluation; fifteen of them were dedicated to the treatment of cancer (Table 7).

Despite reported advancements in clinical setup, several siRNA-based studies were halted, indicating that there are still challenges to overcome before clinical adoption of RNAi-based therapies. These challenges are even more pronounced for miRNA-based therapies (213). Indeed, translating miRNAs from bench to bedside is subjected to stringent criteria within the classical drug discovery workflow (Figure 30).

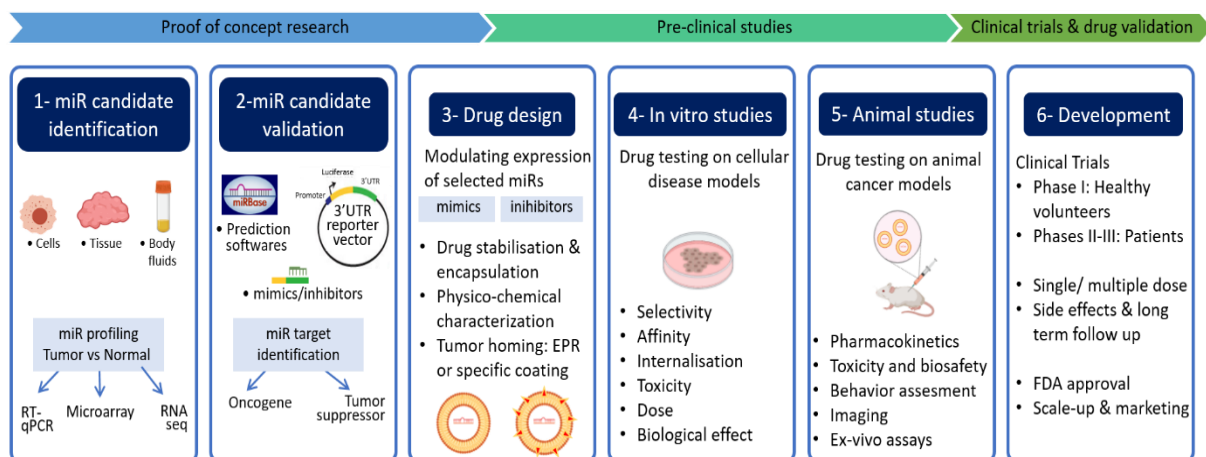


**Figure 30: Translating miRNA biology from bench to bedside in cancer.**

Development of miRNA therapeutics consists of 3 main levels: proof of concept research, preclinical studies, and clinical trials. (1) Identification of candidate miRNAs for therapy. MiRNA expression is quantified in tissue, cells, or body fluids of healthy and tumor specimens (RT-qPCR: Reverse Transcription-quantitative PCR; RNA-Seq: RNA sequencing). (2) Potential targets of differentially expressed miRNAs can be identified using target prediction softwares and validated in reporter gene assays vectors using target transcript 3'-UTR cloned downstream of luciferase reporter and miRNA mimics/inhibitors. (3) Design of therapeutic miRNA requires stabilization and encapsulation of miRNAs in well characterized carriers. (4) Evaluation of the effects of miRNA-loaded nanocarriers on several biological processes in cancer cell models (5) Therapeutic miRNA candidates are tested in animal cancer models alongside animal behavior and recovery before the evaluation of the antitumor effects. (6) Initiation of clinical trials requires a careful assessment of efficacy and toxicity in pre-clinical studies. Doses and side effects are particularly monitored for FDA approval and treatment scale-up.

Drug name	siRNA target(s)	Current status	Condition(s)	Manufacturing company
ONPATTRO (Patisiran, ALN-TTR02)	TTR	Approved	Transthyretin (TTR)-mediated amyloidosis	Anylam Pharmaceuticals
Givlaari (Givosiran, ALN-ASI)	ALAS-1	Approved	Accute hepatic porphyrias	Anylam Pharmaceuticals
Fitusiran (ALN-AT3sc, ALN-APC, SAR439774)	Thrombin	Phase III	Hemophilia A/B	Anylam Pharmaceuticals
Vutrisiran (ALN-TTRsc02)	TTR	Phase III	Transthyretin (TTR)-mediated amyloidosis	Anylam Pharmaceuticals
Tivanisiran (SYL1001)	TRPVI	Phase III	Ocular pain, dry eye	Sylentis, S.A.
Lumasiran (ALN-GO1)	HAO1	Phase III	Primary hyperoxaluria type 1 (PH1)	Anylam Pharmaceuticals
Inclisiran (ALN-PCSc)	PCSK9	Phase III	Hypercholesterolemia	Anylam Pharmaceuticals
Vigil vaccine (FANG, vigil, vigil EATC)	Furin	Phase III	Breast cancer (III), ovarian cancer (II), colorectal cancer (I), Ewing's sarcoma (II), metastatic melanoma (II), metastatic non-small-cell lung cancer (II), solid tumors (I)	Gradalis, Inc.
QPI-1002 (I5NP)	p53	Phase III	Delayed graft function (III), acute kidney injury (II)	Quark Pharmaceuticals
DCR-PHXC	LDHA	Phase III	Primary hyperoxaluria	Dicerna Pharmaceuticals
ARO-HBV	HBV gene	Phase II	Hepatitis B	Arrowhead Pharmaceuticals
PSCT19 (MiHA-loaded PD-L-silenced DC vaccination)	PD-L1/PD-L2	Phase II	Hematological malignancies	Radboud University
Cemdisiran (ALN-CC5)	C5a Receptor	Phase II	Paroxysmal nocturnal hemoglobinuria (PNH)	Anylam Pharmaceuticals
STP705 (cotsiranib)	TGF- $\beta$ 1 and COX-2	Phase II	Hypertrophic scar (wound healing)	Sirnaomics
SYL040012 (bamosiran)	ADRB2	Phase II	Open angle glaucoma, ocular hypertension	Sylentis, S.A.
Lentivirus vector CCR5 shRNA	CCR5	Phase II	AIDS-related lymphoma	AIDS Malignancy Consortium
Cal-1 (LVsh5/C46, Cal-1 modified HSPC, Cal-1 modified CD4 + T lymphocytes)	CCR5	Phase II	HIV/AIDS	Calimmune Inc.



PF-655 (PF-04523655)	RTP801	Phase II	Diabetic macular edema (II), age-related macular degeneration (II)	Quark Pharmaceuticals
----------------------	--------	----------	--	-----------------------

**Table 7: Some of the reported siRNA-based clinical trials.**

To date, only ten miRNA-based drugs have entered clinical trials with none of them reaching phase III and half of them being suspended (Table 8).

Drug name	miRNA	Current status	Condition(s)	Manufacturing company
Lademirsen (SAR339375, RG-012)	miR-21	Phase II	Alport syndrome	Genzyme
MRG-201 (Replarsen)	miR-29	Phase II	Keloid	miRagen Therapeutics, Inc.
RG-125 (AZD4076)	miR-103/107	Phase II	Nonalcoholic fatty liver disease	AstraZeneca
MRG-106	miR-155	Phase I	Lymphoma; leukemia	miRagen Therapeutics, Inc.
MRG-110	miR-92a	Phase I	Skin excisional wound	miRagen Therapeutics, Inc.
MesomiR 1	miR-16	Suspended	Malignant pleural mesothelioma; NSCLC	Asbestos Diseases Research Foundation
Miravirsen	miR-122	Suspended	Chronic hepatitis C	Santaris Pharma A/S
RG-101	miR-122	Discontinued	Chronic hepatitis C	Regulus Therapeutics Inc.
pSil-miR200c and PMIS miR200a	miR-200a/c	Discontinued	Tooth extraction	University of Iowa
MRX34	miR-34a	Discontinued	Melanoma; primary liver cancer; hematologic malignancies	Mirna Therapeutics, Inc.

**Table 8: Reported miRNA-based compounds in clinical trials**

The first miRNA-based drug admitted for clinical trials was an antagomiR targeting miR-122, namely Miravirsen, developed by Santaris Pharma as a therapy against Hepatitis C Virus (HCV) infections (Santaris Pharma, Roche Pharmaceuticals). Miravirsen efficiently reduced viremia in patients infected with HCV [155–157] and subsequently underwent multiple phase II clinical trials (NCT01200420, NCT01872936, NCT02031133, NCT02508090). Regulus Therapeutics

established another miR-122 inhibitor, RG-101, an N-acetyl-D-galactosamine-conjugated antagomiR which showed considerable efficacy in patients with HCV. However, the emergence of severe hyperbilirubinemia led the FDA to discontinue the trial, thus suggesting that miRNA refinement or packaging must be carefully revised for optimal therapeutic outcomes. In cancer contexts, MRX34, a first-in-class cancer therapy manufactured by miRNA Therapeutics was delivered as a mimic of miR-34 encapsulated into a liposomal NP (NOV40). MRX34 exhibited a strong activity in hepatocellular carcinoma, melanoma, NSCLC, and renal carcinoma (NCT01829971). Unfortunately, the phase I trial was halted due to multiple immune-related complications. Despite so far deceiving patient outcomes, miRNA therapeutics are still under clinical investigation, awaiting their Eureka moment. Biopharmaceutical companies are pouring their efforts to develop and commercialize safe miRNA-based compounds for cancer treatment. MiRagen Therapeutics is performing clinical trials of MRG-106 (Cobomarsen, an inhibitor of miR-155) for the treatment of lymphomas and adult T-cell leukemia/lymphoma (NCT02580552, NCT03713320). EnGeneIC is currently testing TargomiRs as 2nd or 3rd Line Treatment for patients with recurrent malignant pleural mesothelioma and non-small cell lung cancer (NCT02369198).

Discordance between reported preclinical hopes and their non-translation into the clinics is justified by numerous issues still hindering miRNA therapeutics, i.e. delivery platforms, administration routes, dosage concerns and off-target effects.

It is now clear that oligonucleotide drugs are subjected to nuclease digestion with a bloodstream half-life of only a few minutes. As discussed earlier, nanotechnologies provided versatile platforms to tackle obstacles related to miRNA shuttling, with the ultimate aim to increase their therapeutic index while minimizing undesired toxicities. Indeed, it is crucial to fully characterize miRNA-loaded NPs before going further with treatment evaluation. Unfortunately, we cannot anticipate the clinical behavior of most nanosystems, as they have not yet been tested in humans. Accurate pharmacokinetic follow-ups of ADME (absorption, distribution, metabolism, and excretion) in animal models may provide a basis for how miRNA mimics/antimiRs might act in humans. Hence, for pre-clinical as for clinical usages, miRNA-delivering vectors should demonstrate functional and biocompatible properties inherent to their constitutive biomaterials, interacting both with their miRNA payload and with recipient

cells. Biocompatibility is achievable thanks to the malleability of synthetic biomaterials, which are custom-tailored for surface functionalization, high active payload, and reduced toxicity. MiRNA mimics or inhibitors are hereby shielded all the way from the injection site to the targeted tissue, in a scenario mirroring natural miRNA shuttling within exosomes.

Moreover, particles' integrity should be regularly controlled via their average diameter and polydispersity index, which widely influence their pharmacological performance i.e. biodistribution, circulating half-life and clearance. Other properties related to charge, shape and surface chemistry are also key determinants for NP fate. In fact, a single nanocarrier is processed to integrate coatings, targeting agents, as well as bioactive miRNA, thus demanding highly complicated steps. These physicochemical complexities certainly contribute to the slow clinical translation of miRNA-based formulations, since they hamper large-scale manufacturing by the pharmaceutical industry. Simplified NP designs should allow efficient and reproducible scale-up for better market access. In addition, conceiving ingestible miRNA pills is obviously a gateway towards easier patient prescriptions, as currently proposed nanoformulations are administrated via intravenous or subcutaneous routes.

Tumor homing via the so-praised EPR of NPs is contested due to the heterogeneous nanocarrier accumulation between different individuals and tumor types. Intratumor pressure and hypoxia were shown to weaken EPR potencies. In fact, the EPR effect is more complex than previously described, and seems to recruit active trans-endothelial pathways rather than simple intravasation through the leaky tumor vasculature. Liver and spleen also entrap NPs via their fenestrated endothelium, thus limiting NP supply to tumor foci. Accordingly, EPR effect, alone, is not sufficient to drive NPs towards the tumor mass; NP composition and active targeting guide selective tissue uptake.

Other challenges are related to the miRNA itself, as most commercial miRNA mimics/antimiRs harbor chemical modifications in their size or sequence for enhanced stability and engraftment efficiency. Modifying miRNA backbones may introduce variations in their activity and pharmacokinetics, thus it is crucial to evaluate each miRNA candidate apart from its harboring vector.

However, the major miRNA-linked concern remains the choice of the dosage and injection route. The therapeutic window to be adopted should take into account NP leakage, thus miRNA loss during bloodstream journey, in addition to low release efficiency from the NP. The perfect anti-miRs posology should achieve total sequestration of endogenous miRNA, thus relieving the repression of confirmed target genes, whereas the defined concentration of miRNA mimics should induce physiological miRNA restorations capable of efficient silencing of a limited panel of targets. An overdose of miRNA mimics/inhibitors is accompanied by an over-amplification of off-target complications with potential life-threatening consequences. Preclinical cell and animal studies should guide the dose choice for phase I/II trials while respecting species-inherent variables such as injection volumes and blood pressure. This underlines the importance of conducting dose-defining studies in large animal models such as non-human primates to fill the gap between preclinical research in mouse cancer models and clinical research in cancer patients.

It is reasonable to expect that improvements in target prediction tools and experimental validation of true miRNA targets might help solving dosing issues. Deciphering targeted networks of a candidate miRNA drug enables anticipating its possible off-target effects, thus evaluation of the benefit/risk balance for appropriate payload determination. In their study, Zhang et al. concluded that the serious immune-related complications that led to the discontinuation of MRX34 were due to a “too many targets for miRNA effect” (TMTME) on several genes involved in cytokine and interleukin cascades (213). A combination of tissue specific knockouts and advanced molecular biology techniques will allow us to determine miRNAs target-selectivity and will help define the specific contribution of a single miRNA to a given biological pathway in different tissues. This will have major impacts on posology setup for clinical trials in attempt to minimize ineffective and potentially toxic over exposures.

On the other hand, the field of nanomedicine is submerged with novel formulations, which makes it hard to appreciate benefits of one nanosystem compared to another. The lack of framed regulatory and safety guidelines for quality control and good manufacturing practices has delayed the clinical shifting of these products. Indeed, the miRNA-NP combination is still "exotic" for the cancer therapy world; hence, research outcomes should be interpreted with caution. Standardization and simplification of NP architecture could be a milestone for the evaluation of miRNA drugs by regulatory authorities.

The cost-benefit ratio is another limitation to the clinical translation of miRNA-based therapies when compared to existing anti-cancer compounds. This owes to the high costs of miRNA research products added to the structural complexity facing purification of innovative NPs. The fact that each country's healthcare system is unique poses a burden for pharmaceutical companies looking to invest on a global scale. Financial constraints and a lack of socioeconomic validation studies may neutralize innovative advances. This suggests that in the next years, only developed nations will be able to improve miRNA-based therapeutics programs. North America is predicted to stay at the forefront and retain the top position in the global miRNA market among all nations. This is due to the rising number of miRNA clinical trials launched in the United States to find new treatment options. In Europe, growing government funding for the startups for R&D activities to develop novel miRNA-based therapies might allow the region to hold the second position in the market.

## **Chapter IV. Lipidots, novel platforms for nucleic acid delivery**

After discussing the major developments in nanomedicine, we move on to the core of this thesis work, which engaged experimental assessments of Lipidots® as miRNA delivery platforms. This chapter exposes the current state of knowledge concerning Lipidots, innovative lipid nanoparticles patented by CEA-LETI more than a decade ago. We describe their components and manufacturing process.

## IV.A. Definition

Lipidots, also denoted LNPs (for lipid nanoparticles), are nanoparticles of the nanostructured lipid carrier (NLC) type consisting of a semi-crystalline lipid core supported by a surfactant crown. The core of LNP is a combination of solid lipids (wax) and liquid lipids (oil), while the surfactant crown is made up of amphiphilic phospholipids and PEG polymer chains. Of note, the oil/wax mixture within the LNP core results in imperfect crystallization allowing the encapsulation of biomolecules such as fluorophores (299). The LNPs' composition was optimized to produce particles with high colloidal stability and a size adjustable from 30 to 200 nm by varying the ratios of the various ingredients. Most importantly, each of the biomaterials needed to synthesize LNPs are Generally Recognized As Safe (GRAS) with an FDA authorization for human use. As a result, LNPs are biocompatible and usable *in vivo* (300). Furthermore, the PEG coating on the LNP surface provides them a stealthy protection for an extended circulation.

LNPs were initially conceived for use in fluorescence imaging. Indeed, these vectors may encapsulate lipophilic fluorophores, improving their optical properties and half-life (301). Tracking LNP fluorescence allowed researchers to follow their biodistribution pattern *in vivo*. After intravenous injection, LNPs naturally accumulates in the liver, lymph nodes, spleen, and steroid tissues (302). Moreover, due to EPR effect, LNPs tend to passively accumulate in subcutaneous tumors, rendering this system extremely useful for malignancy detection (303, 304). Recently, with the rise of nanomedicines, the LNP application has expanded to include drug delivery and vaccine formulations owing to their virtues in terms of stability, safety, and *in vivo* behavior (305, 306).

## IV.B. Constitutive components

### IV.B. 1. Surfactants

LNPs are oil-in-water nanoemulsions, with oil as the dispersed phase and an aqueous solution as the continuous phase. Emulsification is the process of finely dispersing the oily phase in the aqueous phase in the form of droplets of a few tens of nanometers in diameter. Lipid droplets are often stabilized by a layer of surfactants serving as an interface between the dispersed and continuous phases. This layer is made up of lecithin and pegylated surfactants (Figure 31).

#### IV.B. 1.a. Lecithin

Lecithin or phosphatidylcholine is a mixture of natural amphiphilic molecules mostly consisting of phospholipids. Phospholipids are the primary constituents of lipid bilayers that form cell membranes; they are also biocompatible in addition to their emulsifying capabilities. Thus, they confer the nanoemulsions a certain biomimicry with lipoproteins and cells, allowing the particles to be more resilient once suspended in the bloodstream. The lecithin implemented in the formulations is derived from soybeans (Lecithin S75); hence, the fatty acid content is comparable to that of triglycerides in soybean oil, mainly unsaturated fatty acids with 18 carbon atoms (307). For cationic LNPs, quaternised cationic lipids, such as 1,2-dioleoyl-sn-glycero-3-phosphoethanolamine (DOPE) and 1,2-dioleoyl-3-trimethylammonium-propane chloride (DOTAP) are also added to the phospholipids monolayer (308).

#### IV.B. 1.b. Polyethylene glycol

As previously mentioned, the main aim of implementing a PEG stealth into NPs is to provide another degree of complexity, in order to evade the biological defense systems. Pegylated surfactants are synthetic nonionic amphiphilic compounds with polyoxyethylene units in their hydrophilic portion (POE or PEG). These chains are either linear, as in the case of polyoxyethylene stearates (commercialized under the brand name Myrj), or branched, as in the case of Tween (300). Because of the steric repulsion generated by hydrophilic chains, PEG surfactants are biocompatible and demonstrate excellent emulsifying and stabilizing capacities.



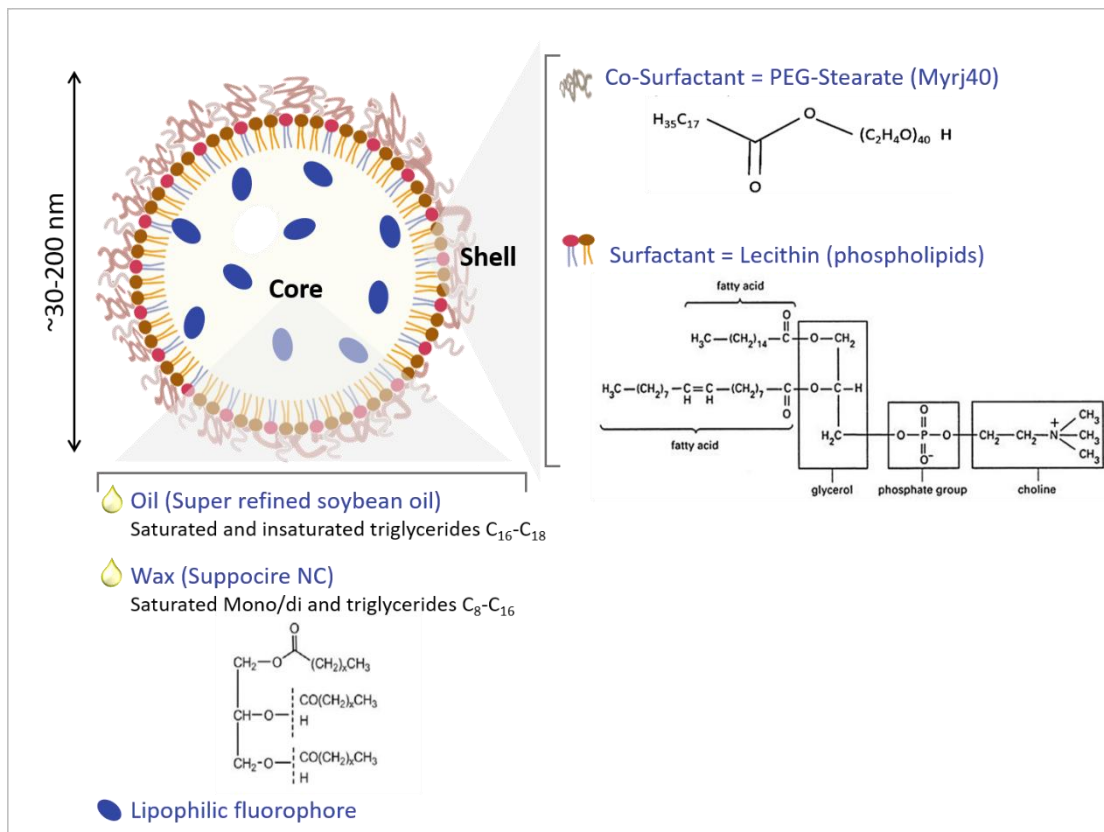


**Figure 31: Schematic representation of oil-in-water nanoemulsions, Lipidots.**

The core shell structure of Lipidots features an oily phase dispersed in an aqueous polyethylene glycol phase. The shell is composed of lecithin surfactants and their PEG co-surfactants, whereas the core contains solid (wax) and oily (Soybean oil) triglycerides.

## IV.B. 2. Lipid core

The lipid core, also serving as dispersion phase, is a mixture of glycerides of oil and/or wax nature to boost the solubility of phospholipids.

### IV.B. 2.a. Soybean oil

One of the constituents of the dispersed phase is a vegetable oil: soybean oil. This biocompatible oil is mainly composed of triglycerides with long unsaturated fatty acids (309). The choice of this oil in particular owes to its water insolubility, which is an essential property to minimize the colloidal destabilization of nanoemulsions. Table 9 shows the average percentage of the main fatty acids composing soybean oil (310).

Fatty acids nature	Percentage in soybean oil
C16	8 – 13%
C16 : 1	<0,2%
C18	2,4 – 5,4%
C18 : 1	17,7 – 26,1%
C18 : 2	49,8 – 57,1%
C18 : 3	5,5 – 9,5%

**Table 9: Composition of soybean oil.**

The fatty acids are reported according to the  $C\alpha : \beta$  nomenclature, where  $\alpha$  corresponds to the number of carbon atoms and  $\beta$  to the number of insaturations in the carbon chain.

#### IV.B. 2.b. Suppocire wax

Suppocire<sup>®</sup> NC wax was employed in the formulation of the nanoemulsions. This wax is obtained through direct esterification of glycerol and fatty acids. The resulting semi-synthetic glycerides (mono-, di-, triglycerides) contain saturated fatty acids with 8 to 18 carbon atoms (Table 10). Suppocire<sup>®</sup> NC is solid at room temperature and melts across a temperature range near 38 ° C. It is weakly soluble in water, but has a high solubilizing capacity (308). According to the envisaged application, the particle size is adjustable by modifying the wax/ oil ratio.

Fatty acid chain length	Percentage in Suppocire
C8	0,1 – 0,9
C10	0,1 – 0,9
C12	25 - 50
C14	10 – 25
C16	10 – 25
C18	10 – 25

**Table 10: Fatty acids composition of Suppocire<sup>®</sup> NC.**

In addition to oil and wax, the LNP core may harbor an imaging dye and the potential therapeutic agent if it is lipophilic.

### IV.C. Formulation method

Oil-in-water nanoemulsions are synthesized by sonicating the oily phase in the aqueous phase (Figure 32). As already mentioned, the dispersion phase is made up of glycerides (Suppocire<sup>®</sup> NC and super refined soybean oil). For solubility reasons, lecithin (phospholipids) is dissolved in the dispersed phase by addition of an organic solvent (dichloromethane).

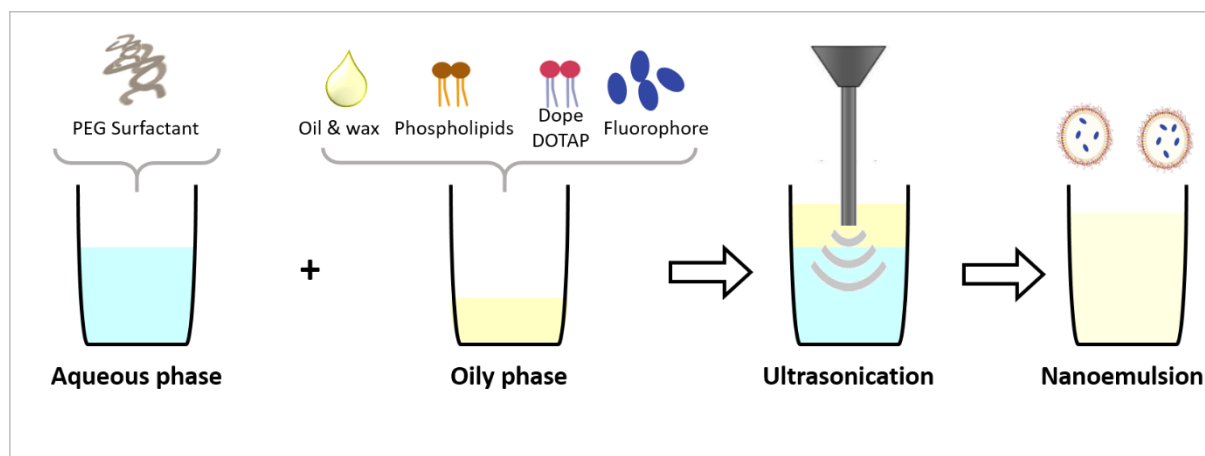


Figure 32: Formulation process of cationic lipid dots as oil-in-water nanoemulsions.

Before discarding the solvent, lipophilic dyes such as Dil (1,1'-Diocadecyl-3,3',3'-Tetramethylindocarbocyanine Perchlorate) are introduced to the lipid phase to allow fluorescence tracking of LNPs. Once all the compounds have dissolved, the solvent is vacuum evaporated at a temperature above the wax melting point. Hence, the oily phase is the combination of lecithin and the oil / wax mixture (307). To assist nucleic acid incorporation, the cationic lipid DOTAP (1,2-dioleoyl-3-trimethylammonium-propane chloride) and the fusogenic lipid DOPE (1,2-dioleoyl-sn-glycero-3-phosphoethanolamine) were added to the lipid phase, thus conferring a positive charge for the resulting formulations (305). Figure 33 depicts a hypothetical structure displaying each component of neutral and cationic LNPs. The interest of such cationic LNPs will be further discussed in section IV.F.

The aqueous phase is prepared by hot mixing glycerol and the pegylated surfactant (Myrj40) in PBS to boost viscosity. Indeed, a constant viscous phase enhances emulsification and aids in preventing projections during sonication. The so-formed lipid and aqueous phases are appropriately conserved at 50°C, combined, and then the resulting two-phased solution is sonicated at high frequency, until obtaining a clear nanoemulsion solution (300). LNP purification steps occur through dialysis in LNP buffer (154 mM NaCl, 10 mM HEPES, pH 7.4) using ultra-pure water and 12–14 kDa MW cut-off membranes. At this level, the LNP solution is freed of non-incorporated compounds and is subjected to a final filtration through a 0.22µm Millipore membrane under a laminar flow PSM. After formulation, the final particles are stored at 4 °C in PBS.

LNPs of different diameters may be obtained by adjusting the ratio of wax relative to aqueous compounds. Accordingly, the oily core can occupy 1-80%, 10-30% or ideally 5-50% of the

particle weight. Delmas et al. demonstrated that increasing the wax content of LNP drops down the average hydrodynamic diameter, whereas the surface charge of LNP remains unaffected (307). This is quite expected since it is the chemical structure of the interface, and not the core composition, that governs LNP surface charge.

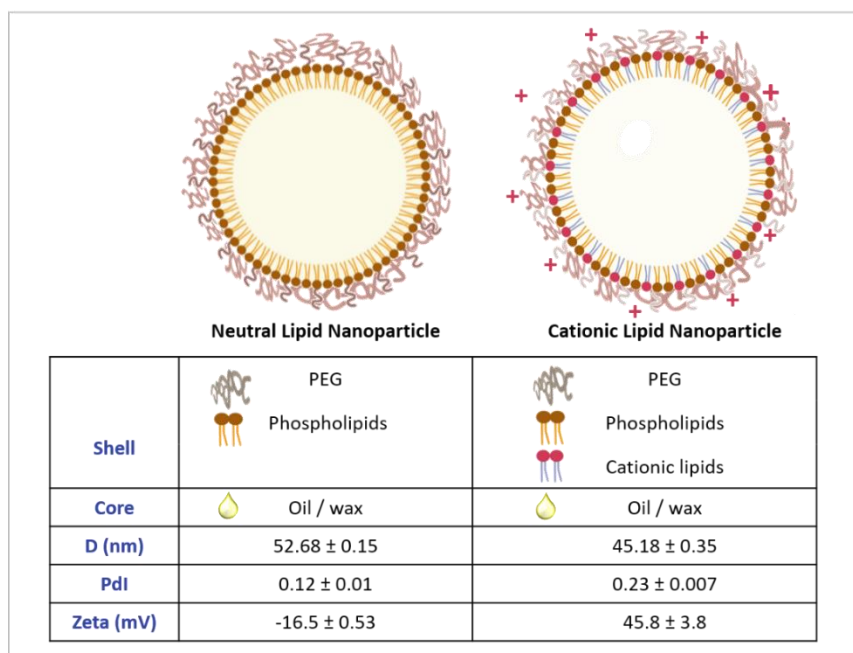


**Figure 33: Physical characterization of neutral and cationic Lipidots.**

Particles are characterized by their hydrodynamic diameter (D), polydispersity index (PdI) and Zeta potential.

This thesis work have been carried out with cationic LNPs, the term LNP afterwards refers strictly to cationic particles of nearly 40 nm size.

## IV.D. Physico-chemical characterization of lipidots

Before further application, it is critical to properly characterize the formulated particles using conventional parameters in the NP field. Dynamic Light Scattering (DLS) is a popular technique for determining particle size and distribution (311). This method relies on particle Brownian motion. When particles in suspension are sufficiently small, they are vulnerable to random motions induced by interactions with solvent molecules. The smaller the particles, the quicker these motions. When a light beam travels through a colloidal solution and encounters a particle, it is diffused according to a diffusion coefficient that is proportional to the particle's Brownian motion, hence its size. It is possible to measure the speed of Brownian motion and

thereby the scattering coefficient of the particles, through repeatedly measuring the scattered light over extremely small time frames. Table 11 reports the basic characterization of the LNP batch used in this thesis work, as measured by the LETI/DTBS laboratory, immediately after formulation.

Batch	Size	PDI	Zeta	Concentration (mg/ml)	[Dil] ( $\mu\text{M}$ )
CL40_Dil19	$35 \pm 0.2$	$0.2 \pm 0.136$	$39 \pm 4$	227	571

**Table 11: Physico-chemical properties of the used LNP formulations after synthesis.**  
These data are generated from DLS on a ZetaSizer NanoZS (Malvern Instruments) measures.

#### IV.D. 1. Morphology and hydrodynamic diameter

The disc-like shape evaluates the integrity of the formulated particles. Indeed, if some particles appear spherical, others appeared more elongated in tube-like shapes. These observations were justified by the fact that the particles indeed have the same morphology, but are visualized in different orientations. Transmission electron microscopy (TEM) may be used to examine the morphology of the purified nano-emulsions (312). This approach enables examination of materials in solution, preventing alteration of their morphological features.

The hydrodynamic diameter of LNPs is measured by DLS. The volume-weighted average diameter of the reference formulation is  $35 \pm 2$  nm (308). TEM may also allow verification of the DLS data, but the sizes of the observed particles may seem slightly smaller. The LNP specific surface is  $66\text{m}^2$ /particle with a molecular weight of  $\sim 8000\text{kDa}$  and a particulate mass of  $1.32 \times 10^8$  ng. LNPs are stable with a shelf life at room temperature  $> 1$  year; they are resistant to a range of pH between 2 and 11 (307).

#### IV.D. 2. Polydispersity index

The polydispersity index (PDI) is an estimation of the size dispersion of particles constituting the same batch, also evaluated by DLS. In other words, PDI reflects the uniformity of a particle solution. The closer the PDI is to zero, the more the population of particles is monodisperse, thereby of homogeneous size (311). PDI can also predict NP aggregation, as well as the consistency of particle surface changes across the LNP sample. PDI of the reference formulation is close to 0.170 at production; the solution is therefore slightly polydisperse. However, the production method yields excellent reproducibility in terms of size distribution, when comparing different batches of LNPs produced with the same formulation (299).

### IV.D. 3. Zeta potential

The zeta potential characterizes the surface charge of colloids in solution. However, it translates the charge acquired in solution and not the actual particle charge (311). A charged particle in suspension is surrounded by counterions from the medium forming an ionic double layer for enhanced stabilization (Figure 34).

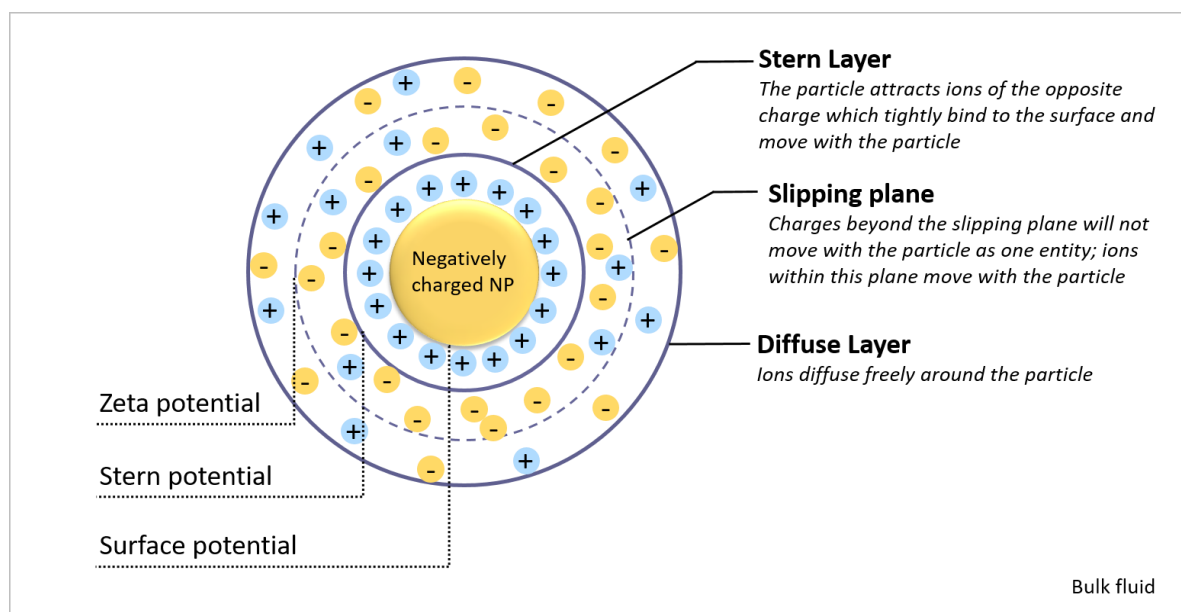


**Figure 34: Representation of a particle's zeta potential according to the Gouy-Stern model.**

The surface potential is the electrical potential surrounding the particle, the stern potential is the electrical potential at the stern layer, and the zeta potential is the electrical potential at the slipping plane. The slipping plane is the hydrodynamic shear beyond which ions diffuse freely.

The layer nearest to the particle, also known as the Stern layer, is made up of ions that have the opposite charge as the particle's surface. In turn, the Stern layer attracts ions with opposed charges (therefore of the same charge as the particle). This second layer is termed the diffuse or Gouy layer, and contains to less extent similar charges as the Stern layer.

When particles are set in motion, whether by Brownian or induced motion (by an electric field), a boundary called the slip plane (shear plane), is formed within the diffuse layer. At this point, the Stern layer and part of the Gouy layer remain linked to the particle and follow its movement, whilst the rest of the diffuse layer remains motionless or displays a delayed motility (313). When an electric field is applied to the suspension of particles, they move towards the anode or the cathode according to their zeta potential. ZetaSizer NanoZS

(Malvern Instruments) then measures their electrophoretic mobility  $\mu_e$ , which is related to the zeta potential  $\zeta$  by the Smoluchowski formula:

$$\zeta = \frac{4 \pi \mu_e \eta}{\varepsilon} \quad (\eta:\text{viscosity}; \varepsilon:\text{dielectric constant})$$

Zeta potential is often measured to predict the stability of suspended particles. The intensity of the electrostatic repulsion force is in fact related to the zeta potential: the more the particles have a high zeta potential (in absolute value), the more they will repel each other and the less they will tend to aggregate.

The zeta potential of the reference formulation is  $-5 \pm 2$  mV. This low value can be explained by the fact that lecithin is mostly composed of zwitterionic phospholipids (which are normally neutral) while pegylated surfactants are already nonionic. The observed negative charges are certainly related to the free fatty acids present in the dispersed phase of lecithin. Because the steric barrier of the polyoxyethylene chains causes the sliding plane to migrate away from the particle, the presence of the pegylated surfactant layer also helps to lower the zeta potential.

#### IV.D. 4. LNP quantification in formulation

The number of LNPs contained in a formulation can be estimated using the following calculation, which is valid for all NLCs (o/w) formulations whether neutral or cationic, with no size restrictions.

$$\text{Total lipid volume in dispersed phase} = \frac{\text{Total mass of dispersed phase (g)}}{\text{Total density of dispersed phase (g/cm}^3\text{)}}$$

*The dispersed phase comprises wax, oil, surfactant and PEGs, which have a known final density of 1.05 g / cm<sup>3</sup>.*

$$\text{Volume of a LNP} = \frac{4}{3} \pi \times R^3 ; R \text{ is the radius of a perfect spherical particle}$$

$$\text{Total LNP number in the formulation} = \frac{\text{Total lipid volume in dispersed phase}}{\text{Volume of a LNP}}$$

#### IV.E. Fluorophore encapsulation

For imaging applications, the LNP formulation comprises an imaging agent, which allows visualizing them in cells or in patient's tissue, and therefore following the distribution of their cargo (301). According to its nature, the imaging dye is adapted for a given imaging type such as Positron Emission Tomography (PET), magnetic resonance imaging (MRI), or optical

imaging. Fluorescence tracking of NPs is simple, non-invasive when compared to these methods requiring gamma-emitting nuclides, radiotracers... However, it is crucial to ensure a sufficient light penetration towards the profound tissues through choosing a stable and powerful dye. Fluorophores with emission and excitation within the near infrared (NIR) wavelengths (600-900 nm) elicit the best depth of precision (314). In vivo fluorescent imaging methods have witnessed increased development with the introduction of small animal imaging equipment. Two fluorescence approaches can be used to track the fate of a NP. The first is to encapsulate a fluorophore within the NP and test the hypothesis that the fluorophore's fate correlates to that of the NP (315). For this, the biodistribution of fluorophore alone should be examined, and the absence of fluorescence leakage from the NP should be confirmed. The second method involves monitoring a brilliant NP that exhibits fluorescence properties on its own, such as Quantum dots (QD). However, because of their substantial metal content, QD pose a considerable toxicological risk, making them harmful and unsuitable for human usage (232). This explains why organic alternatives are required in clinical investigations and applications.

Lipidots are ideal reservoirs for loading of hydrophobic molecules such as organic fluorophores harboring aromatic moieties with limited water solubility. The LNP core offers an apolar viscous environment for lipophilic dyes, thus enabling high fluorescence yield with minimized leakage. Different lipophilic (Di Family) or amphiphilic (indocyanine green ICG) cyanine dyes can be loaded in the oily phase or surfactant shell (Figure 35) prior to aqueous phase addition and ultrasonication. Lipidots are then purified by dialysis, which discards non-encapsulated dyes and surfactants.



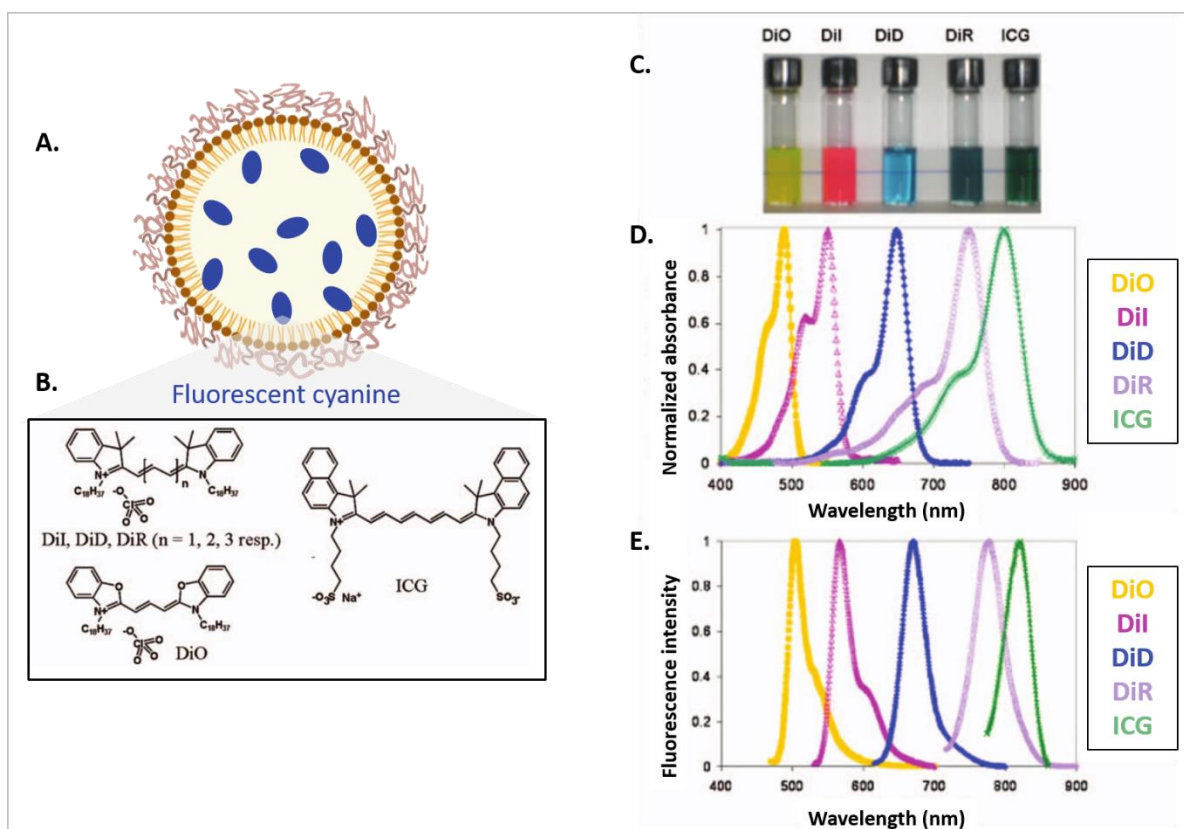


**Figure 35: Cyanines encapsulation in LNP core.**

(A) 50nm Lipidots are nano-emulsions containing (B) lipophilic (DiI, DiO, DiD, DiR) or amphiphilic (Indocyanine green ICG) cyanines enclosed in the lipid core and/or surfactant layer. (C) Dye-loaded LNP formulations hold luminous features as demonstrated by (D) absorption and (E) emission spectra.

Gravier et al. determined the dye loading efficiency of neutral LNPs by comparing dispersion absorbance and fluorescence before and after dialysis (316). Table 12 shows their findings for 50 nm neutral LNPs loaded with a local dye concentration of 1.2 mM. Encapsulation efficiency for all four highly lipophilic indocyanines (DiO, DiI, DiD, and DiR) exceeded 90%. ICG exhibited lower encapsulation yield (77%) mainly because of hydrophilic sulfonate moieties in their structure.

Tracking the fluorescence signals in vivo demonstrates that LNP are primarily localized to the paw surface area, demonstrating that lipidots remain confined to the interstitial space upon intradermal injection. This can assist their gradual drainage via the lymphatic system. When injection sites are veiled with black tape, the DiD- and ICG-loaded lipidots migrate and accumulate in lymph nodes. Herein, fluorescence from DiD-lipidots persisted for several weeks, while ICG fluorescence has vanished 24 hours after injection (303). The partial position

of the ICG dye in the particle shell generates quick diffusion from the particles following in vivo injection and therefore its rapid clearance. Despite larger injection dosages, no signal is detected with the more blueshifted fluorophores (DiO, DiI), highlighting the relevance of NIR wavelengths for in vivo research.

Loaded dye	Loading efficiency	1 year dye stability	Absorption (nm)	Emission (nm)	$\epsilon$ (L/mol/cm)	Fluorescence quantum yield $\Phi$	$\epsilon \times n \times \Phi$ (L/mol/cm)
DiO	93%	48%	489	505	$9 \times 10^4$	$0.39 \pm 0.02$	$1.5 \times 10^6$
DiI	96%	93%	550	567	$1.2 \times 10^5$	$0.31 \pm 0.02$	$1.6 \times 10^6$
DiD	95%	52%	646	668	$1.3 \times 10^5$	$0.53 \pm 0.01$	$2.9 \times 10^6$
DiR	92%	NA	750	775	$7 \times 10^4$	$0.21 \pm 0.02$	$6.2 \times 10^5$
ICG	77%	89%	801	820	$2 \times 10^5$	$0.06 \pm 0.01$	$4.3 \times 10^5$

**Table 12: Optical properties of LNP-loaded dyes.**

For each loaded dye, Gravier et al. have tested: the loading efficiency of incorporating  $0.8 \mu\text{mol}$  of dye into 50nm LNPs; percentage of functional dye loaded in LNP after 1 year of storage at dark; maximum absorption and emission wavelengths; extinction coefficient ( $\epsilon$ ), fluorescence quantum yield ( $\Phi$ ), and the brilliance ( $n$  is the number of dye per particle)

Indeed, Lipidots have long-term colloidal, and photochemical stabilities with limited cytotoxicity. Their wide size and wavelength emissions allow them to be employed in a variety of applications: while shorter wavelengths are ideal for in vitro or ex vivo research, NIR-emitting lipidots are required for sensitive multichannel imaging. Moreover, guided by the EPR phenomenon, brilliant LNPs can accumulate at tumor sites for their extended fluorescence labeling. This could be useful not only in preclinical studies to monitor the efficacy of cancer therapies on a daily basis, but also in clinical contexts to enhance the accuracy of detection of small cancerous nodules, even in deep tissues, using non-invasive fluorescence imaging.

## IV.F. Nucleic acid encapsulation

LNPs are not adapted for encapsulation of hydrophilic compounds such as nucleic acids because of the lipid nature of their core. Loading macromolecules such as RNAi or mRNA is feasible by linkage to the particle's shell, either through chemical modifications of PEG residues (317) or through incorporation of cationic lipids in their phospholipid monolayer. Cationic lipids, such as Dioleoyl-3-trimethylammonium propane (DOTAP), in association with the fusogenic lipid DOPE (1,2-dioleoyl-sn-glycero-3-phosphoethanolamine) are most often added to the formulation at appropriate ratio (308). As a result, nucleic acids binding and

condensing in the particles occurs through electrostatic interactions with positively charged lipids (Figure 35). DOTAP-integrating LNPs have a global positive charge, their toxicity and immunogenicity are still questionable.

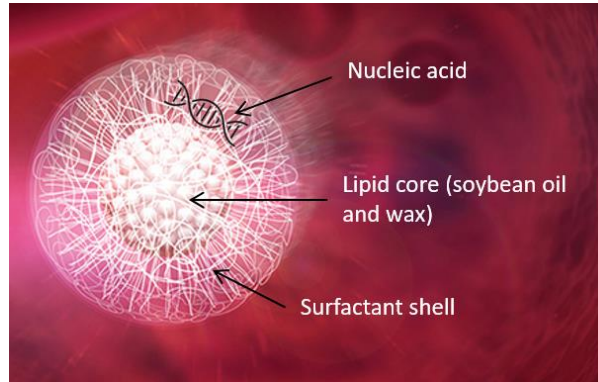
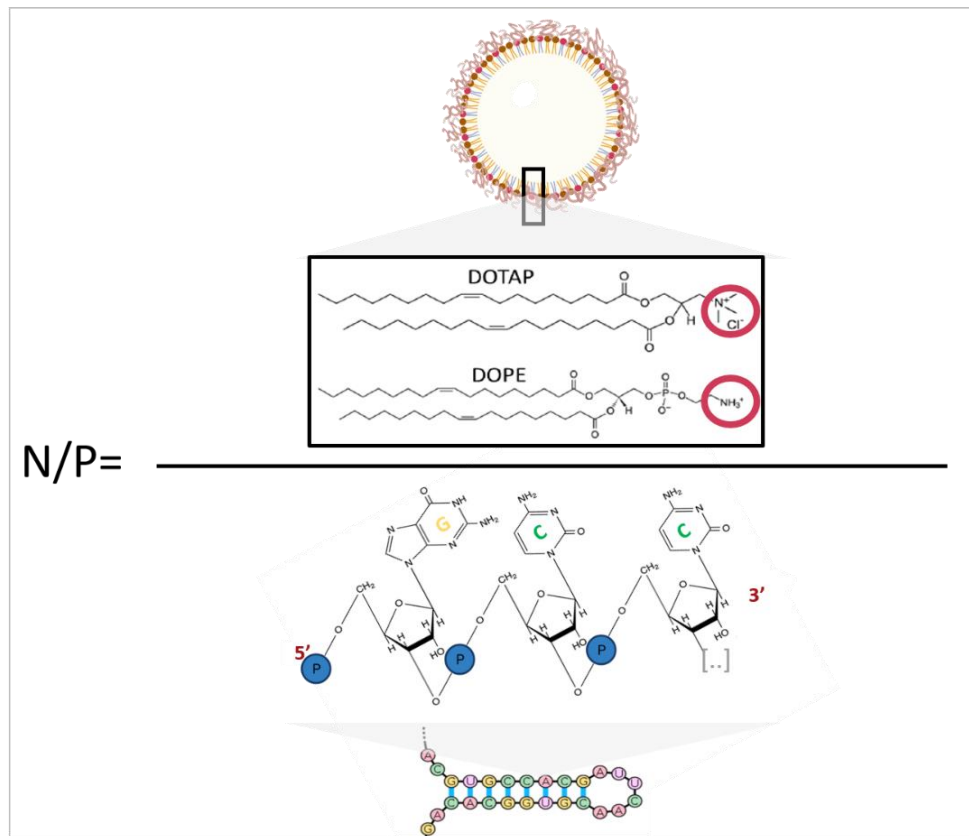


Figure 36: Lipid-nucleic acids complex in blood

#### IV.F. 1. The N/P ratio

The complexation of nucleic acids on the surface of LNPs is determined by the ratio of positive charges carried by the amine functions of cationic lipids (N for amine) and negative charges carried by the phosphate groups (P for phosphate) in each phosphodiester bond inside the nucleic acid sequence. The N/P ratio is then used to calculate the RNAi loading rate on the LNPs (Figure 37). The choice of the N/P ratio for a given application is completely arbitrary and relies on preliminary assessments in terms of efficiency, toxicity and cost. For miRNA research, it is beneficial to opt for minimal effective payloads, thus complying with higher N/P ratios, at a given LNP quantity.



**Figure 37: Definition of the N/P ratio.**

RNAi loading in LNP is enabled by electrostatic interactions. The positive charges are carried by the amines of the cationic lipids DOTAP and DOPE constituting the LNP positive charges, while the phosphate groups connecting the nucleic acids' nucleotides provide the negative charges.

## IV.F. 2. Complexation and nucleic acids payload

Nucleic acids such as miRNA are coupled to LNPs by electrostatic interactions. Negatively charged miRNA is mixed for 5 minutes with cationic particles according to the desired N/P ratio (N/P=16 in our experiments). For a given mass of LNP, the mass of miRNA to be added in concordance with the desired N/P ratio is determined according to the following calculations:

The positive charge in the complex originates from the amines within the DOPE and DOTAP structure; a DOTAP or DOPE molecule contains a positive charge.

**Number of positive charges** =  $(n_{\text{DOTAP}} + n_{\text{DOPE}}) \times \text{Avogadro Number}$

$$= \left( \frac{\text{mass (DOTAP)}}{\text{Molar mass (DOTAP)}} + \frac{\text{mass (DOPE)}}{\text{Molar mass (DOPE)}} \right) \times \text{NA}$$

*The molar masses of DOTAP and DOPE are respectively 699 g/mol and 744 g/mol. Avogadro's number is the number of molecules in a mole and is equal to  $6,022 \times 10^{23}$ .*

We have previously stated that N/P is the ratio of N (positive charge) relative to P (negative charge):

$$\text{Number of negative charges} = \frac{\text{Number of positive charges}}{N/P}$$

The mass of miRNA to be conjugated is determined according to the number of nucleotides; hence, the number of phosphate groups linking these nucleotides. In our approach, we used single-stranded miRNA inhibitors (AntimiRs) made up of 21 nucleotides linked by phosphate groups each carrying a negative charge. An AntimiR strand therefore has 20 negative charges. The molar mass of antimiRs is 12000g/mol.

$$\text{miRNA mass} = \frac{\text{Number of negative charges}}{\text{Number of Phosphate}} \times \text{Molar mass (miRNA)}$$

After mixing the elements according to the N/P ratio, the miRNA loading capacity by LNPs can also be estimated, assuming a perfect complexation at this N/P ratio.

$$\text{miRNA loading rate (\%)} = \frac{\text{miRNA mass}}{\text{LNP mass}} \times 100$$

$$\text{Number of miRNAs per particle} = \frac{\text{Number of miRNA}}{\text{Number of LNP}}$$

In the experimental setup of this thesis, our calculations reported 42 miRNA molecules theoretically engrafted to one particle. Further calculations to determine the expected number of LNPs taken up by one cell in petri dishes also aid in evaluating the complexation efficiency.

## IV.G. In vivo behavior of Lipidots

Before going further, it is essential to understand the behavior of LNPs after in vivo administration, by evaluating their basic pharmacokinetics as well as their routes of metabolism and excretion. Bioavailability and biodistribution are the most popular parameters to monitor. While **bioavailability** refers to the percentage of administered drug that reaches the blood compartment (bioavailability is 100% when administered via the blood), **biodistribution** is the theoretical fluid volume in which the compound should be

dispersed to achieve the same concentration as in plasma (318). This reflects the biomolecule's capacity to diffuse in the organism. In terms of elimination, the **plasmatic half-life** reflects the time period required to observe a 50% decrease in the initial injected dosage. It serves as a reference criterion for determining the stealth of a NP in the body. Total **clearance** is the flow rate that measures the organism's ability to clear out the compound (268). After confirming their emergence to the bloodstream, the behavior of nano-objects in the organism is described by four parameters, often recognized as ADME for absorption, distribution, metabolism and elimination.

#### **IV.G. 1. Absorption**

The process by which a NP transits from its administration site to the interior environment, by passing through the blood plasma, is known as absorption. Absorption varies primarily according to the route of administration and the various barriers that must be overcome during this journey (269): oral (gastric enzymes), nasal, ocular (tear evacuation), pulmonary (alveolar filters), dermal (diffusion through the skin barrier), intratumoral (acidity). Absorption is not an issue for LNPs since they are already systemically injected for an optimal bioavailability (100%). It is worth mentioning that blood administration is often adopted during the initial stages of drug discovery.

#### **IV.G. 2. Distribution**

NP distribution relates to its uptake by different tissues; the most researched areas include vital organs in addition to the vascular, lymphatic and the reticuloendothelial system (RES). The circulatory system is a complex tissue that highly affects the NP fate. As previously mentioned in section III.E, NPs are prone to opsonization by plasma proteins, thus altering their initial physicochemical features (240). The nature of tissue endothelium guides extravasation of NPs to these tissues. For example, a discontinuous endothelium is characteristic of liver, spleen, and bones, which are known accumulation sites for NPs. Fenestrations within angiogenic vessels have widely aided tumor targeting of NPs via the EPR effect. Moreover, blood supply and tissue perfusion are determining parameters for the distribution of the nano-objects. LNPs were well tolerated by endothelial cells at a concentration reaching 400 $\mu$ g/ml (319).

Besides RES and lymphatic drainage, LNPs' biodistribution is easily tracked via fluorescence. An efficient nanocarrier should safely convey its payload to its destination and release it. These conditions are met by DiD-labeled lipidots, which resided over 24h in blood compartment with no signs of tracer leakage (320). Along the same line, the integrity of LNP-doped dyes was evaluated through comparing their biodistribution to that of free tracers; this demonstrated a clear LNP-driven fluorescence pattern.

In their experiments, Merian et al. injected triply labeled LNPs containing the two radiotracers <sup>3</sup>H-CHE and <sup>14</sup>CCHO, as well as a fluorescent NIR dye 1,19-dioctadecyl-3,3,39,39-tetramethylindotricarbocyanine perchlorate (DiD) in the tail vein of FVB mice. Introducing this radiolabeling step allowed quantitative analyses rather than inaccurate fluorescence assessments only. Blood pharmacokinetics studies showed that all three tracers remain active in the circulation when shielded in LNPs, whereas free tracers were immediately washed out after injection (302). The three tracers were identified mostly in the liver, ovaries, and adrenals, with only negligible signals discovered in the heart, brain, fat, muscle, pancreas, and intestines. Also, there was no significant uptake by the spleen, lung, or kidney. Lipidots infiltration in lymph nodes has already been documented and is common to other organic or inorganic NPs (316).

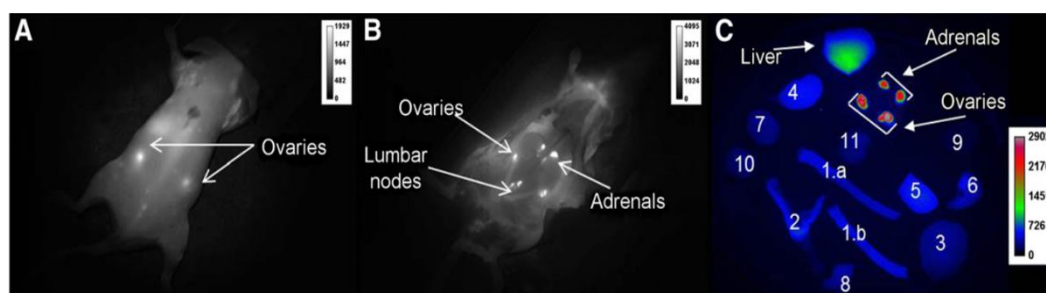


**Figure 38: In vivo distribution of LNP fluorescence.**

(A) Representative image of a FVB mouse 24 hours after receiving  $1.2 \times 10^{13}$  DiD-loaded LNPs, intravenously. (B) Representative image following a laparotomy. (C) Mouse organs ex-vivo 24 hours after injection. 1 intestine (1a duodenum; 1b jejunum); 2 uterus; 3 brain; 4 kidney; 5 spleen; 6 lung; 7 salivary glands; 8 pancreas; 9 muscle; 10 fat; 11 heart. Taken from Merian et al. 2013.

Nevertheless, considerable amounts of the three tracers were retrieved from the bile, but with dramatic interanimal variability because of variable hepatobiliary excretion. Overall, endocrine organs (adrenals, and ovaries) accumulated most fluorescence and tritium signals, thus revealing a specific LNP tropism for these tissues (321). 16 hours after injection, the

fluorescence peak in ovaries was high enough to be perceived through the skin (Figure 38). Moreover, these signals persisted up to 168 hours in adrenals and ovaries. These findings were indeed the pillars for the current thesis, as will be explained throughout this manuscript. Furthermore, injecting labeled lipidots with RGD (Arg-Gly-Asp) surface functionalization, generated fluorescence signals from the subcutaneously established tumors. As ligands of  $\alpha\beta3$  integrins are highly expressed in the tumor vasculature, RGD oligopeptides were involved in the specific homing of LNPs to the tumor (299). However, similar accumulation pattern was observed in non-stealthy LNPs indicating that RGD binding to tumoral integrins was not the primary factor driving lipidots into the tumors. One hypothesis is that lipidots are degraded in plasma, resulting in distinct components that were taken up separately in tumors. Alternatively, tumor absorption of lipidots might be compelled by the EPR effect.

### **IV.G. 3. Metabolization**

Metabolization encompasses all biological processes that modify the physico-chemical characteristics of NPs. After being absorbed, some NPs are immediately metabolized in the lysosomes of RES macrophages, whereas others are hydrolyzed in the aqueous environment. Many NPs, particularly metallic NPs, are not digested by the organism and accumulate in the body, increasing their toxicity. Biodegradability is a major advantage of LNPs' whose components are metabolized in the liver through the natural lipid pathways (322).

### **IV.G. 4. Elimination**

The NP components indicate whether it is cleared out as an intact entity or as degraded metabolites. The liver and kidneys are the primary organs involved in NP excretion. In terms of renal clearance, tiny (5 nm) or hydrophilic NPs, undergo glomerular filtration to be expelled in the urine. Aside from its metabolic role, the liver is a key route of excretion for nanoparticles, particularly lipid-based nanoparticles such as Lipidots. Herein, the hepatocytes sort these NPs towards gallbladder ejection. Other excretory pathways such as milk or sweat may interfere.



## IV.H. Current applications of lipidots

Given their versatile properties, lipidots have emerged as attractive platforms already approved for several applications such as fluorescence imaging, photodynamic therapy, drug delivery, and vaccine formulations. Foremost, dye-loaded LNPs exhibit NIR absorption and emission wavelengths highly appreciated in imaging contexts because of their in-depth efficacy. Thanks to the EPR effect, LNPs act as safe contrast agents, which naturally accumulate in tumors, thus eliciting prolonged fluorescence signals upon in vivo administration. LNPs have emerged as safe competitors to quantum dots; hence they are valuable not only in preclinical studies to monitor the efficacy of cancer therapies, but also in precision oncology to improve the detection of small cancerous nodules (316).

Lipidots were also used to study the photodynamic efficiency of new nanoformulations incorporating mTHPC as a photochemically active agent (323). mTHPC was effectively encapsulated into LNP without compromising the carrier's colloidal characteristics or the photophysical properties of the loaded photosensitizer. This was demonstrated by its phototoxic effects on human breast cancer MCF-7 cells. However, in order to maximize the benefit potential of LNPs in photodynamic therapy, it is necessary to manage their payload, such as the lipid concentration in contact with cells. Moreover, the in vivo behavior of LNPs was extensively characterized and the biodistribution landscape revealed a clear tropism for lipid-avid and lipoprotein receptor-expressing tissues (321). Hence, it is expected that this specific affinity is of diagnostic and therapeutic interest for lipoprotein-receptor-overexpressing cancer cells present in hormone-dependent tumors i.e. breast and prostate cancer. On the other hand, Lipidots have been exploited for vaccine applications. Bayon et al. tailored LNPs for protein antigen delivery in a novel strategy for HIV vaccines. Briefly, ovalbumine conjugation onto the LNP surface was accomplished with good yields while maintaining global colloidal stability (300). These tolerated NP do not stimulate the immune system on their own, but rather serve as an antigen transport mechanism to the lymph nodes. Besides great capacity to induce both humoral and cellular immunity, this study underlined the relevance of NP physicochemical characterization for vaccine applications. Such lipid carriers have a great biocompatibility profile and are easily producible on a wide scale, two key obstacles for the industrial transfer of nanomedicine products. In light of these findings, Lipidots are currently under investigation for COVID-19 mRNA vaccines (NanoCov2-Vac

project) as a response to the current health crisis. Recently, the characterization of siRNA-LNP complexes has raised some concerns in terms of immunogenicity of cationic LNPs. Modulating the N/P ratio by tuning the load of nucleic acids clearly relieved these primary complications (305). Thus the rationale for tuning the nucleic acid load of cationic LNPs is based on whether immunostimulation is demanded or not, in accordance with the intended therapeutic use, such as mRNA vaccines or gene delivery. In the mean time, siRNA LNP formulations are being evaluated for use in inflammatory bowel disease (324). Taken together, this great number of promising data will definitely position LNPs as frontline candidates for gene therapy via surface engraftment of nucleic acids.

## Conclusion

Over the last decades, nanomedicine has been constantly evolving in order to create more efficient, biocompatible, and non-hazardous items. Nanoparticles enabled the encapsulation of environmentally sensitive molecules, such as fluorophores for fluorescence imaging or chemical compounds for drug delivery. In fact, nanoobjects have underwent numerous structural manipulations in order to increase their vectorization capacities *in vivo*. The implementation of hydrophilic surfactants, in particular, remarkably enhanced the circulating half-life, allowing for targeted delivery of the vector and its cargo. Applying different layers of stealth and targeting moieties resulted in extremely sophisticated platforms exerting bi- or trimodal activities.

Therefore, it is critical to analyze the behavior of these particles and their payload in the body using reliable tools. It remains tricky to compare various approaches proposed across the literature, given the wide variety of nanocarriers at current disposal, each being unique in its composition, size, surface chemistry, and processing methods. Additionally, the diversity of the experimental conditions makes it challenging to compare experimental results from one study to another. Such research biases may include the animal model, routes of administration, duration of the experiment and of course, the envisaged application. Nonetheless, fundamental parameters such as pharmacokinetics or tracking of nanoparticle accumulation in the body remain of importance. Long-term monitoring approaches rather than single-point observations are necessary to perform toxicity readouts over a prolonged

period. Furthermore, the use of animal models such as non-human primates would be more relevant to fill the gap between preclinical research conducted in mice and clinical applications. As acquiring authorization for application in patients remains the ultimate goal of novel nanotechnology-based formulations, nanoparticles based on natural lipids continue to be at the forefront of clinically preconized treatment.

## 2- THESIS OBJECTIVES

---



In this thesis project, we proposed the development of an innovative therapeutic strategy for adrenocortical carcinoma, a rare but highly aggressive cancer that remains refractory to conventional therapies. Previous studies of ACC miRnome by our team have revealed that two miRNAs, miR-139-5p and miR-483-5p, are overexpressed in aggressive tumors and associated with poor prognosis. In light of these results, we assumed that inhibition of these two miRNAs could reverse the aggressive phenotype of ACC. Moreover, with the rise of miRNA-based therapies and the emergence of complex carriers for safe and targeted delivery, we opted for an original nanotechnology system, namely Lipidots®. Lipidots® were developed and patented by our colleagues "next-door" at CEA-LETI, and demonstrated a remarkable tropism for adrenal glands, which justifies their use in the context of this thesis.

The main aim of this work was to evaluate miR-139-5p and miR-483-5p as therapeutic targets in ACC by nanovectorizing their respective anti-miRs via Lipidots, and addressing these nanoformulations to tumor-bearing mice.

Before tackling this final goal, three complementary objectives were set:

- (1) To establish in vitro the proof of concept that miR-483-5p and miR-139-5p are relevant therapeutic targets for ACC. This study was carried out using synthetic miRs (mimics) or non-vectorized miRNA anti-miRs in the human cell line NCI H295R, an ACC reference model. This cell line was also used for xenograft experiments. In this part, we basically explored the direct/indirect signaling networks affected by miR-139-5p and miR-483-5p.
- (2) To characterize the in vitro behavior of Lipidots® in cultured NCI H295R in terms of toxicity and cellular uptake.
- (3) To efficiently encapsulate anti-miRs in Lipidots® nanoparticles and analyze their functional effects in NCI H295R cells.



# 3- RESULTS

---





# ARTICLE I

**MicroRNA therapeutics in adrenocortical carcinoma: A lipid nanoparticle-based approach to suppress the oncogenic activity of microRNAs**

(To be published)



## **MicroRNA therapeutics in ACC: A lipid nanoparticle-based approach to suppress the oncogenic activity of microRNAs**

Soha Reda El Sayed<sup>1</sup>, Adrien Nougarede<sup>2</sup>, Josiane Denis<sup>1</sup>, Justine Cristante<sup>1</sup>, Fabrice Navarro<sup>2</sup>, Olivier Chabre<sup>1, 3</sup>, Laurent Guyon<sup>1</sup> and Nadia Cherradi<sup>1</sup>

<sup>1</sup> University Grenoble Alpes, INSERM, CEA, IRIG, Biology and Biotechnologies for Health Lab, UMR\_1292, Grenoble, FRANCE.

<sup>2</sup> University Grenoble Alpes, CEA, LETI, Technologies for Healthcare and Biology Division, Microfluidic Systems and Bioengineering Lab, Grenoble, FRANCE.

<sup>3</sup> University Hospital Grenoble Alpes, Endocrinology Department, Grenoble, FRANCE.

**Word count:** 10980

**Number of references:** 48

**Number of tables and figures:** 7 Figures, 2 Supplementary Figures and 6 Supplementary tables

**Corresponding author:** Dr. Nadia Cherradi, INSERM U1292  
Laboratoire Biologie et Biotechnologies pour la Santé/ IRIG/CEA  
17 rue des Martyrs  
38054 Grenoble Cedex 09, France.  
Phone: + 33 438 78 35 01  
Fax: + 33 438 78 50 58  
e-mail : [nadia.cherradi@cea.fr](mailto:nadia.cherradi@cea.fr)

**Keywords:** MicroRNA therapeutics, Adrenocortical carcinoma, Solid Lipid Nanoparticles, Lipidots, Targeted therapy

## Abstract

Adrenocortical carcinoma (ACC) is a rare endocrine malignancy with dismal prognosis and unmet clinical needs. Aberrant expressions of tumor and circulating microRNA (miRNA) have been reported in ACC patients. Besides their promising potential as biomarkers, the therapeutic value of miRNAs is increasingly studied. However, a major challenge of miRNA-based cancer therapy is to achieve specific and safe delivery *in vivo*. We have shown that miR-483-5p and miR-139-5p are overexpressed in ACC and involved in cancer cell aggressiveness. We aimed to evaluate both miRNAs as therapeutic targets using a 'smart' drug delivery system, namely Lipidots (LNP). Lipidots are biocompatible solid lipid nanoparticles with a natural and unique tropism toward steroid-producing organs. We first investigated potential oncogenic pathways activated by miR-483-5p and miR-139-5p in the human ACC cell line NCI H295R. Using PCR and Antibody arrays, we found that miR-483-5p and miR-139-5p inhibition impairs p38 MAP kinase, AKT/mTOR and Wnt/ $\beta$ -catenin signaling pathways as well as the expression of key genes in cell invasion. We generated cationic antimiRs-(483-5p/139-5p)/LNP complexes and tested their activity in H295R cells. We show that delivered antimiRs retained their ability to relieve the inhibitory effect of miR-483-5p and miR-139-5p on their target transcripts. In addition, antimiRs-LNP impaired H295R cell migration and invasion. Intravenous injection of these nanoformulations in *scid* mice revealed no signs of toxicity with a preferential accumulation of LNP/antimiRs in steroidogenic tissues (adrenals and ovaries). We report in preliminary experiments using subcutaneous xenograft of NCI H295R cells that systemic administration of antimiRs-LNP inhibits tumor growth. This work describes the first use of Lipidots<sup>®</sup> to vectorize miRNAs for therapeutic purposes and suggests that targeting miRNAs deregulations is a relevant strategy for the treatment of ACC. Although the molecular mechanisms involved in miR-139-5p- and miR-483-5p-mediated adrenocortical tumorigenesis remain to be fully elucidated, our combinatorial miRNA therapeutic approach engages components of ACC cell-addictive pathways and highlights the ability to deliver multiple miRNAs in a safe and effective manner to target adrenocortical carcinoma cells.

## Introduction

Adrenocortical carcinoma (ACC) is a malignancy of the adrenal cortex with a yearly incidence of 0.5-2 cases per million, accounting for 0.2% of cancer-related deaths (1). ACC is often associated with pejorative prognosis, with a 5-year survival rate around 38 % (2), due to delayed diagnosis. Approximately 60% of patients manifest hormone excess-related symptoms, 20% present mild abdominal discomfort, and the rest are incidentally diagnosed during other medical inspections (3). To date, radical surgery is the gold-standard treatment for early stage tumors, whereas cytotoxic chemotherapy is adopted for advanced cases (4). Despite tumor resection with clean margins, surgery is often followed by recurrence; chemotherapy and targeted therapies are associated with suboptimal efficacies (5). Hence, managing ACC requires multidisciplinary approaches in order to better understand the disease pathogenesis. With the emergence of integrated pan-genomic strategies, ACC tumors were profiled for their genetic and epigenetic signatures (6, 7). Overexpression of IGF-2 is described in 90% of sporadic ACCs, but also in rare cases of adenomas (ACA). Mutations in Wnt/ $\beta$ -catenin and TP53 signaling pathways have been reported in ~40 % and 25 % of ACC, respectively. Nonetheless, these mutational patterns were not found in all ACCs, implying the involvement of additional deregulations in the disease etiology (8).

Despite the disease rarity, ACC miRnome was extensively analyzed in patient cohorts. MicroRNAs (miRNAs or miRs) are small non-coding RNA which regulate gene expression through imperfect base pairing with the 3'-untranslated region (3'UTR) of target mRNA (9). By virtue to their target variety and broad spectrum of activity, miRNAs can efficiently regulate cancer hallmarks. Mapping miRNA profiles in normal versus tumor tissues revealed cancer-specific signatures, not only useful for diagnosis, but also for therapy and prognosis. Differential miRNA expression in ACC versus ACA or normal cortices revealed a panel of deregulated miRNAs: Common upregulated miRNAs comprise miR-483, miR-184, miR-503, miR-139 and miR-210. On the other hand, miR-195, miR-497 and miR-335 are among the most investigated underexpressed miRNAs in ACC (10). Moreover, circulating miRNA signatures have been identified in patient sera, thus pointing at the miRNAs' potential as non-invasive biomarkers of malignancy or recurrence (11, 12). Beyond diagnostic and prognostic value, miRNAs turned out as appealing tools for anti-cancer gene therapy. However, the challenge of using miRNA compounds for cancer treatment is to entrap safely miRNAs within delivery

vectors, in order to optimize their stability and minimize their off-target effects (13). The revolution in nanotechnology-based carriers offered great venues for improving the cell-specific delivery of miRNAs. A variety of delivery vehicles, including polypeptide, metal and lipid nanoparticles have been employed; however, to date, few of them are validated for use in humans (14). Lipidots are biocompatible solid lipid nanoparticles (LNPs) emerging as unique reservoirs for nucleic acid loading. Most importantly, LNPs are manufactured with FDA-approved biomaterials, are well tolerated and display an outstanding avidity for steroid-producing organs such as adrenals (15). Although ACC miRnome profiling has been performed in numerous studies, miRNA-based therapies are still scarce for this cancer with only one study reporting the potential of miR-7 as a therapeutic target (16). We have previously shown that two miRNAs, miR-483-5p and miR-139-5p are overexpressed in ACC and promoted cancer cell aggressiveness at least by downregulating the N-myc Downstream-Regulated Gene member 2 (NDRG2) and member 4 (NDRG4) (17). We hypothesized that inhibiting these two miRNAs in cancer cells could be a relevant strategy for ACC therapy. We therefore vectorized inhibitors (antimiRs) of miR-139-5p and miR-483-5p *via* cationic LNPs and assessed the effects of these therapeutic formulations *in vitro* and *in vivo*. We show that miR-139-5p and miR-483-5p are involved in tumorigenic pathways in ACC and that systemic delivery of their inhibitors using Lipidots nanoparticles reduces tumor growth in both ACC cells and xenograft models.

## **Materials and methods**

### *Cell culture*

Cell lines were purchased from the American Type Culture Collection (ATCC). The human ACC cells NCI-H295R (ATCC-CRL-2128) were cultured as monolayers on rat-tail collagen-1-coated plates (Corning) in Dulbecco's Modified Eagle Medium: Nutrient Mixture F-12 (DMEM:F12, Gibco Life Technologies, Courtaboeuf, France). Medium was supplemented with 2.5% Nu-Serum (v/v, Corning) and 1% Insulin-Transferrin-Selenium (ITS) premix (v/v, BD Biosciences, Le Pont de Claix, France) in the presence of antibiotics (100 units/ml penicillin, 100µg/ml streptomycin and 50µg/ml gentamicin, Invitrogen, Cergy Pontoise, France). Renal cell carcinoma cell line 786-O (ATCC-CRL-1932) was cultured in RPMI 1640 medium (Gibco Life Technologies) containing 10% fetal bovine serum (BioSera) and 1% antibiotics (100 units/ml penicillin and 100µg/ml streptomycin, Invitrogen). Mouse fibroblast cell line NIH-3T3 (ATCC-

CRL-1658) was cultured in DMEM supplemented with 10% fetal bovine Serum (BioSera) and 1% antibiotics (v/v). All cell lines were cultured at 37°C in a humidified incubator in the presence of 5% CO<sub>2</sub> and were routinely checked for potential contaminations using the MycoAlert™ Mycoplasma Detection Kit (Lonza, Colmar, France). NCI H295R cells were tested for sterility, rodent pathogens (IMPACT Mouse FELASA) and Mouse Kidney Parvovirus (MKPV) (IDEXX BioAnalytics, Kornwestheim, Germany). They were authenticated using STR-based DNA profiling and multiplex PCR to detect inter-species contamination (CellCheck 9) (IDEXX BioAnalytics).

#### *Generation of NCI H295R cells stably expressing Firefly Luciferase reporter gene*

NCI H295R-Luciferase (Luc) cells were generated using a lentivirus expression system (pLenti-II-CMV-Luc-IRES-GFP vector). The infection protocol was performed according to the manufacturer's instructions (Applied Biological Materials Inc., Richmond, BC, Canada. Cat no. LV152). Briefly, NCI H295R cells were seeded at a 30%-confluence and were incubated in lentiviral medium for 6 hours. Subsequently, cells were cultured in selective medium containing 200 µg/ml Neomycin for 7 days. Additional selection of GFP-expressing cells was performed using fluorescence-activated cell sorting (BD FACSMelody™).

#### *miRNA transfections*

Transient transfections of NCI H295R with miRVana inhibitors of hsa-miR-483-5p (ID: MH11749, ThermoFisher Scientific, Courtaboeuf, France) or hsa-miR-139-5p (ID: MH12629, ThermoFisher Scientific) or a mix of both miRNA inhibitors were performed using Lipofectamine RNAimax (Invitrogen, Life Technologies). AntimiRs and lipofectamine were diluted, as recommended by the manufacturer, in Opti-MEM Reduced Serum Medium (Invitrogen, Life Technologies) to a final concentration of 10nM per 100mm petri dish or per well of 6-well plates. For mock transfection conditions, MiRVana Negative Control Inhibitors were transfected as a random miRNA sequence validated to have no detectable effect on known microRNA function. Transfection medium was discarded after 24 hours. Cells were grown in complete or serum-free (kinase phosphorylation assessment) medium for an additional 48 hours before lysis in presence of protease inhibitor cocktail (Sigma-Aldrich, Saint-Quentin Fallavier, France). Lysates were stored at -80°C. The efficiency of miRNA



knockdown was systematically assessed by reverse transcription (RT) and quantitative PCR (RT-qPCR) 72h after transfection.

#### *Measurement of Wnt/ $\beta$ -catenin signaling (TOPflash luciferase reporter assay)*

NCI H295R cells were seeded in triplicates into 12 well-plates (300 000 cells/well) and transfected for 48h with 10nM AntimiRs using Lipofectamine RNAimax, as previously described. After 2 days, a second round of transfection was performed using Lipofectamine 2000 (Invitrogen, Life Technologies): 250ng of pTOPflash or pFOPflash reporter plasmids (Merk Millipore, Darmstadt, Germany) were co-transfected in the presence of 150ng of pRL-TK-Renilla luciferase plasmid (Promega, Charbonnières-les-Bains, France) to compensate for variations in transfection efficiency. Firefly and Renilla luciferase activities were sequentially measured 24h after plasmid transfection using the Twinlite dual luciferase reporter gene assay system (Perkin Elmer, Wellesley, MA, USA) on an automated TECAN luminometer (TECAN Group Ltd. Zürich, Switzerland). FOPflash plasmid holding mutated TCF binding sites was used as negative control. The ratio of Firefly luciferase activity (Relative light units RLU)/Renilla luciferase activity (RLU) was plotted and expressed as fold changes by comparing to that of control cells.

#### *RNA extraction*

Total RNA and protein extracts were simultaneously isolated from the same lysate sample using the mirVANA PARIS Kit (Ambion, Life Technologies) following the manufacturer's guidelines. Cytoplasmic lysate was clarified by centrifugation at 10 000 rpm for 10min. At the final step, total RNA was eluted in 30 $\mu$ l of RNase-free water and quantitated using a NanoQuant plate on a TECAN instrument (TECAN Group Ltd. Zürich, Switzerland).

#### *MiRNA quantification*

MiRNA levels were measured using TaqMan miRNA assay-based quantitative PCR (Thermo Fisher Scientific). 10ng of total RNA were reverse-transcribed using the TaqMan Reverse Transcriptase kit (Applied Biosystems, Life Technologies) and miRNA-specific stem-loop primers (Thermo Fisher Scientific) in a 15 $\mu$ l-RT reaction containing 0.15 $\mu$ l 100mM dNTPs mix, 1.5 $\mu$ l 10x RT buffer, 0.19 $\mu$ l RNase inhibitor (20 units/ $\mu$ l), nuclease free water, 1 $\mu$ l Multiscribe

Reverse Transcriptase, and 5µl input RNA, in a Gradient Thermal Cycler (Bio-Rad) at 16°C for 30min, 42°C for 30 min, and 85°C for 5min. Real time PCR was performed with TaqMan 2X Universal PCR Master Mix and the appropriate TaqMan MicroRNA Assay Mix for each miRNA of interest. Briefly, 4.5µl of 5-fold diluted RT product was combined with 5.5µl of PCR assay reagents in a final volume of 10µl. Real-time PCR was carried out on a C1000 Thermal cycler (CFX96 Real Time system, Bio-Rad) at 95°C for 10min, followed by 40 cycles at 95°C for 15s and 60°C for 1min. Data were analyzed with CFX Manager Software (Bio-Rad version V1.5.534.0511). Normalized fold change was calculated relatively to control samples using the comparative Ct ( $2^{-\Delta\Delta Ct}$ ) method. RNU48 served as an endogenous control for normalization.

#### *Target gene quantification*

Expression of N-Myc Downstream-Regulated Genes 2 and 4 (NDRG2 and NDRG4) was evaluated by RT-qPCR. Reverse transcription of 1µg RNA was carried out using the iScript cDNA Synthesis Kit (Bio-Rad) according to the manufacturer's protocol. Quantitative PCR was performed using 5µl of 2.5-fold diluted RT product and 5µl of reaction mix composed of 4µl of ssoAdvanced Universal SYBR Green Supermix (Bio-Rad) and 1µl of primer mix (forward and reverse PCR primers at a final primer concentration of 0.35µM) in a final PCR volume of 10µl. All primers were purchased from Sigma-Aldrich; primer sequences are reported in Supplementary Table T5. Real-time PCR was carried out at 95°C for 2 min, followed by 40 cycles at 95°C for 15 s and 60°C for 1 min. Normalized expression of NDRG2 and NDRG4 was calculated using RPL13A and HPRT as housekeeping genes and the comparative Ct method. Fold changes were derived from the  $2^{-\Delta\Delta Ct}$  values with the CFX Manager Software (Bio-Rad version V1.5.534.0511).

#### *PCR arrays*

Transcriptomic analyses of signaling pathways were carried out using qPCR SignArrays® (Anygenes, Paris, France) pre-plated with lyophilized primers for specific gene panels. Reverse transcription was performed with 1µg RNA as previously described for target genes. Following the manufacturer's guidelines, a master mix was prepared for each 96 well-plate by combining 1000µl of Anygenes Perfect Master Mix SYBR Green, 800µl of ultra-pure water and 200µl of 12-fold diluted cDNA. 20µl-reaction volume were added in each well. Reverse

transcription was carried out on a C1000 Thermal cycler (CFX96 Real Time system, Bio-Rad) at 95°C for 10min, followed by 40 cycles at 95°C for 10s and 60°C for 30s. Real time PCR was performed at 95°C for 10min, followed by 45 cycles at 95°C for 10s, 65°C for 30s and a final continuous heating at 95°C. Each plate allows profiling of a single experimental condition. Data were analyzed using Anygenes matrix with intraplate quality controls and plotted as logarithmic fold-changes. Genes were filtered out for  $Ct < 35$  and  $\text{Log}_2\text{FC} > 0.5$  or  $\text{Log}_2\text{FC} < -0.5$ .

### *Western Blotting*

Proteins were extracted from NCI H295R cells using Cell Disruption Buffer (Thermo Fisher Scientific) and were quantified with microBCA protein Assay kit (Thermo Fisher Scientific). 20µg of proteins were dissolved in sample buffer (60 mM Tris-HCl, pH 6.8, 10% glycerol, 2 % SDS, 5 % β-mercaptoethanol, 0.01% bromophenol blue), boiled for 5min and loaded onto 4–20% mini-protean TGX precast protein gels. Electrophoresis was carried out at 80V for 30mins and then at 120V for 1 hour in a 10x Tris/glycine/SDS running buffer (Bio-Rad). SDS-PAGE-resolved proteins were transferred onto a nitrocellulose membrane using the Trans-Blot Turbo™ transfer system (Bio-Rad) according to the manufacturer's instructions. After transfer, the membrane was incubated for 1 hour at room temperature in a blocking solution of Tris-buffer saline (TBS) containing 0.1% Tween 20 and 5% nonfat dry milk. The blots were probed with appropriate antibodies (Supplementary Table T6) in TBS/Tween overnight at 4 °C. The membrane was thoroughly washed with the same buffer, then incubated for 1 hour with either HRP-conjugated goat anti-rabbit IgG (1:3000, Thermo Fisher Scientific) or horseradish peroxidase (HRP)-conjugated goat anti-mouse IgG (1:5000, Thermo Fisher Scientific). The membrane was washed again and the antigen-antibody complex was revealed by Enhanced Chemiluminescence on the ChemiDoc MP imaging system (Bio-Rad). Signal intensity was quantified using Image Lab software version 6.0.1 (Bio-Rad). Protein levels were normalized to tubulin to compensate for protein loading variations. Quantification data are presented relative to the protein content of control samples.

### *Antibody arrays*

Cell lysates corresponding to 200-600µg protein extracts from NCI H295R cells transfected with 10nM of AntimiRs, were incubated with nitrocellulose membranes pre-probed for

phosphokinases and oncology-related proteins (Human Proteome Profiler Array Kits, R&D Systems, Lille, France), according to the manufacturer's recommendations. Nearly 100 capture antibodies in duplicate are spotted on each membrane. When present in the sample, target proteins are specifically captured on the membrane and are detected using a HRP-conjugated detection antibody. Membranes from different experimental conditions were revealed simultaneously using the Chemi Reagent Mix (R&D Systems) and the Chemidoc Imaging system (BioRad). Quantification of chemiluminescence signals was performed with ImageLab software (BioRad). Values of duplicate spots representing one protein were averaged. Interarray comparability was verified by measuring equal pixel intensity of positive control spots on each array for data normalization.

#### *Biotin Pulldown*

To identify miR-139-5p and miR-483-5p targetome, pulldown experiments were carried out using previously described protocols (18, 19). In a first step, NCI H295R cells were transiently transfected with 5nM of Biotinylated miRCURY LNA mimics of hsa-miR-139-5p or hsa-miR-483-5p (Qiagen, Courtaboeuf, France) using Lipofectamine RNAimax. Cells were collected 24h later in lysis buffer (150 mM NaCl, 25mM Tris-Cl pH7.5, 5mM DTT, 0.5% IGEPAL, 60U/ml Superase (Ambion/ThermoFisher), 1X Protease inhibitor cocktail (Sigma-Aldrich)). Streptavidin Magnetic beads (Pierce ThermoFisher) were resuspended and blocked overnight at 4°C in blocking buffer (1 mg/ml yeast tRNA (Invitrogen), 1 mg/ml BSA (Sigma)), then rinsed three times in pulldown wash buffer (1 M NaCl, 10mM Tris-Cl pH7.5, 5mM DTT, 0.5% IGEPAL, 60U/ml Superase (Ambion/ThermoFisher), 1X protease inhibitor (Sigma-Aldrich), 10mM KCl, 1.5mM MgCl<sub>2</sub>). Fractions of the cell lysates were kept apart for transcriptomic sequencing while 400µl of lysates were incubated with the pulldown buffer- resuspended beads for 1h at room temperature on a rotating mixer. Three final washes with pulldown buffer were performed. Beads containing miRNA-mRNA complexes were suspended in 100µl of ultra-pure water and 150µl of cell disruption buffer then pulldown RNA was extracted as previously mentioned using miRVana Paris kit.

#### *Library preparation and HiSeq Sequencing*

RNA library preparations and sequencing were performed by GENEWIZ, LLC (South Plainfield, NJ, USA). SMART-Seq v4 Ultra Low Input Kit for Sequencing was used for full-length cDNA synthesis and amplification (Clontech, Mountain View, CA), and Illumina Nextera XT library was used for sequencing library preparation. Briefly, cDNA was fragmented, and adaptor was added using Transposase, followed by limited-cycle PCR to enrich and add index to the cDNA fragments. The final library was assessed with Agilent TapeStation. The sequencing libraries were multiplexed and clustered on a flowcell. After clustering, the flowcell was loaded on the Illumina HiSeq instrument according to manufacturer's instructions. The samples were sequenced using a 2x150 Paired End (PE) configuration. Image analysis and base calling were conducted by the HiSeq Control Software (HCS). Raw sequence data generated from Illumina HiSeq was converted into fastq files and de-multiplexed using Illumina's bcl2fastq 2.17 software. One mis-match was allowed for index sequence identification.

#### *Data Analysis*

After investigating the quality of the raw data, sequence reads were trimmed to remove possible adapter sequences and nucleotides with poor quality using Trimmomatic v.0.36. The trimmed reads were mapped to the Homo sapiens reference genome available on ENSEMBL using the STAR aligner v.2.5.2b. The STAR aligner is a splice aligner that detects splice junctions and incorporates them to help align the entire read sequences. BAM files were generated as a result of this step. Unique gene hit counts were calculated by using feature Counts from the Subread package v.1.5.2. Only unique reads that fell within exon regions were counted. After extraction of gene hit counts, the gene hit counts table was used for downstream differential expression analysis. Using DESeq2, a comparison of gene expression between the groups of samples was performed. The Wald test was used to generate p-values and Log2 fold changes. Genes with adjusted p-values < 0.05 and absolute log2 fold changes > 1 were called as differentially expressed genes for each comparison. A gene ontology analysis was performed on the statistically significant set of genes by implementing the software GeneSCF. The goa\_human GO list was used to cluster the set of genes based on their biological process and determine their statistical significance.

#### *Steroid Hormone measurements*

Aldosterone and cortisol concentrations in NCI H295R conditioned media were measured using Aldosterone and Cortisol Elisa Test Kits from Diagnostics Biochem Canada Inc (London, Ontario, Canada), according to the manufacturer's instructions. Cells were serum starved overnight and were then treated for 24h with Forskolin (10  $\mu$ M, Sigma-Aldrich) or Angiotensin II (10 nM, Tocris Bioscience, Biotechnique, Bristol, UK) after 24h-AntimiR transfections. Colorimetric detection was performed on TECAN instrument (TECAN Group Ltd. Zürich, Switzerland) at 450nm with a correction read at 540nm. Data were normalized to lysate protein concentrations.

#### *LNP preparation*

Cationic LNPs were prepared by the Microfluidic Systems and Bioengineering Lab (CEA LETI) according to an established standardized protocol (15). LNPs were synthesized as oil-in-water nanoemulsions by sonicating the oily phase in the aqueous phase. The lipid phase is made up of triglycerides (Suppocire<sup>®</sup> NB, Gattefossé and super refined soybean oil, Croda Uniqema) and lecithin (phospholipids, Lipoid SPC3). To allow nucleic acid incorporation, the cationic lipid DOTAP (1,2-dioleoyl-3-trimethylammonium-propane chloride) and the fusogenic lipid DOPE (1,2-dioleoyl-sn-glycero-3-phosphoethanolamine) were added to the lipid phase, thus conferring a positive charge to the resulting formulations. Lipophilic dyes such as Dil (D282, Thermo Fisher) were introduced to the lipid phase to allow fluorescence tracking of LNPs. Once all the compounds have dissolved, the solvent was vacuum-evaporated at a temperature above the wax melting point. The aqueous phase was prepared by hot mixing glycerol and the pegylated surfactant (Myrj40, Croda Uniqema) in PBS to boost viscosity. The so-formed lipid and aqueous phases were appropriately conserved at 50°C, combined, and then the resulting two-phased solution was sonicated at high frequency, until obtaining a clear nanoemulsion solution. LNP purification steps occur through dialysis in LNP buffer (154 mM NaCl, 10 mM HEPES, pH 7.4) using ultra-pure water and 12–14 kDa MW cut-off membranes. At this level, the LNP solution is freed of non-incorporated compounds and is subjected to a final filtration through a 0.22 $\mu$ m-Millipore membrane under a laminar flow PSM. The final particles are stored at 4 °C in PBS.

#### *Complexation of LNP with AntimiRs*

LNP solution was homogenized by tube shaking. AntimiRs and LNPs were diluted, then gently mixed together and left for 5min at room temperature to form complexes before subsequent use. Required volumes of AntimiRs and LNPs were adjusted according to the desired N/P ratio of 16 at a constant AntimiRs concentration of 40nM. N/P represents the ratio of positively charged amine groups (N) within the LNP structure to the negatively charged phosphate groups (P) within the miRNA backbones. Complexation was carried out in Opti-Mem Reduced Serum Medium (Invitrogen, Life Technologies), or in PBS where necessary.

#### *Physical characterization of AntimiRs-LNP complexes*

For a suspension of 1mg/ml of LNPs complexed or not with antimiRs at N/P 16 in ultra-pure water, Zeta potential was measured by electrophoretic light scattering (ELS) in water, the hydrodynamic diameter and polydispersity index (PDI) were subsequently determined in PBS 10X by dynamic light scattering (DLS). All assays were performed in triplicates at 25°C using Zeta Sizer Nano cells (Malvern Instrument).

#### *Electrophoretic mobility shift assays*

The miRNA binding ability of LNPs was investigated by electrophoretic mobility shift assays. LNPs were complexed with AntimiRs or miRNA mimics at N/P 16. Samples were mixed with 10× loading buffer containing 1000-fold diluted SYBR Gold (Invitrogen) and then loaded on a 3% (w/v) agarose gel in TAE buffer. Electrophoresis was run for 10 min at 110 V. Naked miRNA mimics/antimiRs as well as native LNPs were loaded as control samples. The gel was photographed using an epi-light module on a Chemidoc Imager (BioRad).

#### *Cellular uptake of LNPs*

AntimiR-LNP nanoformulations were prepared at N/P 16 with antimiR-ctl, antimiR-139-5p, antimiR-483-5p or mixed antimiRs, then added to 500 000 NCI H295R cells cultured in six well-plates. The final volume was adjusted to 800µl per well by adding OptiMem. After 6h, medium was discarded and replaced by fresh medium for downstream experiments.

#### *Fluorescence labeling of AntimiR*

AntimiRs of hsa-miR-483-5p and hsa-miR-139-5p (miRVana inhibitors) were fluorescently labeled with Fluorescein FAM (Ex 492nm, Em 518nm) Labeling Reagent using Silencer® siRNA Labeling Kit (Life Technologies, Carlsbad, CA, USA) according to the manufacturer's instructions.

#### *Confocal microscopy*

NCI H295R cells were incubated in 6-well plates in the presence of complexed DiI-labeled lipidots and FAM-labeled antimiRs. After 24h, cells were trypsinized then seeded on 8-well-Lab-Tek chambered slides (Thermo Fisher Scientific) for 24h. Nuclei were stained with 1 $\mu$ M of Hoechst 3342 (Thermo Fisher Scientific, Rockford, IL, USA). After rinsing with Hanks' Balanced Salt solution, cells were fixed in 4% paraformaldehyde (PFA) (Sigma-Aldrich, Saint-Quentin Fallavier, France). Lab-tek chambers were detached and cover slips were mounted on the glass slides. Cells were visualized using a laser scanning confocal microscope equipped with an Airyscan detector (LSM 800, Carl Zeiss, Jena, Germany) at 20 or 40 magnification. Images were processed with Zen 2.3 Software (blue edition, Carl Zeiss, Jena, Germany).

#### *Fluorescence-activated Cell Sorting*

NCI H295R, 786-O or 3T3 cells were cultured in presence of DiI-labeled LNPs for 30min, 6h, or 24h. LNP uptake kinetics were analyzed by flow cytometry measurements on a BD FACSMelody cell sorter (BD Biosciences) using a yellow-green (561 nm) laser. 20 000 events (cells) were analyzed with FlowJo software (FlowJo, LLC, BD Biosciences). DiI fluorescence was expressed as DiI geometric means per 10 000 cells to compensate for inter-cell line doubling variations. For complex uptake experiments, NCI H295R cells were incubated with FAM-labeled-AntimiRs and DiI-labeled LNPs at N/P 16, then sequentially subjected to FACS analysis using the yellow-green (561 nm) and bleu laser (488nm) configurations of the FACSMelody cell sorter. Double fluorescence readouts were analyzed with FlowJo software (FlowJo, LLC, BD Biosciences).

#### *Toxicity assays*

NCI H295R cells were cultured in 96 well-plates in presence of LNP doses ranging from 2 to 250 $\mu$ g/ml. LNP-driven toxicity was evaluated by adding 0.5  $\mu$ g/ml Propidium iodide (Sigma-



Aldrich) or 5  $\mu$ M IncuCyte Caspase-3/7 Red Dye (Sartorius, France) in wells. Plates were incubated in the IncuCyte<sup>®</sup> Live Cell Analysis Imaging System (ESSEN BioScience, France) for 24h; real-time images were acquired every 2 hours. Red fluorescence signals from acquired images were quantified as number of counts per  $\text{mm}^2$  using algorithms integrated in the IncuCyte ZOOM Software (Royston Hertfordshire, UK). Propidium Iodide readouts were fitted to logarithmic scale and expressed in sigmoid curves as percentage of dying cells. IC50 was determined using GraphPad Prism software version 4.03 (San Diego, California, USA).

#### *Transwell migration and invasion assays*

NCI H295R cells were incubated with AntimiR-LNP complexes for 48h. 30 000 cells were resuspended in low-serum medium (0.5% Nuserum, 2 $\mu$ g/ml mitomycin) and transferred to 8 $\mu$ m-pore-sized-transwell chambers (BD Falcon) coated with rat-tail Collagen I (Corning). Cell-seeded inserts were placed in 24 well plates containing complete serum-enriched medium (15% Nuserum, 2 $\mu$ g/ml mitomycin). After 48h of migration, unmigrated cells in the top chambers were cleared out using moistened cotton swabs, whereas migrating cells were fixed at the bottom side of the inserts using 4% Paraformaldehyde solution (Sigma), then stained using a Crystal Violet solution (in 10% ethanol). Images of five random fields were acquired for each insert on an axioplan microscope (Zeiss); migratory cells were counted using Image J Software v1.53a (Maryland, USA). Results are illustrated as percentage of migrating cells to control conditions by considering the mean counts of three independent experiments performed in duplicates. Invasion was evaluated using transwells pre-coated with matrigel basement membrane matrix (Corning). Cells were seeded in low-serum medium in the upper chamber while serum-enriched medium was added in the bottom chambers. After 4 days, invading cells were processed as described for migration assays.

#### *Animal studies*

All animal experimentations were approved by the institutional guidelines and those of the European Community for the Use of Experimental Animals (Animal Research authorization APAFIS#25915-2020060809547835 v1). Six-weeks-old female *scid/cb17* mice were purchased from Janvier Labs and maintained in the department's animal facility. For biodistribution tracking, 20 $\mu$ g of FAM-labeled antimiRs were complexed with 10<sup>13</sup> Dil-fluorescent LNPs and

injected in the mice tail veins for 24h, 48h, or 96h. Mice were sacrificed by cervical dislocation, vital organs were carefully collected and imaged with IVIS Lumina II imaging system (Xenogen, Caliper Life Science). The system was configured for fluorescence imaging mode with DsRed (Ex 535nm Em: DsRed ) or FAM (Ex 465nm Em: GFP) settings. Fluorescence signals reflecting the AntimiR/ LNP distribution were acquired as normalized fluorescence efficiency calculated using Xenogen Living Image software version 3.2 with fluorescence background subtraction. Afterwards, tissue were weighted and either fixed overnight in 4% paraformaldehyde (PFA) (Sigma-Aldrich, Saint-Quentin Fallavier, France) or stored at -80°C in RNAlater solution (Invitrogene) for molecular analysis.

For tumor xenograft experiments,  $7.10^6$  NCI H295R-Luc cells were suspended in 50 $\mu$ l of complete growth medium and mixed with 50 $\mu$ l of growth factor reduced matrigel (BD Biosciences). The cell suspension was subcutaneously injected into the hind flank of isoflurane-anesthetized animals. When tumors reached a volume of 100mm<sup>3</sup>, animals were randomly divided into four groups, and treatment was started. 20 $\mu$ g of antimiRs were complexed with  $10^{13}$  Dil-fluorescent LNPs and injected in the tail vein every other day for a total of 8 injections. Tumor growth was routinely monitored either by measuring the emitted bioluminescence or by measuring tumor volume with caliper using the formula  $V = 0.5ab^2$  (a: largest diameter; b: smallest diameter). Results are plotted as tumor volume per day of treatment. For bioluminescence assessments, 150mg/kg of D-Luciferin (Perkin Elmer, Courtaboeuf, France) was injected in the mouse peritoneum. After 15min, anesthetized animals were imaged with the IVIS Lumina II system. Bioluminescence signals, reflecting the number of living tumor cells, are presented as Region of interest (ROI) luminescence and are expressed in photons/sec/cm<sup>2</sup> /sr (Xenogen Living Image software version 3.2). Anesthetized animals mice were sacrificed by cardiac puncture after 24 days of treatment. Tumors and vital organs were collected, weighted and imaged for ex-vivo fluorescence tracking, as previously described.

### *Immunohistochemistry*

5  $\mu$ m-thick paraffin sections of PFA-fixed tumors were deparaffinised and rehydrated. Nuclei were stained with haematoxylin and eosinophilic structures with eosin (Sigma-Aldrich). For Ki67 immunodetection, sections were microwaved in 10 mM citrate buffer pH 6 at 800 W for

2 x 5 min. Endogenous peroxidase activity was blocked by incubating sections with 1 % H<sub>2</sub>O<sub>2</sub> in methanol for 20 min. Slides were then incubated for 20 min in PBS buffer containing 1.5% horse serum (Vectastain Elite ABC Kit, Vector Laboratories) for 20 min at 4°C then with mouse anti-human Ki67 overnight (Ki67 clone MIB1, dilution 1/300 in TBS containing 2% BSA ; Agilent Courtabeuf, Les Ulis, France). After two washes of 5 min in TBS containing 0.1 % Tween 20, sections were sequentially incubated for 30 min with biotinylated anti-mouse secondary antibodies (Vectastain Elite ABC Kit) and for 30 min with an avidin/biotinylated horseradish peroxidase complex (Vectastain Elite ABC kit). Peroxidase activity was revealed using diaminobenzidine tetrachloride as a chromogen (DAKO A/S). Sections were briefly counterstained with haematoxylin, dehydrated and mounted. Slides were examined using a Zeiss Axioplan microscope equipped with an Axiocam HRC camera and Axiovision software version 4.8. Ki67 index was determined by an expert technician pathologist on five random fields with the highest index values for each tumor section.

#### *Statistical analyses*

Statistical analyses were performed with GraphPad Prism software version 4.03 (San Diego, California, USA) using One way ANOVA or unpaired t-tests, where appropriate. Results are expressed as mean ± S.E.M. Statistical significance is indicated as \* for p ≤ 0.05, \*\* for p ≤ 0.01 and \*\*\* for p ≤ 0.001.

## **Results**

### **Inhibition of miR-139-5p and miR-483-5p impedes expression of cancer-related genes**

We have previously shown that miR-139-5p and miR-483-5p are upregulated in ACC and associated with poor prognosis. To determine the relationship between these two miRNA and ACC aggressiveness, NCI H295R cells were transiently transfected with either negative control antimiRs, antimiR-139-5p, antimiR-483-5p or a combination of both antimiRs (Mix AntimiRs). Transfection efficiency and specificity was confirmed within 72h by a significant downregulation of the corresponding miRNA by its inhibitor when transfected alone or in combination (**Figure 1A**). We have previously demonstrated that miR-483-5p and miR-139-5p target two members of the N-myc Downstream Regulated gene family of proteins NDRG2 and NDRG4, respectively (17). Both members were found to play a significant role in the regulation

of NCI H295R and SW13 ACC cell line migration and invasion. We therefore investigated whether miRNA inhibition could restore target gene expression. **Figure 1B** indicates that blockade of miR-139-5p enhanced the expression of NDRG4 by 3-fold when transfected alone and by 1.8-fold when mixed with AntimiR-483-5p. Unexpectedly, the ability of AntimiR-483-5p to restore NDRG2 expression was less pronounced, yet the tendency was maintained (**Figure 1B right panel**). A thorough examination of NDRG2 3'UTR and of the latest release of TargetScan webserver (TargetScanHuman 7.0) revealed that NDRG2 is also a predicted target of miR-139-5p, hence explaining its expression relief upon miR-139-5p inhibition (**Figure 1B right panel**). Inhibition of both miRNAs maintained NDRG4 upregulation while no significant changes were found for NDRG2 (**Figure 1B right panel**). These results led us to dissect further the signaling pathways engaged by miR-139-5p and miR-483-5p to promote ACC aggressiveness. We investigated specific proteomic and transcriptomic landscapes of miR-depleted NCI H295R cells using antibody or PCR arrays dedicated to oncogenic pathways. The expressions of 84 cancer-related proteins were simultaneously detected in lysates of AntimiR control- and Mix AntimiRs-transfected cells with an overall downregulated proteome. Only detectable spots were quantified and plotted in **Figure 1C**. The highest signals were obtained for Epithelial Growth Factor Receptor (EGFR), Enolase, Survivin, Vimentin, Progranulin, Secreted protein acidic and cysteine rich (SPARC), Cathepsin D, Osteopontin, Matrix Metalloproteinase 2 (MMP2). Along the same line, PCR array analyses showed a panel of deregulated genes involved in epithelial-mesenchymal transition (**Figure 1D**). Among the genes filtered out, various WNT ligands, STAT3, Bone Morphogenetic Protein 1 (BMP1), AKT1, Integrin subunit alpha 5 (ITGA5), Transforming Growth Factor Beta 1 (TGFB1), Transcription factor 3 (TCF3), Meosin (MSN), Frizzled 7 (FZD7) and again the pro-migratory protein SPARC, are repressed after inhibiting miR-139-5p and miR-483-5p simultaneously. Conversely, Insulin-like growth factor binding protein 4 (IGFBP4), Vitronectin (VTN) and Keratins were found upregulated upon miRNA blockade. Next, we validated some of these observations by Western Blotting as shown in **Figure 1E**. Typically, MMP2 expression exhibited a 35%-decrease in the presence of AntimiR-483-5p, which was also observed in the Mix AntimiR condition. For Vimentin, protein repression was only detected when both miRNAs were repressed, suggesting a synergic action on this protein. An important mesenchymal marker, N-cadherin

demonstrated a discrete repression when miR-483-5p is inhibited alone or in combination with anti-miR-139-5p.

### **Inhibition of miR-139-5p and miR-483-5p alters NCI H295R cell signaling pathways**

As previously shown in Figure 1D, inhibiting miR-139-5p and miR-483-5p repressed the expression of various components of WNT/ $\beta$ -catenin pathway (WNT ligands, frizzled family member 7 and Transcription Factor 3 (Fzd7, TCF3), a master signaling pathway in ACC. It is worth mentioning that WNT4, an important driver of WNT pathway activation in ACC was not present in the PCR array shown in Figure 1. In order to check whether WNT/ $\beta$ -catenin signaling was affected following miR-139-5p and miR-483-5p repression in NCI H295R cells, we performed TOPflash transfection experiments using reporter plasmids containing TCF binding domains cloned upstream of the TK promoter and Luciferase open reading frame. Luciferase activity indicates binding of  $\beta$ -catenin to the TCF reporter vector, hence activation of downstream TCF-responsive genes in the cell extracts. Our data from five independent experiments showed a discrete, yet significant inhibition of  $\beta$ -catenin activity in the presence of both anti-miRs inhibitors (**Figure 2A**). No effect was observed on  $\beta$ -catenin itself at the protein level, suggesting that miR-139-5p and miR-483-5p target other components of the pathway (**Figure 2B**). The impact of miRNA suppression on tumorigenic signaling pathways was further explored using phosphokinase arrays. **Figure 2C** shows that the phosphorylation status of several kinases including Akt, Chk-2, AMPK, Mitogen and stress activated protein kinase 1 and 2 (MSK1/2), MAP kinases JNK, ERK and p38 were decreased when miR-139-5p and miR-483-5p were repressed. Phosphorylation of two key kinases were validated in **Figure 2D**, which shows a marked decrease in p38 and Akt phosphorylation in NCI H295R cells treated with miRNA inhibitor combination. Taken together, our results provide evidence that downregulation of miR-139-5p and miR-483-5p expression disrupt tumorigenic signaling pathways in ACC. Therefore, counteracting their overexpression could provide a relevant therapeutic approach for ACC.

### **Identification of miR-139-5p and miR-483-5p target genes in ACC**

A single miRNA can target multiple genes through its binding to sequences in the 3'UTR of target mRNA. Thus, it is expected that NDRG2 and NDRG4 transcripts are not the only targets

of miR-139-5p and miR-483-5p. Uncovering novel target genes and their associated signaling pathways may help to better define miR-139-5p and miR-483-5p function in ACC (**Supplementary figure S1**). Hence, we sought to identify additional direct target genes of both miRNAs in ACC. To this end, miRNA pulldown experiments were carried out by transfecting biotinylated mimics into NCI H295R cells for 72h, then miRNA-RNA complexes were isolated from cell lysates. Before proceeding to RNA sequencing (RNAseq), several quality controls were performed, of which RT-qPCR analysis for specific miRNA enrichment in pulldown RNA is depicted in **Supplementary figure S.1.A**. Bioinformatics analysis of RNAseq data revealed upregulated and downregulated genes in pulldowns while we were expecting only enriched miRNA targets. We postulated that these experiments rather reflect the global transcriptomic changes induced by miR-139-5p and miR-483-5p overexpression, including indirect and direct targets of both miRNAs. Significantly differentially expressed genes are represented in volcano plots according to their log<sub>2</sub> fold change compared to control (**Figure S.1.B**). Clustering the top 30 differentially expressed genes (DEG) across the treatment conditions showed a panel of 13 genes co-regulated by miR-139-5p and miR-483-5p (**Figure S.1.C, Supplementary tables T.1 and T.2**), thus suggesting a synergic function of miR-139-5p and miR-483-5p. Among these Top 30 differentially expressed transcripts in miR-139-5p pulldown, none has been described as key gene in adrenal physiology or tumorigenesis. However, gene ontology enrichment (GO) revealed a tight link between miR-139-5p and oxidation-reduction processes in ACC (**Figure S.1D**). These findings are in line with the steroidogenic function of adrenocortical cells, which express several cytochromes P450s enzymes involved in steroid hormone synthesis. It is worth mentioning that cytochromes CYP11B1 and CYP11B2 were found in the gene list of this enriched oxidative pathway (data not shown). Other genes related to phosphorylation cascades, cell adhesion and migration and MAPK signaling pathway were also enriched in miR-139-5p pulldown. For miR-483-5p, the master transcription factor of adrenal physiology NR5A1/SF1 belongs to the Top30 genes significantly differentially expressed in the corresponding pulldown (**Figure S.1.C**). GO analysis revealed that genes involved in positive regulation of transcription, mRNA processing, cell adhesion and migration as well as Wnt signaling pathway are enriched in miR-483-5p pulldown (**Figure S.1D**).

In order to identify putative direct targets of miR-139-5p and miR-483-5p, we performed gene set enrichment analysis (GSEA) for genes with more than 100 counts and that are predicted

as targets for each miRNA by TargetScan prediction program (TargetScan<http://www.targets.org>), using a weighted Targetscan score  $<-0.3$  (**Figure S.1.E**). This filtering allowed for the identification of 190 targets for miR-139-5p and 213 for miR-483-5p. GSEA showed a significant enrichment of negatively-regulated genes by miR-139-5p with an enrichment score of  $-0.39$  ( $p$ -value=0.007); whereas the enrichment was non-significant for miR-483-5p ( $p$ -value=0.165). The leading edges corresponding to the subsets of genes most contributing to the enrichment score comprises 61 genes for miR-139-5p and 44 genes for miR-483-5p (**Supplementary Tables T.3 and T.4**). Interestingly, NDRG2 and NDRG4 were among the top targets of miR-139-5p and were found downregulated when compared to control. Various genes implicated in mitochondrial function and oxidation-reduction were also sorted in GSEA. Altogether, our results indicate that miR-139-5p and miR-483-5p are implicated in the direct/indirect regulation of tumorigenesis-related pathways and control of the differentiated function of adrenocortical cells (i.e. steroidogenesis). The finding that several negatively-regulated genes were enriched in the pulldowns suggests that transfections of miRNA mimics for 72 hours might be too long so that miRNA-triggered degradation of target mRNAs hampers the capture of miRNA-mRNA complexes. Hence, reducing transfection kinetics should improve the identification of direct targets of miR-139-5p and miR-483-5p.

#### **Effects of miR-139-5p and miR-483-5p repression on NCI H295R steroid hormone secretion**

With the recurrence of steroidogenesis-related genes in our sequencing data from the pulldown experiments, we analyzed hormone secretion by NCI H295R cells in basal or stimulated conditions, after efficient miRNA inhibition. Supplementary Figure S2 shows that as expected, forskolin (FSK) or angiotensin II (ATII) induce aldosterone and cortisol secretion as compared to basal non-stimulated conditions. No significant effect of miR-139-5p or miR-483-5p inhibition on aldosterone synthesis was observed either on basal levels or after Angiotensin II stimulation. Interestingly, cortisol levels decreased after forskolin stimulation in anti-miR-139-5p-treated cells. These results suggest a link between miR-139-5p and cortisol regulatory pathways and are in line with our previous observations in patients showing a correlation between miR-139-5p expression in tumors and urinary cortisol levels in patients (Chabre, Libé et al. 2013).

### **Lipidots are well tolerated and preferentially internalized by NCI H295R cells**

One of the major challenges in miRNA-based therapy is that naked RNAs are highly unstable in the circulation. It is therefore critical to develop carriers that can shield miRNAs against degradation (20). Lipidots are solid Lipid Nanoparticles (LNPs) that emerged as promising reservoirs for nucleic acid loading. LNPs feature a core-shell structure with an oily inner content, which allow the incorporation of lipophilic dyes such as Dil, and an outer layer of lecithin stabilized by PEG (21). We first characterized the behavior of "naked" LNPs in NCI H295R cells. The physicochemical properties of LNPs were assessed using Dynamic Light Scattering (**Figure 3A**). These measurements confirmed their nanometric size (35nm), their pharmaceutically acceptable polydispersity index (0.2), as well as their overall positive charge (zeta potential) conferred by the cationic lipids embedded in the shell (39mV). We then evaluated the LNP cytotoxicity in NCI H295R cells and identified an IC<sub>50</sub> of 35µg/ml, highlighting the sensitivity of lipid-avid cells to LNPs (**Figure 3B**) as compared to other cell types (22). Upon incubation with Dil-labeled LNPs, NCI H295R cells rapidly and massively internalized the particles as shown by confocal imaging analysis (**Figure 3C**), with a stable fluorescence signal up to 72h post-treatment (data not shown). To check the in vitro avidity for NCI H295R cell line, kinetics of LNP uptake were performed on two non-steroidogenic cell lines in addition to H295R, namely renal cell carcinoma cell line 786-O and fibroblasts 3T3. Dil fluorescence was quantified by flow cytometry and demonstrated that, at all-time points, Lipidots preferentially accumulated in NCI H295R cells (**Figure 3D**).

### **AntimiRs are efficiently entrapped by Lipidots and delivered to NCI H295R cells**

Once we validated that NCI H295R cells efficiently internalized the LNPs, different nanoformulations were prepared by fine-tuning the ratio of positively charged amine groups from LNPs (N) to negatively charged phosphate groups (P) from miRNA sequence, referred as the N/P ratio. Here, miRNA payload was determined following an N/P ratio of 16. AntimiRs complexation to LNPs was enabled by electrostatic interactions with the cationic LNP shell. MiRNA entrapment was demonstrated by an electrophoretic retardation of miRNA-LNP complexes run on agarose gels, as compared to naked non-complexed miRNA (**Figure 4A**). We then measured the hydrodynamic diameter and Zeta potential of different AntimiR-LNP complexes using DLS (**Figure 4B**). Compared to naked LNPs, apparent sizes of the miRNA-



conjugated LNPs were slightly increased, whereas their surface charge (zeta potential) was decreased from 50mV to nearly 39mV for AntimiR-139-5p and 46 mV for AntimiR-483-5p. This suggests the presence of negatively charged AntimiRs inducing LNP surface charge neutralization. Considering particle aggregation in solution, polydispersity indexes remained within pharmaceutical tolerance (<0.2) no matter the formulation. We next evaluated the uptake of AntimiR-LNP complexes by NCI H295R cells. AntimiR-139-5p was labeled with a FAM dye and complexed with Dil-labeled LNPs at N/P 16. Complexes were added to cell cultures over a timeframe of 72h. Subsequently, cells were subjected to flow cytometry analyses at different time points, for measurement of Dil and FAM fluorescence (**Figure 4C**). Of note, all analyzed cells (100%) were Dil+ all over the experiment, when compared to non-treated cells, thus confirming the stable LNP internalization by NCI H295R cells. Moreover, no fluorescence was captured on the FAM channel alone, thus indicating the only intracellular trafficking of miRNA via LNPs. Analysis of doubly-labeled cells revealed a maximum fluorescence at 24h (50% cells Dil+, FAM+). Importantly, confocal microscopy analysis showed a co-localization of FAM-labeled antimiRs and Dil-labeled LNPs after 6 and 24h of incubation (**Figure 4D**), thus indicating the efficient internalization of Lipidots-AntimiR complexes in NCI H295R cells.

### **Lipidots-delivered antimiRs are biologically active and impair H295R cell migration and invasion**

To determine whether antimiRs were released from LNPs once delivered to the intracellular compartment, endogenous miR-139-5p and miR-483-5p levels were measured by RT-qPCR. Lipidots-delivered antimiRs significantly and specifically repress expression of the corresponding miRNA (**Figure 5A**). Subsequently, we investigated the capacity of Lipidots-AntimiR complexes to relieve the downregulation of the previously identified target genes NDRG4 and NDRG2 (**Figure 5B**). Indeed, RT-qPCR analyses of four experiments showed a 1.4 fold increase in NDRG4 expression upon inhibition of miR-139-5p. A significant 2-fold upregulation of NDRG4 and NDRG2 expression was observed with antimiR-483-5p alone. On the other hand, a significant 1.5-fold upregulation of NDRG4 was measured with antimiR-139-5p and antimiR-483-5p combination. Next, we evaluated the efficacy of the therapeutic formulations by assessing their impact on major cancer hallmarks. Cell death and proliferation assays revealed no significant effect of our miRNA candidates as compared to control (**Figure**

**5C-D).** These results are in agreements with our previous observations showing no impact of both miRNAs on cell cycle progression or apoptosis (17). We then examined the impact of AntimiRs-LNP complexes on NCI H295R cell migration and invasion using Boyden chambers. **Figures 5E and 5F** show that LNP-delivered miR-483-5p and miR-139-5p antimiRs, significantly impaired the migration and invasion of NCI H295R cells as compared to controls. Altogether, our data show that delivering antimiRs via LNPs reversed the aggressive phenotype of NCI H295R cells as observed previously with naked antimiRs (17). Importantly, vectorization of AntimiRs via Lipidots does not interfere with their inhibitory function.

### **In vivo characterization of AntimiRs-LNP treatment as a novel ACC therapy**

Based on our results in vitro, we conducted in vivo experiments using a preclinical mouse model of ACC. We address the potential nanoparticle-driven toxicity, biodistribution as well as treatment effects on tumor growth. We first analyzed the LNP biodistribution when complexed or not with AntimiRs in healthy mice, by tracking the Dil-associated fluorescence. Because of the high skin autofluorescence in *scid/CB17* mice, all fluorescence assays were performed ex-vivo on collected organs. Forty-eight hours after LNP injection, we observed a striking accumulation of LNPs in the adrenal glands and ovaries of treated mice (**Figure 6A**). Such fluorescence pattern persisted up to 96h post-LNP injection (data not shown). Next, we aimed to visualize the in vivo behavior of FAM-labeled AntimiRs and Dil-labeled LNPs complexes upon systemic injection. **Figure 6B** shows that FAM and Dil fluorophores co-localized in the adrenals and ovaries, suggesting the delivery of AntimiRs within LNPs in vivo. Tumors were established by subcutaneously engrafting NCI H295R-Luciferase cells in the hind flanks of *scid/CB17* mice. When tumor size reached 100 mm<sup>3</sup>, treatment was started by injecting AntimiR-LNP formulations in the tail vein every other day. Mice behavior and body weight were regularly monitored for possible signs of toxicity. As seen in **Figure 6G**, injecting different LNP formulations did not affect mice body weight up to 22 days post-injection, hence no LNP-driven toxicity was inferred. Tumor growth was monitored by measuring luciferase luminescence signal intensity as well as tumor volumes over time by caliper measurements (**Figure 6C and 6D**). As shown in **Figure 6D**, a significant growth retardation was observed in mice treated with mixed antimiRs-LNP, which was even more significant in mice injected with antimiR-483-5p nanoformulations. Resected tumors were imaged (**Figure 6E**) and weighted

(**Figure 6F**), thus confirming that tumors from antimiR-483-5p- or mixed antimiRs-LNP were smaller than controls after 24 days of treatment. Moreover, ex-vivo fluorescence from treated mice organs showed an intense Dil accumulation in adrenals, ovaries as well as in the tumor, with a weak signal in the liver (**Figure 6H**). Quantification of fluorescence in lungs, liver, heart, spleen, kidneys, ovaries, adrenals and tumors from all mice groups showed that tumors and adrenals indeed harbored the highest fluorescence signals (**Figure 6I**). Altogether, these first results in vivo suggest that antimiRs delivery using LNPs impeded ACC tumor growth in immunodeficient mice.

### **Molecular analysis of tumor tissues from AntimiRs-LNP-treated mice**

We next evaluated miRNA inhibition in tumors resected from AntimiR-LNP-treated mice using RT-qPCR. No significant changes in targeted miR-139-5p or miR-483-5p were detected, due to the variability between individuals in the same treatment group (**Figure 7A**). However, a trend towards reduced miR-483-5p expression was observed in tumors from animals injected with the corresponding antimiR, which was correlated with a slight increase in NDRG2 expression (**Figure 7B**). We then performed Hematoxylin & Eosin (H&E) staining of tumor sections. **Figure 7C** show that treatment with antimiRs-LNPs did not disrupt tissue integrity. Moreover, there was no detectable tumor necrosis. Immunohistochemical analysis of Ki67, a major prognostic marker for ACC did not show significant changes between mouse treated with AntimiR-ctrl-LNP, AntimiR-139-5p-LNP or Mix-antimiRs (Ki67 index:  $50 \pm 5\%$ ,  $55 \pm 5\%$ ,  $50 \pm 5\%$ ). Again, the tumor from antimiR-483-5p-LNP-treated mouse displayed a decrease in Ki67 labeling ( $40 \pm 5\%$ ). However, it is noteworthy that these observations concern only one random mouse per group and further detailed quantifications remain to be performed.

### **Discussion**

ACC is a rare malignancy with dismal prognosis and unmet clinical needs. Therapeutic options include surgical resection, radiotherapy and adjuvant chemotherapy with mitotane as first line therapy for metastatic cases. To our knowledge, no molecular therapy has proven to be effective. It is well known that prior characterization of the tumor biology is critical for treatment development. Over the last decades, breakthroughs in the fields of molecular biology and next generation sequencing have greatly enhanced our knowledge of ACC

pathogenesis. Anti-angiogenic agents were tested in ACC considering the increased VEGF/VEGFR expression (23). Devastating outcomes have been declared in terms of progression-free survival (24). Clinicians have placed much hope in IGF targeting drugs, as IGF2 and IGF-1R are significantly overexpressed in ACC (8). Unfortunately, a phase III retrospective study reported suboptimal efficacy (25). Despite its central role in carcinogenesis, the Wnt/ $\beta$ -catenin pathway still lacks specific targeted therapy in clinical trials, though preclinical work shows some promise (26). In addition to the transcriptome and methylome, ACC miRnome has been thoroughly analyzed. Aberrant expression of tumor and circulating miRNAs has been reported in ACC patients (6, 11). Besides their diagnostic and prognostic potential, miRNAs have emerged as promising targets for therapeutic applications when shuttled in safe delivery vectors.

In light of our previous study, we focused on two miRNAs upregulated in ACC, miR-483-5p and miR-139-5p (17). Here, we validated their function as oncomiRs mediating ACC aggressiveness, and showed their relevance as candidates for therapeutic targeting. As our strategy aimed to downregulate miR-139/483-5p, all of our experiments were conducted using sequence-specific miRNA inhibitors, also referred as AntimiRs. We encapsulated miRNA inhibitors via lipid nanoparticles, and addressed these nanoformulations in vitro and in vivo, where we assessed their therapeutic potential on cell/tumor phenotype. Moreover, we evaluated for the first time, the combined effects of both miRNAs, which exerted a synergic activity on key signaling pathways at least in vitro, suggesting that their simultaneous targeting may potentiate the therapeutic outcome.

We first showed that inhibiting miR-483-5p and miR-139-5p could restore the expression of their previously validated targets N-Myc Downstream Regulated Genes 2 and 4 (NDRG2 and NDRG4), with a cross-regulation of these genes by both miRNAs. The first gene discovered of the NDRG family, NDRG1, can be repressed by the c-myc and N-Myc proto-oncogenes. Nonetheless, even though each family member has been given the same name, they are not all regulated by either c- or N-myc. NDRG1 and NDRG2 have been shown to display tumor-suppressive activities in cancer (27). The NDRG family comprises four members with a 53-65% shared amino acid identity (28). More precisely, NDRG2 expression is significantly repressed in several tumors such as liver, colorectal, breast, thyroid cancer and glioblastoma (29, 30). NDRG4 however, is less documented, but acts either as oncogene or as tumor suppressor

according to the tissue context (31). Although NDRG2 and NDRG4 have been implicated in the control of proliferation, metastasis and stress responses via repressing the AKT/PI3K pathway (32), the molecular mechanisms underlying their activities in ACC remain to be explored. It is noteworthy that our focus on NDRG2/4 was based on three predictions softwares and anti-correlations of mRNA/miRNA expression profiles in ACC patients (Agosta et al, 2018). We could further validate experimentally the direct interaction of NDRG2 and NDRG4 with their regulatory miRNA. Treatment of NCI H295R cells with NDRG4 or NDRG2 siRNAs increases their migration and invasion (17). Conversely, their overexpression impeded both processes. Interestingly, we also found that NDRG4 underexpression in ACC was highly associated with patient poor prognosis.

We next analyzed the expression of selected cancer-related genes in NCI H295R cells simultaneously depleted in miR-139-5p and miR-483-5p. Among a panel of deregulated proteins, epithelial growth factor receptor (EGFR) was found most expressed and was reduced upon miRNA inhibition. EGFR is overexpressed in ACC versus ACA and is considered as an indicator of malignancy and metastasis (33). Downstream EGFR-dependent signaling pathways (34), including on one hand, the phosphorylation of AKT and its effector TOR, and on the other hand, the phosphorylation of ERK1/2, were also decreased in miRNA-depleted NCI H295R; Activation of these pathways is involved in many cancer hallmarks including cell proliferation and invasion. However, our proliferation tests in vitro did not reveal any significant effect on cell cycle progression and proliferation ((17) and this work), suggesting that others mechanisms are involved. Indeed, AKT phosphorylates a plethora of nuclear and cytoplasmic factors, which modulate various interconnected pathways mediating cell survival, differentiation, protein synthesis, angiogenesis and migration (35). For instance, AKT enhances cell survival and modulates metabolic homeostasis in part via phosphorylating the transcriptional activity of the FOXO subfamily of Forkhead transcription factors, which includes FKHR (Foxo1) (36). We found a reduced Foxo1 expression in NCI H295R cells simultaneously depleted in miR-139-5p and miR-483-5p. In addition, there are nearly 70 downstream effectors of AKT, of which Survivin was correlated to epithelio-mesenchymal transition (EMT) in colorectal cancer (37). We found reduced Survivin expression, which may occur in response to inhibited AKT signaling after miR-139-5p and miR-483-5p silencing in NCI H295R cells. Besides EGFR, Enolase expression was decreased in our antibody array analyses

as compared to controls. Enolase was shown to promote PI3K/AKT and MAPK/ERK signaling in neurological tissues (38). Enolase is a glycolytic enzyme, which catalyzes the interconversion of 2-phosphoglycerate to phosphoenolpyruvate. Its overexpression in cancer accounts for the Warburg effect, an adaptive response of tumor cells to hypoxia. Although it is considered as a marker for neuroendocrine tissues, immunohistochemical examination of ACC tumors revealed abundant staining for Enolase (39). Moreover, serum enolase levels were found markedly high before surgery and were proposed as useful biomarkers for patient management. Collectively, our data support the growing evidence from animal and in vitro models and from analysis of human tumors for the involvement of PI3K/AKT signaling in ACC. Epithelial-mesenchymal transition, a process associated with metastases in several epithelial cancers is highly controversial in ACC because of the mesodermal origin of the adrenal gland. Recently, Sbiera et al. reported that adrenocortical tissues lack expression of epithelial markers and exhibit closer similarity to mesenchymal tissues (40). This in contrast with our study where we were able to detect epithelial markers like keratins and EpCAM in NCI H295R cells. In addition, several pivotal genes of EMT such as the transcription factor TWIST, N-cadherin, Vimentin and metalloproteinase MMP2 were found downregulated upon miR-139-5p and miR-483-5p knockdown. Surprisingly, while N-cadherin expression is correlated with poor prognosis in most carcinomas, it was associated to structure maintenance in normal adrenals and not to ACC aggressiveness (40). Activation of EMT-related genes may be triggered by bone morphogenic proteins (BMP), TGF $\beta$  and hepatocyte growth factor (HGF), upon binding to their respective receptors BMPR, TGFR and MET (41). Of note, our experiments revealed reduced expression of TGF $\beta$ 1 while Follistatin, a reported antagonist of the TGF $\beta$  family member, Activin, exhibited increased expression upon miRNA knockdown. Foremost, the Activin pathway has demonstrated anti-apoptotic activity in ACC (42). A limitation of our study is that we do not have normal adrenocortical cells. Efforts have been recently spilled to establish commercial primary cultures of human adrenocortical cells from normal cortices that will allow us to better apprehend our observations.

Another migration marker worth to be investigated is secreted protein acidic rich in cysteine (SPARC) of which overexpression has been reported in ACC compared with normal cortices (43). As observed at RNA and protein levels (PCR and Antibody arrays), SPARC expression was decreased in presence of both antimicroRNAs. SPARC was shown to induce glioma cell migration

through increased p-P38 MAPK, which prompts actin reorganization, thus cell migration (44). Our data demonstrate a striking decrease in phosphorylated P38 MAPK (p-P38) after anti-miR-transfection, which supports the role of miR-139-5p and miR-483-5p in cell migration.

In terms of activated signaling pathways in ACC, Wnt/ $\beta$ -catenin is on top of the list (activated in 39%-41% of ACC) as determined by integrated genomic analyses led by Assié et al. and Zheng et al (6, 7). Gain-of-function mutations in CTNNB1 (the gene encoding  $\beta$ -catenin) and deletion or loss of function mutation in ZNRF3 (a negative regulator of the Wnt/ $\beta$ -catenin pathway) lead to constitutive activation of Wnt/ $\beta$ -catenin signaling in ACC. We did not find any effect of miRNA silencing on  $\beta$ -catenin expression. Our analysis of Wnt/ $\beta$ -catenin signaling revealed a decreased expression of various Wnt ligands, Frizzled receptors (Fzd7) and TCF transcription factors upon miR-139-5p and miR-483-5p inhibition. Measurement of  $\beta$ -catenin activity using TCF/LEF reporter constructs showed a discrete, yet significant decrease in combined miRNA inhibition. Along the same line, Kim et al. reported that NDRG2 negatively regulates TCF/ $\beta$ -catenin signaling via GSK-3 $\beta$  in colon carcinoma (45). As we observed a significant upregulation of NDRG2/NDRG4 following miRNA inhibition, the potential role of these genes as attenuators of Wnt/ $\beta$ -catenin signaling in ACC deserves further investigation. Moreover, looking at a potential regulatory feedback loop, we have evidenced that constitutively active  $\beta$ -catenin is involved in miR-139-5p overexpression in NCI H295R cells and downregulation of its target gene NDRG4 (unpublished data from our team). This suggests a complex interplay between miR-139-5p and this oncogenic pathway.

The identification of the whole targetome of miR-139-5p and miR-483-5p and associated signaling pathways may help to better characterize their role in ACC development and progression. In the present study, we aimed to identify miR-139-5p and miR-483-5p targetome using pulldown experiments followed by RNA sequencing of miRNA-bound mRNAs. To stay in line with our in vitro assays, a first pulldown experiment was carried out after 72h of biotinylated miRNA mimics transfection. Binding of the transcripts to their biotinylated regulatory miRNAs is expected to translate into enrichment of the targeted mRNA in the pulldown material. Nevertheless, our RNA-sequencing analyses revealed that 54% and 37% of differentially expressed gene were downregulated in miR-139-5p and miR-483-5p pulldowns, respectively, making identification of bona fide targets challenging. These results might be attributable to too long kinetics and indicate that the time window to be used for miRNA

mimic transfections is critical for such experiments, in order to capture target transcripts before their degradation by the mRNA decay machinery. As a striking correlation was obtained between our pulldown data and transcriptomic data (correlation coefficient  $r=0.92$ , data not shown), we decided to go further and to analyze the pulldown data as classical transcriptomic data of miRNA mimics-transfected cells, where downregulation of direct and indirect target genes is expected. Using this approach, we found that genes involved in cell migration and cell adhesion were enriched in GO analysis, thus confirming our in vitro functional studies. Very interestingly, key P450 cytochrome enzymes catalyzing steroid hormone biosynthesis as well as SF1, a master regulator of steroidogenesis, were also identified in GO and GSEA analyses, respectively. These results are in line with our findings that miR-139-5p interplays with adrenal cortisol secretion, in addition to cancer-related pathways.

Through the “fine tuning” of multiple signaling pathways, miRNA-based therapy might restore homeostasis and provide an effective strategy to abolish transcriptome or proteome dysregulations in cancer cells. In our study, we believe that we have collected a panel of indirect and direct target transcripts of miR-139-5p and miR-483-5p. Nonetheless, our molecular analyses demonstrate that miR-139-5p and miR-483-5p anti-miRs simultaneously alter various cancer-related pathways, and therefore have the potential to exert therapeutic effects. In light of these observations, we decided to test miRNA inhibitors in therapeutic settings by delivering them via the lipid nanoparticles Lipidots (LNPs), first in vitro then in vivo. With regard to our cancer model and envisaged approach, cationic LNPs were best adapted. Their positive charges favor electrostatic interactions with negatively charged nucleic acids, hence ensuring their engraftment on LNP surface. Moreover, physico-chemical characterization of naked Lipidots at time of manufacture then two years later in our experiments confirmed an outstanding stability of these nanoparticles. A conserved size of about 35nm and an acceptable polydispersity index indicate no subsequent aggregation, which could drive toxicity. Importantly, we demonstrated for the first time that the strong tropism observed initially with the neutral LNPs for adrenocortical cells, is maintained with cationic LNPs. As shown previously in vivo with neutral LNPs (46), we observed a striking uptake of cationic LNPs by the ACC cell line NCI H295R. These cells were clearly sensitive to LNPs as witnessed by the low IC<sub>50</sub> of 35µg/ml as compared to other cell lines (46). This



observation is reminiscent of lipid adrenal hyperplasia where accumulation of unmetabolized cholesterol becomes toxic for cellular metabolism, leading to cell death. After complexation at N/P 16, DLS characterization of AntimiRs-LNP complexes showed a slight increase in size with miRNA engraftment as compared to naked LNPs. Most importantly, charge variations were barely detectable in zeta potential measurements, when compared to naked LNPs, indicating a charge imbalance between positively charged LNPs and negatively charged AntimiRs in the nanoformulations. These observations suggest that, at N/P 16, LNPs are still far from saturation and that higher miRNA trapping may be considered. This engages lower N/P ratios, thereby lower zeta potentials (closer to zero). Previous observations with siRNA indicated marked zeta potential variations starting at N/P 8, which accounts for double the miRNA concentration used for N/P 16 formulations (21). It is worth mentioning that AntimiRs are single-stranded sequences complementary to the miRbase sequences of miR-139-5p and miR-483-5p; for this reason, their detection on agarose gels was more complex than that of double-stranded miRNA mimics. Moreover, the activity of nucleic acids after discharge from LNPs is a major concern in nanomedicine, since impurities formed through lipid:RNA reactions may induce cargo instability, thus loss of function (47). Not only did we visualize the antimiR-LNP colocalization and internalization by NCI H295R cells, but we also showed the release of bioactive antimiRs from LNPs in vitro. Indeed LNP-delivered antimiRs conserved their specific miRNA inhibiting capacities, hence reproducing the previously reported impacts of miR-139-5p and miR-483-5p on cell invasion and migration. While the choice of N/P 16 was based on previous work from our LNP suppliers, we achieved significant miRNA inhibition in vitro, despite the positive charge of our nanoformulations. The possibility of trapping additional miRNA to reach nanoparticle saturation highlights the potential of LNPs as important reservoirs for miRNA vectorisation.

We then administered AntimiRs-LNP complexes systemically into ACC-bearing mice. The high skin autofluorescence may be avoided in upcoming experiments by using near-infrared-fluorophores such as DiD, incorporated in the core of LNPs. Ex-vivo fluorescence of major organs showed the expected accumulation pattern of antimiRs-LNPs in steroidogenic tissues, in addition to tumors. This natural LNP tropism to lipid avid organs is probably due to LNPs' activity as lipoproteins, and the enrichment of these tissues with lipid receptors. LNP

accumulation in tumors is attributed to the Enhanced Permeability and Retention effect through the leaky tumor vasculature. Thanks to their biodegradability, LNPs' components are metabolized in the liver through the natural lipid pathways (48), which explains the occasional Dil signals collected in this organ. No visible signs of toxicity were detected all over the treatment campaign; This remain to be confirmed by dosing liver enzymes like aspartate aminotransferase (AST) and (alanine aminotransferase) ALT. At this stage, we provided a pilot experiment to validate the proof of concept of the therapeutic strategy. We are aware that any off-tumor accumulation represents a loss of drug bioavailability, not to forget the potential reprotoxicity induced by repetitive injections and accumulation in ovaries/testis. Adding an EGFR targeting antibodies on the surface of LNPs may enhance their accumulation in EGFR-expressing ACC tumors and prevent accumulation in the contro-lateral normal adrenal or reproductive tissues; on the other hand, we should consider mouse models with pseudo-orthotopic tumors embedded under the renal capsule to best mimic tumor physiology.

We observed a significantly reduced tumor growth and weight upon intravenous injections of our novel formulations, notably those containing AntimiR-483-5p. However, our in vitro assays showed no impacts of miR-139-5p and miR-483-5p on NCI H295R cell proliferation. This discrepancy suggest a potential role of the tumor microenvironment, which is not observable in vitro. In line with these results, Ki67 labeling of tumor sections did not reveal significant changes in tumor cell proliferation. One hypothesis is that inhibiting miR-139-5p and miR-483-5p negatively modulates tumor angiogenesis. Indeed, our unpublished data indicate that both miRNAs are shuttled within NCI H295R-derived microvesicles (exosomes) which are internalized by endothelial cells and promote angiogenesis (unpublished data). Therefore, miRNA silencing may prevent tumor vascularization, hence tumor growth. Immunohistochemical analysis of tumor vessels remains to be performed. Unfortunately, we could not detect significant miRNA inhibition in collected tumors. Our RT-qPCR data revealed inter-individual variability of miRNA expression within the same treatment group, even in control mice, though a slight inhibition was observed for miR-483-5p. Our hypothesis is that miRNA inhibition is likely to be masked by residual miRNAs from murine cells. Indeed, we could detect species cross-contaminations by RT-qPCR since the established tumors comprise mouse macrophages and endothelial cells, expressing miR-139-5p and miR-483-5p, in addition

to NCI H295R cells. In order to circumvent such issues, in addition to reduced availability of AntimiRs at the tumor site due to para-tumor accumulations of LNPs, it seems essential to test additional miRNA doses in vivo. Here, we have injected 20µg of AntimiRs engrafted to LNPs (~120 miRNA molecules/nanoparticle) and repeated injections 8 times for each mouse. The release efficiencies of AntimiRs from LNPs as well as the potential loss of cargo during the particles' bloodstream journey remain to be defined. Tracking double-fluorescently labeled LNPs and AntimiRs all over the treatment cycle would be helpful.

## **Conclusion**

This study reports the first use of Lipidots® to vectorize miRNAs in a therapeutic context. We evidenced that targeting oncogenic miRNAs is a promising strategy for the treatment of ACC. Most importantly, we have shown that delivering inhibitors of miR-139-5p and miR-483-5p through lipid nanoparticles reduces the aggressive and invasive phenotype of cultured ACC cells by impeding pro-cancer signaling pathways. Although the molecular processes behind the nanoformulations' behavior in vivo remain to be thoroughly investigated, our findings open new avenues for the development of novel therapeutics for ACC. Moreover, with the emergence of combinatorial therapy approaches, it would be particularly interesting to test LNPs loaded with mitotane in addition to AntimiRs. Finally, our approach is at the heart of nanomedicine and could be extended to other more frequent cancers associated with alterations of microRNAs.

## **Funding**

This research was funded by the Institut National de la Santé et de la Recherche Médicale, the Ligue Nationale Contre le Cancer (Comités Loire et Isère, R16167CC and R19013CC) and the Cancéropôle Rhône-Alpes Auvergne CLARA Oncostarter (CVPPRCAN000183) and the Institut National du Cancer (INCA-DGOS-8663, COM-ETE-TACTIC). This work has been performed in a laboratory receiving support from the GRAL LabEX (ANR-10- LABX-49-01) within the frame of the CBH-EUR-GS (ANR-17-EURE-0003). This project received help from MuLife imaging facility, which is funded by GRAL, a programme from the Chemistry Biology Health Graduate School of University Grenoble Alpes (ANR-17-EURE-0003).

## **Conflicts of Interest**

The authors declare no conflict of interest.

## Figures

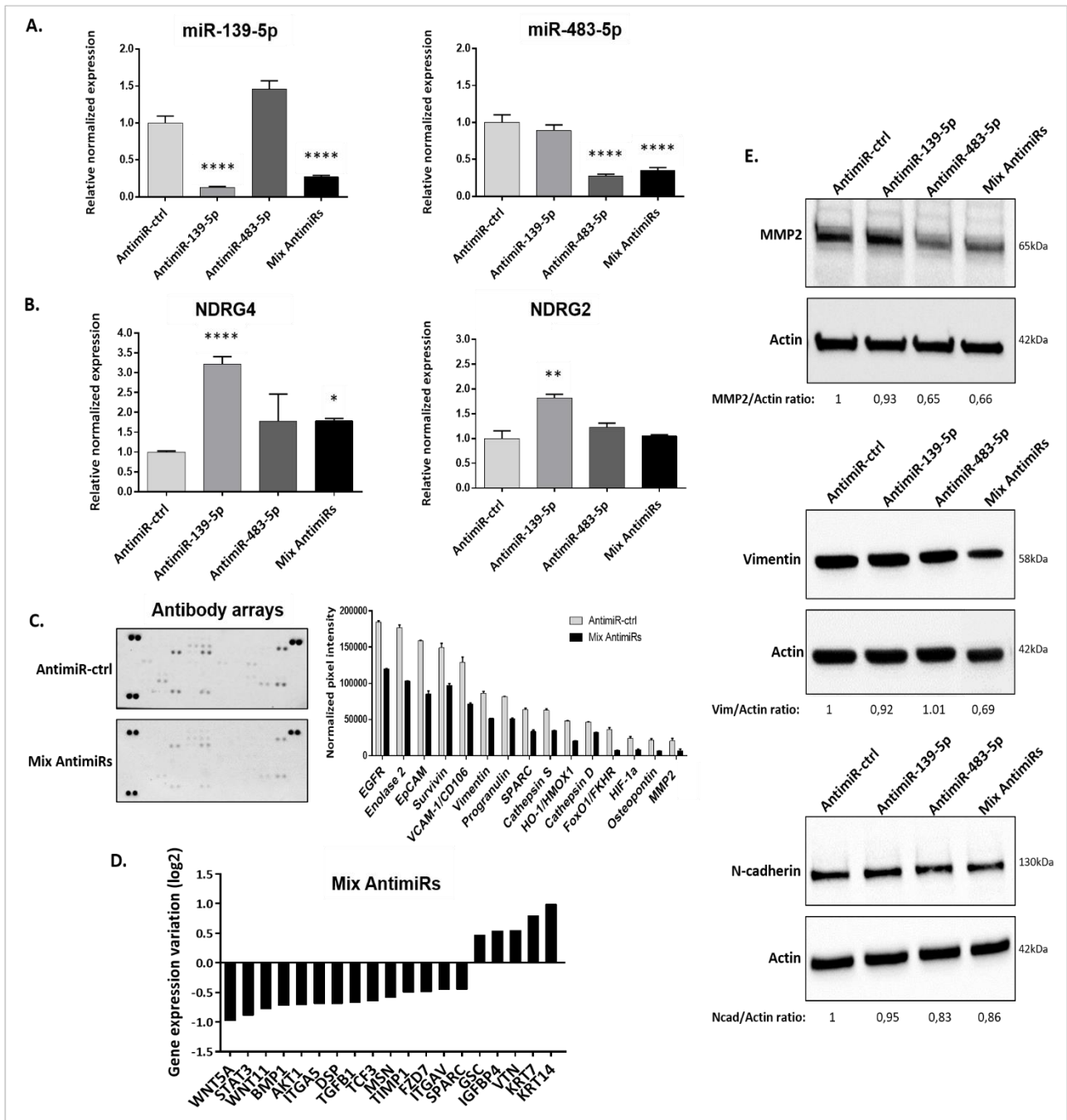


**Figure 1. Downregulation of miR-139-5p and miR-483-5p levels in NCI H295R cells impairs the expression of cancer-related genes**

(A) NCI H295R cells were transiently transfected for 72h with inhibitors (antimiRs) of miR-139-5p or miR-483-5p alone or antimiRs combined together or with a negative control inhibitor. MiRNA inhibition was checked by RT-qPCR. Normalized expression was plotted relative to control (n=4). (B) Effects of miRNA inhibition on endogenous NDRG2 and NDRG4 expression (n=4). (C) Human oncology antibody array analysis of Control and AntimiRs-treated NCI H295R (n=2 per group). Arrays illustrated on the left panel were imaged simultaneously on a Chemidoc imaging system, and pixel intensity was measured and normalized using ImageLab software. (D) PCR array analysis of two independent experiments where NCI H295R cells were transfected with mix AntimiRs or negative controls. Unexpressed genes (Ct>35) were discarded. Gene expression was normalized and plotted as log2 fold-change relative to AntimiR-ctrl. (E) Western Blot analysis of MMP2, Vimentin and N-cadherin protein expression in NCI H295R cells transfected with 10nM of miRNA inhibitors. Shown are blots representative of three independent experiments. Protein expression was quantified using ImageLab software and normalized to actin. Data are Means ± SEM. \* p≤ 0.05, \*\* p≤ 0.01 and \*\*\*\* p<0.0001

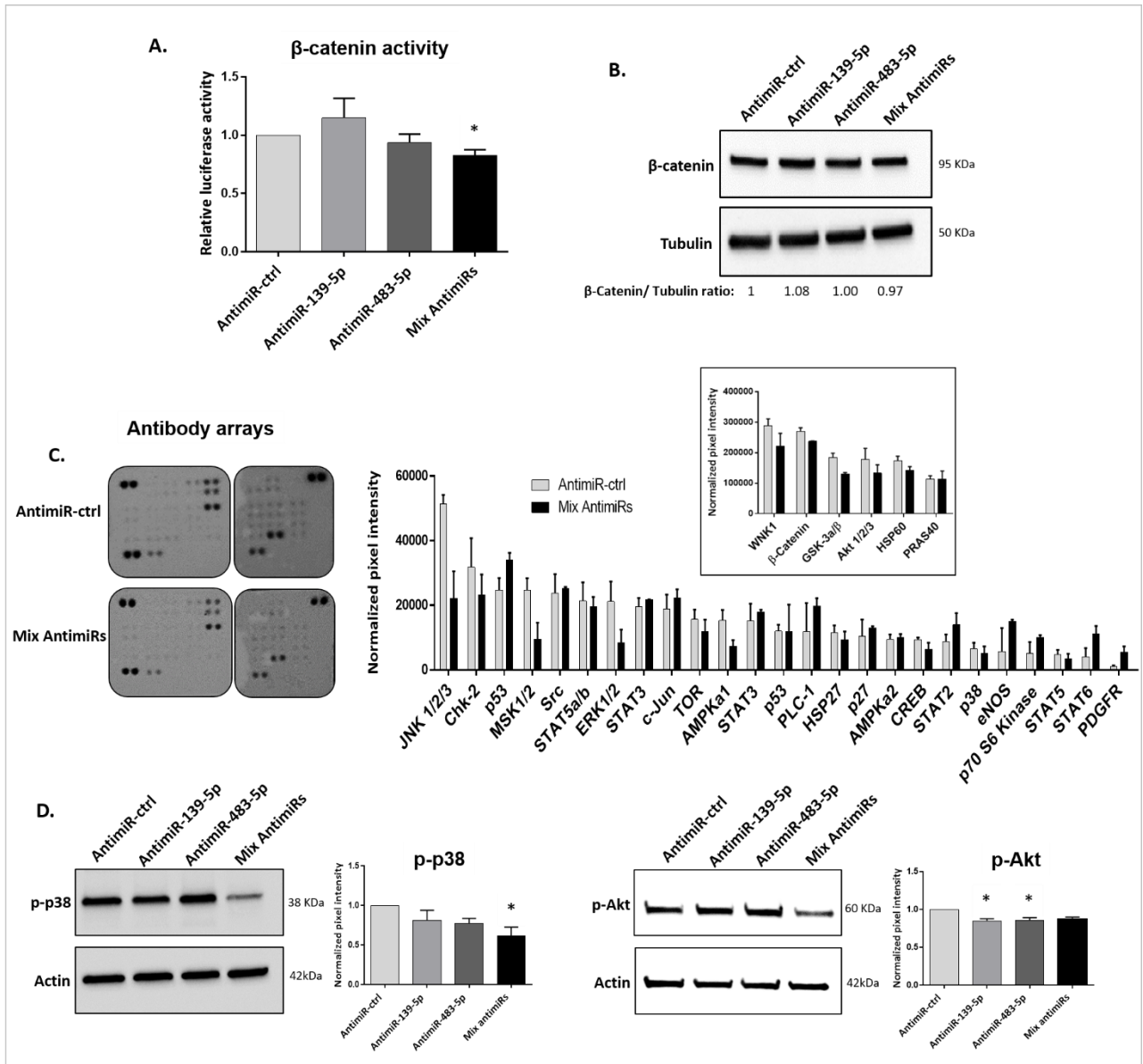


**Figure 2. Downregulation of miR-139-5p and miR-483-5p levels alters NCI H295R signaling pathways**

(A) The TOPflash reporter system, which contains a luciferase reporter plasmid with TCF/LEF-binding sites upstream of the minimum thymidine kinase promoter was used to investigate the role of miR-139-5p and miR-483-5p in Wnt/ $\beta$ -catenin signaling pathway regulation. Plotted are Firefly/Renilla luciferase activity ratios  $\pm$  SEM for five independent experiments performed in triplicates. (B) miR-139-5p and miR-483-5p repression does not affect  $\beta$ -catenin protein expression. (C) Proteome profiling of phosphokinases in cells transfected with control anti-miRs or combined inhibitors of miR-139-5p and miR-483-5p. Each array comprised two membranes for the analysis of a single sample and all arrays were imaged simultaneously. Spot intensities were quantified for detectable kinases. The right inset represents highly expressed proteins. (D) Phospho-p38 (p-p38) and phospho-Akt (p-Akt) protein expression in NCI H295R cells transfected with control AntimiR, AntimiR-139-5p, AntimiR-483-5p or both inhibitors. Shown western blots are representative of four experiments with the same trend. Protein expression was quantified and normalized to Actin; Fold-change to control was plotted as mean  $\pm$  SEM. Statistical significance was determined using ANOVA, with \*:  $p < 0.05$ .

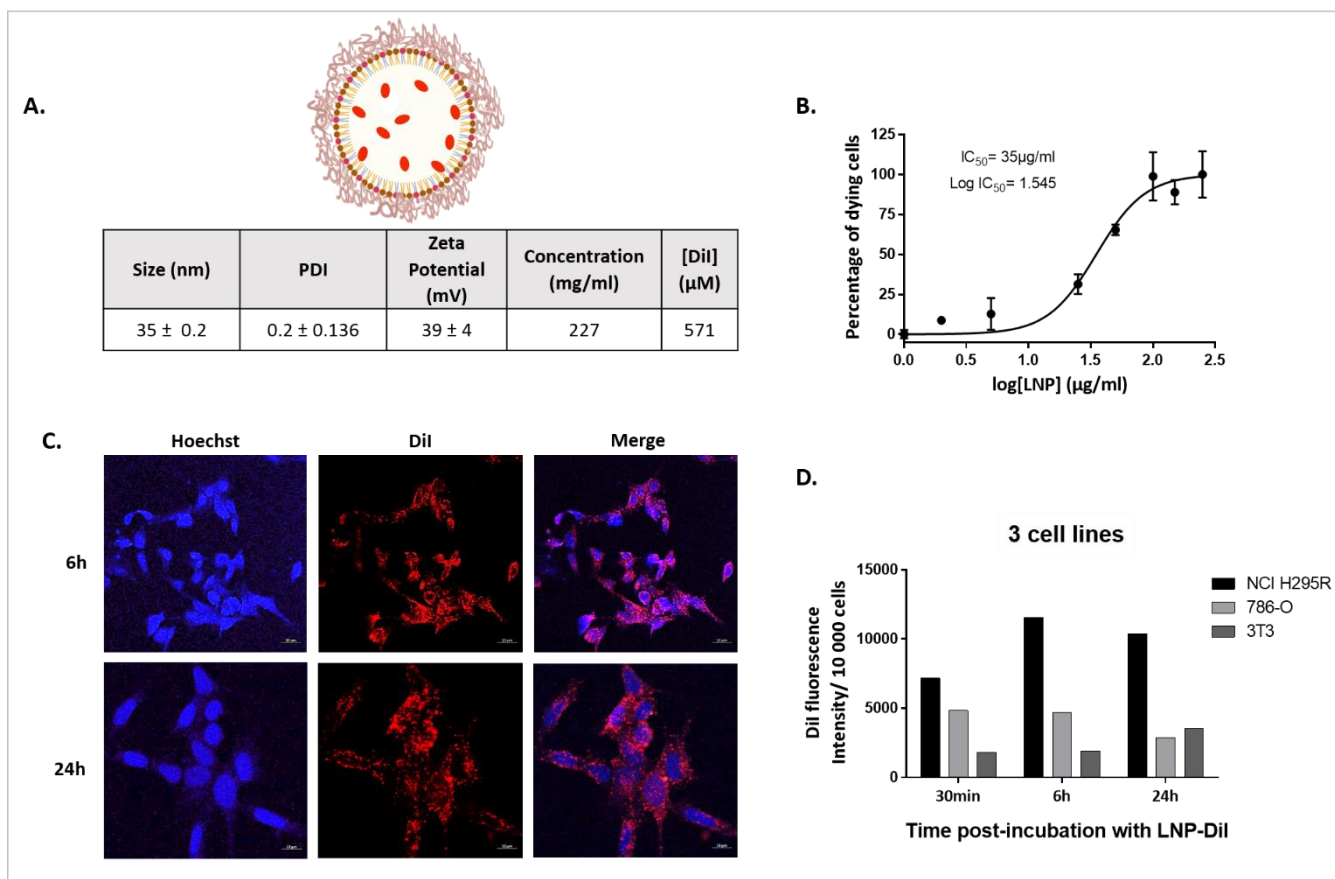


**Figure 3: In vitro characterization of Lipidots**

(A) Schematic representation of a lipid nanoparticle (LNP) with a lipid core containing the DiI dye (red ovals) and an outer shell of phospholipids and polyethylene glycol. Physico-chemical properties of manufactured LNPs were measured by DLS and ELS on a Zetasizer (Malvern Instruments). (B) Cytotoxicity assays of NCI H295R incubated with increased doses of LNPs were performed by counting propidium iodide incorporation. IC<sub>50</sub> was determined after logarithmic fitting. (C) Laser confocal microscopy analysis of NCI H295R cells incubated with DiI-LNP for 6h or 24h and visualized at 20x- or 40x-magnification, respectively. Nuclei were stained with Hoechst. Scale bar, 20  $\mu$ m. (D) FACS quantification of DiI fluorescence in three cell lines after 30min, 6h or 24h of incubation with LNP-DiI. Data were normalized per 10 000 cells to compensate for inter-cell line doubling time variabilities.

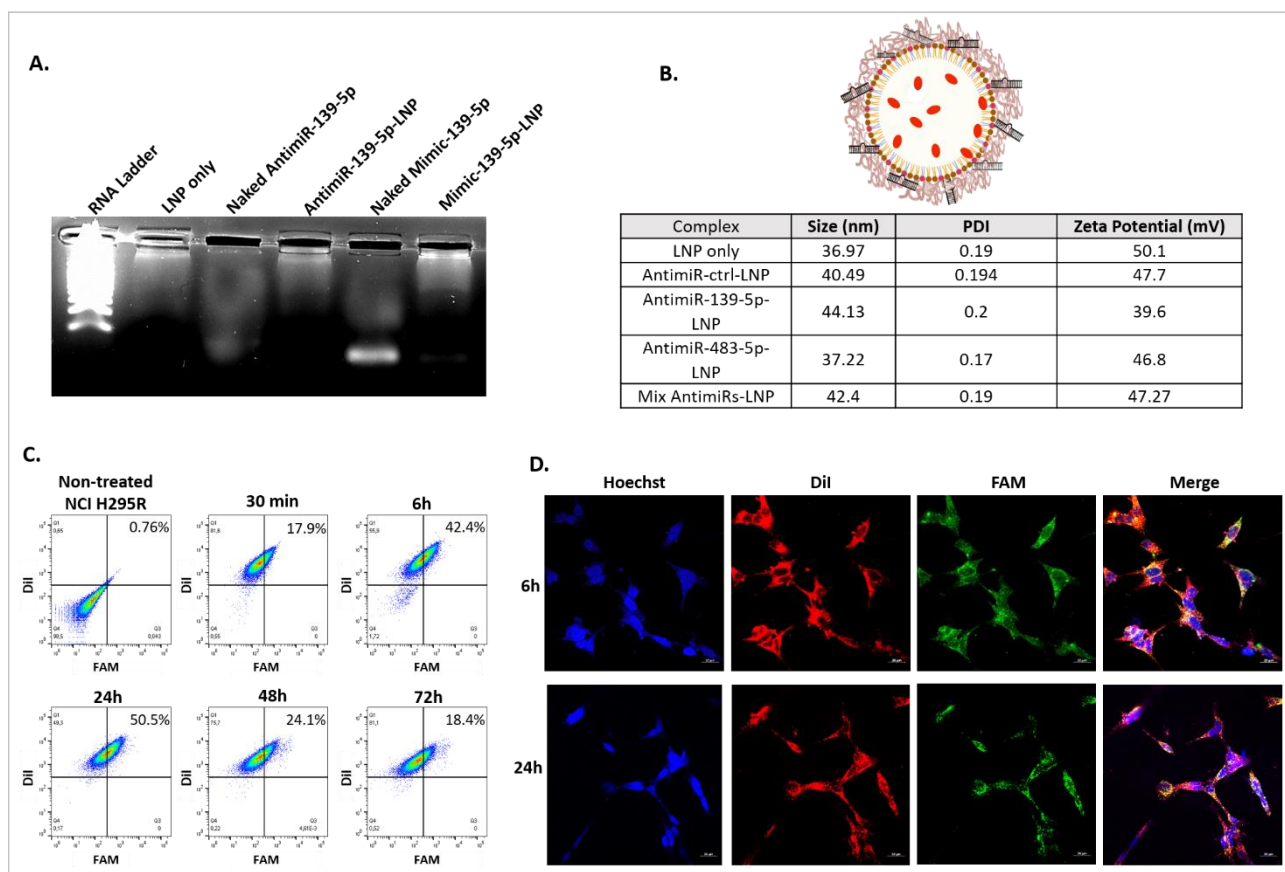


**Figure 4. Complexation and cellular uptake of AntimiR-LNP complexes.**

**(A)** MiRNA binding to LNPs at N/P 16 was investigated by gel electrophoresis mobility shift assay. In each lane was loaded either naked LNP or naked miRNA mimics/inhibitors or LNP-miRNAs complexed at N/P 16. miRNA conjugation to LNP is revealed by electrophoretic mobility shift. **(B)** The hydrodynamic diameters and polydispersity index of LNP-AntimiRs complexes at N/P 16 were measured in PBS buffer on a zetasizer instrument by DLS. Zeta potential measurements were performed on a zetasizer instrument by ELS. **(C)** FACS analysis of double fluorescence signals from NCI H295R cells incubated with FAM-labeled AntimiR-139-5p and DiI-labeled LNPs complexes for 30 minutes, 6, 24, 48 and 72 hours. **(D)** Confocal microscopy analysis of the uptake of doubly-labeled complexes by NCI H295R cells. Scale bar 20 $\mu$ m.



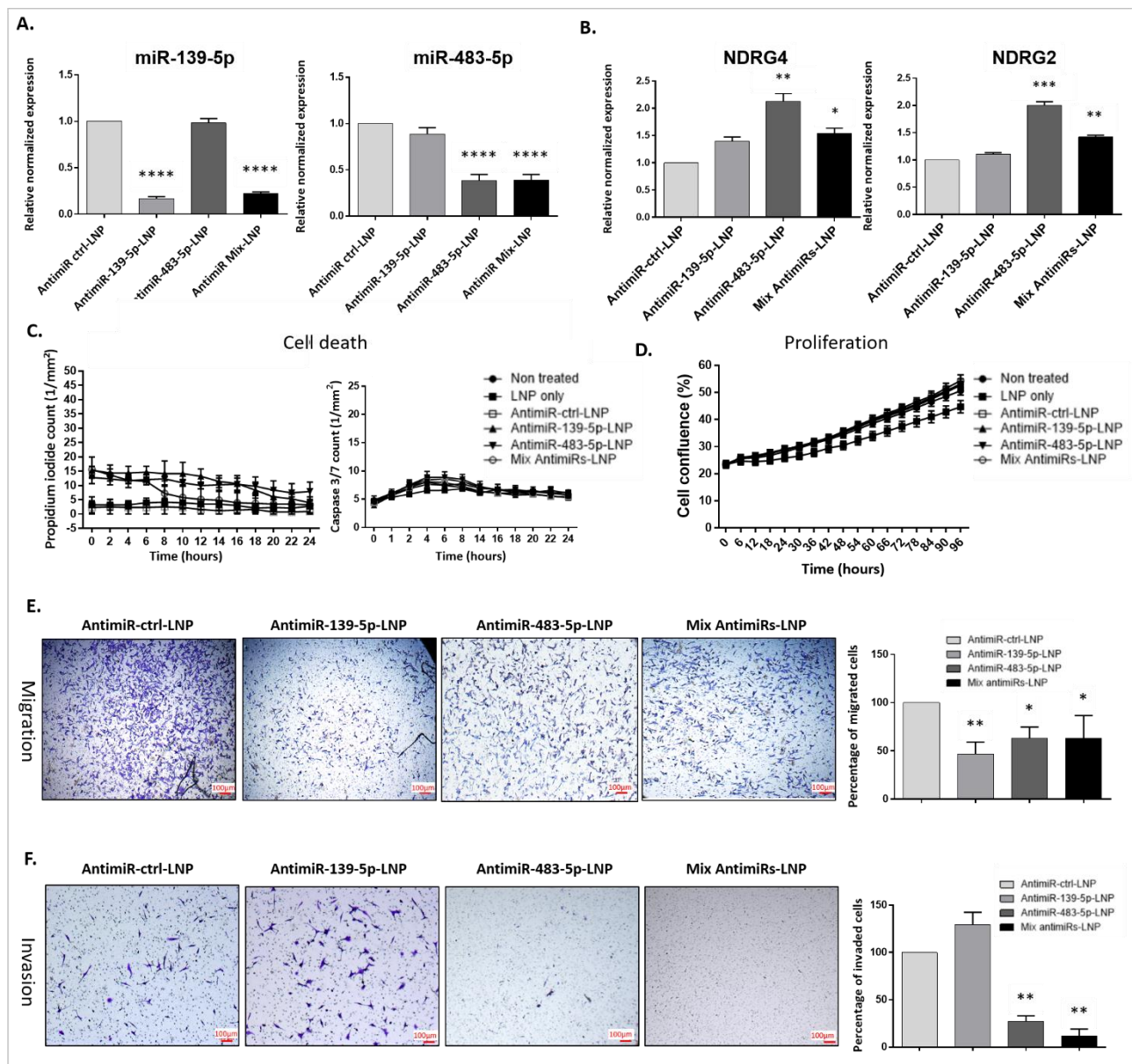


**Figure 5. AntimiRs-LNP complexes efficiently repress endogenous miR-139-5p and miR-483-5p expression and impede NCI H295R cells migration and invasion.**

(A) Determination of AntimiRs-LNP complexes efficiency. Expression levels of miR-139-5p and miR-483-5p in NCI H295R cells treated with AntimiRs-LNP were quantified by RT-qPCR (n=7), and plotted as fold change to control (mean  $\pm$  SEM). Statistical analysis was performed using ANOVA, \*\*\*\*p<0.0001. (B) Effects of AntimiRs-LNP on endogenous NDRG2 and NDRG4 expression (n=4), \*\*p<0.01, \*\*\*p<0.001. (C) Treated and mock-treated cells were stained with propidium iodide and analyzed using Incucyte Living imaging system. Live images were acquired every 2h for 24h. Propidium iodide incorporation was analyzed with the Incucyte Zoom software and plotted as number of Red object counts per mm<sup>2</sup> of a single well (n=3). No significant difference was observed between the treatment conditions. Caspase-mediated apoptosis was assessed using the Incucyte system as described for Propidium iodide. (D) NCI H295R cells were seeded at 20% confluence in 96-well plates, then incubated in the presence or in the absence of AntimiRs-LNP at N/P 16 for 96h. Cell proliferation was calculated using built-in algorithms of the Incucyte Zoom software and was correlated to confluence percentage (n=3). (E) and (F) NCI H295R cells were incubated with AntimiR-LNP complexes, then analyzed on transwell chambers for their migration and invasion capacities. Invasion chambers were pre-coated with a matrigel layer. The right panels show cell number quantification acquired using ImageJ from five random fields per well (mean  $\pm$  SEM) and are representative of 3 independent experiments, \*p<0.05, \*\*p<0.01.

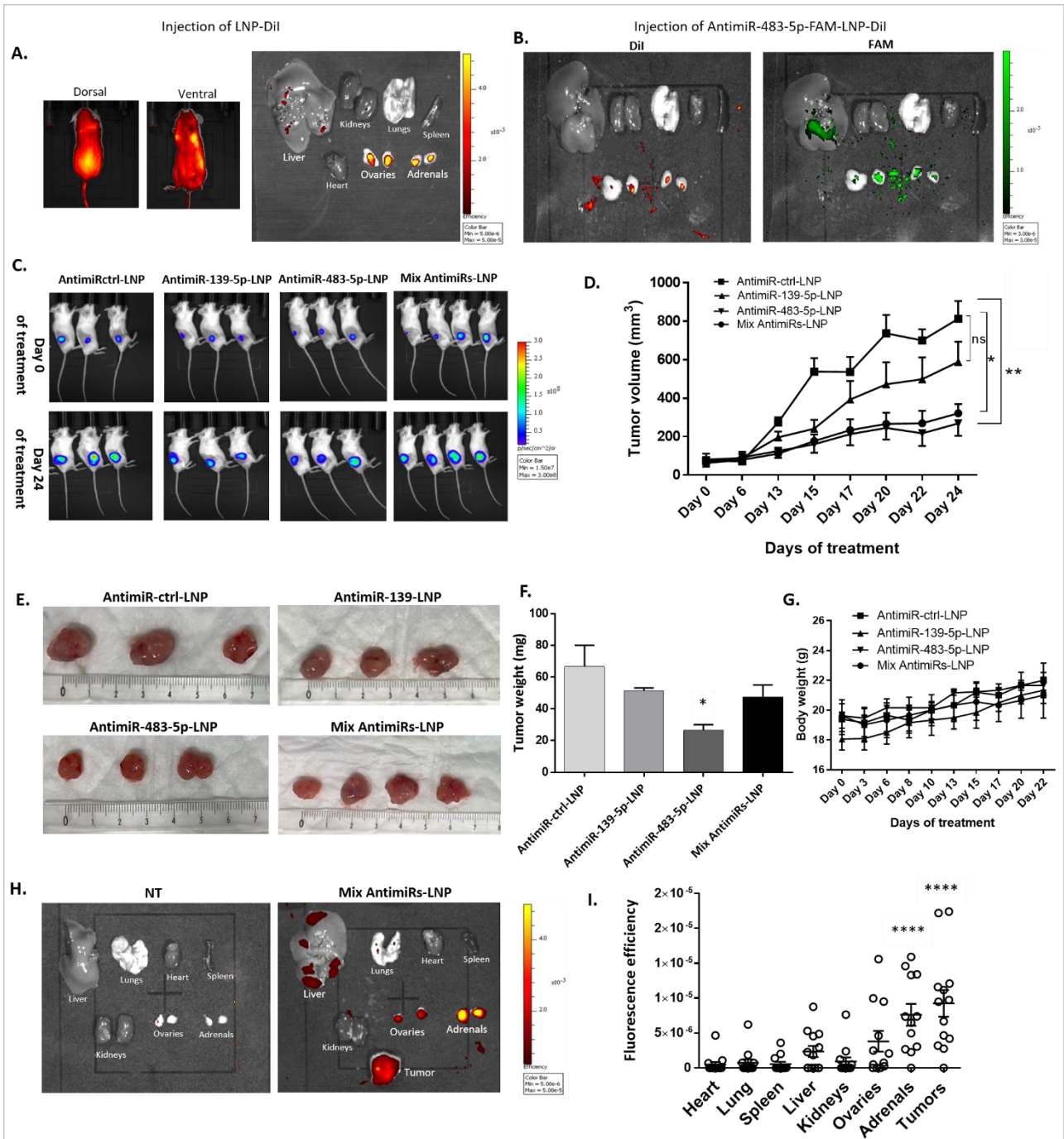


**Figure 6. Determination of AntimiRs-LNP effects on tumor growth in vivo.**

(A) Biodistribution studies of  $10^{13}$  LNPs injected in the tail vein of healthy Scid/CB17 mice. The left panels show skin autofluorescence of the whole animal. Shown in the right panel is a representative image of 2 independent experiments with 22 mice. (B)  $20\mu\text{g}$  of FAM-AntimiRs were complexed with  $10^{13}$  LNPs-Dil. Fluorescence signals from red and green channels reflecting the AntimiR/LNP distribution were acquired on IVIS Lumina II imaging system. (C) NCI H295R-luc cells were subcutaneously implanted into immunodeficient Scid/CB17 mice ( $n=3$  or  $n=4$  per group). Tumor growth was monitored by the measurement of emitted bioluminescence at day 0 and 24 of treatment. (D) Tumor volume was determined by caliper measurements using the formula  $V = 0.5ab^2$  ( $a$ : largest diameter;  $b$ : smallest diameter). Results are plotted as tumor volume per day of treatment. Statistical analysis were performed with two-way ANOVA with multiple comparisons to control group. (E) Macroscopic images of tumors from each treatment group after sacrifice at day 24. Scale bar, 1cm. (F) Tumor weight at day 24 are presented for each treatment group as mean  $\pm$  SEM. Statistical analyses were performed using ANOVA,  $*p < 0.05$ . (G) Multiple injections did not affect mouse body weight. (H) Biodistribution of LNP fluorescence in non-treated or AntimiRs-LNP injected mice reveals a clear accumulation of LNPs in adrenals, ovaries and tumor. (I) Fluorescence efficiency was analyzed with background subtraction and quantified using Xenogen Living Image software. Dots represent fluorescence efficiency per each organ of all treated mice ( $n=13$ ). Statistical significance were determined using ANOVA with  $****p < 0.0001$ .

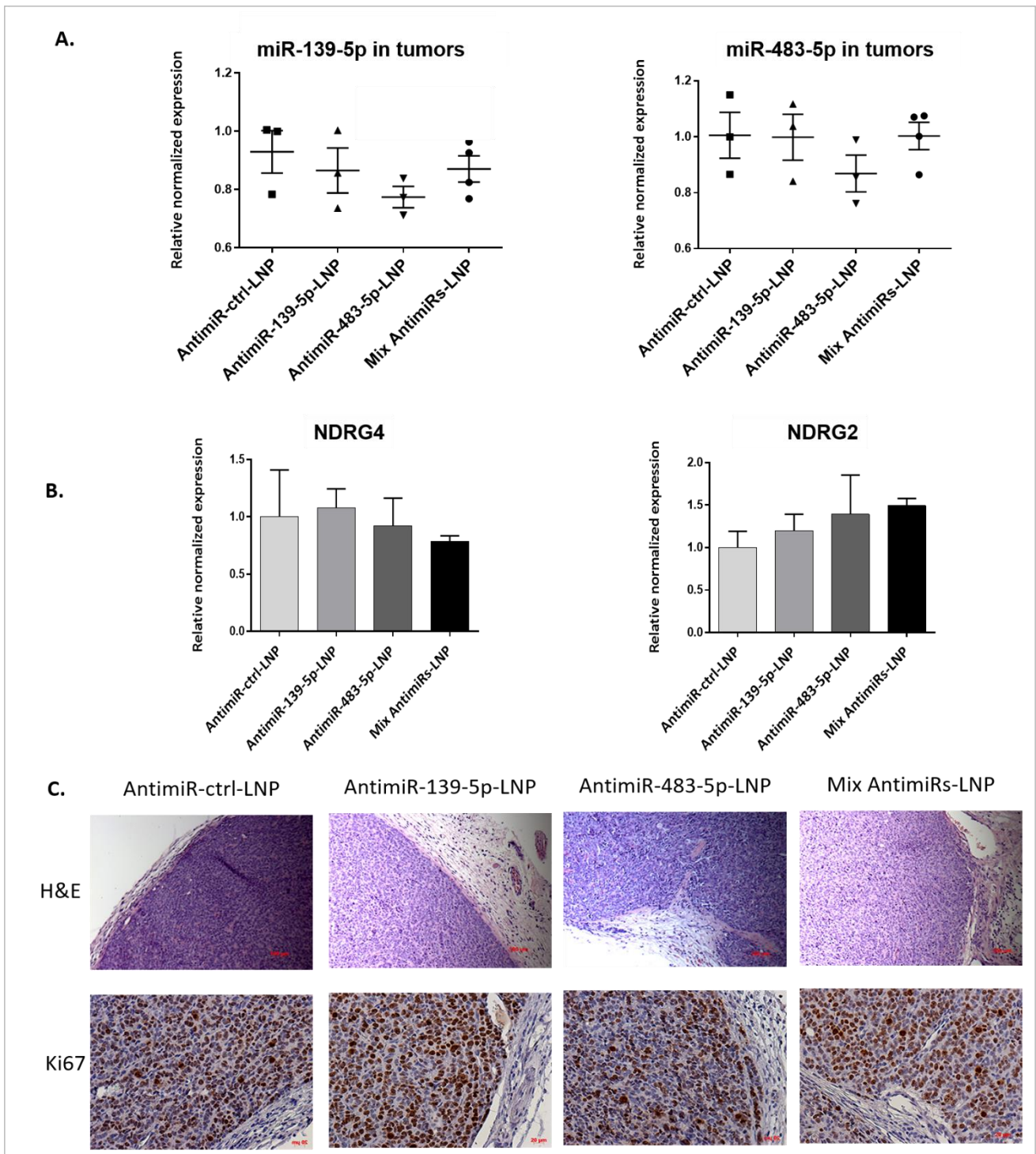


**Figure 7. Molecular analyses of tumor tissues.**

**(A)** RT-qPCR analysis of miRNA expression in tumor tissue of AntimiRs-treated mice. For each mouse of a treatment group, normalized expression data are plotted relative to controls. Error bars correspond to mean  $\pm$  SEM. **(B)** Expression of NDRG2 and NDRG4 mRNAs in tumors of treated mice. **(C)** H&E staining and immunohistochemical analysis of Ki67 of one random mouse per treatment group, scale bars 100 $\mu$ m and 20 $\mu$ m respectively.

## References

1. Prilutskiy A, Nosé V. Update on adrenal cortical neoplasia. *Diagnostic Histopathology*. 2021;27(6):240-51.
2. Bilimoria KY, Shen WT, Elaraj D, Bentrem DJ, Winchester DJ, Kebebew E, et al. Adrenocortical carcinoma in the United States: treatment utilization and prognostic factors. *Cancer*. 2008;113(11):3130-6.
3. Koschker AC, Fassnacht M, Hahner S, Weismann D, Allolio B. Adrenocortical carcinoma -- improving patient care by establishing new structures. *Experimental and clinical endocrinology & diabetes : official journal, German Society of Endocrinology [and] German Diabetes Association*. 2006;114(2):45-51.
4. Fassnacht M, Dekkers OM, Else T, Baudin E, Berruti A, de Krijger RR, et al. European Society of Endocrinology Clinical Practice Guidelines on the management of adrenocortical carcinoma in adults, in collaboration with the European Network for the Study of Adrenal Tumors. *European Journal of Endocrinology*. 2018;179(4):G1-G46.
5. Raj N, Zheng Y, Kelly V, Katz SS, Chou J, Do RKG, et al. PD-1 Blockade in Advanced Adrenocortical Carcinoma. *Journal of clinical oncology : official journal of the American Society of Clinical Oncology*. 2020;38(1):71-80.
6. Assié G, Letouzé E, Fassnacht M, Jouinot A, Luscap W, Barreau O, et al. Integrated genomic characterization of adrenocortical carcinoma. *Nature Genetics*. 2014;46(6):607-12.
7. Zheng S, Cherniack Andrew D, Dewal N, Moffitt Richard A, Danilova L, Murray Bradley A, et al. Comprehensive Pan-Genomic Characterization of Adrenocortical Carcinoma. *Cancer Cell*. 2016;29(5):723-36.
8. Almeida MQ, Fragoso MC, Lotfi CF, Santos MG, Nishi MY, Costa MH, et al. Expression of insulin-like growth factor-II and its receptor in pediatric and adult adrenocortical tumors. *J Clin Endocrinol Metab*. 2008;93(9):3524-31.
9. Ambros V. The functions of animal microRNAs. *Nature*. 2004;431(7006):350-5.
10. Singh P, Soon PSH, Feige J-J, Chabre O, Zhao JT, Cherradi N, et al. Dysregulation of microRNAs in adrenocortical tumors. *Mol Cell Endocrinol*. 2012;351(1):118-28.
11. Chabre O, Libé R, Assie G, Barreau O, Bertherat J, Bertagna X, et al. Serum miR-483-5p and miR-195 are predictive of recurrence risk in adrenocortical cancer patients. *Endocr Relat Cancer*. 2013;20(4):579-94.
12. Oreglia M, Sbiera S. Early Postoperative Circulating miR-483-5p Is a Prognosis Marker for Adrenocortical Cancer. *Cancers*. 2020;12(3).
13. Zhang Y, Wang Z, Gemeinhart RA. Progress in microRNA delivery. *Journal of controlled release : official journal of the Controlled Release Society*. 2013;172(3):962-74.
14. Zhang S, Cheng Z, Wang Y, Han T. The Risks of miRNA Therapeutics: In a Drug Target Perspective. *Drug design, development and therapy*. 2021;15:721-33.
15. Courant T, Bayon E, Reynaud-Dougier HL, Villiers C, Menneteau M, Marche PN, et al. Tailoring nanostructured lipid carriers for the delivery of protein antigens: Physicochemical properties versus immunogenicity studies. *Biomaterials*. 2017;136:29-42.
16. Cherradi N. microRNAs as Potential Biomarkers in Adrenocortical Cancer: Progress and Challenges. *Frontiers in endocrinology*. 2015;6:195.

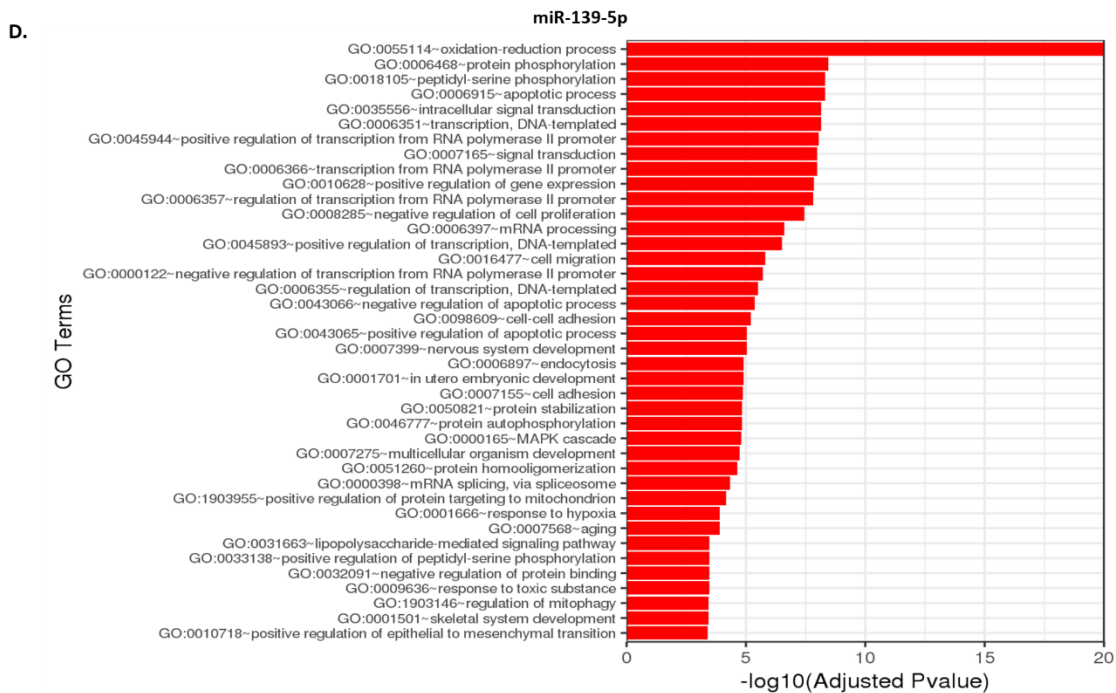
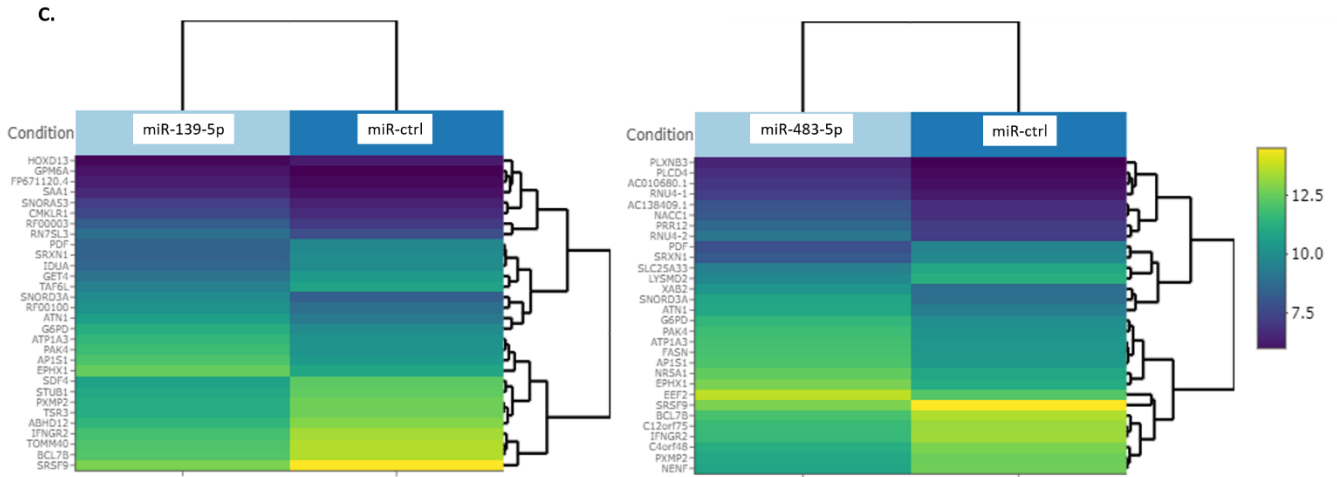
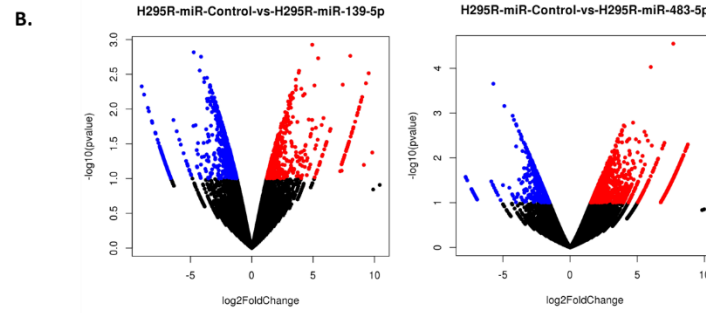
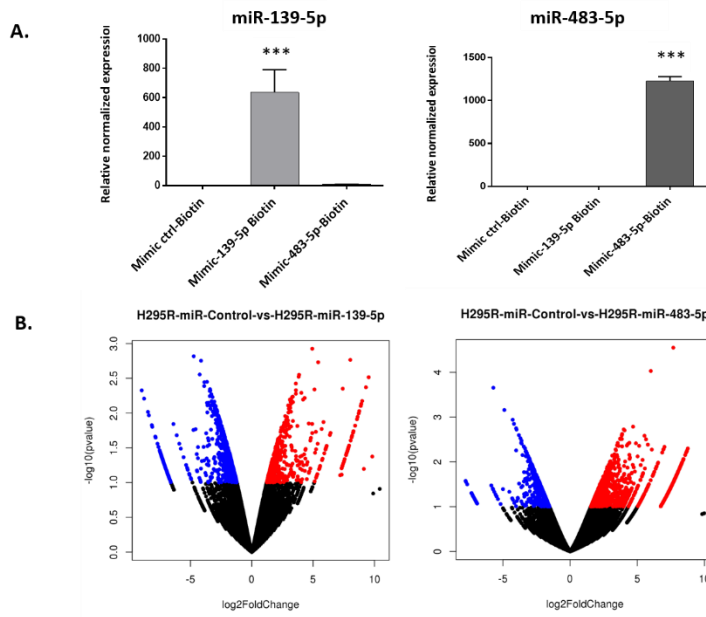
17. Agosta C, Laugier J, Guyon L, Denis J, Bertherat J, Libé R, et al. MiR-483-5p and miR-139-5p promote aggressiveness by targeting N-myc downstream-regulated gene family members in adrenocortical cancer. *International journal of cancer*. 2018;143(4):944-57.
18. Dash S, Balasubramaniam M, Dash C, Pandhare J. Biotin-based Pulldown Assay to Validate mRNA Targets of Cellular miRNAs. *Journal of visualized experiments : JoVE*. 2018(136).
19. Tan Shen M, Kirchner R, Jin J, Hofmann O, McReynolds L, Hide W, et al. Sequencing of Captive Target Transcripts Identifies the Network of Regulated Genes and Functions of Primate-Specific miR-522. *Cell Reports*. 2014;8(4):1225-39.
20. Zhang L, Yang X, Lv Y, Xin X, Qin C, Han X, et al. Cytosolic co-delivery of miRNA-34a and docetaxel with core-shell nanocarriers via caveolae-mediated pathway for the treatment of metastatic breast cancer. *Scientific Reports*. 2017;7(1):46186.
21. Dey AK, Nougarede A, Clément F, Fournier C, Jouvin-Marche E, Escudé M, et al. Tuning the Immunostimulation Properties of Cationic Lipid Nanocarriers for Nucleic Acid Delivery. *Frontiers in Immunology*. 2021;12.
22. Bayon E, Morlieras J, Dereuddre-Bosquet N, Gonon A, Gosse L, Courant T, et al. Overcoming immunogenicity issues of HIV p24 antigen by the use of innovative nanostructured lipid carriers as delivery systems: evidences in mice and non-human primates. *npj Vaccines*. 2018;3(1):46.
23. Cerquetti L, Bucci B, Raffa S, Amendola D, Maggio R, Lardo P, et al. Effects of Sorafenib, a Tyrosin Kinase Inhibitor, on Adrenocortical Cancer. *Frontiers in endocrinology*. 2021;12:667798.
24. Berruti A, Sperone P, Ferrero A, Germano A, Ardito A, Priola AM, et al. Phase II study of weekly paclitaxel and sorafenib as second/third-line therapy in patients with adrenocortical carcinoma. *Eur J Endocrinol*. 2012;166(3):451-8.
25. Fassnacht M, Berruti A, Baudin E, Demeure MJ, Gilbert J, Haak H, et al. Linsitinib (OSI-906) versus placebo for patients with locally advanced or metastatic adrenocortical carcinoma: a double-blind, randomised, phase 3 study. *The Lancet Oncology*. 2015;16(4):426-35.
26. Batisse-Lignier M, Sahut-Barnola I, Tissier F, Dumontet T, Mathieu M, Drelon C, et al. P53/Rb inhibition induces metastatic adrenocortical carcinomas in a preclinical transgenic model. *Oncogene*. 2017;36(31):4445-56.
27. Melotte V, Qu X, Ongenaert M, van Criekinge W, de Bruïne AP, Baldwin HS, et al. The N-myc downstream regulated gene (NDRG) family: diverse functions, multiple applications. *The FASEB Journal*. 2010;24(11):4153-66.
28. Hwang J, Kim Y, Kang HB, Jaroszewski L, Deacon AM, Lee H, et al. Crystal structure of the human N-Myc downstream-regulated gene 2 protein provides insight into its role as a tumor suppressor. *The Journal of biological chemistry*. 2011;286(14):12450-60.
29. Hu XL, Liu XP, Lin SX, Deng YC, Liu N, Li X, et al. NDRG2 expression and mutation in human liver and pancreatic cancers. *World journal of gastroenterology*. 2004;10(23):3518-21.
30. Lorentzen A, Lewinsky RH, Bornholdt J, Vogel LK, Mitchelmore C. Expression profile of the N-myc Downstream Regulated Gene 2 (NDRG2) in human cancers with focus on breast cancer. *BMC cancer*. 2011;11:14.
31. Chu D, Zhang Z, Zhou Y, Li Y, Zhu S, Zhang J, et al. NDRG4, a novel candidate tumor suppressor, is a predictor of overall survival of colorectal cancer patients. *Oncotarget*. 2015;6(10):7584-96.
32. Morishita K, Nakahata S, Ichikawa T. Pathophysiological significance of N-myc downstream-regulated gene 2 in cancer development through protein phosphatase 2A phosphorylation regulation. *Cancer science*. 2021;112(1):22-30.

33. Kamio T, Shigematsu K, Sou H, Kawai K, Tsuchiyama H. Immunohistochemical expression of epidermal growth factor receptors in human adrenocortical carcinoma. *Human Pathology*. 1990;21(3):277-82.
34. Miyamoto Y, Suyama K, Baba H. Recent Advances in Targeting the EGFR Signaling Pathway for the Treatment of Metastatic Colorectal Cancer. *International Journal of Molecular Sciences*. 2017;18(4):752.
35. Robbins HL, Hague A. The PI3K/Akt Pathway in Tumors of Endocrine Tissues. *Frontiers in endocrinology*. 2015;6:188.
36. Matsuzaki H, Daitoku H, Hatta M, Tanaka K, Fukamizu A. Insulin-induced phosphorylation of FKHR (Foxo1) targets to proteasomal degradation. *Proceedings of the National Academy of Sciences*. 2003;100(20):11285-90.
37. Lee SC, Kim OH, Lee SK, Kim SJ. IWR-1 inhibits epithelial-mesenchymal transition of colorectal cancer cells through suppressing Wnt/ $\beta$ -catenin signaling as well as survivin expression. *Oncotarget*. 2015;6(29):27146-59.
38. Haque A, Polcyn R, Matzelle D, Banik NL. New Insights into the Role of Neuron-Specific Enolase in Neuro-Inflammation, Neurodegeneration, and Neuroprotection. *Brain Sciences*. 2018;8(2):33.
39. Ide H, Terado Y, Tokiwa S, Nishio K, Saito K, Isotani S, et al. Novel Germ Line Mutation p53-P177R in Adult Adrenocortical Carcinoma Producing Neuron-specific Enolase as a Possible Marker. *Japanese Journal of Clinical Oncology*. 2010;40(8):815-8.
40. Sbiera I, Kircher S, Altieri B. Epithelial and Mesenchymal Markers in Adrenocortical Tissues: How Mesenchymal Are Adrenocortical Tissues? *Cancers*. 2021;13(7).
41. Cano CE, Motoo Y, Iovanna JL. Epithelial-to-mesenchymal transition in pancreatic adenocarcinoma. *TheScientificWorldJournal*. 2010;10:1947-57.
42. Hofland J, de Jong FH. Inhibins and activins: Their roles in the adrenal gland and the development of adrenocortical tumors. *Mol Cell Endocrinol*. 2012;359(1):92-100.
43. Demeure MJ, Stephan E, Sinari S, Mount D, Gately S, Gonzales P, et al. Preclinical investigation of nanoparticle albumin-bound paclitaxel as a potential treatment for adrenocortical cancer. *Annals of surgery*. 2012;255(1):140-6.
44. Alam R, Schultz CR, Golembieski WA, Poisson LM, Rempel SA. PTEN suppresses SPARC-induced pMAPKAPK2 and inhibits SPARC-induced Ser78 HSP27 phosphorylation in glioma. *Neuro-oncology*. 2013;15(4):451-61.
45. Kim Y-J, Yoon SY, Kim J-T, Song EY, Lee HG, Son HJ, et al. NDRG2 expression decreases with tumor stages and regulates TCF/ $\beta$ -catenin signaling in human colon carcinoma. *Carcinogenesis*. 2009;30(4):598-605.
46. Mérian J, Boisgard R, Declèves X, Thezé B, Texier I, Tavitian B. Synthetic Lipid Nanoparticles Targeting Steroid Organs. *Journal of Nuclear Medicine*. 2013;54(11):1996-2003.
47. Packer M, Gyawali D, Yerabolu R, Schariter J, White P. A novel mechanism for the loss of mRNA activity in lipid nanoparticle delivery systems. *Nature communications*. 2021;12(1):6777.
48. Bibette J. BR, Boisseau P., Coll J.L., Couffin A.C., Delmas T., Dufort S., Fraichard A., Gravier J., Heinrich E., Mérian J., Navarro F., Tavitian B., Texier I., Thomann J.S.,. Lipid nanoparticles: tumor-targeting nanocargos for drug and contrast agent delivery. *TechConnect Briefs*. 2011;3, *Nanotechnology 2011: Bio Sensors, Instruments, Medical, Environment and Energy*.

## Supplementary Figures and Tables

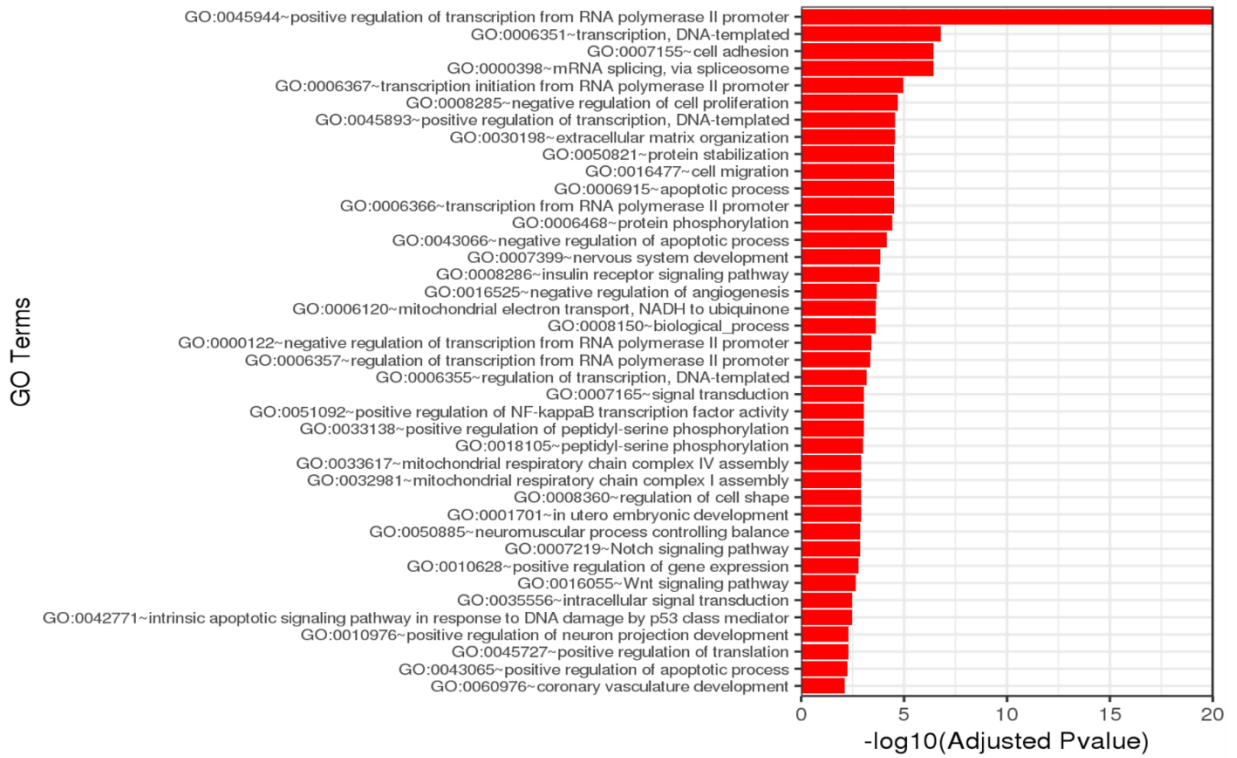
**Figure S. 1. Bioinformatics analyses of RNA sequencing data from miR-139-5p or miR-483-5p pulldowns in NCI H295R cells.**

(A) For pulldown experiments, NCI H295R cells were transiently transfected for 72h with biotinylated miR-139-5p or miR-483-5p. MiRNA enrichment in pulldowns was checked by RT-qPCR. MiRNA expression was normalized and plotted relative to control. **(B)** Global transcriptional changes across the compared groups are visualized by Volcano plots. Each data point represents a gene. The log<sub>2</sub> fold change of each gene is represented on the x-axis and the log<sub>10</sub> of its p-value is on the y-axis. Genes with a p-value less than 0.1 and a log<sub>2</sub> fold change greater than 1 are indicated by red dots. These represent up-regulated genes. Genes with a p-value less than 0.1 and a log<sub>2</sub> fold change less than -1 are indicated by blue dots. These represent down-regulated genes. **(C)** Bi-clustering heatmap visualizing the expression profile of the top 30 differentially expressed genes sorted by their p-value and their log<sub>2</sub> transformed expression values. This analysis is useful to identify co-regulated genes across the treatment conditions. **(D)** Gene ontology enrichment. Significant differentially expressed genes were clustered by their gene ontology and the enrichment of gene ontology terms was tested using Fisher exact test (GeneSCF v1.1-p2). We selected gene ontology terms, if any, that are significantly enriched with an adjusted P-value less than 0.05 in the differentially expressed gene sets (up to 40 terms). **(E)** GSEA for predicted TargetScan targets of miR-139-5p and miR-483-5p in pulldown sequencing. The barcode plot indicates the position of the genes in each gene set; Predicted targets from Target Scan v7.2, confident targets (score < -0.3): 190 predicted targets for miR-139-5p, and 213 for miR-483-5p. Leading edge (corresponding to the enrichment score, bottom of the curve) is indicated in red. It corresponds to LFC = -0.79 for miR-139-5p and LFC = -0.71 for miR-483-5p.

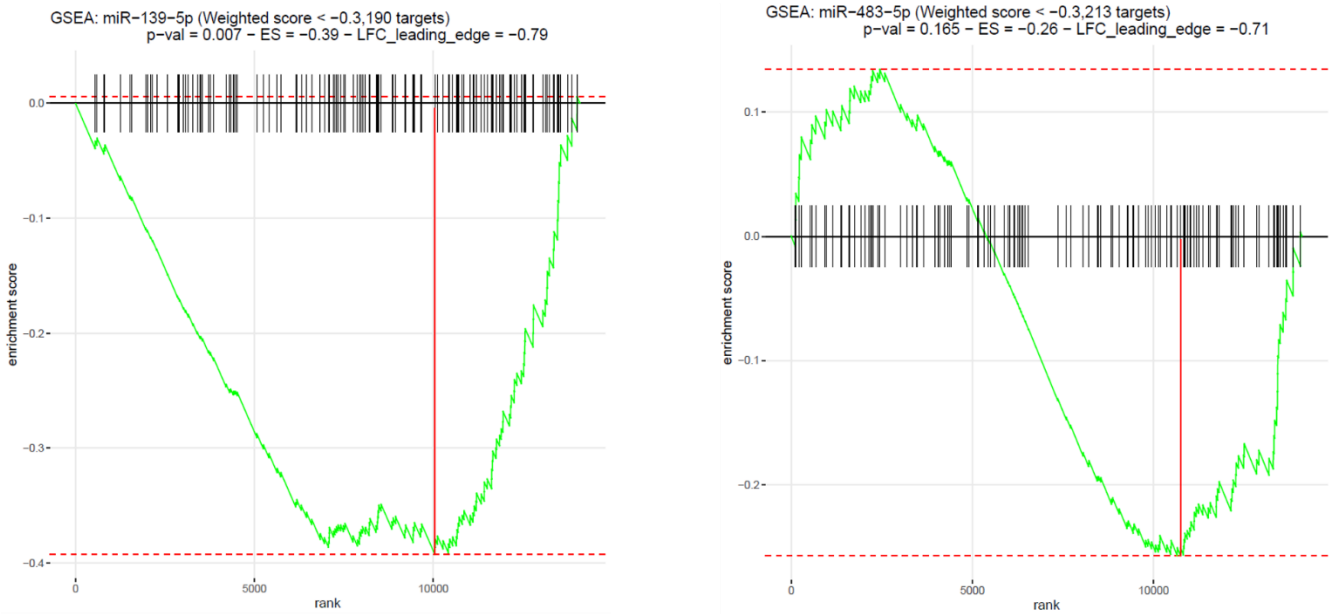




miR-483-5p

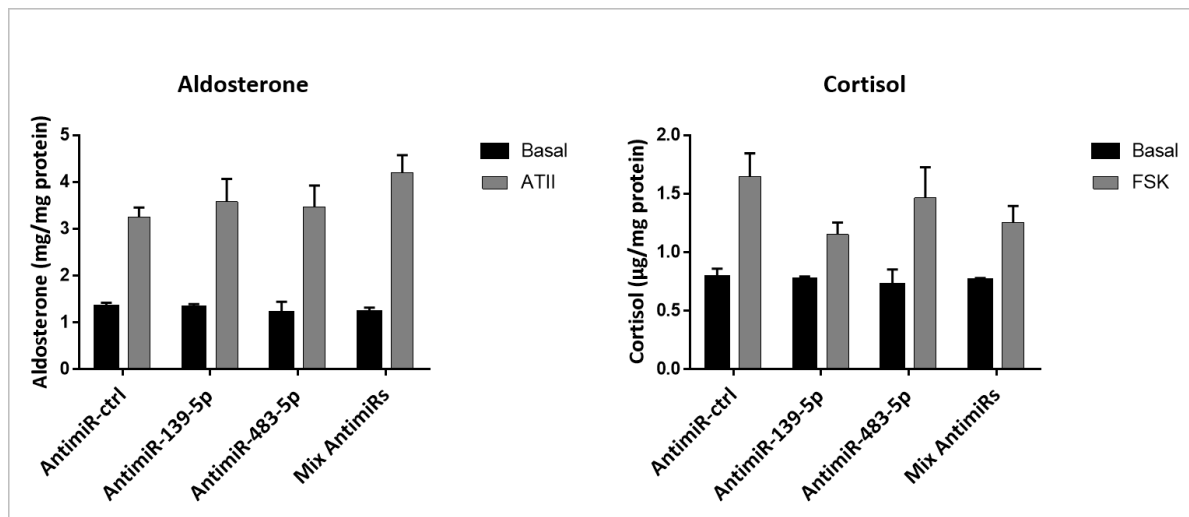


E.



**Supplementary Figure S.2. Hormone measurements in NCI H295R cells transfected with anti-miRs.**

Anti-miRs-transfected NCI H295R cells were serum-starved overnight and were then stimulated for 24h with Angiotensin II or Forskolin. Aldosterone and cortisol levels were determined in culture media from 24h-non-stimulated or stimulated cells. Shown are means  $\pm$  SD (n=2) of aldosterone and cortisol concentrations normalized to total protein content.



**Supplementary Table T.1. Clustering heatmap of miR-139-5p vs miR-ctrl pulldown.**

The heatmap corresponds to the log2-transformed expression of the top 30 differentially expressed genes in miR-139-5p transfected cells vs miR-ctrl. Genes in red are co-regulated by both miR-139-5p and miR-483-5p.

Gene ID	Gene name	Full gene name	miR-139-5p (normalized counts)	miR-ctrl (normalized counts)	Log Fold Change miR-139	p-value
ENSG00000281383	FP671120,4	5,8S rRNA	115	0	9,527	0,0031
ENSG00000150625	GPM6A	Glycoprotein M6A	98	0	9,302	0,0043
ENSG00000212443	<b>SNORA53</b>	Small Nucleolar RNA, H/ACA Box 53	221	1	8,032	0,0017
ENSG00000173432	SAA1	Serum Amyloid A1	144	1	7,415	0,0045
ENSG00000270722	RF00003	RNA, variant U1 small nuclear 31	432	10	5,411	0,0019
ENSG00000174600	CMKLR1	Chemokine-Like Receptor 1	263	8	5,109	0,0046
ENSG00000263934	SNORD3A	Small Nucleolar RNA, C/D Box 3A	1364	45	4,928	0,0012
ENSG00000278771	RN7SL3	RNA Component Of Signal Recognition Particle 7SL3	640	39	4,041	0,0051
ENSG00000106367	<b>AP1S1</b>	Adaptor Related Protein Complex 1 Subunit Sigma 1	5665	392	3,852	0,0028
ENSG00000130669	<b>PAK4</b>	P21 (RAC1) Activated Kinase 4	4621	327	3,820	0,0030
ENSG00000111676	<b>ATN1</b>	Atrophia 1	2070	171	3,600	0,0047
ENSG00000202198	RF00100	RNA Component Of 75K Nuclear Ribonucleoprotein	1494	123	3,598	0,0053
ENSG00000143819	<b>EPHX1</b>	Epoxide Hydrolase 1	7407	615	3,591	0,0038
ENSG00000160211	<b>G6PD</b>	Glucose-6-Phosphate Dehydrogenase	3061	302	3,343	0,0058
ENSG00000105409	<b>ATP1A3</b>	ATPase Na+/K+ Transporting Subunit Alpha 3	3835	389	3,302	0,0059
ENSG00000106635	<b>BCL7B</b>	BAF Chromatin Remodeling Complex Subunit BCL7B	1701	15578	-3,195	0,0059
ENSG00000103266	STUB1	STIP1 Homology And U-Box Containing Protein 1	707	6931	-3,293	0,0055
ENSG00000007520	TSR3	Transferase Ribosome Maturation Factor	814	8030	-3,303	0,0054
ENSG00000159128	<b>IFNGR2</b>	Interferon Gamma Receptor 2	1336	13829	-3,372	0,0047
ENSG00000100997	ABHD12	Abhydrolase Domain Containing 12, Lysophospholipase	974	10189	-3,388	0,0047
ENSG00000130204	TOMM40	Translocase Of Outer Mitochondrial Membrane 40	1483	15686	-3,402	0,0045
ENSG00000162227	TAF6L	TATA-Box Binding Protein Associated Factor 6 Like	216	2310	-3,415	0,0057
ENSG00000176894	<b>PXMP2</b>	Peroxisomal Membrane Protein 2	768	8230	-3,422	0,0048
ENSG00000078808	SDF4	Stromal Cell Derived Factor 4	535	6700	-3,647	0,0036
ENSG00000239857	GET4	Guided Entry Of Tail-Anchored Proteins Factor 4	127	1841	-3,863	0,0036
ENSG00000127415	IDUA	Alpha-L-Iduronidase	88	1288	-3,879	0,0041
ENSG00000111786	<b>SRSF9</b>	Serine And Arginine Rich Splicing Factor 9	1960	34403	-4,134	0,0018
ENSG00000258429	<b>PDF</b>	Peptide Deformylase, Mitochondrial	64	1211	-4,245	0,0028
ENSG00000271303	<b>SRXN1</b>	Sulfiredoxin 1	51	1350	-4,730	0,0015
ENSG00000128714	HOXD13	Homeo Box D13	0	109	-8,969	0,0047

**Supplementary Table T.2. Clustering heatmap of miR-483-5p vs miR-ctrl pulldown.**

The heatmap corresponds to log2-transformed expression of the top 30 differentially expressed genes in miR-483-5p transfected cells vs miR-ctrl. Genes in red are co-regulated by miR-139-5p and miR-483-5p.

Gene ID	Gene name	Full gene name	miR-483-5p (normalized counts)	miR-ctrl (normalized counts)	LFC miR-483	p-value
ENSG00000202538	RNU4-2	RNA, U4 Small Nuclear 2	1058	5	7,681	0,0000
ENSG00000263934	SNORD3A	Small Nucleolar RNA, C/D Box 3A	3517	55	6,008	0,0001
ENSG00000198753	PLXNB3	Plexin B3	171	3	5,786	0,0041
ENSG00000115556	PLCD4	Phospholipase C Delta 4	207	4	5,646	0,0031
ENSG00000267784	AC010680,1	Novel transcript, antisense to titin	240	5	5,538	0,0026
ENSG00000200795	RNU4-1	RNA, U4 Small Nuclear 1	276	9	4,896	0,0038
ENSG00000126464	PRR12	Proline Rich 12	717	28	4,686	0,0016
ENSG00000215156	AC138409,1	POM121-Like Protein 1 Pseudogene	438	21	4,410	0,0038
ENSG00000160877	NACC1	Nucleus Accumbens Associated 1/Transcriptional Repressor NAC1	470	24	4,310	0,0040
ENSG00000111676	ATN1	Atrophin 1	3463	208	4,055	0,0020
ENSG00000143819	EPHX1	Epoxide Hydrolase 1	11926	750	3,992	0,0019
ENSG00000169710	FASN	Fatty Acid Synthase	6580	450	3,871	0,0024
ENSG00000106367	AP1S1	Adaptor Related Protein Complex 1 Subunit Sigma 1	6995	478	3,870	0,0024
ENSG00000076924	XAB2	XPA Binding Protein 2/SYF1 pre-mRNA-splicing factor	2105	146	3,846	0,0031
ENSG00000130669	PAK4	P21 (RAC1) Activated Kinase 4	5721	399	3,842	0,0026
ENSG00000160211	G6PD	Glucose-6-Phosphate Dehydrogenase	4888	368	3,731	0,0031
ENSG00000105409	ATP1A3	ATPase Na <sup>+</sup> /K <sup>+</sup> Transporting Subunit Alpha 3	6283	474	3,728	0,0030
ENSG00000167658	EEF2	Eukaryotic Translation Elongation Factor 2	21666	1862	3,540	0,0038
ENSG00000136931	NR5A1/ SF1	Nuclear Receptor Subfamily 5 Group A Member 1	8826	785	3,492	0,0043
ENSG00000140280	LYSM2	LysM Domain Containing 2	329	3994	-3,603	0,0039
ENSG00000106635	BCL7B	BAF Chromatin Remodeling Complex Subunit BCL7B	1553	19002	-3,613	0,0034
ENSG00000171612	SLC25A33	Solute Carrier Family 25 Member 33	259	3242	-3,646	0,0038
ENSG00000235162	C12orf75	Chromosome 12 Open Reading Frame 75/Overexpressed In Colon Carcinoma 1 Protein	1221	15854	-3,699	0,0030
ENSG00000176894	PXMP2	Peroxisomal Membrane Protein 2	713	10038	-3,816	0,0025
ENSG00000243449	C4orf48	Chromosome 4 Open Reading Frame 48/Neuropeptide-like protein	757	12010	-3,987	0,0019
ENSG00000159128	IFNGR2	Interferon Gamma Receptor 2	1043	16869	-4,016	0,0018
ENSG00000117691	NENF	Neudesin Neurotrophic Factor/Cell Growth-Inhibiting Protein 47	588	10624	-4,176	0,0014
ENSG00000111786	SRSF9	Serine And Arginine Rich Splicing Factor 9	2170	41964	-4,273	0,0011
ENSG00000271303	SRXN1	Sulfiredoxin 1	55	1647	-4,897	0,0007
ENSG00000258429	PDF	Peptide Deformylase, Mitochondrial	28	1478	-5,715	0,0002

**Supplementary Table T.3. Top genes enriched in miR-139-5p pulldown after GSEA.**

These genes correspond to the leading edge subset. Criteria: count\_ctrl > 100, Log Fold Change (LFC) < -0.79), TargetScan 7.2 prediction score < -0.3

Gene ID	Target miR-139-5p	Full Gene Name	miR139_Weighted Score	Target miR-483-5p	miR-483 Weighted Score	LFC miR-139	LFC miR-483
ENSG00000123472	ATPAF1	ATP synthase mitochondrial F1 complex assembly factor 1	-0,44			-3,31	-2,44
ENSG00000011295	TTC19	tetratricopeptide repeat domain 19	-0,33			-2,69	-1,14
ENSG00000197265	GTF2E2	general transcription factor IIE, polypeptide 2, beta 34kDa	-0,64			-2,39	-1,71
ENSG00000104341	LAPTM4B	lysosomal protein transmembrane 4 beta	-0,67			-2,08	-0,47
ENSG00000182287	AP1S2	adaptor-related protein complex 1, sigma 2 subunit	-0,46			-2,02	-1,80
ENSG00000136048	DRAM1	D-damage regulated autophagy modulator 1	-0,36			-1,99	-1,22
ENSG00000173917	HOXB2	homeobox B2	-0,57	HOXB2	-0,24	-1,97	-2,02
ENSG00000057019	DCBLD2	discoidin, CUB and LCCL domain containing 2	-0,32			-1,95	-0,23
ENSG00000105968	H2AFV	H2A histone family, member V	-0,77	H2AFV	-0,11	-1,84	-1,36
ENSG00000116350	SRSF4	serine/arginine-rich splicing factor 4	-0,4	SRSF4	-0,44	-1,82	-1,15
<b>ENSG00000103034</b>	<b>NDRG4</b>	<b>NDRG family member 4</b>	<b>-0,34</b>			<b>-1,71</b>	<b>-0,25</b>
ENSG00000165379	LRFN5	leucine rich repeat and fibronectin type III domain containing 5	-0,46			-1,65	-0,53
ENSG00000122779	TRIM24	tripartite motif containing 24	-0,39			-1,64	-0,36
ENSG00000174007	CEP19	centrosomal protein 19kDa	-0,4			-1,60	-0,89
ENSG00000162885	B3GALNT2	beta-1,3-N-acetylgalactosaminyltransferase 2	-0,33			-1,55	-0,64
ENSG00000148429	USP6NL	USP6 N-termil like	-0,43			-1,38	-0,64
ENSG00000095906	NUBP2	nucleotide binding protein 2	-0,45			-1,38	-0,79
ENSG00000171729	TMEM51	transmembrane protein 51	-0,32			-1,38	-0,97
ENSG00000115616	SLC9A2	solute carrier family 9, subfamily A (NHE2, cation proton antiporter 2), member 2	-0,53			-1,26	0,63
ENSG00000214114	MYCBP	MYC binding protein	-0,33	MYCBP	-0,02	-1,26	-0,90
ENSG00000180884	ZNF792	zinc finger protein 792	-0,42			-1,25	0,30
ENSG00000123091	RNF11	ring finger protein 11	-0,51	RNF11	0	-1,24	-1,24
ENSG00000188938	FAM120AOS	family with sequence similarity 120A opposite strand	-0,36			-1,22	-1,34
ENSG00000170775	GPR37	G protein-coupled receptor 37 (endothelin receptor type B-like)	-0,45			-1,17	-0,20
ENSG00000130962	PRRG1	proline rich Gla (G-carboxyglutamic acid) 1	-0,41			-1,15	-0,12
ENSG00000177606	JUN	jun proto-oncogene	-0,38			-1,15	-0,14
ENSG00000147650	LRP12	low density lipoprotein receptor-related protein 12	-0,39			-1,12	0,04
ENSG00000076554	TPD52	tumor protein D52	-0,46			-1,11	-0,65
ENSG00000170852	KBTD2	kelch repeat and BTB (POZ) domain containing 2	-0,55			-1,10	-0,33
ENSG00000161551	ZNF577	zinc finger protein 577	-0,36			-1,05	-0,63
ENSG00000171160	MORN4	MORN repeat containing 4	-0,6			-1,05	-0,88
ENSG00000154920	EME1	essential meiotic structure-specific endonuclease 1	-0,54			-1,04	0,10
ENSG00000103335	PIEZO1	piezo-type mechanosensitive ion channel component 1	-0,42			-1,03	1,11
ENSG00000100568	VTI1B	vesicle transport through interaction with t-SREs 1B	-0,33			-1,01	-1,52

ENSG00000189241	TSPYL1	TSPY-like 1	-0,31	TSPYL1	0	-1,01	-0,03
ENSG00000170348	TMED10	transmembrane emp24-like trafficking protein 10 (yeast)	-0,44			-0,99	-0,50
ENSG00000136146	MED4	mediator complex subunit 4	-0,54			-0,98	-1,53
ENSG00000162961	DPY30	dpy-30 homolog (C. elegans)	-0,73			-0,98	-1,11
ENSG00000147145	LPAR4	lysophosphatidic acid receptor 4	-0,4			-0,98	-0,48
ENSG00000131127	ZNF141	zinc finger protein 141	-0,51	ZNF141	0	-0,96	0,23
ENSG00000152380	FAM151B	family with sequence similarity 151, member B	-0,33	FAM151B	-0,02	-0,94	-1,53
ENSG00000184182	UBE2F	ubiquitin-conjugating enzyme E2F (putative)	-0,38			-0,94	-1,05
ENSG00000149636	DSN1	DSN1, MIS12 kinetochore complex component	-0,44			-0,93	-0,64
ENSG00000066185	ZMYND12	zinc finger, MYND-type containing 12	-0,39			-0,91	-0,40
ENSG00000164109	MAD2L1	MAD2 mitotic arrest deficient-like 1 (yeast)	-0,42	MAD2L1	-0,02	-0,91	-0,98
ENSG00000175324	LSM1	LSM1 homolog, U6 small nuclear R associated (S. cerevisiae)	-0,6			-0,90	-1,46
ENSG00000110321	EIF4G2	eukaryotic translation initiation factor 4 gamma, 2	-0,48			-0,90	-0,08
ENSG00000221994	ZNF630	zinc finger protein 630	-0,52			-0,89	-0,51
ENSG00000124657	OR2B6	olfactory receptor, family 2, subfamily B, member 6	-0,62			-0,87	-1,00
ENSG00000197841	ZNF181	zinc finger protein 181	-0,4			-0,86	-0,17
ENSG00000109099	PMP22	peripheral myelin protein 22	-0,39			-0,85	-0,56
ENSG00000162062	C16orf59	chromosome 16 open reading frame 59	-0,43			-0,85	-0,37
ENSG00000135334	AKIRIN2	akirin 2	-0,52			-0,85	-0,30
ENSG00000072401	UBE2D1	ubiquitin-conjugating enzyme E2D 1	-0,57			-0,84	-0,72
ENSG00000164649	CDCA7L	cell division cycle associated 7-like	-0,56			-0,83	-0,13
ENSG00000164330	EBF1	early B-cell factor 1	-0,43			-0,83	0,08
ENSG00000125166	GOT2	glutamic-oxaloacetic transaminase 2, mitochondrial	-0,35			-0,82	-0,05
ENSG00000119986	AVPI1	arginine vasopressin-induced 1	-0,32			-0,81	-0,75
ENSG00000185305	ARL15	ADP-ribosylation factor-like 15	-0,67			-0,79	-0,84
ENSG00000145349	CAMK2D	calcium/calmodulin-dependent protein kinase II delta	-0,43			-0,79	-0,14
ENSG00000164305	CASP3	caspase 3, apoptosis-related cysteine peptidase	-0,42			-0,79	-0,37
ENSG00000150753	CCT5	chaperonin containing TCP1, subunit 5 (epsilon)	-0,46			-0,75	-0,16
<b>ENSG00000165795</b>	<b>NDRG2</b>	<b>NDRG family member 2</b>	<b>-0,57</b>	<b>NDRG2</b>	<b>-0,24</b>	<b>-0,75</b>	<b>0,06</b>
ENSG00000119787	ATL2	atlastin GTPase 2	-0,39			-0,73	0,23
ENSG00000172115	CYCS	cytochrome c, somatic	-0,43	CYCS	-0,04	-0,73	-1,58
ENSG00000120992	LYPLA1	lysophospholipase I	-0,37	LYPLA1	-0,01	-0,73	-0,99
ENSG00000108468	CBX1	chromobox homolog 1	-0,53			-0,71	-0,19
ENSG00000116213	WRAP73	WD repeat containing, antisense to TP73	-0,31			-0,71	-0,12

**Supplementary Table T.4. Top genes enriched in miR-483-5p pulldown after GSEA.**

These genes correspond to the leading edge subset. Criteria : count\_ctrl > 100 , Log Fold Change (lfc) < -0.71, TargetScan 7.2 prediction : score < -0.3

Gene ID	Target miR-483-5p	Full Gene Name	miR483_Weighted Score	Target_139	miR-139 Weighted Score	LFC 139	LFC 483
ENSG00000167799	NUDT8	nudix (nucleoside diphosphate linked moiety X)-type motif 8	-0,4			-2,39	-2,96
ENSG00000237190	CDKN2AIPNL	CDKN2A interacting protein N-terminal like	-0,45			-1,02	-2,13
ENSG00000115468	EFHD1	EF-hand domain family, member D1	-0,32	EFHD1	-0,11	-2,75	-2,12
ENSG0000036448	MYOM2	myomesin 2	-0,63	MYOM2	0	-0,89	-1,83
ENSG00000137409	MTCH1	mitochondrial carrier 1	-0,42			-2,22	-1,80
ENSG00000183784	C9orf66	chromosome 9 open reading frame 66	-0,52			-2,51	-1,71
ENSG00000124733	MEA1	male-enhanced antigen 1	-0,47			-0,95	-1,63
ENSG00000167536	DHRS13	dehydrogese/reductase (SDR family) member 13	-0,32			-1,92	-1,60
ENSG00000106236	NPTX2	neuroI pentraxin II	-0,33			-2,21	-1,59
ENSG00000148655	C10orf11	chromosome 10 open reading frame 11	-0,32			-1,05	-1,59
ENSG00000196182	STK40	serine/threonine kise 40	-0,35			-1,71	-1,59
ENSG00000172366	FAM195A	family with sequence similarity 195, member A	-0,38			-1,10	-1,58
ENSG00000142444	C19orf52	chromosome 19 open reading frame 52	-0,46			-1,96	-1,54
ENSG00000138794	CASP6	caspase 6, apoptosis-related cysteine peptidase	-0,36			-1,62	-1,53
ENSG00000175130	MARCKSL1	MARCKS-like 1	-0,58			-1,31	-1,51
ENSG00000146700	SRCRB4D	scavenger receptor cysteine rich domain containing, group B (4 domains)	-0,5			-1,95	-1,45
ENSG00000205791	LOH12CR2	loss of heterozygosity, 12, chromosomal region 2 (non-protein coding)	-0,4			0,09	-1,30
ENSG00000184924	PTRHD1	peptidyl-tR hydrolase domain containing 1	-0,48			-0,40	-1,27
ENSG00000215014	AL645728.1	Uncharacterized protein	-0,41			-2,02	-1,15
ENSG00000116350	SRSF4	serine/arginine-rich splicing factor 4	-0,44	SRSF4	-0,4	-1,82	-1,15
ENSG00000228696	ARL17B	ADP-ribosylation factor-like 17B	-0,31			-1,29	-1,11
ENSG00000160213	CSTB	cystatin B (stefin B)	-0,33			-0,33	-1,08
ENSG00000187514	PTMA	prothymosin, alpha	-0,43			-0,03	-1,08
ENSG00000166407	LMO1	LIM domain only 1 (rhombotin 1)	-0,62			-0,88	-1,06
ENSG00000230124	ACBD6	acyl-CoA binding domain containing 6	-0,61			-1,15	-1,05
ENSG00000168395	ING5	inhibitor of growth family, member 5	-0,38			-1,89	-1,05
ENSG00000138395	CDK15	cyclin-dependent kise 15	-0,52			-0,66	-0,95
ENSG00000117280	RAB7L1	RAB7, member RAS oncogene family-like 1	-0,62			-0,66	-0,94
ENSG00000006042	TMEM98	transmembrane protein 98	-0,34	TMEM98	0	-0,76	-0,93
ENSG00000105402	PA	N-ethylmaleimide-sensitive factor attachment protein, alpha	-0,32			-0,77	-0,93
ENSG00000179029	TMEM107	transmembrane protein 107	-0,34	TMEM107	-0,1	-0,75	-0,89
ENSG00000171604	CXXC5	CXXC finger protein 5	-0,34			-1,36	-0,88
ENSG00000007255	TRAPP6A	trafficking protein particle complex 6A	-0,42			-0,96	-0,85
ENSG00000153896	ZNF599	zinc finger protein 599	-0,38			-0,69	-0,82
ENSG00000172992	DCAKD	dephospho-CoA kise domain containing	-0,31			-0,58	-0,80

ENSG00000180185	FAHD1	fumarylacetoacetate hydrolase domain containing 1	-0,35			-0,76	-0,79
ENSG00000214253	FIS1	fission 1 (mitochondrial outer membrane) homolog (S. cerevisiae)	-0,43			-0,48	-0,79
ENSG00000165102	HGST	heparan-alpha-glucosaminide N-acetyltransferase	-0,38	HGST	-0,01	-1,39	-0,77
ENSG00000171960	PPIH	peptidylprolyl isomerase H (cyclophilin H)	-0,38			-0,49	-0,76
ENSG00000181773	GPR3	G protein-coupled receptor 3	-0,37			-0,04	-0,75
ENSG00000161558	TMEM143	transmembrane protein 143	-0,41			-0,67	-0,73
ENSG00000162174	ASRGL1	asparagise like 1	-0,37			-1,01	-0,73
ENSG00000067560	RHOA	ras homolog family member A	-0,31			-0,43	-0,72
ENSG00000180543	TSPYL5	TSPY-like 5	-0,47			-0,89	-0,71



**Supplementary Table T.5. PCR primers used for gene expression analysis.**

Gene	Accession number	Forward primer	Reverse primer
NDRG2	NM_201535.1	5'-GCTCTGTCACTTTCACGTCTAT-3'	5'-AGTGGCTGGAAGCAAGATTTA-3'
NDRG4	NM_020465.3	5'-CCGGCCTAACTAGCACTTTAC-3'	5'-GTTACCACGTTCCCAATCT -3'
HPRT	NM_000194.2	5'- ATGGACAGGACTGAACGTCTTGCT-3'	5'- TTGAGCACACAGAGGGCTACAATG -3'
RPL13A	NM_012423.3	5'-TTAATTCCTCATGCGTTGCCTGCC-3'	5'-TTCCTTGCTCCCAGCTTCTATGT-3'

**Supplementary Table T.6. List of antibodies used for western blot analyses.**

Antibody	Supplier	Species	MW (kDa)	Dilution
N-cadherin	BD Bioscience	Mouse	130	1:2500
MMP2	Cell signaling	Rabbit	65	1:1000
P-Akt	Cell signaling	Rabbit	60	1:2000
P-p38	Cell signaling	Rabbit	38	1:1000
Tubulin	Sigma-Aldrich	Mouse	50	1:2000
Vimentin	Sigma-Aldrich	Mouse	58	1:1000
$\beta$ -actin	Cell signaling	Rabbit	45	1:1000
$\beta$ -catenin	R&D Biotechne	Mouse	95	1:1000

## **4-CONCLUSION AND PERSPECTIVES**

---



Cancer is a multifactorial pathology that disrupts cell homeostasis. Despite a broad range of approaches to treat malignancy or prevent delayed diagnosis and relapse of patients, multidrug resistance and therapeutic failure remain problematic for cancer eradication. MiRNAs exert a pleiotropic activity and are involved in the acquisition of major cancer traits. The finding that aberrant expression of miRNAs in cancer promotes upregulation of oncogenes and downregulation of tumor suppressor genes led the scientific community to propose that these nucleic acids are relevant candidates for anti-cancer therapies. In ACC, miRNAs have been successfully explored as diagnostic or prognostic biomarkers. However, their potential therapeutic activity remains to be evaluated. Encouraged by our prior research, we hereby tested for the first time the relevance of two miRNAs, miR-483-5p and miR-139-5p, as therapeutic targets in ACC in vitro and in vivo. Our data provide evidence that miRNA-based therapies should be considered for ACC. Indeed, the combined effects of miR-139-5p/miR-483-5p inhibitors demonstrated synergistic impact on critical signaling pathways, suggesting that their simultaneous targeting may improve treatment outcomes.

Theoretically, miRNA expression abnormalities would be simple to "correct", using synthetic oligonucleotides to restore downregulated miRNAs, or artificial antagonists to silence overexpressed miRNAs. Hence, as miR-483-5p/miR-139-5p are overexpressed in ACC, our experiments were carried out using sequence-specific miRNA inhibitors (antimiRs), in order to downregulate miRNA expression. In a first approach, we assessed their function as oncomiRs mediating ACC aggressiveness by interfering with several cancer-related pathways. As a result of their multi-target action, miR-483-5p and miR-139-5p silencing led to the impairment of ACC cell migration and invasion, two major cancer hallmarks. Our very next step is to decipher the direct targetome of miR-139-5p and miR-483-5p in ACC. Our pulldown experiments were performed within 72 hours of transfection with biotinylated miRNA mimics to comply with our in vitro assessments. We were expecting that the binding of the transcripts to their biotinylated regulatory miRNAs would result in enrichment of the miRNA-targeted mRNA in the pulldown material. Nonetheless, our RNA sequencing data revealed that differentially expressed genes were rather downregulated in miR-139-5p and miR-483-5p pulldowns, making identification of genuine targets challenging. These findings might be attributed to too long kinetics and indicate that the duration for miRNA mimic transfections is crucial for such

experiments. We are currently revisiting our experimental setup for pulldown assays, in order to maximize our chances of collecting true targets of miR-139-5p/miR-483-5p, before their sequestration by the mRNA decay machinery. Moreover, crossing sequencing data from pulldown experiments with simultaneous whole transcriptome sequencing is under consideration for the upcoming experiments.

It is well established that nucleic acids are rapidly degraded by blood-borne nucleases, and are incapable of cell entry by their own. The ultimate success of miRNA therapeutics therefore relies on overcoming these pharmacokinetic barriers by properly addressing miRNA formulations within delivery platforms. Over the last decade, nanomedicine has offered novel venues for drug- or RNA-mediated cancer therapies. Innovations and strategies implemented in this topic are described in details in our review attached at the end of this manuscript. The implementation of nanoparticles (NPs) in precision oncology has gained particular value, for diagnosis, imaging and tumor-specific drug delivery. NPs are made up of organic or inorganic biomaterials that are generally engineered to fulfill theranostic requirements. Indeed, the NP architecture tightly influences their stability, aggregation, encapsulation and targeting capacities. Regardless of their cargo, NPs' shape, charge and surface chemistry should be carefully considered, in compliance with the desired application. While cationic NPs may elicit higher toxicity than neutral vectors, their positive charge is indispensable for engraftment of negatively charged nucleic acids such as miRNAs or siRNAs. Moreover, even though some NPs exhibited remarkable biocompatibility, they are not devoid of cytotoxicity. Integrating stealth and targeting agents in addition to the bioactive miRNA within the NP design would help restrain the NP-driven toxicity. However, this physicochemical complexity undoubtedly contributes to the delayed clinical translation of miRNA-based formulations, since it impedes large-scale pharmaceutical manufacture.

In the present study, we used positively charged Lipidots (LNPs) to convey anti-miRNAs inhibitors to ACC cells, either in culture or grafted in vivo. The primary miRNA-related concern we faced in this work is the dose of anti-miRNAs to be complexed with LNPs. LNPs did not demonstrate NP-related issues within the concentration range tested in both conditions. LNPs bear biocompatible components in a core shell structure, with an overall positive charge, which ensured miRNA complexation by simple electrostatic interaction. Also, their well characterized pharmacokinetics are in agreement with our expectations, in terms of

biocompatibility and preferential accumulation in steroidogenic tissue. Indeed, in addition to LNPs homing to pre-established tumors, we could also detect para-tumor accumulation in adrenals and ovaries, suggesting that the build-up of LNPs in the tumors relies on intrinsic properties of endocrine organs in addition to the EPR effect. It is worth mentioning that the EPR effect is still debated in the NP community, due to heterogeneous nanocarrier accumulation between individuals and tumor types. While EPR is weakened by intratumor pressure and hypoxia, the liver and spleen can similarly capture NPs through their fenestrated endothelium, thus limiting bioavailability of NPs and NP-shuttled therapeutics, within the tumor foci. As a result, it is the NP chemistry and active targeting that govern specific tissue uptake, rather than EPR only.

Regarding anti-miR-LNP activity *in vivo*, we provided at this stage a pilot experiment to validate the proof of concept of our therapeutic strategy. We plan experimental improvements in the short term to better document the anti-tumor effects observed in our study, and in the mid-term to make the preclinical model more relevant to ACC biology. Finding the appropriate anti-miR dose is definitely our priority for our very next campaigns *in vivo*. The selected miRNA concentration should compensate for NP leakage, which results in miRNA loss in the bloodstream. Defining the doses required to achieve total endogenous miRNA sequestration with anti-miRs, or endogenous physiological miRNA concentration with miRNA mimics, is a key stage of preclinical toxicity and pharmacokinetic studies. The ideal anti-miR posology should result in sequestration of endogenous miRNA, alleviating repression of specific target genes only. In addition, a dose scale-up should be considered imperatively when transitioning from cells to complex organisms or even in humans. Most importantly, the risk/benefit balance should always be kept in mind; an excess of miRNA inhibitors/mimics is often associated with exacerbation of off-target effects, which can be fatal. Indeed, suspension of the MRX34 trial due to severe immune complications was later explained by a "too many targets for miRNA effect" (TMTME) on numerous genes implicated in cytokine and interleukin cascades. As shown in our work, miRNAs could interfere with several signaling pathways in direct or indirect ways. Deciphering the targetome of a miRNA candidate allows for the prediction of potential off-target effects, hence evaluation of the benefit/risk balance for suitable payload selection. While no visible signs of toxicity were detected in our mice all over the treatment campaign, we plan to confirm these observations in the next experiments by dosing liver enzymes like

aspartate aminotransferase (AST) and alanine aminotransferase (ALT) in mice. Moreover, we are aware that off-tumor accumulation accounts for a loss of drug bioavailability, not to forget the potential toxicity induced by repetitive injections and accumulation in ovaries/testis. In the mid-term, adding EGFR targeting antibodies on the surface of LNPs should be considered, to enhance LNP accumulation in EGFR-expressing ACC tumors and to prevent reprotoxicity. On the other hand, we plan to use pseudo-orthotopic tumors embedded under the renal capsule to better mimic tumor physiology. This experimental design has not been implemented due to lack of time. Another limitation of our study is that the best characterized ACC cell line, namely NCI H295R, do not metastasize in mice. This feature makes it impossible to study the effects of anti-miR-LNPs on tumor cell metastasis towards other organs. To overcome this hurdle, we plan to use the newly generated ACC cell line MUC-1 as soon as we get permission from the laboratory that developed this model from ACC metastasis to the neck. Moreover, it is worth testing whether the combination of both anti-miRs with mitotane in LNPs would reduce the toxicity of this drug. Importantly, our approach could later be expanded to other miRNAs deregulated in ACC, such as miR-195, miR-503 and miR-335, using a cocktail of miRNA inhibitors and mimics to restore normal miRNA signatures.

Apart from the preclinical model and nanocarriers, other challenges are linked to the miRNA itself, since modifying miRNA backbones might alter their activity and pharmacokinetics. Hence, it is critical to analyze each miRNA candidate independently of its harboring vector and to fully characterize its spectrum of activity and potential off-target effects. Then, thorough characterization of miRNA-loaded NPs is essential before proceeding to therapeutic assessment. Besides complexation efficiency, it is crucial to assess cellular release of miRNA from NPs, *in vitro* and *in vivo*. Because most nanosystems have not yet been evaluated in human, we cannot predict their clinical behavior. Accurate pharmacokinetic monitoring of ADME (absorption, distribution, metabolism, and excretion) in animal models may offer a pipeline for understanding how miRNA mimics/anti-miRs could operate in humans.

To conclude, it is clear that miRNA therapies are still awaiting their golden era. Despite all these hurdles, rising mounts of pre-clinical evidence support the relevance of miRNAs as anti-cancer drugs. The field of nanotechnology is now mature enough to envisage potential shifting to clinical studies in the next few years. The Anti-Covid-19 vaccines based on mRNA encapsulation constitute a game-changing milestone in nanomedicine credibility. This will

definitely aid some of the most promising miRNA nanocarriers to reach the market. Developing miRNA tablets is clearly a step towards patient-friendly prescriptions, since currently suggested nanoformulations are administered intravenously or subcutaneously. Meanwhile, regulatory authorities have gained awareness of the use of nanoparticles for drug delivery as multiple liposomal medications are already on the market, clearing the path for miRNA therapies.





## 5-ANNEX

---



## ARTICLE 2



### **MicroRNA Therapeutics in Cancer: Current Advances and Challenges**

Soha Reda El Sayed, Justine Cristante, Laurent Guyon, Josiane Denis, Olivier Chabre and Nadia Cherradi\*. MicroRNA Therapeutics in Cancer: Current Advances and Challenges. *Cancers* (Basel). 2021 May 29;13(11):2680. doi: 10.3390/cancers13112680.



Review

# MicroRNA Therapeutics in Cancer: Current Advances and Challenges

Soha Reda El Sayed <sup>1</sup>, Justine Cristante <sup>1,2</sup> , Laurent Guyon <sup>1</sup> , Josiane Denis <sup>1</sup>, Olivier Chabre <sup>1,2</sup> and Nadia Cherradi <sup>1,\*</sup> 

- <sup>1</sup> University Grenoble Alpes, INSERM, CEA, Interdisciplinary Research Institute of Grenoble (IRIG), Biology and Biotechnologies for Health UMR\_1292, F-38000 Grenoble, France; soha.redaelsayed@cea.fr (S.R.E.S.); jcristante@chu-grenoble.fr (J.C.); laurent.guyon@cea.fr (L.G.); josiane.denis@cea.fr (J.D.); OlivierChabre@chu-grenoble.fr (O.C.)
- <sup>2</sup> Centre Hospitalier Universitaire Grenoble Alpes, Service d'Endocrinologie, F-38000 Grenoble, France
- \* Correspondence: nadia.cherradi@cea.fr; Tel.: +33-(0)4-38783501; Fax: +33-(0)4-38785058

**Simple Summary:** Cancer is a complex disease associated with deregulation of numerous genes. In addition, redundant cellular pathways limit efficiency of monotarget drugs in cancer therapy. MicroRNAs are a class of gene expression regulators, which often function by targeting multiple genes. This feature makes them a double-edged sword (a) as attractive targets for anti-tumor therapy and concomitantly (b) as risky targets due to their potential side effects on healthy tissues. As for conventional antitumor drugs, nanocarriers have been developed to circumvent the problems associated with miRNA delivery to tumors. In this review, we highlight studies that have established the pre-clinical proof-of concept of miRNAs as relevant therapeutic targets in oncology. Particular attention was brought to new strategies based on nanovectorization of miRNAs as well as to the perspectives for their applications.



**Citation:** Reda El Sayed, S.; Cristante, J.; Guyon, L.; Denis, J.; Chabre, O.; Cherradi, N. MicroRNA Therapeutics in Cancer: Current Advances and Challenges. *Cancers* **2021**, *13*, 2680. <https://doi.org/10.3390/cancers13112680>

Academic Editor: Sempere Lorenzo

Received: 31 March 2021  
Accepted: 24 May 2021  
Published: 29 May 2021

**Publisher's Note:** MDPI stays neutral with regard to jurisdictional claims in published maps and institutional affiliations.



**Copyright:** © 2021 by the authors. Licensee MDPI, Basel, Switzerland. This article is an open access article distributed under the terms and conditions of the Creative Commons Attribution (CC BY) license (<https://creativecommons.org/licenses/by/4.0/>).

**Abstract:** The discovery of microRNAs (miRNAs) in 1993 has challenged the dogma of gene expression regulation. MiRNAs affect most of cellular processes from metabolism, through cell proliferation and differentiation, to cell death. In cancer, deregulated miRNA expression leads to tumor development and progression by promoting acquisition of cancer hallmark traits. The multi-target action of miRNAs, which enable regulation of entire signaling networks, makes them attractive tools for the development of anti-cancer therapies. Hence, supplementing downregulated miRNA by synthetic oligonucleotides or silencing overexpressed miRNAs through artificial antagonists became a common strategy in cancer research. However, the ultimate success of miRNA therapeutics will depend on solving pharmacokinetic and targeted delivery issues. The development of a number of nanocarrier-based platforms holds significant promises to enhance the cell specific controlled delivery and safety profile of miRNA-based therapies. In this review, we provide among the most comprehensive assessments to date of promising nanomedicine platforms that have been tested preclinically, pertaining to the treatment of selected solid tumors including lung, liver, breast, and glioblastoma tumors as well as endocrine malignancies. The future challenges and potential applications in clinical oncology are discussed.

**Keywords:** cancer; preclinical research; multi-target therapy; microRNA delivery; nanotechnology; nanoparticles; nanomedicine platforms

## 1. Introduction

MicroRNAs (miRNAs) are highly conserved small non-coding RNAs, which regulate gene expression through imperfect base pairing to the 3'-untranslated region (3'-UTR) of target mRNA. For the most part, miRNA binding through partial complementarity to the target transcript leads to its degradation or repression of its translation [1]. MiRNAs have a particular biogenesis that makes their expression both spatially and temporarily

controlled [2]: miRNA genes are transcribed into hairpin-containing primary transcripts (pri-miRNA). Pri-miRNAs are cleaved by the Double-Stranded RNA-Specific Endoribonuclease DROSHA (RNase III) and its cofactor DiGeorge syndrome Critical Region 8 (DGCR8) into short hairpin pre-miRNAs in the nucleus. Pre-miRNAs are then transported into the cytoplasm by an Exportin-5 RanGTP complex to undergo further processing into approximately 22 nucleotides-double-stranded mature miRNAs by the Dicer RNase III/TRBP (HIV-1 transactivating response (TAR) RNA-binding protein) complex. The resulting small RNA duplex is then assembled into AGO (Argonaute) protein within the RNA-Induced Silencing Complex (RISC) where the guide strand is selected to exert its effect on the target transcript [3].

Given their small size of ~22 nucleotides, miRNAs can regulate various genes, in a developmental and tissue-specific manner [4]. To date, about 1917 human precursors and 2654 mature miRNAs have been described in miRBase (<http://www.mirbase.org/>; accessed on 22 October 2018), some of which have been implicated in human pathologies. Their involvement in cancer was first demonstrated in 2002, when miR-15 and miR-16-1 were found to be downregulated in Chronic Lymphocytic Leukemia [5]. Since then, high throughput molecular profiling allowed detection of aberrant miRNA expression in various tumors as compared to healthy tissue [6]. These cancer-associated miRNA signatures result from alterations of several mechanisms including structural genetic alterations (chromosomal deletions/amplifications and mutations), defects in the miRNA biogenesis machinery [7], and epigenetic changes such as altered DNA methylation [8]. Tumor hypoxia is also a key regulator of miRNA expression. Notably, Hypoxia Inducible Factor-1 $\alpha$  (HIF-1 $\alpha$ ) downregulates miR-34a, thus promoting epithelial to mesenchymal transition by targeting the Notch signaling pathway in epithelial cells [9]. Further genetic studies indicated that the specific localization of more than 50% of miRNA genes in fragile genomic regions favors their imbalanced expression, thus their involvement in tumorigenesis. In general, miRNAs embedded in cancer-deleted loci (such as the miR-15a-miR-16-1 cluster at 13q14) act as tumor suppressors, whereas miRNAs located in cancer-amplified genomic regions (such as the miR-17-92 cluster) function as oncogenes [10].

In addition to their major involvement in tumorigenesis and metastasis, miRNAs have been linked to drug resistance, the principal limiting factor to achieving cures in patients with cancer [11,12]. Indeed, alterations in miRNA expression profiles lead to anticancer drug resistance by abnormally regulating the expression of genes involved in multi-drug-resistance (MDR) mechanisms, such as ATP-binding cassette (ABC) transporter genes, apoptosis- and autophagy-related genes, and drug metabolism-related genes [13]. For example, over-expression of miR-223 or miR-298 in doxorubicin (DOX)-resistant hepatocellular carcinoma (HCC) cells or in breast cancer cells, respectively, increased their sensitivity to DOX through ABCB1 (ABC Subfamily B Member 1) downregulation [14,15]. In chronic myeloid leukemia, miR-212 inhibition resulted in ABCG2 (ABC Subfamily G Member 2) upregulation and increased ABCG2-dependent efflux of Imatinib [16]. Knock-down of miRNA-182 and miRNA-205 improve the sensitivity of non-small-cell lung cancer (NSCLC) to cisplatin, and enhanced apoptosis through upregulation of the pro-apoptotic proteins phosphatase and tensin homolog (PTEN) and programmed cell death-4 (PDCD4), respectively [17,18]. Autophagy is activated in cancer cells during chemotherapy and often contributes to drug resistance [19]. Zou et al. found that ectopic expression of miRNA-30a significantly reduced beclin 1 and cisplatin-induced autophagy while significantly increasing HCC and breast cancer cell apoptosis [20]. MiRNAs also regulate drug-metabolizing enzymes such as the cytochrome P450 (CYP) superfamily, which catalyzes the metabolism of most drugs. As observed for ABC transporters, the expression level of drug-metabolizing enzymes is frequently higher in various types of cancers compared with normal tissues. MiR-27b and miR-892a were found to respectively target and downregulate CYP1B1 and CYP1A1 expression in breast cancer [21,22] and to impair the benzo(a)pyrene-mediated decrease in cancer cell viability [22]. All these findings reinforce the idea that subsets of miRNAs may have clinical relevance as therapeutics agents.

Besides their validation as powerful tools for diagnosis, inhibition of miRNA activity and/or enhancement of miRNA function (miRNA replacement) strategies led to promising results in terms of antitumor effects in preclinical models [23–26]. It is worth mentioning that the development of miRNA-based therapies continues to benefit from the major advances made in siRNA/RNA therapeutics. As components of the RNA interference (RNAi) process, both miRNA and siRNA are able to knockdown oncogenic genes by targeting mRNA expression. MiRNA and siRNA have similar physicochemical properties (double-stranded RNA with 21–23 nucleotides) and use the same intracellular machinery to be active (function of the RNA-induced Silencing Complex). Therefore, it is conceivable that similar technologies can be applied to both types of RNA for therapeutic purposes. However, the origin and mechanisms of action of miRNA and siRNA differ: miRNA are encoded by the cell genome and regulate endogenous genes while siRNA function after exogenous delivery; miRNA mostly use 7–8 nucleotides from their 5′-end to identify target mRNA sequence and to induce mRNA degradation or inhibition of translation. Consequently, a single miRNA is able to bind and target more than one mRNA, thus allowing multi-target action on several genes, which often work together as a network within the same pathway [27]. This property is attractive for the treatment of multifactorial diseases such as cancer but can also lead to potential off-target effects. In contrast, siRNA use their full length to recognize their target sequence and mediate cleavage of the target mRNA, thus permitting target specificity and the ability to inhibit the expression of a mutant oncogenic protein without affecting the wild type. Nevertheless, siRNAs can in turn cause unintended gene silencing due to miRNA-like effects when their 5′-end of the guide strand is complementary to the 3′-UTR of the mRNA.

A series of stringent criteria must be met before bringing miRNAs from bench to bedside (Figure 1). These include safe delivery, limitation of off-target effects which are inherent to miRNA mechanisms of action, and reduction of toxicity and immune responses. In this review, we summarize the emergence of miRNA-based therapy as a strategy to treat cancer by specifically targeting signaling pathways leading to the disease. We cover the approaches implemented for the delivery of miRNA mimics or anti-miRNAs (antimiRs) with an emphasis on nanotechnology-based formulations for the treatment of major cancer types and rare endocrine tumors in preclinical models. The challenges that persist for translating laboratory breakthroughs to the clinic are discussed.

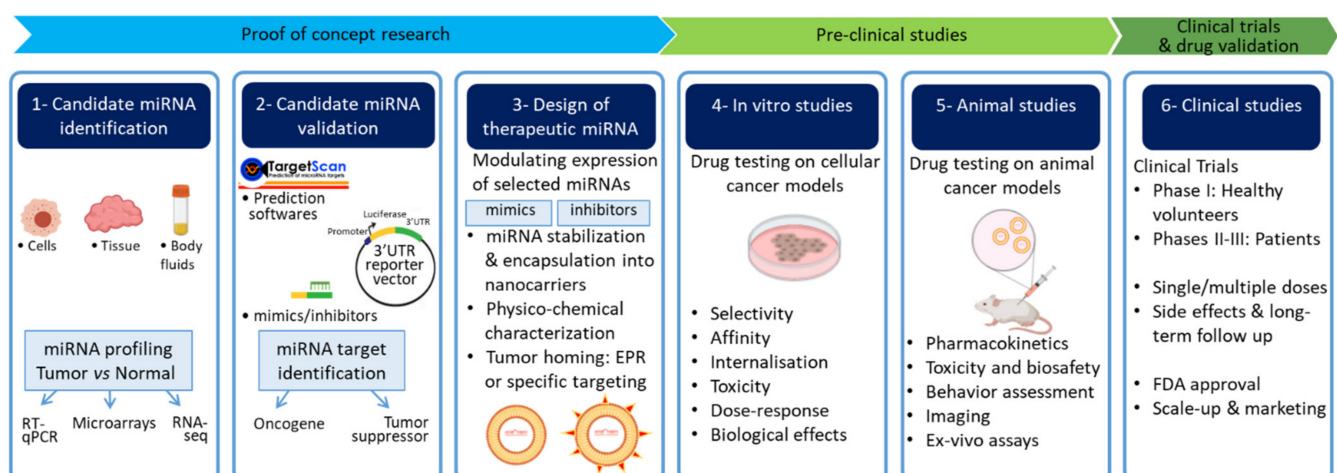


**Figure 1.** Translating miRNA biology from bench to bedside in cancer. As for the classical drug discovery workflow, development of miRNA therapeutics consists of 3 main levels: proof of concept research, preclinical studies, and clinical trials. (1) Identification of candidate miRNAs for therapy. MiRNA expression is quantified in tissue, cells, or body fluids of healthy and tumor specimens (RT-qPCR: Reverse Transcription-quantitative PCR; RNA-Seq: RNA sequencing). (2) Potential



targets of differentially expressed miRNAs can be identified using target prediction softwares and validated in reporter gene assays vectors using target transcript 3'-UTR cloned downstream of luciferase reporter and miRNA mimics/inhibitors. (3) Design of therapeutic miRNA requires stabilization and encapsulation of miRNAs in well characterized carriers. (4) Evaluation of the effects of miRNA-loaded nanocarriers on several biological processes in cancer cell models is a pre-requisite for the development of therapeutic protocols in vivo. (5) Therapeutic miRNA candidates are tested in animal cancer models alongside animal behavior and recovery before the evaluation of the antitumor effects. (6) Initiation of clinical trials requires a careful assessment of efficacy and toxicity in pre-clinical studies. Doses and side effects are particularly monitored for FDA approval and treatment scale-up.

## 2. Main Approaches for Therapeutic Targeting of miRNAs

MiRNA expression patterns can be modulated to abolish or restore miRNA biological function. To inhibit oncogenes or restore tumor suppressors, one anti-cancer strategy consists of silencing the overexpressed oncomiRs or replacing the downregulated tumor suppressor miRNAs [28]. There are three approaches to achieve miRNA loss of function: miRNA sponges, antisense oligonucleotides (antagomiRs, antimiRs), and genetic knockouts based on the application of Clustered Regularly Interspaced Short Palindromic Repeats/CRISPR-associated protein 9 (CRISPR/Cas9) genome-editing technologies [29,30]. Synthetic miRNA sponge vectors express transcripts with miRNA binding sites that mimic those found in natural mRNAs and complementary to the targeted miRNA [31]. This system sequesters endogenous intracellular miRNAs, thus preventing their binding availability for the target mRNAs [32]. By transducing a retroviral miRNA sponge to inhibit miR-9, Ma et al. demonstrated that metastasis was significantly reduced in a syngeneic mouse model of breast cancer [33]. High affinity-inhibition is also feasible via chemically modified oligonucleotides such as locked nucleic acids (LNA). As a part of the cell endogenous DNA repair machinery, the CRISPR/Cas9 system has been reported recently as a potent genetic engineering tool for miRNA-based therapeutic intervention. Yoshino and colleagues targeted miR-210-3p and miR-210-5p using the CRISPR/Cas9 system in renal cell carcinoma cell lines and demonstrated that deletion of miR-210-3p increased tumorigenesis, both in vitro and in vivo [34]. Another growing field in miRNA therapeutics is miRNA replacement therapy which aims at restoring miRNAs, which are downregulated or deleted in cancer cells [35]. With the recurrence of downregulated tumor suppressor miRNAs in human malignancies, mainly miR-34 and let-7, administration of miRNA mimics can re-establish miRNA levels to their basal non-pathological states. Indeed, a decrease of let-7 promotes expression of a number of oncogenic factors, including RAS, Myc, cyclins, and cyclin-dependent kinases [36]. In cultured lung cancer cells as well as in pre-clinical models of lung cancer, re-introduction of let-7 mimics impedes cell proliferation and reduces growth of lung tumors [37]. MiR-34a is markedly under-expressed in most human cancer types. Re-expression of miR-34a induces growth arrest and apoptosis, by silencing pro-proliferative and anti-apoptotic genes [38].

## 3. Delivery Platforms for miRNA Therapeutics

Improvement of miRNA mimics or antimiRs stability and development of safe and efficient delivery systems are critical steps to bring miRNA therapies from bench to bedside. Indeed, synthetic miRNA mimics or antimiR oligonucleotides have short half-life and are immediately degraded in biological fluids by nucleases [39]. To overcome this hurdle, several strategies have been devised, including chemical modifications such as phosphodiester and phosphorothioate internucleotide linkages, addition of a 2'-O-methyl group or synthesis of locked nucleic acids in which the ribose ring is constrained by a methylene linkage between the 2-oxygen and the 4-carbon. In addition to chemical modifications, entrapment of therapeutic miRNAs within functionalized nanoparticles allowed further improvement in their protection from degradation, decreased the immune response and enhanced the circulation time. Finally, conjugation of nanoparticles with targeting ligands such as proteins, peptides, and antibodies improved cellular uptake and specific targeting of the tumor site.

Several viral and non-viral miRNA delivery systems have been used successfully *in vitro* and *in vivo*. Nevertheless, whether based on chemically modified oligonucleotides, miRNA sponges or miRNA mimics, developing therapeutic approaches still present clearance, accessibility, tissue-specific targeting and safety issues [40]. The exponential growth in nanotechnology research is expected to help to overcome these barriers: oligonucleotides can be encapsulated into complex nanoparticles (NPs) capable of efficient and targeted drug delivery. Besides improved endosomal escape, these nanocarriers achieve tumor-selective accumulation through the Enhanced Permeability and Retention (EPR) effect, a central paradigm in cancer nanomedicine [41]. This passive targeting mechanism results from the extravasation of long-circulating nanoparticles (diameter < 100 nm) through the leaky tumor microvasculature into the tumor interstitium. Subsequent nanoparticle cellular uptake and intracellular fate are strongly influenced by their size, shape and surface properties [42].

Genetically modified viral vectors, including retroviruses, lentiviruses, adenoviruses and adeno-associated viruses (AAVs) have long been used for gene therapy and also designed to deliver transgenes encoding miRNA mimics or antagonists [43]. Virus-like nanoparticles (VLNPs) are noninfectious protein shells or capsids, composed of virus-derived structural proteins and devoid of the pathogenic elements of the viral genome. VLNPs can be produced from infections of host cells or by recombinant protein expression and self-assembly. The advantage of viral vectors is to provide high infection efficiency and persistent expression of the transgene. For example, systemic lentiviral delivery of miR-15a/16 in a mouse model of Chronic Lymphocytic Leukemia restored the expression of miR-15a/16, reduced malignancy with decreased proliferation and increased apoptosis of malignant lymphoid cells [44]. However, lentiviruses and retroviruses can integrate their own reverse transcribed DNA into the host genome, which may lead to insertional mutagenesis and activation of oncogenic pathways. Thus, non-integrating adenoviruses and AAVs have been used as alternative miRNA carriers as they keep their own genomes in episomal form. For example, systemic delivery of miR-26a carried by AAVs showed cell cycle arrest and apoptosis induction in hepatocellular carcinoma cells and tumor growth inhibition [45]. Although the viral vectors used are replication-deficient, some problems such as toxicity, immunogenicity, and manufacturing complexity shifted the research in nanomedicine towards non-viral carriers. Thus, polymeric non-viral vectors, which have been favored due to their low immunogenicity, ease of production, controlled composition, and chemical flexibility, have represented an attractive alternative to viral vectors (Figure 2).

Various types of natural and synthetic polymers have been used in miRNA-based therapies. Interest in synthetic cationic polymers resulted from their potential to form polyelectrolyte complexes with nucleic acids. Polyethyleneimine (PEI), an organic macromolecule with a high cationic-charge-density potential, is the most commonly used polymeric gene delivery system. The overall positive charge of PEI makes it convenient for condensing large negatively charged molecules such as nucleic acids, resulting in the formation of polyplexes through electrostatic complexation. Following endocytosis, PEI undergoes protonation of its amine groups within endosomes and thereby exerts a proton-sponge effect. Proton accumulation triggers cytosolic water towards the endosomes, leading therefore to osmotic swelling, endosome bursting, and PEI polyplex release into the cytosol [46]. Systemic or local application of PEI/miR-145 complexes into a mouse model of colon carcinoma significantly reduced tumor proliferation and increased apoptosis, with concomitant repression of c-Myc and ERK5 [47]. Natural cationic polymers including chitosan and dextran (polysaccharides) were also successfully tested for miRNA delivery to treat multiple myeloma and osteosarcoma in preclinical models [48,49]. Chitosan has a strong binding affinity for nucleic acids at low pH as its protonated amine groups rapidly interact with negatively charged molecules such as miRNAs. A major drawback of chitosan nanoparticles is that these interactions are almost irreversible thus preventing efficient drug release. Lipid chains or negatively charged polymers have been combined with chitosan to improve nucleic acid delivery [50].

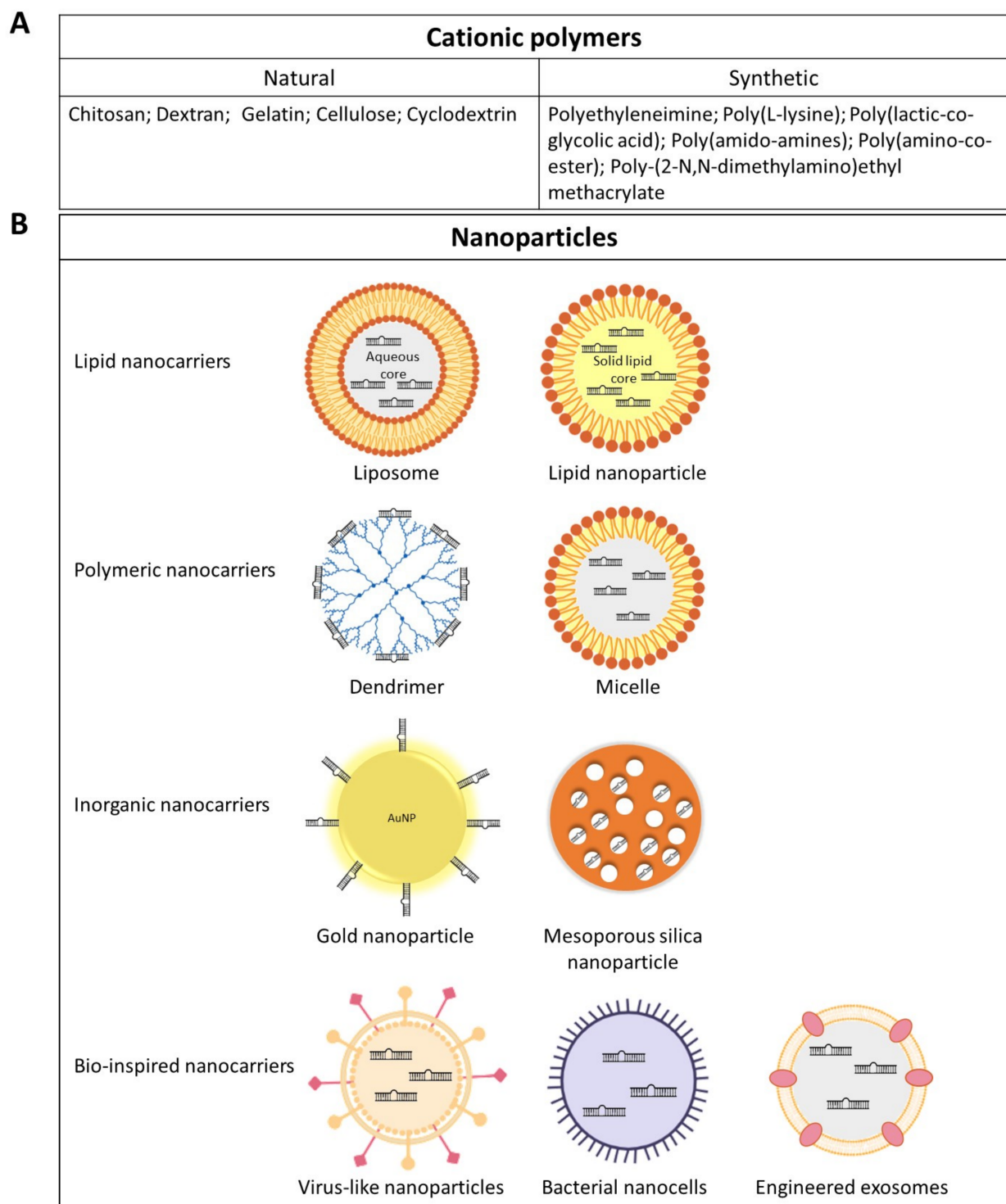


**Figure 2.** Schematic representation of commonly used and emerging nanoplatforms for miRNA delivery. **(A)** Natural and synthetic polymers can form electrostatic complexes with nucleic acids such as miRNAs. **(B)** Nanoparticle-based platforms are characterized by tunable size, shape, and surface characteristics, which enable them to have compatibility with different administration routes. Specific recognition molecules such as antibodies or peptides can be grafted to target tissues more specifically. Tumor-derived exosomes are being increasingly explored as delivery systems in cancer research since their identification as drivers of organotropic metastatic spread. However, their complex composition and still non-established biological functions led to the development of Exosome-Mimetic Nanosystems that recapitulate natural exosomes structure with a controlled composition.

Other studies investigated the potential of inorganic materials such as gold (Au) or silica NPs in miRNA-based therapy. Inorganic NPs feature several advantages, including tunable size, surface properties, and multifunctional capabilities. Multiple strategies have been used for the functionalization of Au-NPs to increase their bonding with biological molecules and facilitate the intracellular payload release. Gold nanoparticles (Au-NPs) can be functionalized with thiol groups to increase their bonding with miRNA [51]. This approach has been reported by Ekin et al. to successfully convey miR-145 to prostate PC3 and breast MCF-7 cell lines [52]. An additional polyethylene glycol (PEG) layer was shown to stabilize Au-NPs nanoformulations by limiting their aggregation and miRNA degradation [53]. Moreover, Au-NPs binding with the target site can be addressed by decorating their surface with target specific ligands. Even though Au-NPs have received a lot of interest over the past few years, more investigations related to biocompatibility, cytotoxicity, retention, and clearance time are needed to conceive conjugated Au-NPs with minimal side effects [54,55]. Mesoporous silica nanoparticles (MSN) are a special group of inorganic NPs that have porosities at the nanoscale. They provide a high surface area, thermal stability, and easy surface modification, with biocompatible and non-toxic properties. Their large and active surface allows the attachment of different functional groups for targeted drug delivery. Among the many strategies that are used to functionalize MSNs, chemical modifications within the pores to increase the retention time of loaded molecules, coating with PEG for stabilization and attachment of targeting ligands to target specific cell receptors have been extensively investigated. Tivnan et al. exploited the high expression level of the tumor-associated antigen disialoganglioside (GD2) in neuroblastoma to develop GD2-targeting MSN for the delivery of miR-34 into neuroblastoma murine models [56]. However, the synthesis of functionalized MSN requires multiple steps with complex chemical reactions that limited their fabrication at industrial scale.

Lipid-based nanoparticles (LNPs) are widely used due to their efficient cellular uptake through the cell membrane. Different types of nanoformulations, such as liposomes and solid lipid nanoparticles (SLNs) prove to be less toxic than other delivery systems such as polymer nanoparticles, owing to their biocompatibility and biodegradability. MiRNA-loaded LNPs are usually a cocktail of cationic lipids (*N*-[1-(2,3-dioleoyloxy)propyl]-*N,N,N*-trimethylammonium chloride (DOTMA) or 1,2-dioleoyl-3-trimethylammonium-propane (DOTAP)), neutral lipids and PEG, which shield miRNAs either in their aqueous core or by forming a stable complex via electrostatic interactions with the negatively charged phosphate groups in miRNA molecules [57]. Helper lipids, i.e., neutral lipids like cholesterol and dioleoylphosphatidyl ethanolamine (DOPE), can be incorporated in LNPs in order to reduce the charge-driven toxicity and to enhance delivery efficiency [58,59]. LNPs increased the therapeutic index of many drugs and offered improved drug targeting and controlled release. As for the other drug delivery nanosystems, targeted liposomal formulations have been developed by coating liposomes with specific ligands, which bind to cancer-associated antigens. For example, taking advantage of the selective internalization of GAH antibodies by gastric cancer cells, Hosokawa et al. showed that doxorubicin exerted better anti-tumor activity when vectorized in PEG-GAH liposomes than in non-coated liposomes [60,61]. In the context of miRNA-based therapy, miR-135a-loaded cationic immunoliposomes coated with anti-EGFR (Epidermal Growth Factor Receptor) antibodies (Anti-EGFR-CIL-miR-135a) were shown to inhibit gallbladder carcinoma invasion (GBC) and metastasis, and to promote apoptosis. The GBC tumor growth rate was 60% lower in xenograft-bearing mice treated with Anti-EGFR-CIL-miR-135a as compared to controls [62]. PD-L1 monoclonal antibody-conjugated miR-130a/oxaliplatin-loaded immunoliposomes (PD-miOXNP) showed a high efficacy in HGC27 gastric cancer tumors with reduced Ki67+ cells and increased TUNEL+ cells [63]. SLNs offer additional advantages over polymeric NPs and liposomes. Indeed, incorporation of both hydrophilic and hydrophobic drugs is achievable along with controlled release of the drug for up to several weeks [64]. Moreover, the lipids used in the preparation of SLNs are biodegradable and safe. SLN formulations are also characterized by a high stability and loading capacity as compared to their lipid

counterparts. The main components of SLN formulation are solid lipids, surfactants, and water. Solid lipids include fatty acids, triglycerides, steroids, and waxes. Cationic lipids facilitate interaction with the cell membrane, improving transfection efficiency. Combining miRNA with chemotherapeutic drugs using SLNs was shown to be a powerful anticancer strategy. Shi et al. demonstrated that co-incorporation of miR-34a and paclitaxel (PTX) in SLNs (miSLNs-34a/PTX) increases the uptake of these nanoparticles by B16F10-CD44+ melanoma cells and induces more cell death than single drug-loaded nanoparticles [65]. MiR-34a and PTX exerted a synergistic induction of melanoma cell death. In another study, cationic SLNs were successfully used to deliver anti-miR-21 oligonucleotide and Pemetrexed for glioblastoma therapy in vitro [66]. Micelles are nanoparticles that are formed from the self-assembling of amphiphilic molecules in an aqueous environment. Reported advantages of micelles include simple preparation, low toxicity and good tissue penetration properties [67]. However, similar to liposomes, they are prone to dilution following intravenous administration. Modifications of micelles at their core and their shell can improve encapsulation efficiency and in vivo stability. Mittal et al. designed gemcitabine-conjugated cationic micelles for the co-delivery of gemcitabine and miRNA-205 in pancreatic cancer [68]. Combination formulations efficiently reversed chemoresistance, invasion and migration in gemcitabine-resistant pancreatic cancer cells in vitro, and showed significant growth inhibition in vivo.

A powerful delivery vehicle based on bacterially derived nanocells, called EDV<sup>TM</sup> (EnGeneIC Dream Vectors) has been developed by EnGeneIC Ltd. (Sydney, Australia) [69]. Bacterial nanocells are achromosomal nanoparticles produced by inactivation of the genes that control normal bacterial cell division. They can package a range of anticancer chemotherapeutic drugs [70]. Targeted delivery was achieved by using bispecific antibodies, which are capable of binding the EDVs with one arm and the tumor antigen with the other arm. In addition, the bacterial cell wall of the nanocells stimulates key components of the immune system, which are then activated to kill cancer cells. The EDVs proved to be safe and well tolerated despite high and repeated doses in different animal models [70,71]. This system has been used to deliver miR-16 to mesothelioma in vivo [72] as well as to mesothelioma patients (MesomiR-1 clinical trial NCT02369198). Another elegant strategy for miRNA delivery was inspired by natural exosomes, which shield and convey miRNAs into the tumor niche. Nevertheless, besides the validation of exosomes as biocompatible molecular carriers, their clinical translation is still hampered by their complex composition and poor harvesting yields [73]. To overcome these issues, Vazquez-Rios et al. took advantage of the existing liposome technology to develop Exosome-Mimetic Nanosystems (EMNs) [74]. These nanostructures reproduce cell-derived exosomes structure, physicochemical properties, and loading capacities.

#### 4. Application of miRNA-Based Therapeutics in Selected Cancers

In their recent review, Bonneau et al. reported the clinical advances for miRNA therapeutics in several human diseases, including cancer [75]. In the following sections, we will describe the preclinical advances in anti-cancer strategies using miRNA-based therapy for selected common and rare solid tumors. Table 1 provides several examples of in vitro and in vivo studies using different delivery systems and administration routes to replace or inhibit miRNAs in cancer cells.

##### 4.1. Lung Cancer

Lung cancer is the most frequent cause of cancer-related deaths worldwide with 5-year survival rates ranging from 4–17% depending on stage and populations. Liposomes have been reported to be particularly convenient for drug delivery to the lungs, since they can be prepared from lung endogenous surfactants. This makes them relevant carriers for miRNA-targeting molecules to this organ. To date, miR-34a is the most well documented tumor suppressor miRNA, capable of cell cycle arrest and induction of apoptosis. Its downregulation is reported in various solid tumors including lung cancer, suggesting that replacement

therapy might be effective for retrieving its physiological levels [76]. Wiggins et al. [77] showed that systemic delivery of synthetic miR-34a in liposomal formulation could indeed inhibit tumor growth in NSCLC-bearing mice. No immunogenicity or toxicity were observed. These results were in agreement with prior *in vitro* experiments on genetic variants of NSCLC cell lines, showing that transfection of miR-34a reduced cell growth and colony formation in a p53 dependent manner [77]. In the same line, Kasinski et al. suggested a combinatorial approach to co-deliver the tumor suppressors miR-34 and let-7b using NOV340 liposomes in NSCLC. This strategy reduced tumor burden and induced a 40%-increase in survival rate of  $Kras^{G12D/+}/Trp53^{flx/flx}$  mutant mice [78]. Systemic delivery of miR-200c loaded-NOV340 liposomes has been shown to enhance radiosensitivity in lung cancer by increasing the oxidative stress response and by inhibiting repair of radiation-induced DNA double-strand breaks [79]. Thus, rendering treatment-resistant lung cancer sensitive to radiotherapy through lipid nanoparticle-mediated miRNA replacement appeared as a promising approach. On the clinical side, miR-34 mimics, encapsulated in NOV340 liposomes (MRX34), were the first miRNA-based therapy approach that entered phase I clinical testing in 2013 for several solid and hematological malignancies (NCT01829971, Mirna Therapeutics) [80]. Unfortunately, this study was halted in 2016 following multiple immune-related severe adverse events observed in the patients [81].

Another approach demonstrated that DOTMA-based cationic lipoplexes (LPs) successfully conveyed miR-29b (LP-miR-29b) to both NSCLC A549 cells in culture and NSCLC xenograft mouse model [82]. After several injections of miR-29b-loaded-lipoplexes in the tail vein, the treated mice displayed reduced tumor size as compared to negative controls (LP-miR-NC) and untreated mice. MiR-29b expression in tumor tissue of treated mice was 5-fold higher, confirming the efficient release of miR-29b from DOTMA lipoplexes. As for the biological impact of restoring miR-29b expression, Wu et al. [82] observed a significant decrease in miR-29b oncogenic targets DNMT3B (DNA (cytosine-5-)-methyltransferase 3 beta), CDK6 (Cell division protein kinase 6) and MCL1 (Induced myeloid leukemia cell differentiation protein) with minor toxicity. Nonliving bacterial nanocells (EDVs or TargomiRs) were used as carriers for miR-16 delivery to 26 NSCLC patients in a phase I clinical study (NCT02369198). The targeting moiety of this bacterially derived delivery system was an anti-EGFR bispecific antibody to target EGFR-expressing cancer cells. Tumor growth was impaired after systemic administration of TargomiRs at low dosages. However, dose-dependent toxicities were reported, i.e., anaphylaxis, inflammation as well as cardiac events. Variable response rates were observed with 5% of the patients showing partial response, 68% showing stable disease and 27% showing progressive disease [83]. Based on these observations, the authors recommended to conduct a new trial combining TargomiRs with chemotherapy or immunotherapy in larger groups of patients. More recently, Exosome-Mimetic Nanosystems were engineered with organ specific proteins such as Integrin  $\alpha 6\beta 4$  for the targeted delivery of miR-145 mimics to lung adenocarcinoma cells. *In vivo* experiments were carried out using intraperitoneal or retro-orbital injection of labeled miR-145-EMNs into nude mice bearing lung tumors. Fluorescence was mainly detected at tumor sites and mild off-target effects were found in the liver and spleen [74].

**Table 1.** Examples of in vitro (cell lines) and in vivo studies (preclinical mouse cancer models) that have been conducted to test miRNA-based therapies in the absence or in the presence of accompanying anticancer drugs.

Cancer Type	miRNAs	Delivery System	MiRNA Loading Strategy	Cell Lines	Delivery Route In Vivo	Results	References
Lung cancer	miR-34a	Neutral Lipid Reagent (RNA-LANCER II)	Encapsulation in phospholipid-oil emulsion	A549, BJ, NCI-H460, Calu-3, NCI-H596, NCI-H1650, HCC2935, SW-900, NCI-H226, NCI-H522, NCI-H1299, Wi-38 and TE353.sk	it, iv	Reduced cell proliferation and colony formation; Tumor growth inhibition	[77]
	miR-34 let-7	Neutral Lipid Nanoemulsions	Encapsulation in phospholipid-oil emulsion	KRAS/TP53-mutated NSCLC cell lines: H358, H23, and H441	iv	Decreased MET and MYC expression; 40% better survival rate	[78]
	miR-29	Cationic DOTMA Lipoplexes	Electrostatic interaction	A549	iv	Decreased expression of miR-29b oncogenic targets DNMT3B, CDK6 and MCL1	[82]
	miR-16	Bacterial Minicells (with EGFR antibody coating)	Loading via non-specific Porin channels	-	iv	Inhibition of tumor growth but dose-dependent toxicities	[83]
	miR-145	Liposomal Exosome-Mimetic Nanoplat-forms (Integrin $\alpha 6\beta 4$ coating)	Encapsulation in aqueous phase	A549	ip, ro	Preferential accumulation at tumor sites	[74]
Liver cancer	miR-122	Lentivirus	Viral vector expression system	Mahlavu SK-HEP-1	sc	Reduced ADAM17 expression; Inhibition of tumor growth, angiogenesis, and intrahepatic metastasis	[84]
		Cationic Liposomes	Encapsulation	Sk-Hep-1	it	50% growth suppression of Sk-Hep-1 xenografts; impairment of angiogenesis; Downregulation of SRF, IGF1R and ADAM10	[85]
	Anti-miR-221	PEI-modified PLGA nanoparticles	Electrostatic interaction	HepG2	sc	Inhibition of tumor growth; Increased circulating miR-221	[86]
	miR-199a/b-3p/anti-miR-10b	PEI-Cyclodextrin-PEG polymeric nanoparticles	Electrostatic interaction	Huh-7 PDX	iv	Inhibition of Huh-7 tumor growth by targeting mTOR, PAK4, RHOC and EMT pathways. Tumor suppression on PDX	[87]

Table 1. Cont.

Cancer Type	miRNAs	Delivery System	MiRNA Loading Strategy	Cell Lines	Delivery Route In Vivo	Results	References
	miR-27a Sorafenib	Anti-GPC3 antibody-targeted lipid nanoparticles	Electrostatic interaction	HepG2	-	Suppression of tumor burden; increased apoptosis	[88]
Breast cancer	miR-125a	Liposomes (with hyaluronic acid coating)	Electrostatic interaction	SKBR3, 21MT-1	-	Reduced HER-2 expression	[89]
	miR-34a Doxorubicin	Hyaluronic acid-chitosan nanoparticles	Electrostatic interaction	MDA-MB-231	iv	Enhanced response to chemotherapy	[90,91]
	Anti-miR-21 Adriamycin	PEI graphene oxide nanocarriers	PEI-mediated electrostatic interaction	MCF-7	-	Increased Adriamycin uptake	[92]
	miR-9 miR-21 miR-145	PEI-modified magnetic nanoparticles	Electrostatic interaction	MCF-7	iv	Effective tumor targeting; Reduced tumor burden	[93]
	miR-34	Silica nanoparticles	Electrostatic interaction with added amine groups	Comma D $\beta$ , SUM159pt	it	Inhibition of tumor growth	[94]
Glioblastoma	miR-100 anti-miR-21	Gold-iron oxide nanoparticles (with T7 peptide-cyclodextrin-chitosan coating)	Electrostatic interaction	U87-MG	in	Diagnosis by MRI tracking of gold nanoparticles; Presensitization to temozolomide	[95]
	Anti-miR-21	Cationic polyamine-co-ester	Electrostatic interaction	U87	ced	Apoptosis of GBM cells; Better survival rates	[96]
	miR-34a	Dendritic polyglycerolamine	Electrostatic interaction	Patient-derived GBM cells	iv	Reduced tumor burden	[97]
Thyroid cancer	Anti-miR-146	Invivofectamine	Electrostatic interaction	Cal62	it	Impaired tumor growth; Restored PTEN expression	[98]
	Anti-miR-21	LNA	Chemical modifications	RTL-5	sc	Inhibition of tumor growth	[99]
	miR-204-5p	Lentivirus	Viral vector expression system	TCP-1 BCPAP	sc	Inhibition of tumor growth	[100]
Adrenocortical cancer	miR-7	Bacterial Minicell particles "EnGene/c Delivery Vehicles" (EDVs) (with EGFR antibody coating)	Loading via non-specific porin channels	NCI-H295R SW13	iv	Inhibition of tumor growth by targeting CDK1/Raf1/mTOR signaling	[101]



Table 1. Cont.

Cancer Type	miRNAs	Delivery System	MiRNA Loading Strategy	Cell Lines	Delivery Route In Vivo	Results	References
	miR-431 Doxorubicin Mitotane	Lipofectamine	Electrostatic interaction	NCI-H295R	-	Reversed EMT phenotype	[102]
Ovarian cancer	miR-200c Paclitaxel	Lipofectamine	Electrostatic interaction	SCOV3	-	Impaired migration and invasion, enhanced chemosensitivity	[103]
	miR-200a miR-141	Lentivirus	Viral vector expression system	SCOV3	-	Improved sensitivity to paclitaxel	[104]
	miR-7 Paclitaxel	Polymeric Nanoparticles (monomethoxy (poly(ethylene glycol))-poly(D,L-lactide-co-glycolide)-poly(L-lysine)	Electrostatic interaction with the poly(L-lysine) chains in the core	SCOV3	iv	Improved sensitivity to paclitaxel and apoptosis of cancer cells through inhibition of EGFR/ERK pathway	[105]
	miR-15a miR-16 Cisplatin	Liposomes	Electrostatic interaction	A2780 A2780-CP20 OVCAR4	iv	Reduced tumor burden; decreased expression of BMI1 oncogene and EMT markers	[106]
	Anti-miR-21	Mesoporous Silica Nanoparticles (with CGKRR peptide coating)	Calcium silicate trapping procedure	OAW42	iv	Reduced tumor mass	[107]
	Anti-miR-21	Gold Nanoparticles	Surface functionalization with amine or thiol groups	-	-	Disrupted cell colony formation ability	[108]
	miR-155	PEI	Electrostatic interaction	OvCa-associated dendritic cells	ip	Boosted immunity and better survival	[109]
Prostate Cancer	miR-34a	Chitosan Nanoparticles	Electrostatic interaction via the protonated amino groups at low pH	PC3	iv	Inhibited tumor growth and metastasis	[110]
	Anti-miR-221	Mesoporous Silica Nanoparticles	Electrostatic interaction within the pore	PC3	-	Less cancer expansion	[111]
	miR-205 Docetaxel	Iron oxide nanoplatforms	Electrostatic interaction	PC3 C4-2	-	Induced apoptosis and Chemosensitization	[112]
	miR-145	SSPEI with R11 peptide coating	Electrostatic interaction	PC3 LNCAP	iv	Impaired tumor growth Enhanced survival	[113]

It = intratumor; iv = intravenous; ip = intraperitoneal; ro = retroorbital; in = intranasal; ced = convection-enhanced delivery; PDX = Patient-Derived Xenografts.

#### 4.2. Liver Cancer

Liver cancer is one of the most common malignancies worldwide and the third leading cause of cancer-associated mortality. It has a poor prognosis due to largely ineffective therapeutic options. Surgical removal or liver transplantation is the only curative treatments

for early-stage HCC, the most frequent type of primary liver cancer [114]. Alterations of miRNAs landscape and their potential as therapeutic targets in liver diseases, including liver metabolism dysregulation, liver fibrosis and liver cancer have been the focus of several reviews [115–117]. Plasma levels of synthetic miRNA antagonists or miRNA mimics distribute broadly after intravenous administration but later accumulate mostly in the liver and kidney and remain high up to 24 h after injection [118]. On the other hand, NPs biodistribution studies have demonstrated that the majority of injected nanomaterials usually accumulate in the liver before undergoing hepatic clearance [119]. This makes liver cancer a good model for testing miRNA-based therapy approaches as this organ can be easily targeted with different delivery systems. Nevertheless, miRNA delivery through NPs to treat HCC has to take into consideration passive and active mechanisms to avoid or delay liver elimination. MiR-122, a highly abundant, liver-specific miRNA that accounts for approximately 70% of the whole hepatic miRNome in humans, was found to be markedly downregulated in HCC. Restoring miR-122 using a lentiviral expression vector in metastatic liver cancer cell lines inhibited migration and invasion in vitro as well as tumorigenesis, angiogenesis, and metastasis in vivo [84]. It was further demonstrated that miR-122 inhibits hepatocellular carcinoma metastasis by modulating ADAM17 (a disintegrin and metalloprotease 17) [84] and cyclin G1 (CCNG1) [120]. Hsu et al. demonstrated that delivery of miR-122 to HCC cells using cationic lipid nanoparticles consisting of 2-dioleoyloxy-*N,N*-dimethyl-3-aminopropane (DODMA), egg phosphatidylcholine, cholesterol, and cholesterol-polyethylene glycol (LNP-DP1) dramatically downregulated miR-122 target genes [85]. In vivo, LNP-DP1-encapsulated miR-122 mimic induced HCC xenografts growth suppression without causing systemic toxicity. MiR-26a is expressed at high levels in normal adult liver but is dramatically downregulated in both human and murine liver tumors. MiR-26a replacement using AAV as delivery vector potently suppressed cancer cell proliferation and activated tumor apoptosis in vivo, leading to marked suppression of tumor growth [45]. It was further shown that miR-26a arrested the cell cycle at G1 phase in human liver cancer cells by downregulating cyclins D2 and E2. MiR-21 is highly overexpressed in HCC [121]. Inhibition of miR-21 in cultured HCC cells increased expression of PTEN tumor suppressor, and decreased tumor cell proliferation, migration, and invasion [122]. Meng et al. investigated poly(lactic-co-glycolic) acid (PLGA)-based nanoparticle for the delivery of anti-miR-221 to HCC cells and tested its therapeutic efficacy in vitro and in vivo [86]. PLGA nanoparticles encapsulating anti-miR-221 suppressed HCC cell growth, colony formation ability, migration, invasion, and impaired tumor growth in mice. Interestingly, Shao et al. developed a combination therapy by encapsulating miR-199a/b-3p mimics and anti-miR-10b into a polymer-based nanopatform PEI-βCD@Ad-CDM-PEG (PCACP) to treat HCC. PCACP significantly inhibited HCC cell proliferation and tumor growth by targeting mTOR (mechanistic target of rapamycin), PAK4 (p21-Activated kinase 4), RHOC (Rho-related GTP-binding protein) and epithelial mesenchymal transition (EMT) pathways both in vitro and in vivo [87]. In an elegant study, Sorafenib (SRF), and anti-miR-27a-loaded anti-GPC3 antibody targeted cationic LNPs were developed to treat HepG2 cell xenograft-bearing mice [88]. Combination of SRF and anti-miR-27a (G-S27LN) decreased cell viability and potentiated cell apoptosis compared to SRF alone, suggesting a synergistic anticancer effect. A significant reduction of tumor burden and marked TUNEL positive apoptosis were observed in animals treated with G-S27LN formulation.

#### 4.3. Breast Cancer

As HER-2 (Human Epidermal Growth Factor Receptor 2) positive breast cancers account for 30% of cases associated with poor prognosis, more attention is being brought to efficiently target this overexpressed receptor. In this context, in vivo studies in mice models of breast cancer have demonstrated that lentiviral delivery of the tumor suppressor miR-125a-5p reduced tumor growth, metastasis, and angiogenesis by directly targeting HDAC4 (Histone deacetylase 4) [123]. Hayward et al. further showed that transfection of miR-125a-5p in hyaluronic acid-coated liposomes indeed knocked down the HER-2

proto-oncogene in 21MT-1 breast cancer cells. This resulted in reduced migratory and proliferative potential due to inactivation of MAPK and PI3K/AKT signaling [89]. Taking into consideration the overexpressed hyaluronic acid (HA) receptors in breast cancer, HA/miRNA nanoparticles hold great promises for targeted clinical approaches. Interestingly, HA-chitosan nanoparticles were used to co-encapsulate doxorubicin and miR-34a. Deng et al. showed that administration of these formulations into nude mice enhanced the response to chemotherapy and decreased cancer cell migration due to inactivation of Notch signaling by miR-34a [90,91]. In a similar approach, Adriamycin uptake by MCF-7 cells was increased when delivered together with anti-miR-21 in PEI graphene oxide carriers [92]. As cancer cells consistently display alterations in multiple microRNAs, combinatorial strategies have been implemented. Indeed, in vivo studies conducted by Yu et al. showed a 58%-reduction in tumor volume when packaging miR-9, miR-21 and miR-145 sponges into PEI-modified magnetic particles [93]. Recently, Panebianco et al. demonstrated that silica nanoparticles (SiO<sub>2</sub>NPs) allowed delivery of miR-34a into mammospheres and mammary tumors [94]. MiR-34a/SiO<sub>2</sub>NPs complexes decreased sphere formation efficiency and reduced tumor growth in mice. The levels of well-known target genes of miR-34a such as NOTCH1 (Notch Receptor 1), Cyclin E2 and c-Myc were significantly reduced, indicating the biological activity of delivered miR-34a.

#### 4.4. Glioblastoma

Despite conventional therapeutic options involving surgery, radiology, and chemotherapy (mainly Temozolomide), glioblastoma (GBM) remains a lethal malignancy with unmet clinical needs. The implementation of the RNA interference technology provided new insights for GBM gene therapy. For example, miR-21 has been recognized as a major oncomiR upregulated in GBM. It contributes to tumorigenesis by directly targeting PTEN, thus blocking expression of key apoptosis-enabling genes such as caspases and p53. MiR-21 overexpression is also associated with drug resistance, hence chemotherapy failure [124,125]. Conversely, the tumor suppressor miR-100 was shown to trigger the p53 network through regulation of the PLK1 (Polo-Like Kinase gene 1) signaling in tumor-initiating cells [126]. Of note, this apoptotic pathway is also activated by the gold-standard GBM treatment, Temozolomide, suggesting a potential chemo-sensitization via miRNA remodeling [127]. In a combined theranostic-chemotherapeutic approach, gold-iron oxide NPs were used to co-deliver miR-100 and anti-miR-21 into GBM xenograft-bearing mice. The carriers were tailored with a GBM cell-targeting T7 peptide and a cyclodextrin-chitosan polymer layer for specific brain targeting [95]. In vivo experiments were carried out by intranasal inhalation of these nanoformulations to bypass the blood-brain barrier. In parallel, a group of mice received systemic doses of temozolomide. Remarkably, mice co-treated with miR-loaded-NPs and temozolomide chemotherapy showed better survival than animals receiving either miR-NPs or chemotherapy alone, or no therapy. Furthermore, given their magnetic resonance property, it was possible to track gold-iron formulations by MRI imaging. Similar results were obtained by intratumor administration of miR-21-inhibiting NPs named PACE (cationic polyamine-co-ester) [96]. As for most solid cancers, miR-34a was also investigated in GBM for its apoptosis-inducing capacities. When complexed in a dendritic polyglycerolamine (dPG-NH<sub>2</sub>) cationic carrier, miR-34a stability was enhanced, thus disabling in vitro proliferation and migration of glioma cell lines via C-MET, CDK6, NOTCH1, and BCL-2 inhibition [97]. In vivo studies revealed reduced tumor burdens upon tail vein injection of dPG-NH<sub>2</sub>-miR-34a polyplexes. Interestingly, the protected miR-34a was able to cross the blood brain barrier with no reported toxicity.

#### 4.5. Endocrine Cancers

With regard to endocrine tissues, miRNAs are indeed relevant players given their hormone-like effects with endocrine, autocrine or paracrine regulatory functions mediating intercellular communication [128]. A reciprocal interplay between hormones and microRNAs has been described: miRNAs can alter hormone metabolism via their binding

to genes coding for hormones, hormone antagonists, enzymes of hormone biosynthesis, or even hormone receptors [129]. Conversely, many hormones were shown to modulate microRNA expression patterns through regulation of miRNA transcription or biogenesis. Understanding these regulatory feedback loops and how they are perturbed in cancer are critical for the development of miR-based therapeutics and biomarkers in endocrine tissues.

#### 4.5.1. Thyroid Cancer

Thyroid carcinoma is the most common form of endocrine cancers. According to the Surveillance, Epidemiology, and End Results (SEER) registry, thyroid cancers account for 3% of new cancer cases in the US and 0.4% of all cancer deaths with a 2.9-times higher rate in women. Such tumors normally disrupt hormone secretion and are associated with hormone-related complications. Papillary thyroid cancer (PTC) is the most common form of differentiated thyroid neoplasia, which arise from the follicular cells of the thyroid gland. MiRNA profiling in thyroid tumors led to the identification of specific signatures that could be useful for diagnosis and possibly for therapy [130,131]. Among others, miR-146b is highly expressed in PTC and is correlated with pejorative outcome. It was further demonstrated that the tumor suppressor PTEN holds a miR-146 binding site in its 3'-untranslated region. MiR-146b-mediated downregulation of PTEN triggers the PI3K/AKT signaling pathway thus promoting cell proliferation, survival, migration, and invasion. In agreement with these findings, intratumor delivery of miR-146b inhibitors using lipid formulations—namely invivofectamine—suppressed miR-146b-induced aggressiveness in xenograft models [98]. RAS activating mutations have been widely reported in thyroid cancer. Besides their major effects on the global transcription of protein-coding genes, activated RAS proteins have been found to promote the increase of a subset of miRNAs, of which miR-21. Frezzetti et al. showed that LNA-mediated knockdown of miR-21 in RAS-transformed FRTL-5 thyroid cells was able to inhibit markedly the growth of tumor xenografts [99]. The Wnt/ $\beta$  catenin pathway was shown to be activated in PTC as an indirect target of the oncogenic miR-155 [132]. Moreover, miR-155 overexpression in PTC was associated with enhanced survival and colony formation in PTC cell lines. These observations were confirmed in nude mice inoculated with miR-155-transduced TPC-1 cells where larger and highly proliferating tumors were obtained, thus suggesting that silencing miR-155 may be a potential therapeutic strategy for treating PTC. MiRNA replacement therapy has been also conducted in PTC preclinical models. Functional assays by Lianyong et al. showed that miR-204-5p impairs tumor growth through repression of IGF1R (Insulin-like growth factor-binding protein 5). In nude mice, subcutaneous engraftment of human PTC cells stably expressing miR-204-5p induced smaller tumors as compared to controls [100]. In addition to their role in the regulation of cancer hallmarks, miRNAs could also modulate response to adjuvant therapy in thyroid cancer. Approximately 30% of patients with advanced stages of differentiated thyroid cancer are refractory to radioiodine therapy, due to reduced expression of the Sodium Iodide Symporter (NIS) [133]. High levels of miR-146b were shown to disrupt thyroid differentiation and iodide uptake by direct repression of the transcription factor PAX8 and its target gene NIS. Other genes involved in iodide transport mechanisms such as Dehalogenase 1 and Deiodinase 2 are also regulated by miR-146b thus confirming its pivotal role in radioiodine therapy [134]. The authors suggested that miR-146b-3p/PAX8 (Paired box gene 8)/NIS regulatory axis might be a relevant therapeutic target to modulate thyroid cell differentiation and iodide uptake for improved treatment of advanced thyroid cancer. All these important findings are waiting for further exploitation using nanoparticle-based delivery of therapeutic miRNAs in thyroid cancer.

#### 4.5.2. Adrenocortical Cancer

Adrenocortical carcinoma (ACC) is a rare and highly aggressive malignancy (incidence of 4–12 cases per million per year) which develops in the cortex of the adrenal gland. Cortisol hypersecretion, causing rapidly progressive Cushing's syndrome, is the most com-

mon hormone excess in ACC patients. The clinical outcome of ACC is poor, with a 5-year survival ranging from 15 to 35% [135]. About half of the patients presents with advanced disease or develop local recurrence and distant metastasis after surgery. Complete surgical removal of the tumor remains the mainstay treatment option for ACC. Mitotane, the only FDA-approved drug for this cancer, displays some single-agent activity (10–30% tumor response rates) based on its adrenolytic activity, but its broad clinical use is challenged by an unfavorable toxicity profile [136]. Response to combination of mitotane and cisplatin-based chemotherapies do not exceed 20% for patients with advanced ACC, either recurring or metastasizing [137]. Targeted therapies including inhibitors of IGF (Insuline-like Growth Factor)/mTOR pathway, VEGFRs and other tyrosine kinase receptors such as EGFR and FGFR have been largely ineffective as monotherapy. The multiple genomic and molecular alterations reported in ACC (TP53, Wnt/ $\beta$ -catenin, and IGF pathway) include extensive deregulations of miRNA expression [138–145]. Among the most frequently deregulated miRNAs in ACC, miR-483, miR-139-5p, miR-503, and miR-210 were found to be upregulated, whereas miR-195 and miR-335 were found to be downregulated [146]. However, miRNA-based therapeutic approaches for ACC are still scarce as most studies focused on the biomarker potential of tumor or circulating miRNAs [146]. A first preclinical approach was performed using the genetically modified bacterial nanocells (EDVs) to deliver systemically the tumor suppressor miR-7 into a human ACC mouse model [101]. Specific tumor homing was ensured by using EGFR-tailored EDVs. MiR-7-loaded nanoparticles could effectively reduce ACC xenograft growth arising from both an ACC cell line and patient-derived xenografts, without any evidence of off-target effects. Mechanistically, this phenotype was mediated by repression of RAF1, mTOR, and CDK1 (Figure 3). As miR-7 replacement therapy acted synergistically with Erlotinib therapy in head and neck cancer [147], it is crucial to assess whether combination of miR-7 and mitotane would have similar effects in ACC. Such was the case of miR-431, which efficiently sensitized ACC cell lines to mitotane and doxorubicin. In fact, miR-431 was 100-fold underexpressed in patients who were resistant to adjuvant therapy, when compared to sensitive ones. Following transfection of the ACC cell line H295R with miR-431 mimics followed by treatment with doxorubicin or mitotane, H295R cells showed reduced proliferation and increased apoptosis. Restoring miR-431 expression could reverse the EMT phenotype as shown by ZEB1 (Zinc finger E-box-binding homeobox 1) transcription factor repression [102]. These findings support a great potential of miRNA therapeutics for ACC alongside clinical trials based on combined chemotherapy [137]. Jung et al. proposed an experimental setup with liposome-encapsulated chemotherapeutics (L-EDP-M etoposide (E), doxorubicin (D), cisplatin (P), and mitotane (M)) in order to minimize unintended targeting [148]. Treatment of the ACC cell line SW-13-derived xenografts in mice induced necrosis and reduction in tumor size. Interestingly, the research group reported an increased expression of circulating miR-210 in the L-EDP-M-responsive animals. Since miR-210 is a frequently described as an oncomiR in ACC, its release from the tumor to the circulation may be valuable for monitoring response to therapy.

#### 4.5.3. Ovarian Cancer

Intensive analysis of the Cancer Genome Atlas (TCGA) data revealed a large panel of miRNA deregulations in the three ovarian cancer (OvCa) subtypes (serous, endometrioid, and clear cell carcinoma). The miR-200 family proved to be of great prognostic value as it gathers five tumor suppressor miRs arising from 2 genomic clusters, namely miR-200b, miR-200a, miR-429, miR-200c, and miR-141 [149]. MiR-200c upregulation is predictive of good prognosis in OvCa. Its overexpression impaired migratory and invasive capacities of SCOV3 cell lines and significantly increased their susceptibility to microtubule-targeting chemotherapeutics, i.e., paclitaxel (PTX) [103]. Animal studies conducted by Mateescu et al. demonstrated that restoring miR-200a and miR-141 favored tumor growth, but simultaneously enhanced chemosensitivity to PTX, which is among the first-line chemotherapy agents used for OvCa [104]. According to the authors, these miRNAs drive a persistent

oxidative stress response through inhibition of p38 $\alpha$ , which is associated with an improved sensitivity to PTX. However, a major drawback of this compound is induction of survival, proliferation, and drug resistance upon activation of the EGFR/ERK pathway. Interestingly, miR-7 was shown to suppress this signaling network, thereby suggesting that combining miR-7 therapy with PTX in nanoparticles could enhance sensitivity to chemotherapy [105]. Indeed, upon intravenous administration, PTX/miR-7 nanoparticles revealed anti-cancer properties in OvCa models through the inhibition of PTX-induced EGFR/ERK pathway. Responsiveness to cisplatin chemotherapy was also improved when liposomal miR-15a and miR-16 were injected in a chemo-resistant orthotopic OvCa mouse model [106]. A reduced tumor burden along with decreased expressions of the BMI1 oncogene, the EMT markers as well as the cisplatin transporter ATP7B were reported in treated mice as compared to negative controls. Peptide modified-porous silicon nanoparticles were used by Bertucci et al. [107] to encapsulate an anti-miR-21 LNA. A tumor specific-peptide CGKRRK was grafted on the surface of the nanocarriers for targeted distribution. Internalization, silencing efficiency, and antitumor activity were firstly determined in cultures of OAW42 OvCa cell lines. In mice bearing subcutaneous xenografts, five doses of anti-miR-21 formulations at 25 mg/kg injected in the tail vein every other day significantly reduced the tumor mass [107]. Another study demonstrated that gold nanoparticles were attractive platforms for anti-miR-21 delivery to OvCa cells as they efficiently silenced endogenous miR-21 and disrupted cell colony formation [108]. Lactic-co-glycolic acid-modified polyethylenimine (LGA-PEI) could successfully transfer miR-520h mimics into ovarian xenograft tumors [150]. Along the same line, miR-155 loaded-PEI nanocomplexes were used for OvCa immunotherapy. While miR-155 was demonstrated to have an immune-stimulatory role [151], it was found underexpressed in OvCa-derived dendritic cells. After intraperitoneal injection, miR-155-PEI were selectively taken up by dendritic cells residing in ovarian tumors, thus boosting anti-cancer immunity and increasing mice survival rates by 65% [109].

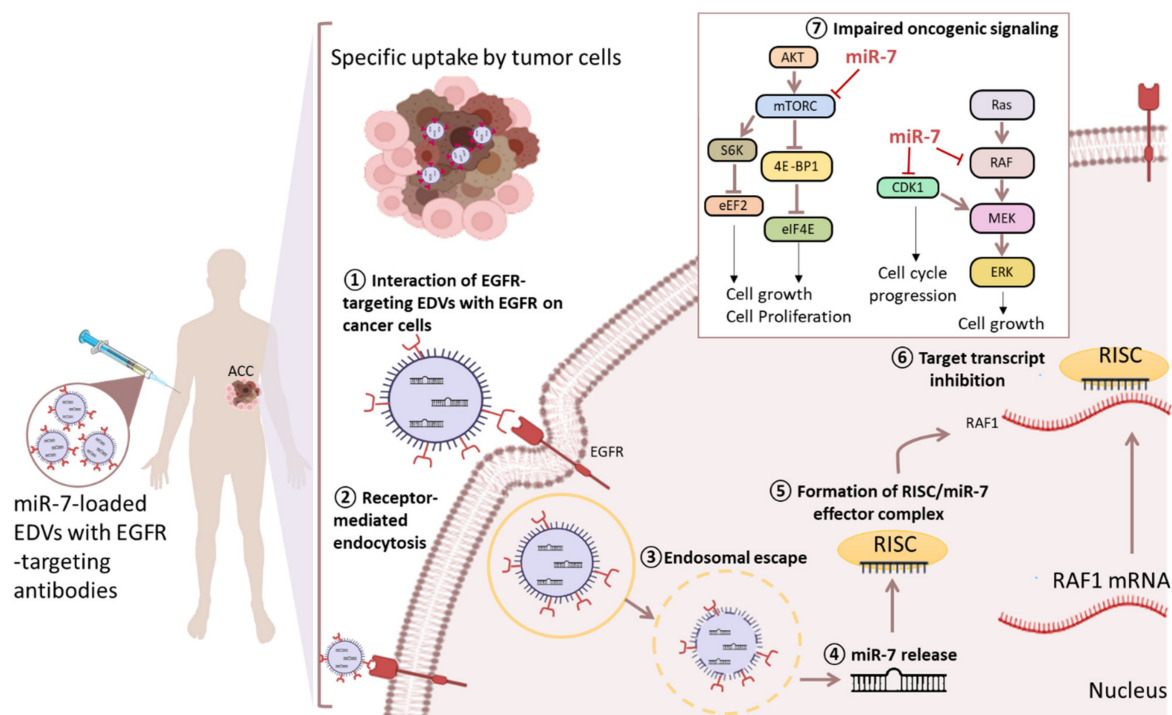


**Figure 3.** A proposed model in which miR-7 replacement via EDVs (EnGeneIC Delivery Vehicle) in Adrenocortical Carcinoma could inhibit multiple oncogenic pathways including mTOR, MAPK and CDK1 signaling pathways [70]. mTORC: mammalian target of rapamycin Complex; 4EBP1: eukaryotic translation initiation factor 4E- (eIF4E-) binding protein 1; eIF4E: eukaryotic translation initiation factor 4E; S6K: ribosomal protein S6 kinase; eEF2: eukaryotic elongation factor 2; CDK1: cyclin dependent kinase 1.

#### 4.5.4. Prostate Cancer

The taxanes docetaxel and cabazitaxel remain the standard of care for prostate cancer (PCa). However, drug resistance remains a major issue, which imply the development of new therapeutic strategies. There has been rapidly growing interest in alternative therapeutic molecules such as miRNAs for PCa. For example, systemic injection of miR-34a-enriched-chitosan nanoparticles inhibited prostate tumor growth in subcutaneous xenograft models and prevented bone metastasis [110]. Besides downregulation of its target genes including MET, Axl, and c-Myc, nanoparticle-mediated restoration of miR-34a expression in PC3 cells induced apoptosis and autophagy, and decreased PC3 cell proliferation, invasion, and migration [110]. MiR-221 is one of the most studied oncogenic miRNA in prostate cancer. By inducing p27 cell cycle checkpoint arrest, miR-221 supports uncontrolled proliferation, hence cancer expansion. Moreover, high circulating levels of miR-221 were detected in patients with PCa. This has led Farina et al. to propose a therapeutic approach consisting of miR-221 inhibitor encapsulation into mesoporous silica nanoparticles (MSN) [111]. MSN are biocompatible nanoparticles with a high molecular loading capacity and a possible controlled release of payload. MiR-221 mimic-loaded MSN were successfully delivered to PC3 cell lines where they recapitulated the biological effects of miR-221 [111]. The anti-tumor function of miR-205 was highlighted in prostate cancer using magnetic iron oxide core nanoparticles coated with PEG-PEI layers [112]. MiR-205 nanoplateforms were internalized into PC3 and C4-2 cells as measured by flow cytometry analysis. Western blot analysis revealed an important induction of pro-apoptotic proteins such as cleaved PARP and cleaved Caspase 3 after treatment with miR-205-nanoparticles and Docetaxel. Globally, these formulations reversed cancer hallmarks with a marked anti-migratory and anti-invasive effects as well as chemo-sensitization in vitro [112]. An original approach based on the combination of chemically modified PEI (disulfide linkage in the branched PEI or SSPEI) with the cell permeable peptide R11 (R11-SSPEI nanocarriers) was set up by Zhang et al. [113]. Taking advantage of R11 specific uptake by prostate cancer cells in vivo, they demonstrated that R11-SSPEI nanomaterials were able to deliver miR-145 in intraperitoneal prostate cancer models [113]. Northern blotting of tumor tissue after three weeks of treatment revealed a substantial increase of miR-145 levels in the treated group, thus underscoring the excellent transfection efficiency of PEI formulations. Importantly, MiR-145 overexpression significantly impaired tumor growth and prolonged mice survival.

#### 5. Challenges in the Clinical Translation of miRNA Therapeutics

More than fifty therapeutic siRNA programs have entered clinical trials in the past decade (phase I, II, and III) [152]. Patisiran and givosiran (Alnylam Pharmaceuticals), two siRNA-based drugs, were approved by the Food and Drug Administration in 2018 and 2019 for hereditary transthyretin-mediated amyloidosis and acute hepatic porphyria, respectively [153,154]. About fifteen phase I-, II-, and III-programs based on siRNA drugs are dedicated to the treatment of diverse cancer types [152]. Despite such successes in clinical development, several clinical trials have been discontinued, indicating that there are still several challenges to overcome before the clinical application of RNAi-based therapies becomes widespread. These challenges are even more significant for miRNA-based therapies.

So far, only 10 miRNA-based drugs have reached clinical trials with none of them entering Phase III and half of them were halted. MiRNA-based therapy programs for cancer treatment are mainly driven by four biopharmaceutical companies, including miRagen Therapeutics (Boulder, CO, USA), Regulus therapeutics (San Diego, CA, USA), Mirna Therapeutics Inc. (Carlsbad, CA, USA) and EnGeneIC (Sydney, Australia). MiRagen Therapeutics is performing clinical trials of MRG-106 (Cobomarsen, an inhibitor of miR-155) for the treatment of cutaneous T-cell lymphoma, chronic lymphocytic leukemia, diffuse large B-cell lymphoma, and adult T-cell leukemia/lymphoma (NCT02580552, NCT03713320). EnGeneIC is currently testing TargomiRs as 2nd or 3rd Line Treatment for patients with

recurrent malignant pleural mesothelioma and non-small cell lung cancer (NCT02369198). The first miRNA-based drug entering clinical trials was Miravirsen, an antagomiR targeting miR-122, as a therapy against Hepatitis C Virus (HCV) infections (Santaris Pharma, Roche Pharmaceuticals). Miravirsen showed a strong efficacy by reducing viremia in patients with HCV [155–157] and underwent multiple phase II clinical trials (NCT01200420, NCT01872936, NCT02031133, NCT02508090). Regulus Therapeutics developed another miR-122 inhibitor, RG-101, an *N*-acetyl-D-galactosamine-conjugated antagomiR which showed considerable efficacy in patients with HCV. However, some serious adverse events of severe hyperbilirubinemia led the FDA to suspend the trial. MRX34, a first-in-class cancer therapy developed by miRNA Therapeutics was delivered as a mimic of miR-34 encapsulated into a liposome-formulated nanoparticle (NOV40). MRX34 displayed a strong activity in melanoma, hepatocellular carcinoma, NSCLC, and renal carcinoma (NCT01829971). Unfortunately, miRNA Therapeutics halted the phase I due to multiple immune-related severe adverse events. These successive failures indicate that miRNA-based therapies are still awaiting their Eureka moment.

Delivery systems and administration routes, dosage concerns and off-target effects remain major challenges to be overcome for the development of miRNA-based therapies for cancer and other diseases. Despite a great number of preclinical studies in mouse models of cancer, only a very small number of miRNA candidates have reached clinical development so far. Performing rigorous pharmacokinetics (absorption, distribution, metabolism, and excretion or ADME) studies in animals will provide a basis for anticipating how miRNA mimics/antimiRs will behave in humans. As detailed earlier, nanotechnologies provided versatile platforms for safe biomolecule delivery (polymers, lipid compounds, inorganic nanomaterial). Nanoparticle-based delivery of miRNA aims to increase therapeutic efficacy, decrease the effective dose, and/or reduce the risk of systemic side effects. However, most of these systems have yet to reach their testing in humans. Hence, the challenge is to establish functional, yet biocompatible carrier systems for miRNA therapy. Indeed, nanoparticles are potent reservoirs in which molecular cargo can be particularly enriched. Due to their synthetic malleability, polymeric biomaterials are tailored for specific applications with surface functionalization, high active payload, and minimized toxicity. MiRNA mimics or inhibitors could be therefore shielded from the injection site to the targeted area. This mechanism mirrors the natural shielding of endogenous miRNAs by extracellular vesicles such as exosomes. However, the applicability of nanocarrier formulations for drug administration depends on several parameters including their average diameter and their polydispersity index. Controlling and validating these parameters are of major importance for nanoparticle circulating time, biodistribution and cellular uptake with a view of their effective clinical applications. Other parameters related to charge, shape, surface chemistry, and clearance are also key determinants for nanoparticle fate. Integration of miRNAs, coatings and targeting agents into a single nanocarrier requires multiple steps in the production process. These structural and physicochemical complexities contribute certainly to the slow rates in clinical translation since they hamper large-scale manufacturing by the pharmaceutical industry. Simplification in the design of nanoparticles should allow efficient and reproducible large-scale manufacturing. The EPR effect of nanoparticles in tumors has long stood as an important driver of cancer nanomedicine. However, the reliability of the EPR effect in human patients have been recently debated as the extent of nanocarriers accumulation varies profoundly between patients and tumor types [158]. The mechanism by which nanoparticles enter solid tumors appears more complex than previously thought and probably involves active trans-endothelial pathways [159]. The EPR-dependent drug delivery is compromised by high tumor interstitial fluid pressure and poor blood flow inside human tumors. Despite nanoparticle stabilization and surface manipulations, perfect tumor targeting is not yet achieved [160]. Liver and spleen remain the first accumulation sites for nanoparticles due in part to their fenestrated endothelium. Thus, these organs are major barriers to clinical translation of nanomaterials adminis-



tered intravenously [161]. Understanding the mechanisms behind this accumulation more extensively will help develop new strategies for tumor targeting and liver or spleen escape.

Dosage concerns must be addressed before introduction of miRNA therapeutics into the clinic because an overdose of miRNA mimics/antimiRs may amplify off-target adverse effects, non-specific immune responses, and toxicities. Dose finding in miRNA therapy studies is complex because exposing patients to either a non-active dose or a potentially toxic dose is not ethical. The initial dose for a phase I/II trial is extrapolated from preclinical animal and cell studies to humans. Several variables should be accounted for, including the differences in size and volume between animal and human organs and the spread of the volume delivered. This further underlines the importance of proper dose-range finding studies in large animal models (such as non-human primates) to fill the gap between preclinical research in mouse cancer models and clinical research in cancer patients. In addition, administration routes of oligonucleotide drugs are still problematic since they are prone to nuclease digestion with a bloodstream half-life of only a few minutes. Currently, miRNA mimics/antimiRs can only be administered through intravenous or subcutaneous routes. The development for oral delivery vehicles will be a key step in advancing this class of drugs to clinical use in patients. Most commercial miRNA mimics/antimiRs undergo different chemical modifications or length changes to increase their stability, which may introduce variations in their activity, pharmacokinetics, and biodistribution. Thus, it is important to characterize each candidate miRNA drug and to evaluate the impact of its specific modifications in early stage of preclinical evaluation. Information on the half-life of the miRNA mimics/antimiRs and the turnover rate of the miRNA targets is mandatory to determine dosing and dosing schedules. For example, measurement of the rate of clearance of antimiRs would allow to replace only the miRNA molecules that are cleared or those required to sequester newly synthesized miRNAs. Defining the doses required to achieve total endogenous miRNA sequestration with antimiRs or endogenous physiological miRNA concentration with miRNA mimics is a key stage of nonclinical toxicity and pharmacokinetic studies. The selected concentration of miRNA mimics/antimiRs should completely silence or upregulate a limited number of target mRNAs in a cell. Any antimiR given in excess of the dose required to fully sequester the available miRNA target will produce non-target-related effects. For example, earlier work showed that LNA-modified anti-miR-122 oligonucleotides could upregulate miR-122 target aldolase A in non-human primates at much lower dose of 1–25 mg/kg [162], compared to the previously reported dose of 120–240 mg/kg of cholesterol-conjugated oligonucleotides in mice [163]. It is reasonable to expect that solving miRNA-dosing issues will be also facilitated by continuous improvement in miRNA target prediction tools and validations of true miRNA targets. Interestingly, Zhang et al. [152] recently analyzed the reasons for the delayed development of miRNA-based therapies compared to siRNA-based therapies. Combining clinical trial information [164], Drugs@FDA database, target prediction softwares and gene ontology enrichment tools allowed them to conclude that the serious immune-related adverse events that led to the discontinuation of MRX34 were due to a “too many targets for miRNA effect” (TMTME) on several genes involved in cytokine and interleukin signaling in the immune system [152]. A combination of tissue specific knockout mouse models and advanced molecular biology techniques will allow us to determine miRNAs target-selectivity and will help us to define the specific contribution of a single miRNA in controlling a biological pathway and gene network in different tissues. This will have major implications for the design of dosage for clinical trials to minimize ineffective and potentially toxic over exposures.

Another challenge is the current regulatory gap for both nanomedicines and RNAi-driven therapies, including miRNA-based therapies [165]. The lack of clear regulatory and safety guidelines for quality control and safety has delayed the development of these products toward effective clinical translation. The increased number of novel polymeric nanomaterials, complex polymeric-based nanoformulations and chemical modifications require appropriate regulatory rules to help in miRNA drug assessment (good manufacturing

practices, production process, and quality controls). Simplification in formulation design could be a key step in the evaluation by regulatory authorities. On the other hand, the cost–benefit ratio is another limitation to the clinical translation of miRNA-based therapies when compared to existing anti-cancer therapies, due to the high cost of both miRNA biology products and emerging nanocarriers, which are more complex in structure and more expensive than conventional drugs [166]. The fact that the healthcare system is different in each country is a threat for pharmaceutical companies who want to invest at the international level. The decrease of financial resources and the lack of socio-economic validation studies may neutralize innovative advances. This means that only developed countries will be able to advance miRNA-based therapy programs in the forthcoming years. Among all the countries, North America is expected to remain at the forefront and hold the highest position in the global miRNA market. In the USA, this is attributable to the increasing miRNA clinical trials launched to develop advanced therapeutic solutions. In Europe, growing government funding for the startups for R&D activities to develop novel miRNA-based therapies might allow the region to hold the second position in the market.

## 6. Conclusions

The pleiotropic action of miRNAs suggests that targeting these molecules could efficiently reverse phenotypes of multifactorial pathologies like cancer. As they are short-sequence molecules naturally produced by the cell, miRNA inhibition or replacement are relatively easy and hold great promises for clinical translation [156,167]. The power of Systems biology will allow a better understanding of the high complexity of miRNA-mediated gene regulatory networks and hence, a better evaluation of the therapeutic value of miRNA drugs. The relevance of miRNAs as anti-cancer agents is supported by 11,439 studies referenced in Pubmed under the search terms “microRNA” AND “cancer therapy”. The field of nanotechnology is now mature enough to envisage reproducible scale-up for potential clinical studies in the next few years. Messenger RNA-based anti-Covid-19 vaccines are a groundbreaking innovation in nanomedicine and a huge scientific achievement in a very short period of time that could help some of the most promising miRNA nanocarriers to reach the market [168]. Moreover, regulatory authorities gained awareness of nanoparticle use for drug delivery given that several liposomal drugs are now on the market, directly paving the way for miRNA therapeutics to the clinics.

**Author Contributions:** Writing—original draft preparation, S.R.E.S. and N.C.; writing—review and editing, N.C., L.G., O.C., J.C. and J.D.; supervision, N.C.; funding acquisition, N.C. All authors have read and agreed to the published version of the manuscript.

**Funding:** This research was funded by the Institut National de la Santé et de la Recherche Médicale, the Ligue Nationale Contre le Cancer to N.C. (Comités Loire et Isère, R16167CC and R19013CC) and S.R.E.S. (LNCC), the Cancéropôle Rhône-Alpes Auvergne CLARA Oncostarter to NC (CVP-PRCAN000183) and the Institut National du Cancer to N.C. (INCA-DGOS-8663, COM-ETE-TACTIC). This work has been performed in a laboratory receiving support from the GRAL LabEX (ANR-10-LABX-49-01) within the frame of the CBH-EUR-GS (ANR-17-EURE-0003).

**Conflicts of Interest:** The authors declare no conflict of interest.

## References

1. Ambros, V. The functions of animal microRNAs. *Nature* **2004**, *431*, 350–355. [[CrossRef](#)]
2. Ha, M.; Kim, V.N. Regulation of microRNA biogenesis. *Nat. Rev. Mol. Cell. Biol.* **2014**, *15*, 509–524. [[CrossRef](#)]
3. Leichter, A.L.; Sullivan, M.J.; Eccles, M.R.; Chatterjee, A. MicroRNA expression patterns and signalling pathways in the development and progression of childhood solid tumours. *Mol. Cancer* **2017**, *16*, 15. [[CrossRef](#)]
4. Guo, Z.; Maki, M.; Ding, R.; Yang, Y.; Zhang, B.; Xiong, L. Genome-wide survey of tissue-specific microRNA and transcription factor regulatory networks in 12 tissues. *Sci. Rep.* **2014**, *4*, 5150. [[CrossRef](#)]
5. Calin, G.A.; Dumitru, C.D.; Shimizu, M.; Bichi, R.; Zupo, S.; Noch, E.; Aldler, H.; Rattan, S.; Keating, M.; Rai, K.; et al. Frequent deletions and down-regulation of micro-RNA genes miR15 and miR16 at 13q14 in chronic lymphocytic leukemia. *Proc. Natl. Acad. Sci. USA* **2002**, *99*, 15524–15529. [[CrossRef](#)]
6. Hanahan, D.; Weinberg, R.A. Hallmarks of cancer: The next generation. *Cell* **2011**, *144*, 646–674. [[CrossRef](#)]

7. Hata, A.; Kashima, R. Dysregulation of microRNA biogenesis machinery in cancer. *Crit. Rev. Biochem. Mol. Biol.* **2016**, *51*, 121–134. [[CrossRef](#)] [[PubMed](#)]
8. Lin, S.; Gregory, R.I. MicroRNA biogenesis pathways in cancer. *Nat. Rev. Cancer* **2015**, *15*, 321–333. [[CrossRef](#)] [[PubMed](#)]
9. Du, R.; Sun, W.; Xia, L.; Zhao, A.; Yu, Y.; Zhao, L.; Wang, H.; Huang, C.; Sun, S. Hypoxia-induced down-regulation of microRNA-34a promotes EMT by targeting the Notch signaling pathway in tubular epithelial cells. *PLoS ONE* **2012**, *7*, e30771. [[CrossRef](#)] [[PubMed](#)]
10. Calin, G.A.; Croce, C.M. MicroRNA signatures in human cancers. *Nat. Rev. Cancer* **2006**, *6*, 857–866. [[CrossRef](#)] [[PubMed](#)]
11. Rupaimoole, R.; Calin, G.A.; Lopez-Berestein, G.; Sood, A.K. miRNA Deregulation in Cancer Cells and the Tumor Microenvironment. *Cancer Discov.* **2016**, *6*, 235–246. [[CrossRef](#)] [[PubMed](#)]
12. Li, H.; Yang, B.B. Friend or foe: The role of microRNA in chemotherapy resistance. *Acta Pharmacol. Sin.* **2013**, *34*, 870–879. [[CrossRef](#)] [[PubMed](#)]
13. Si, W.; Shen, J.; Zheng, H.; Fan, W. The role and mechanisms of action of microRNAs in cancer drug resistance. *Clin. Epigenet.* **2019**, *11*, 25. [[CrossRef](#)] [[PubMed](#)]
14. Yang, T.; Zheng, Z.M.; Li, X.N.; Li, Z.F.; Wang, Y.; Geng, Y.F.; Bai, L.; Zhang, X.B. MiR-223 modulates multidrug resistance via downregulation of ABCB1 in hepatocellular carcinoma cells. *Exp. Biol. Med.* **2013**, *238*, 1024–1032. [[CrossRef](#)]
15. Bao, L.; Hazari, S.; Mehra, S.; Kaushal, D.; Moroz, K.; Dash, S. Increased expression of P-glycoprotein and doxorubicin chemoresistance of metastatic breast cancer is regulated by miR-298. *Am. J. Pathol.* **2012**, *180*, 2490–2503. [[CrossRef](#)]
16. Kaehler, M.; Ruemenapp, J.; Gonnermann, D.; Nagel, I.; Bruhn, O.; Haenisch, S.; Ammerpohl, O.; Wesch, D.; Cascorbi, I.; Bruckmueller, H. MicroRNA-212/ABCG2-axis contributes to development of imatinib-resistance in leukemic cells. *Oncotarget* **2017**, *8*, 92018–92031. [[CrossRef](#)]
17. Ning, F.L.; Wang, F.; Li, M.L.; Yu, Z.S.; Hao, Y.Z.; Chen, S.S. MicroRNA-182 modulates chemosensitivity of human non-small cell lung cancer to cisplatin by targeting PDCD4. *Diagn. Pathol.* **2014**, *9*, 143. [[CrossRef](#)] [[PubMed](#)]
18. Lei, L.; Huang, Y.; Gong, W. miR-205 promotes the growth, metastasis and chemoresistance of NSCLC cells by targeting PTEN. *Oncol. Rep.* **2013**, *30*, 2897–2902. [[CrossRef](#)]
19. Levy, J.M.M.; Towers, C.G.; Thorburn, A. Targeting autophagy in cancer. *Nat. Rev. Cancer* **2017**, *17*, 528–542. [[CrossRef](#)] [[PubMed](#)]
20. Zou, Z.; Wu, L.; Ding, H.; Wang, Y.; Zhang, Y.; Chen, X.; Chen, X.; Zhang, C.Y.; Zhang, Q.; Zen, K. MicroRNA-30a sensitizes tumor cells to cis-platinum via suppressing beclin 1-mediated autophagy. *J. Biol. Chem.* **2012**, *287*, 4148–4156. [[CrossRef](#)] [[PubMed](#)]
21. Tsuchiya, Y.; Nakajima, M.; Takagi, S.; Taniya, T.; Yokoi, T. MicroRNA Regulates the Expression of Human Cytochrome P450 1B1. *Cancer Res.* **2006**, *66*, 9090–9098. [[CrossRef](#)]
22. Choi, Y.M.; An, S.; Lee, E.M.; Kim, K.; Choi, S.J.; Kim, J.S.; Jang, H.H.; An, I.S.; Bae, S. CYP1A1 is a target of miR-892a-mediated post-transcriptional repression. *Int. J. Oncol.* **2012**, *41*, 331–336. [[PubMed](#)]
23. Ling, H.; Fabbri, M.; Calin, G.A. MicroRNAs and other non-coding RNAs as targets for anticancer drug development. *Nat. Rev. Drug. Discov.* **2013**, *12*, 847–865. [[CrossRef](#)] [[PubMed](#)]
24. Shah, M.Y.; Ferrajoli, A.; Sood, A.K.; Lopez-Berestein, G.; Calin, G.A. microRNA Therapeutics in Cancer—An Emerging Concept. *EBioMedicine* **2016**, *12*, 34–42. [[CrossRef](#)]
25. Hanna, J.; Hossain, G.S.; Kocerha, J. The Potential for microRNA Therapeutics and Clinical Research. *Front. Genet.* **2019**, *10*, 478. [[CrossRef](#)]
26. Rupaimoole, R.; Slack, F.J. MicroRNA therapeutics: Towards a new era for the management of cancer and other diseases. *Nat. Rev. Drug Discov.* **2017**, *16*, 203–222. [[CrossRef](#)] [[PubMed](#)]
27. Shu, J.; e Silva, B.V.R.; Gao, T.; Xu, Z.; Cui, J. Dynamic and Modularized MicroRNA Regulation and Its Implication in Human Cancers. *Sci. Rep.* **2017**, *7*, 13356. [[CrossRef](#)]
28. Berindan-Neagoe, I.; Monroig Pdel, C.; Pasculli, B.; Calin, G.A. MicroRNAome genome: A treasure for cancer diagnosis and therapy. *CA Cancer J. Clin.* **2014**, *64*, 311–336. [[CrossRef](#)]
29. Mattes, J.; Collison, A.; Foster, P.S. Emerging role of microRNAs in disease pathogenesis and strategies for therapeutic modulation. *Curr. Opin. Mol. Ther.* **2008**, *10*, 150–157.
30. Aquino-Jarquín, G. Emerging Role of CRISPR/Cas9 Technology for MicroRNAs Editing in Cancer Research. *Cancer Res.* **2017**, *77*, 6812–6817. [[CrossRef](#)]
31. Ebert, M.S.; Sharp, P.A. MicroRNA sponges: Progress and possibilities. *RNA* **2010**, *16*, 2043–2050. [[CrossRef](#)]
32. Simonson, B.; Das, S. MicroRNA Therapeutics: The Next Magic Bullet? *Mini Rev. Med. Chem.* **2015**, *15*, 467–474. [[CrossRef](#)]
33. Ma, L.; Young, J.; Prabhala, H.; Pan, E.; Mestdagh, P.; Muth, D.; Teruya-Feldstein, J.; Reinhardt, F.; Onder, T.T.; Valastyan, S.; et al. miR-9, a MYC/MYCN-activated microRNA, regulates E-cadherin and cancer metastasis. *Nat. Cell Biol.* **2010**, *12*, 247–256. [[CrossRef](#)] [[PubMed](#)]
34. Yoshino, H.; Yonemori, M.; Miyamoto, K.; Tatarano, S.; Kofuji, S.; Nohata, N.; Nakagawa, M.; Enokida, H. microRNA-210-3p depletion by CRISPR/Cas9 promoted tumorigenesis through revival of TWIST1 in renal cell carcinoma. *Oncotarget* **2017**, *8*, 20881–20894. [[CrossRef](#)] [[PubMed](#)]
35. Bader, A.G.; Brown, D.; Winkler, M. The promise of microRNA replacement therapy. *Cancer Res.* **2010**, *70*, 7027–7030. [[CrossRef](#)] [[PubMed](#)]

36. Johnson, C.D.; Esquela-Kerscher, A.; Stefani, G.; Byrom, M.; Kelnar, K.; Ovcharenko, D.; Wilson, M.; Wang, X.; Shelton, J.; Shingara, J.; et al. The let-7 microRNA represses cell proliferation pathways in human cells. *Cancer Res.* **2007**, *67*, 7713–7722. [[CrossRef](#)] [[PubMed](#)]
37. Kumar, M.S.; Erkeland, S.J.; Pester, R.E.; Chen, C.Y.; Ebert, M.S.; Sharp, P.A.; Jacks, T. Suppression of non-small cell lung tumor development by the let-7 microRNA family. *Proc. Natl. Acad. Sci. USA* **2008**, *105*, 3903–3908. [[CrossRef](#)]
38. He, L.; He, X.; Lowe, S.W.; Hannon, G.J. microRNAs join the p53 network—another piece in the tumour-suppression puzzle. *Nat. Rev. Cancer* **2007**, *7*, 819–822. [[CrossRef](#)]
39. Chaudhary, V.; Jangra, S.; Yadav, N.R. Nanotechnology based approaches for detection and delivery of microRNA in healthcare and crop protection. *J. Nanobiotechnol.* **2018**, *16*, 40. [[CrossRef](#)]
40. Juliano, R.; Bauman, J.; Kang, H.; Ming, X. Biological barriers to therapy with antisense and siRNA oligonucleotides. *Mol. Pharm.* **2009**, *6*, 686–695. [[CrossRef](#)]
41. Danhier, F.; Feron, O.; Pr at, V. To exploit the tumor microenvironment: Passive and active tumor targeting of nanocarriers for anti-cancer drug delivery. *J. Control Release* **2010**, *148*, 135–146. [[CrossRef](#)]
42. Shi, J.; Kantoff, P.W.; Wooster, R.; Farokhzad, O.C. Cancer nanomedicine: Progress, challenges and opportunities. *Nat. Rev. Cancer* **2017**, *17*, 20–37. [[CrossRef](#)]
43. Fu, Y.; Chen, J.; Huang, Z. Recent progress in microRNA-based delivery systems for the treatment of human disease. *ExRNA* **2019**, *1*, 24. [[CrossRef](#)]
44. Kasar, S.; Salerno, E.; Yuan, Y.; Underbayev, C.; Vollenweider, D.; Laurindo, M.F.; Fernandes, H.; Bonci, D.; Addario, A.; Mazzella, F.; et al. Systemic in vivo lentiviral delivery of miR-15a/16 reduces malignancy in the NZB de novo mouse model of chronic lymphocytic leukemia. *Genes Immun.* **2012**, *13*, 109–119. [[CrossRef](#)] [[PubMed](#)]
45. Kota, J.; Chivukula, R.R.; O'Donnell, K.A.; Wentzel, E.A.; Montgomery, C.L.; Hwang, H.W.; Chang, T.C.; Vivekanandan, P.; Torbenson, M.; Clark, K.R.; et al. Therapeutic microRNA delivery suppresses tumorigenesis in a murine liver cancer model. *Cell* **2009**, *137*, 1005–1017. [[CrossRef](#)]
46. Boussif, O.; Lezoualc'h, F.; Zanta, M.A.; Mergny, M.D.; Scherman, D.; Demeneix, B.; Behr, J.P. A versatile vector for gene and oligonucleotide transfer into cells in culture and in vivo: Polyethylenimine. *Proc. Natl. Acad. Sci. USA* **1995**, *92*, 7297–7301. [[CrossRef](#)] [[PubMed](#)]
47. Ibrahim, A.F.; Weirauch, U.; Thomas, M.; Gr unweller, A.; Hartmann, R.K.; Aigner, A. MicroRNA replacement therapy for miR-145 and miR-33a is efficacious in a model of colon carcinoma. *Cancer Res.* **2011**, *71*, 5214–5224. [[CrossRef](#)] [[PubMed](#)]
48. Cosco, D.; Cilurzo, F.; Maiuolo, J.; Federico, C.; Di Martino, M.T.; Cristiano, M.C.; Tassone, P.; Fresta, M.; Paolino, D. Delivery of miR-34a by chitosan/PLGA nanoplexes for the anticancer treatment of multiple myeloma. *Sci. Rep.* **2015**, *5*, 17579. [[CrossRef](#)]
49. Zhang, L.; Lyer, A.K.; Yang, X.; Kobayashi, E.; Guo, Y.; Mankin, H.; Hornicek, F.J.; Amiji, M.M.; Duan, Z. Polymeric nanoparticle-based delivery of microRNA-199a-3p inhibits proliferation and growth of osteosarcoma cells. *Int. J. Nanomed.* **2015**, *10*, 2913–2924.
50. Layek, B.; Singh, J. N-hexanoyl, N-octanoyl and N-decanoyl chitosans: Binding affinity, cell uptake, and transfection. *Carbohydr. Polym.* **2012**, *89*, 403–410. [[CrossRef](#)]
51. Ding, Y.; Jiang, Z.; Saha, K.; Kim, C.S.; Kim, S.T.; Landis, R.F.; Rotello, V.M. Gold nanoparticles for nucleic acid delivery. *Mol. Ther.* **2014**, *22*, 1075–1083. [[CrossRef](#)]
52. Ekin, A.; Karatas, O.F.; Culha, M.; Ozen, M. Designing a gold nanoparticle-based nanocarrier for microRNA transfection into the prostate and breast cancer cells. *J. Gene Med.* **2014**, *16*, 331–335. [[CrossRef](#)]
53. Ghosh, R.; Singh, L.C.; Shohet, J.M.; Gunaratne, P.H. A gold nanoparticle platform for the delivery of functional microRNAs into cancer cells. *Biomaterials* **2013**, *34*, 807–816. [[CrossRef](#)]
54. Pugazhendhi, A.; Edison, T.; Karuppusamy, I.; Kathirvel, B. Inorganic nanoparticles: A potential cancer therapy for human welfare. *Int. J. Pharm.* **2018**, *539*, 104–111. [[CrossRef](#)]
55. Zhang, Y.; Wang, Z.; Gemeinhart, R.A. Progress in microRNA delivery. *J. Control Release* **2013**, *172*, 962–974. [[CrossRef](#)]
56. Tivnan, A.; Orr, W.S.; Gubala, V.; Nooney, R.; Williams, D.E.; McDonagh, C.; Prenter, S.; Harvey, H.; Domingo-Fern andez, R.; Bray, I.M.; et al. Inhibition of neuroblastoma tumor growth by targeted delivery of microRNA-34a using anti-disialoganglioside GD2 coated nanoparticles. *PLoS ONE* **2012**, *7*, e38129. [[CrossRef](#)]
57. Scheideler, M.; Vidakovic, I.; Prassl, R. Lipid nanocarriers for microRNA delivery. *Chem. Phys. Lipids* **2020**, *226*, 104837. [[CrossRef](#)]
58. Cheng, X.; Lee, R.J. The role of helper lipids in lipid nanoparticles (LNPs) designed for oligonucleotide delivery. *Adv. Drug Deliv. Rev.* **2016**, *99*, 129–137. [[CrossRef](#)] [[PubMed](#)]
59. Hong, C.A.; Nam, Y.S. Functional nanostructures for effective delivery of small interfering RNA therapeutics. *Theranostics* **2014**, *4*, 1211–1232. [[CrossRef](#)] [[PubMed](#)]
60. Hosokawa, S.; Tagawa, T.; Niki, H.; Hirakawa, Y.; Ito, N.; Nohga, K.; Nagaike, K. Establishment and evaluation of cancer-specific human monoclonal antibody GAH for targeting chemotherapy using immunoliposomes. *Hybrid Hybridomics* **2004**, *23*, 109–120. [[CrossRef](#)] [[PubMed](#)]
61. Matsumura, Y.; Gotoh, M.; Muro, K.; Yamada, Y.; Shirao, K.; Shimada, Y.; Okuwa, M.; Matsumoto, S.; Miyata, Y.; Ohkura, H.; et al. Phase I and pharmacokinetic study of MCC-465, a doxorubicin (DXR) encapsulated in PEG immunoliposome, in patients with metastatic stomach cancer. *Ann. Oncol.* **2004**, *15*, 517–525. [[CrossRef](#)] [[PubMed](#)]
62. Yang, G.; Yin, B. Therapeutic effects of long-circulating miR-135a-containing cationic immunoliposomes against gallbladder carcinoma. *Sci. Rep.* **2017**, *7*, 5982. [[CrossRef](#)] [[PubMed](#)]

63. Wang, F.; Sun, Y.; Shi, J. Programmed death-ligand 1 monoclonal antibody-linked immunoliposomes for synergistic efficacy of miR-130a and oxaliplatin in gastric cancers. *Nanomedicine* **2019**, *14*, 1729–1744. [[CrossRef](#)] [[PubMed](#)]
64. Kaur, I.P.; Bhandari, R.; Bhandari, S.; Kakkar, V. Potential of solid lipid nanoparticles in brain targeting. *J. Control Release* **2008**, *127*, 97–109. [[CrossRef](#)] [[PubMed](#)]
65. Shi, S.; Han, L.; Deng, L.; Zhang, Y.; Shen, H.; Gong, T.; Zhang, Z.; Sun, X. Dual drugs (microRNA-34a and paclitaxel)-loaded functional solid lipid nanoparticles for synergistic cancer cell suppression. *J. Control Release* **2014**, *194*, 228–237. [[CrossRef](#)]
66. Küçüktürkmen, B.; Bozkır, A. Development and characterization of cationic solid lipid nanoparticles for co-delivery of pemetrexed and miR-21 antisense oligonucleotide to glioblastoma cells. *Drug Dev. Ind. Pharm.* **2018**, *44*, 306–315. [[CrossRef](#)]
67. Yousefpour Marzbali, M.; Yari Khosroushahi, A. Polymeric micelles as mighty nanocarriers for cancer gene therapy: A review. *Cancer Chemother. Pharmacol.* **2017**, *79*, 637–649. [[CrossRef](#)]
68. Mittal, A.; Chitkara, D.; Behrman, S.W.; Mahato, R.I. Efficacy of gemcitabine conjugated and miRNA-205 complexed micelles for treatment of advanced pancreatic cancer. *Biomaterials* **2014**, *35*, 7077–7087. [[CrossRef](#)]
69. Taylor, K.; Howard, C.B.; Jones, M.L.; Sedliarou, I.; MacDiarmid, J.; Brahmabhatt, H.; Munro, T.P.; Mahler, S.M. Nanocell targeting using engineered bispecific antibodies. *MAbs* **2015**, *7*, 53–65. [[CrossRef](#)]
70. MacDiarmid, J.A.; Mugridge, N.B.; Weiss, J.C.; Phillips, L.; Burn, A.L.; Paulin, R.P.; Haasdyk, J.E.; Dickson, K.A.; Brahmabhatt, V.N.; Pattison, S.T.; et al. Bacterially derived 400 nm particles for encapsulation and cancer cell targeting of chemotherapeutics. *Cancer Cell* **2007**, *11*, 431–445. [[CrossRef](#)]
71. MacDiarmid, J.A.; Madrid-Weiss, J.; Amaro-Mugridge, N.B.; Phillips, L.; Brahmabhatt, H. Bacterially-derived nanocells for tumor-targeted delivery of chemotherapeutics and cell cycle inhibitors. *Cell Cycle* **2007**, *6*, 2099–2105. [[CrossRef](#)] [[PubMed](#)]
72. Reid, G.; Pel, M.E.; Kirschner, M.B.; Cheng, Y.Y.; Mugridge, N.; Weiss, J.; Williams, M.; Wright, C.; Edelman, J.J.; Valley, M.P.; et al. Restoring expression of miR-16: A novel approach to therapy for malignant pleural mesothelioma. *Ann. Oncol.* **2013**, *24*, 3128–3135. [[CrossRef](#)]
73. Luan, X.; Sansanaphongpricha, K.; Myers, I.; Chen, H.; Yuan, H.; Sun, D. Engineering exosomes as refined biological nanoplat-forms for drug delivery. *Acta Pharmacol. Sin.* **2017**, *38*, 754–763. [[CrossRef](#)]
74. Vazquez-Rios, A.J.; Molina-Crespo, A.; Bouzo, B.L.; Lopez-Lopez, R.; Moreno-Bueno, G.; de la Fuente, M. Exosome-mimetic nanoplat-forms for targeted cancer drug delivery. *J. Nanobiotechnol.* **2019**, *17*, 85. [[CrossRef](#)]
75. Bonneau, E.; Neveu, B.; Kostantin, E.; Tsongalis, G.J.; De Guire, V. How close are miRNAs from clinical practice? A perspective on the diagnostic and therapeutic market. *EJIFCC* **2019**, *30*, 114–127. [[PubMed](#)]
76. Li, Y.L.; Liu, X.M.; Zhang, C.Y.; Zhou, J.B.; Shao, Y.; Liang, C.; Wang, H.M.; Hua, Z.Y.; Lu, S.D.; Ma, Z.L. MicroRNA-34a/EGFR axis plays pivotal roles in lung tumorigenesis. *Oncogenesis* **2017**, *6*, e372. [[CrossRef](#)]
77. Wiggins, J.F.; Ruffino, L.; Kelnar, K.; Omotola, M.; Patrawala, L.; Brown, D.; Bader, A.G. Development of a lung cancer therapeutic based on the tumor suppressor microRNA-34. *Cancer Res.* **2010**, *70*, 5923–5930. [[CrossRef](#)]
78. Kasinski, A.L.; Kelnar, K.; Stahlhut, C.; Orellana, E.; Zhao, J.; Shimer, E.; Dysart, S.; Chen, X.; Bader, A.G.; Slack, F.J. A combinatorial microRNA therapeutics approach to suppressing non-small cell lung cancer. *Oncogene* **2015**, *34*, 3547–3555. [[CrossRef](#)] [[PubMed](#)]
79. Cortez, M.A.; Valdecanas, D.; Zhang, X.; Zhan, Y.; Bhardwaj, V.; Calin, G.A.; Komaki, R.; Giri, D.K.; Quini, C.C.; Wolfe, T.; et al. Therapeutic delivery of miR-200c enhances radiosensitivity in lung cancer. *Mol. Ther.* **2014**, *22*, 1494–1503. [[CrossRef](#)] [[PubMed](#)]
80. Beg, M.S.; Brenner, A.J.; Sachdev, J.; Borad, M.; Kang, Y.K.; Stoudemire, J.; Smith, S.; Bader, A.G.; Kim, S.; Hong, D.S. Phase I study of MRX34, a liposomal miR-34a mimic, administered twice weekly in patients with advanced solid tumors. *Investig. New Drugs* **2017**, *35*, 180–188. [[CrossRef](#)]
81. Hong, D.S.; Kang, Y.K.; Borad, M.; Sachdev, J.; Ejadi, S.; Lim, H.Y.; Brenner, A.J.; Park, K.; Lee, J.L.; Kim, T.Y.; et al. Phase 1 study of MRX34, a liposomal miR-34a mimic, in patients with advanced solid tumours. *Br. J. Cancer* **2020**, *122*, 1630–1637. [[CrossRef](#)]
82. Wu, Y.; Crawford, M.; Mao, Y.; Lee, R.J.; Davis, I.C.; Elton, T.S.; Lee, L.J.; Nana-Sinkam, S.P. Therapeutic Delivery of MicroRNA-29b by Cationic Lipoplexes for Lung Cancer. *Mol. Ther. Nucleic Acids* **2013**, *2*, e84. [[CrossRef](#)] [[PubMed](#)]
83. van Zandwijk, N.; Pavlakis, N.; Kao, S.C.; Linton, A.; Boyer, M.J.; Clarke, S.; Huynh, Y.; Chrzanowska, A.; Fullham, M.J.; Bailey, D.L.; et al. Safety and activity of microRNA-loaded minicells in patients with recurrent malignant pleural mesothelioma: A first-in-man, phase 1, open-label, dose-escalation study. *Lancet Oncol.* **2017**, *18*, 1386–1396. [[CrossRef](#)]
84. Tsai, W.C.; Hsu, P.W.; Lai, T.C.; Chau, G.Y.; Lin, C.W.; Chen, C.M.; Lin, C.D.; Liao, Y.L.; Wang, J.L.; Chau, Y.P.; et al. MicroRNA-122, a tumor suppressor microRNA that regulates intrahepatic metastasis of hepatocellular carcinoma. *Hepatology* **2009**, *49*, 1571–1582. [[CrossRef](#)]
85. Hsu, S.H.; Yu, B.; Wang, X.; Lu, Y.; Schmidt, C.R.; Lee, R.J.; Lee, L.J.; Jacob, S.T.; Ghoshal, K. Cationic lipid nanoparticles for therapeutic delivery of siRNA and miRNA to murine liver tumor. *Nanomedicine* **2013**, *9*, 1169–1180. [[CrossRef](#)]
86. Li, F.; Wang, F.; Zhu, C.; Wei, Q.; Zhang, T.; Zhou, Y.L. miR-221 suppression through nanoparticle-based miRNA delivery system for hepatocellular carcinoma therapy and its diagnosis as a potential biomarker. *Int. J. Nanomed.* **2018**, *13*, 2295–2307. [[CrossRef](#)]
87. Shao, S.; Hu, Q.; Wu, W.; Wang, M.; Huang, J.; Zhao, X.; Tang, G.; Liang, T. Tumor-triggered personalized microRNA cocktail therapy for hepatocellular carcinoma. *Biomater. Sci.* **2020**, *8*, 6579–6591. [[CrossRef](#)]
88. Wang, Z.; Zhao, K.; Zhang, Y.; Duan, X.; Zhao, Y. Anti-GPC3 Antibody Tagged Cationic Switchable Lipid-Based Nanoparticles for the Co-Delivery of Anti-miRNA27a And Sorafenib in Liver Cancers. *Pharm. Res.* **2019**, *36*, 145. [[CrossRef](#)] [[PubMed](#)]

89. Hayward, S.L.; Francis, D.M.; Kholmatov, P.; Kidambi, S. Targeted Delivery of MicroRNA125a-5p by Engineered Lipid Nanoparticles for the Treatment of HER2 Positive Metastatic Breast Cancer. *J. Biomed. Nanotechnol.* **2016**, *12*, 554–568. [[CrossRef](#)] [[PubMed](#)]
90. Deng, X.; Cao, M.; Zhang, J.; Hu, K.; Yin, Z.; Zhou, Z.; Xiao, X.; Yang, Y.; Sheng, W.; Wu, Y.; et al. Hyaluronic acid-chitosan nanoparticles for co-delivery of MiR-34a and doxorubicin in therapy against triple negative breast cancer. *Biomaterials* **2014**, *35*, 4333–4344. [[CrossRef](#)]
91. Imani, S.; Wu, R.C.; Fu, J. MicroRNA-34 family in breast cancer: From research to therapeutic potential. *J. Cancer* **2018**, *9*, 3765–3775. [[CrossRef](#)]
92. Zhi, F.; Dong, H.; Jia, X.; Guo, W.; Lu, H.; Yang, Y.; Ju, H.; Zhang, X.; Hu, Y. Functionalized graphene oxide mediated adriamycin delivery and miR-21 gene silencing to overcome tumor multidrug resistance in vitro. *PLoS ONE* **2013**, *8*, e60034. [[CrossRef](#)]
93. Yu, Y.; Yao, Y.; Yan, H.; Wang, R.; Zhang, Z.; Sun, X.; Zhao, L.; Ao, X.; Xie, Z.; Wu, Q. A Tumor-specific MicroRNA Recognition System Facilitates the Accurate Targeting to Tumor Cells by Magnetic Nanoparticles. *Mol. Ther. Nucleic Acids* **2016**, *5*, e318. [[CrossRef](#)] [[PubMed](#)]
94. Panebianco, F.; Climent, M.; Malvindi, M.A.; Pompa, P.P.; Bonetti, P.; Nicassio, F. Delivery of biologically active miR-34a in normal and cancer mammary epithelial cells by synthetic nanoparticles. *Nanomedicine* **2019**, *19*, 95–105. [[CrossRef](#)]
95. Sukumar, U.K.; Bose, R.J.C.; Malhotra, M.; Babikir, H.A.; Afjei, R.; Robinson, E.; Zeng, Y.; Chang, E.; Habte, F.; Sinclair, R.; et al. Intranasal delivery of targeted polyfunctional gold-iron oxide nanoparticles loaded with therapeutic microRNAs for combined theranostic multimodality imaging and presensitization of glioblastoma to temozolomide. *Biomaterials* **2019**, *218*, 119342. [[CrossRef](#)]
96. Seo, Y.E.; Suh, H.W.; Bahal, R.; Josowitz, A.; Zhang, J.; Song, E.; Cui, J.; Noorbakhsh, S.; Jackson, C.; Bu, T.; et al. Nanoparticle-mediated intratumoral inhibition of miR-21 for improved survival in glioblastoma. *Biomaterials* **2019**, *201*, 87–98. [[CrossRef](#)] [[PubMed](#)]
97. Ofek, P.; Calderón, M.; Mehrabadi, F.S.; Krivitsky, A.; Ferber, S.; Tiram, G.; Yerushalmi, N.; Kredon-Russo, S.; Grossman, R.; Ram, Z.; et al. Restoring the oncosuppressor activity of microRNA-34a in glioblastoma using a polyglycerol-based polyplex. *Nanomedicine* **2016**, *12*, 2201–2214. [[CrossRef](#)] [[PubMed](#)]
98. Ramirez-Moya, J.; Wert-Lamas, L.; Santisteban, P. MicroRNA-146b promotes PI3K/AKT pathway hyperactivation and thyroid cancer progression by targeting PTEN. *Oncogene* **2018**, *37*, 3369–3383. [[CrossRef](#)]
99. Frezzetti, D.; Menna, M.D.; Zoppoli, P.; Guerra, C.; Ferraro, A.; Bello, A.M.; Luca, P.D.; Calabrese, C.; Fusco, A.; Ceccarelli, M.; et al. Upregulation of miR-21 by Ras in vivo and its role in tumor growth. *Oncogene* **2011**, *30*, 275–286. [[CrossRef](#)]
100. Liu, L.; Wang, J.; Li, X.; Ma, J.; Shi, C.; Zhu, H.; Xi, Q.; Zhang, J.; Zhao, X.; Gu, M. miR-204-5p suppresses cell proliferation by inhibiting IGFBP5 in papillary thyroid carcinoma. *Biochem. Biophys. Res. Commun.* **2015**, *457*, 621–626. [[CrossRef](#)]
101. Glover, A.R.; Zhao, J.T.; Gill, A.J.; Weiss, J.; Mugridge, N.; Kim, E.; Feeney, A.L.; Ip, J.C.; Reid, G.; Clarke, S.; et al. MicroRNA-7 as a tumor suppressor and novel therapeutic for adrenocortical carcinoma. *Oncotarget* **2015**, *6*, 36675–36688. [[CrossRef](#)]
102. Kwok, G.T.Y.; Zhao, J.T.; Glover, A.R.; Gill, A.J.; Clifton-Bligh, R.; Robinson, B.G.; Ip, J.C.Y.; Sidhu, S.B. microRNA-431 as a Chemosensitizer and Potentiator of Drug Activity in Adrenocortical Carcinoma. *Oncologist* **2019**, *24*, e241–e250. [[CrossRef](#)] [[PubMed](#)]
103. Leskelä, S.; Leandro-García, L.J.; Mendiola, M.; Barriuso, J.; Inglada-Pérez, L.; Muñoz, I.; Martínez-Delgado, B.; Redondo, A.; Santiago, J.d.; Robledo, M.; et al. The miR-200 family controls  $\beta$ -tubulin III expression and is associated with paclitaxel-based treatment response and progression-free survival in ovarian cancer patients. *Endocr. Relat. Cancer* **2011**, *18*, 85–95. [[CrossRef](#)] [[PubMed](#)]
104. Mateescu, B.; Batista, L.; Cardon, M.; Grusso, T.; de Feraudy, Y.; Mariani, O.; Nicolas, A.; Meyniel, J.P.; Cottu, P.; Sastre-Garau, X.; et al. miR-141 and miR-200a act on ovarian tumorigenesis by controlling oxidative stress response. *Nat. Med.* **2011**, *17*, 1627–1635. [[CrossRef](#)] [[PubMed](#)]
105. Cui, X.; Sun, Y.; Shen, M.; Song, K.; Yin, X.; Di, W.; Duan, Y. Enhanced Chemotherapeutic Efficacy of Paclitaxel Nanoparticles Co-delivered with MicroRNA-7 by Inhibiting Paclitaxel-Induced EGFR/ERK pathway Activation for Ovarian Cancer Therapy. *ACS Appl. Mater. Interfaces* **2018**, *10*, 7821–7831. [[CrossRef](#)] [[PubMed](#)]
106. Dwivedi, S.K.; Mustafi, S.B.; Mangala, L.S.; Jiang, D.; Pradeep, S.; Rodriguez-Aguayo, C.; Ling, H.; Ivan, C.; Mukherjee, P.; Calin, G.A.; et al. Therapeutic evaluation of microRNA-15a and microRNA-16 in ovarian cancer. *Oncotarget* **2016**, *7*, 15093–15104. [[CrossRef](#)] [[PubMed](#)]
107. Bertucci, A.; Kim, K.H.; Kang, J.; Zuidema, J.M.; Lee, S.H.; Kwon, E.J.; Kim, D.; Howell, S.B.; Ricci, F.; Ruoslahti, E.; et al. Tumor-Targeting, MicroRNA-Silencing Porous Silicon Nanoparticles for Ovarian Cancer Therapy. *ACS Appl. Mater. Interfaces* **2019**, *11*, 23926–23937. [[CrossRef](#)] [[PubMed](#)]
108. Kafshdooz, L.; Pourfathi, H.; Akbarzadeh, A.; Kafshdooz, T.; Razban, Z.; Sheervalilou, R.; Ebrahimi Sadr, N.; Khalilov, R.; Saghfi, S.; Kavetsky, T.; et al. The role of microRNAs and nanoparticles in ovarian cancer: A review. *Artif. Cells Nanomed. Biotechnol.* **2018**, *46*, 241–247. [[CrossRef](#)]
109. Cubillos-Ruiz, J.R.; Baird, J.R.; Tesone, A.J.; Rutkowski, M.R.; Scarlett, U.K.; Camposeco-Jacobs, A.L.; Anadon-Arnillas, J.; Harwood, N.M.; Korc, M.; Fiering, S.N.; et al. Reprogramming tumor-associated dendritic cells in vivo using miRNA mimetics triggers protective immunity against ovarian cancer. *Cancer Res.* **2012**, *72*, 1683–1693. [[CrossRef](#)] [[PubMed](#)]

110. Gaur, S.; Wen, Y.; Song, J.H.; Parikh, N.U.; Mangala, L.S.; Blessing, A.M.; Ivan, C.; Wu, S.Y.; Varkaris, A.; Shi, Y.; et al. Chitosan nanoparticle-mediated delivery of miRNA-34a decreases prostate tumor growth in the bone and its expression induces non-canonical autophagy. *Oncotarget* **2015**, *6*, 29161–29177. [[CrossRef](#)]
111. Farina, N.H.; Zingiryan, A.; Vrolijk, M.A.; Perrapato, S.D.; Ades, S.; Stein, G.S.; Lian, J.B.; Landry, C.C. Nanoparticle-based targeted cancer strategies for non-invasive prostate cancer intervention. *J. Cell. Physiol.* **2018**, *233*, 6408–6417. [[CrossRef](#)]
112. Nagesh, P.K.B.; Chowdhury, P.; Hatami, E.; Boya, V.K.N.; Kashyap, V.K.; Khan, S.; Hafeez, B.B.; Chauhan, S.C.; Jaggi, M.; Yallapu, M.M. miRNA-205 Nanoformulation Sensitizes Prostate Cancer Cells to Chemotherapy. *Cancers* **2018**, *10*, 289. [[CrossRef](#)]
113. Zhang, T.; Xue, X.; He, D.; Hsieh, J.-T. A prostate cancer-targeted polyarginine-disulfide linked PEI nanocarrier for delivery of microRNA. *Cancer Lett.* **2015**, *365*, 156–165. [[CrossRef](#)]
114. Villanueva, A. Hepatocellular Carcinoma. *N. Engl. J. Med.* **2019**, *380*, 1450–1462. [[CrossRef](#)]
115. Wang, X.; He, Y.; Mackowiak, B.; Gao, B. MicroRNAs as regulators, biomarkers and therapeutic targets in liver diseases. *Gut* **2021**, *70*, 784–795. [[CrossRef](#)]
116. Schueller, F.; Roy, S.; Vucur, M.; Trautwein, C.; Luedde, T.; Roderburg, C. The Role of miRNAs in the Pathophysiology of Liver Diseases and Toxicity. *Int. J. Mol. Sci.* **2018**, *19*, 261. [[CrossRef](#)] [[PubMed](#)]
117. Zhang, G.; Wang, Q.; Xu, R. Therapeutics Based on microRNA: A New Approach for Liver Cancer. *Curr. Genomics* **2010**, *11*, 311–325. [[CrossRef](#)] [[PubMed](#)]
118. Wang, H.; Chiu, M.; Xie, Z.; Chiu, M.; Liu, Z.; Chen, P.; Liu, S.; Byrd, J.C.; Muthusamy, N.; Garzon, R.; et al. Synthetic microRNA cassette dosing: Pharmacokinetics, tissue distribution and bioactivity. *Mol. Pharm.* **2012**, *9*, 1638–1644. [[CrossRef](#)] [[PubMed](#)]
119. Baboci, L.; Capolla, S.; Di Cintio, F.; Colombo, F.; Mauro, P.; Dal Bo, M.; Argenziano, M.; Cavalli, R.; Toffoli, G.; Macor, P. The Dual Role of the Liver in Nanomedicine as an Actor in the Elimination of Nanostructures or a Therapeutic Target. *J. Oncol.* **2020**, *2020*, 4638192. [[CrossRef](#)] [[PubMed](#)]
120. Gramantieri, L.; Ferracin, M.; Fornari, F.; Veronese, A.; Sabbioni, S.; Liu, C.G.; Calin, G.A.; Giovannini, C.; Ferrazzi, E.; Grazi, G.L.; et al. Cyclin G1 is a target of miR-122a, a microRNA frequently down-regulated in human hepatocellular carcinoma. *Cancer Res.* **2007**, *67*, 6092–6099. [[CrossRef](#)] [[PubMed](#)]
121. Jiang, J.; Gusev, Y.; Aderca, I.; Mettler, T.A.; Nagorney, D.M.; Brackett, D.J.; Roberts, L.R.; Schmittgen, T.D. Association of MicroRNA expression in hepatocellular carcinomas with hepatitis infection, cirrhosis, and patient survival. *Clin. Cancer Res.* **2008**, *14*, 419–427. [[CrossRef](#)] [[PubMed](#)]
122. Meng, F.; Henson, R.; Wehbe-Janek, H.; Ghoshal, K.; Jacob, S.T.; Patel, T. MicroRNA-21 regulates expression of the PTEN tumor suppressor gene in human hepatocellular cancer. *Gastroenterology* **2007**, *133*, 647–658. [[CrossRef](#)] [[PubMed](#)]
123. Hsieh, T.H.; Hsu, C.Y.; Tsai, C.F.; Long, C.Y.; Chai, C.Y.; Hou, M.F.; Lee, J.N.; Wu, D.C.; Wang, S.C.; Tsai, E.M. miR-125a-5p is a prognostic biomarker that targets HDAC4 to suppress breast tumorigenesis. *Oncotarget* **2015**, *6*, 494–509. [[CrossRef](#)] [[PubMed](#)]
124. Shi, L.; Chen, J.; Yang, J.; Pan, T.; Zhang, S.; Wang, Z. MiR-21 protected human glioblastoma U87MG cells from chemotherapeutic drug temozolomide induced apoptosis by decreasing Bax/Bcl-2 ratio and caspase-3 activity. *Brain Res.* **2010**, *1352*, 255–264. [[CrossRef](#)] [[PubMed](#)]
125. Wang, G.; Wang, J.J.; Tang, H.M.; To, S.S. Targeting strategies on miRNA-21 and PDCD4 for glioblastoma. *Arch. Biochem. Biophys.* **2015**, *580*, 64–74. [[CrossRef](#)]
126. Alrfaei, B.M.; Clark, P.; Vemuganti, R.; Kuo, J.S. MicroRNA miR-100 Decreases Glioblastoma Growth by Targeting SMARCA5 and Erbb3 in Tumor-Initiating Cells. *Technol. Cancer Res. Treat.* **2020**, *19*, 1533033820960748. [[CrossRef](#)] [[PubMed](#)]
127. Lee, S.Y. Temozolomide resistance in glioblastoma multiforme. *Genes Dis.* **2016**, *3*, 198–210. [[CrossRef](#)]
128. Pardini, B.; Calin, G.A. MicroRNAs and Long Non-Coding RNAs and Their Hormone-Like Activities in Cancer. *Cancers* **2019**, *11*, 378. [[CrossRef](#)]
129. Peng, C.; Wang, Y.L. Editorial: MicroRNAs as New Players in Endocrinology. *Front. Endocrinol.* **2018**, *9*, 459. [[CrossRef](#)]
130. Nikiforova, M.N.; Tseng, G.C.; Steward, D.; Diorio, D.; Nikiforov, Y.E. MicroRNA Expression Profiling of Thyroid Tumors: Biological Significance and Diagnostic Utility. *J. Clin. Endocrinol. Metab.* **2008**, *93*, 1600–1608. [[CrossRef](#)]
131. Wojcicka, A.; Kolanowska, M.; Jazdzewski, K. Mechanisms in Endocrinology: MicroRNA in diagnostics and therapy of thyroid cancer. *Eur. J. Endocrinol.* **2016**, *174*, R89–R98. [[CrossRef](#)] [[PubMed](#)]
132. Zhang, X.; Li, M.; Zuo, K.; Li, D.; Ye, M.; Ding, L.; Cai, H.; Fu, D.; Fan, Y.; Lv, Z. Upregulated miR-155 in Papillary Thyroid Carcinoma Promotes Tumor Growth by Targeting APC and Activating Wnt/ $\beta$ -Catenin Signaling. *J. Clin. Endocrinol. Metab.* **2013**, *98*, E1305–E1313. [[CrossRef](#)]
133. Spitzweg, C.; Bible, K.C.; Hofbauer, L.C.; Morris, J.C. Advanced radioiodine-refractory differentiated thyroid cancer: The sodium iodide symporter and other emerging therapeutic targets. *Lancet Diabetes Endocrinol.* **2014**, *2*, 830–842. [[CrossRef](#)]
134. Riesco-Eizaguirre, G.; Wert-Lamas, L.; Perales-Patón, J.; Sastre-Perona, A.; Fernández, L.P.; Santisteban, P. The miR-146b-3p/PAX8/NIS Regulatory Circuit Modulates the Differentiation Phenotype and Function of Thyroid Cells during Carcinogenesis. *Cancer Res.* **2015**, *75*, 4119–4130. [[CrossRef](#)] [[PubMed](#)]
135. Fassnacht, M.; Dekkers, O.M.; Else, T.; Baudin, E.; Berruti, A.; de Krijger, R.; Haak, H.R.; Mihai, R.; Assie, G.; Terzolo, M. European Society of Endocrinology Clinical Practice Guidelines on the management of adrenocortical carcinoma in adults, in collaboration with the European Network for the Study of Adrenal Tumors. *Eur. J. Endocrinol.* **2018**, *179*, G1–G46. [[CrossRef](#)]
136. Veytsman, I.; Nieman, L.; Fojo, T. Management of endocrine manifestations and the use of mitotane as a chemotherapeutic agent for adrenocortical carcinoma. *J. Clin. Oncol.* **2009**, *27*, 4619–4629. [[CrossRef](#)]

137. Fassnacht, M.; Terzolo, M.; Allolio, B.; Baudin, E.; Haak, H.; Berruti, A.; Welin, S.; Schade-Brittinger, C.; Lacroix, A.; Jarzab, B.; et al. Combination chemotherapy in advanced adrenocortical carcinoma. *N. Engl. J. Med.* **2012**, *366*, 2189–2197. [[CrossRef](#)] [[PubMed](#)]
138. Assie, G.; Letouze, E.; Fassnacht, M.; Jouinot, A.; Luscap, W.; Barreau, O.; Omeiri, H.; Rodriguez, S.; Perlemino, K.; Rene-Corail, F.; et al. Integrated genomic characterization of adrenocortical carcinoma. *Nat. Genet.* **2014**, *46*, 607–612. [[CrossRef](#)] [[PubMed](#)]
139. Zheng, S.; Cherniack, A.D.; Dewal, N.; Moffitt, R.A.; Danilova, L.; Murray, B.A.; Lerario, A.M.; Else, T.; Knijnenburg, T.A.; Ciriello, G.; et al. Comprehensive Pan-Genomic Characterization of Adrenocortical Carcinoma. *Cancer Cell* **2016**, *30*, 363. [[CrossRef](#)] [[PubMed](#)]
140. Chabre, O.; Libe, R.; Assie, G.; Barreau, O.; Bertherat, J.; Bertagna, X.; Feige, J.J.; Cherradi, N. Serum miR-483-5p and miR-195 are predictive of recurrence risk in adrenocortical cancer patients. *Endocr. Relat. Cancer* **2013**, *20*, 579–594. [[CrossRef](#)]
141. Igaz, P.; Igaz, I.; Nagy, Z.; Nyírő, G.; Szabó, P.M.; Falus, A.; Patócs, A.; Rácz, K. MicroRNAs in adrenal tumors: Relevance for pathogenesis, diagnosis, and therapy. *Cell. Mol. Life Sci.* **2015**, *72*, 417–428. [[CrossRef](#)] [[PubMed](#)]
142. Özata, D.M.; Caramuta, S.; Velázquez-Fernández, D.; Akçakaya, P.; Xie, H.; Höög, A.; Zedenius, J.; Bäckdahl, M.; Larsson, C.; Lui, W.O. The role of microRNA deregulation in the pathogenesis of adrenocortical carcinoma. *Endocr. Relat. Cancer* **2011**, *18*, 643–655. [[CrossRef](#)]
143. Patterson, E.E.; Holloway, A.K.; Weng, J.; Fojo, T.; Kebebew, E. MicroRNA profiling of adrenocortical tumors reveals miR-483 as a marker of malignancy. *Cancer* **2011**, *117*, 1630–1639. [[CrossRef](#)] [[PubMed](#)]
144. Singh, P.; Soon, P.S.; Feige, J.J.; Chabre, O.; Zhao, J.T.; Cherradi, N.; Lalli, E.; Sidhu, S.B. Dysregulation of microRNAs in adrenocortical tumors. *Mol. Cell. Endocrinol.* **2012**, *351*, 118–128. [[CrossRef](#)]
145. Soon, P.S.; Tacon, L.J.; Gill, A.J.; Bambach, C.P.; Sywak, M.S.; Campbell, P.R.; Yeh, M.W.; Wong, S.G.; Clifton-Bligh, R.J.; Robinson, B.G.; et al. miR-195 and miR-483-5p Identified as Predictors of Poor Prognosis in Adrenocortical Cancer. *Clin. Cancer Res.* **2009**, *15*, 7684–7692. [[CrossRef](#)]
146. Cherradi, N. microRNAs as Potential Biomarkers in Adrenocortical Cancer: Progress and Challenges. *Front. Endocrinol.* **2015**, *6*, 195. [[CrossRef](#)]
147. Kalinowski, F.C.; Giles, K.M.; Candy, P.A.; Ali, A.; Ganda, C.; Epis, M.R.; Webster, R.J.; Leedman, P.J. Regulation of epidermal growth factor receptor signaling and erlotinib sensitivity in head and neck cancer cells by miR-7. *PLoS ONE* **2012**, *7*, e47067. [[CrossRef](#)]
148. Jung, S.; Nagy, Z.; Fassnacht, M.; Zambetti, G.; Weiss, M.; Reincke, M.; Igaz, P.; Beuschlein, F.; Hantel, C. Preclinical progress and first translational steps for a liposomal chemotherapy protocol against adrenocortical carcinoma. *Endocr. Relat. Cancer* **2016**, *23*, 825–837. [[CrossRef](#)] [[PubMed](#)]
149. Koutsaki, M.; Libra, M.; Spandidos, D.A.; Zaravinos, A. The miR-200 family in ovarian cancer. *Oncotarget* **2017**, *8*, 66629–66640. [[CrossRef](#)]
150. Lü, J.M.; Liang, Z.; Wang, X.; Gu, J.; Yao, Q.; Chen, C. New polymer of lactic-co-glycolic acid-modified polyethylenimine for nucleic acid delivery. *Nanomedicine* **2016**, *11*, 1971–1991. [[CrossRef](#)]
151. Rodriguez, A.; Vigorito, E.; Clare, S.; Warren, M.V.; Couttet, P.; Soond, D.R.; van Dongen, S.; Grocock, R.J.; Das, P.P.; Miska, E.A.; et al. Requirement of microRNA-155 for Normal Immune Function. *Science* **2007**, *316*, 608–611. [[CrossRef](#)]
152. Zhang, S.; Cheng, Z.; Wang, Y.; Han, T. The Risks of miRNA Therapeutics: In a Drug Target Perspective. *Drug Des. Dev. Ther.* **2021**, *15*, 721–733. [[CrossRef](#)] [[PubMed](#)]
153. Mullard, A. 2018 FDA drug approvals. *Nat. Rev. Drug Discov.* **2019**, *18*, 85–89. [[CrossRef](#)] [[PubMed](#)]
154. Mullard, A. 2019 FDA drug approvals. *Nat. Rev. Drug Discov.* **2020**, *19*, 79–84. [[CrossRef](#)]
155. Janssen, H.L.; Reesink, H.W.; Lawitz, E.J.; Zeuzem, S.; Rodriguez-Torres, M.; Patel, K.; van der Meer, A.J.; Patick, A.K.; Chen, A.; Zhou, Y.; et al. Treatment of HCV infection by targeting microRNA. *N. Engl. J. Med.* **2013**, *368*, 1685–1694. [[CrossRef](#)] [[PubMed](#)]
156. Lindow, M.; Kauppinen, S. Discovering the first microRNA-targeted drug. *J. Cell Biol.* **2012**, *199*, 407–412. [[CrossRef](#)]
157. van der Ree, M.H.; van der Meer, A.J.; van Nuenen, A.C.; de Bruijne, J.; Ottosen, S.; Janssen, H.L.; Kootstra, N.A.; Reesink, H.W. Miravirsen dosing in chronic hepatitis C patients results in decreased microRNA-122 levels without affecting other microRNAs in plasma. *Aliment. Pharmacol. Ther.* **2016**, *43*, 102–113. [[CrossRef](#)]
158. Shi, Y.; van der Meel, R.; Chen, X.; Lammers, T. The EPR effect and beyond: Strategies to improve tumor targeting and cancer nanomedicine treatment efficacy. *Theranostics* **2020**, *10*, 7921–7924. [[CrossRef](#)]
159. Sindhwani, S.; Syed, A.M.; Ngai, J.; Kingston, B.R.; Maiorino, L.; Rothschild, J.; MacMillan, P.; Zhang, Y.; Rajesh, N.U.; Hoang, T.; et al. The entry of nanoparticles into solid tumours. *Nat. Mater.* **2020**, *19*, 566–575. [[CrossRef](#)] [[PubMed](#)]
160. Blanco, E.; Shen, H.; Ferrari, M. Principles of nanoparticle design for overcoming biological barriers to drug delivery. *Nat. Biotechnol.* **2015**, *33*, 941–951. [[CrossRef](#)]
161. Haute, D.V.; Berlin, J.M. Challenges in realizing selectivity for nanoparticle biodistribution and clearance: Lessons from gold nanoparticles. *Ther. Deliv.* **2017**, *8*, 763–774. [[CrossRef](#)]
162. Elmén, J.; Lindow, M.; Schütz, S.; Lawrence, M.; Petri, A.; Obad, S.; Lindholm, M.; Hedtjörn, M.; Hansen, H.F.; Berger, U.; et al. LNA-mediated microRNA silencing in non-human primates. *Nature* **2008**, *452*, 896–899. [[CrossRef](#)] [[PubMed](#)]
163. Krützfeldt, J.; Rajewsky, N.; Braich, R.; Rajeev, K.G.; Tuschl, T.; Manoharan, M.; Stoffel, M. Silencing of microRNAs in vivo with ‘antagomirs’. *Nature* **2005**, *438*, 685–689. [[CrossRef](#)]
164. Zarin, D.A.; Tse, T.; Williams, R.J.; Califf, R.M.; Ide, N.C. The ClinicalTrials.gov results database—Update and key issues. *N. Engl. J. Med.* **2011**, *364*, 852–860. [[CrossRef](#)]



165. Sainz, V.; Connot, J.; Matos, A.I.; Peres, C.; Zupancic, E.; Moura, L.; Silva, L.C.; Florindo, H.F.; Gaspar, R.S. Regulatory aspects on nanomedicines. *Biochem. Biophys. Res. Commun.* **2015**, *468*, 504–510. [[CrossRef](#)] [[PubMed](#)]
166. Hare, J.I.; Lammers, T.; Ashford, M.B.; Puri, S.; Storm, G.; Barry, S.T. Challenges and strategies in anti-cancer nanomedicine development: An industry perspective. *Adv. Drug. Deliv. Rev.* **2017**, *108*, 25–38. [[CrossRef](#)] [[PubMed](#)]
167. Monroig-Bosque Pdel, C.; Rivera, C.A.; Calin, G.A. MicroRNAs in cancer therapeutics: “from the bench to the bedside”. *Expert Opin. Biol. Ther.* **2015**, *15*, 1381–1385. [[CrossRef](#)] [[PubMed](#)]
168. Nanomedicine and the COVID-19 vaccines. *Nature Nanotechnol.* **2020**, *15*, 963. [[CrossRef](#)] [[PubMed](#)]

## Scientific production

### Publications :

1. Soha Reda El Sayed, Justine Cristante, Laurent Guyon, Josiane Denis, Olivier Chabre and Nadia Cherradi\*. MicroRNA Therapeutics in Cancer: Current Advances and Challenges. *Cancers* (Basel). 2021 May 29;13(11):2680. doi: 10.3390/cancers13112680.
2. Soha Reda El Sayed, Adrien Nougarede, Josiane Denis, Olivier Chabre, Fabrice Navarro Laurent Guyon, and Nadia Cherradi. MicroRNA therapeutics in ACC: A lipid nanoparticle-based approach to suppress the oncogenic activity of microRNAs (presented in the thesis, to be submitted)
3. Justine Cristante, Soha Reda El Sayed, Laurent Guyon, Josiane Denis, Olivier Chabre, Nadia Cherradi. Non-coding RNAs in adrenocortical carcinoma. Review, imminent submission.
4. Soha Reda El Sayed, Josiane Denis, Tala Al Tabosh, Delphine Pflieger, Christophe Battail, Olivier Chabre, Laurent Guyon and Nadia Cherradi\*. Proteogenomic analyses of adrenocortical cancer cell-derived exosomes reveal their angiogenic and oncogenic functions (in preparation).

### Oral communications :

1. 13 – 15 September 2021: Extracellular Vesicle Summer School, organized by “Société Française en Nanomédecine” (SFNano) and “French Society for Extracellular Vesicles” (FSEV),  
La Grande Motte, FRANCE
2. 30 September – 2 October 2021: 8th International Adrenal Cancer symposium, Brescia, ITALY – Virtual

### Posters :

1. 20 April 2020 : Journée des Jeunes Chercheurs Ligue Contre le Cancer, Université Sorbonne, Paris, FRANCE – Virtual
2. 29 March – 2 April 2021 : Canceropole CLARA, Lyon, FRANCE – Virtual



## 6-REFERENCES

---



1. Rosol TJ, Yarrington JT, Latendresse J, Capen CC. Adrenal gland: structure, function, and mechanisms of toxicity. *Toxicologic pathology*. 2001;29(1):41-8.
2. Angara V, Digiacomio JC. Adrenal gland injury due to gunshot. *Chinese Journal of Traumatology*. 2020;23(3):149-51.
3. El Otmani W, Bhatia K. Clinical aspects of endocrinology: parathyroid and adrenal gland disorders. *Anaesthesia & Intensive Care Medicine*. 2020;21(11):531-8.
4. Wood MA, Acharya A, Finco I, Swonger JM, Elston MJ, Tallquist MD, et al. Fetal adrenal capsular cells serve as progenitor cells for steroidogenic and stromal adrenocortical cell lineages in *M. musculus*. *Development*. 2013;140(22):4522-32.
5. Simon DP, Hammer GD. Adrenocortical stem and progenitor cells: implications for adrenocortical carcinoma. *Mol Cell Endocrinol*. 2012;351(1):2-11.
6. Drelon C, Berthon A, Mathieu M, Martinez A, Val P. Adrenal cortex tissue homeostasis and zonation: A WNT perspective. *Mol Cell Endocrinol*. 2015;408:156-64.
7. Yates R, Katugampola H, Cavlan D, Cogger K, Meimaridou E, Hughes C, et al. Chapter Seven - Adrenocortical Development, Maintenance, and Disease. In: Thomas P, editor. *Current Topics in Developmental Biology*. 106: Academic Press; 2013. p. 239-312.
8. Sushko TA, Gilep AA, Usanov SA. Genetics, structure, function, mode of actions and role in cancer development of CYP17. *Anti-cancer agents in medicinal chemistry*. 2014;14(1):66-76.
9. Bose HS, Whittal RM, Baldwin MA, Miller WL. The active form of the steroidogenic acute regulatory protein, StAR, appears to be a molten globule. *Proceedings of the National Academy of Sciences of the United States of America*. 1999;96(13):7250-5.
10. Papadopoulos V, Amri H, Boujrad N, Cascio C, Culty M, Garnier M, et al. Peripheral benzodiazepine receptor in cholesterol transport and steroidogenesis. *Steroids*. 1997;62(1):21-8.
11. Rainey WE. Adrenal zonation: clues from 11beta-hydroxylase and aldosterone synthase. *Mol Cell Endocrinol*. 1999;151(1-2):151-60.
12. Nogueira EF, Bollag WB, Rainey WE. Angiotensin II regulation of adrenocortical gene transcription. *Mol Cell Endocrinol*. 2009;302(2):230-6.
13. de Joussineau C, Sahut-Barnola I, Levy I, Saloustros E, Val P, Stratakis CA, et al. The cAMP pathway and the control of adrenocortical development and growth. *Mol Cell Endocrinol*. 2012;351(1):28-36.
14. Freedman Bethany D, Kempna Petra B, Carlone Diana L, Shah MS, Guagliardo Nick A, Barrett Paula Q, et al. Adrenocortical Zonation Results from Lineage Conversion of Differentiated Zona Glomerulosa Cells. *Developmental Cell*. 2013;26(6):666-73.
15. Martinez A, Schedl A. Dissecting a zoned organ - Special issue on adrenal biology. *Mol Cell Endocrinol*. 2022;539:111486.

16. Drelon C, Berthon A, Mathieu M, Martinez A, Val P. Adrenal cortex tissue homeostasis and zonation: A WNT perspective. *Mol Cell Endocrinol.* 2015;408:156-64.
  17. Basham KJ, Rodriguez S, Turcu AF, Lerario AM, Logan CY, Rysztak MR, et al. A ZNRF3-dependent Wnt/ $\beta$ -catenin signaling gradient is required for adrenal homeostasis. *Genes Dev.* 2019;33(3-4):209-20.
  18. Burford NG, Webster NA, Cruz-Topete D. Hypothalamic-Pituitary-Adrenal Axis Modulation of Glucocorticoids in the Cardiovascular System. *International Journal of Molecular Sciences.* 2017;18(10).
  19. Nagamine M, Noguchi H, Takahashi N, Kim Y, Matsuoka Y. Effect of cortisol diurnal rhythm on emotional memory in healthy young adults. *Scientific Reports.* 2017;7(1):10158.
  20. Endoh A, Kristiansen SB, Casson PR, Buster JE, Hornsby PJ. The zona reticularis is the site of biosynthesis of dehydroepiandrosterone and dehydroepiandrosterone sulfate in the adult human adrenal cortex resulting from its low expression of 3 beta-hydroxysteroid dehydrogenase. *The Journal of Clinical Endocrinology & Metabolism.* 1996;81(10):3558-65.
  21. Lyraki R, Schedl A. Adrenal cortex renewal in health and disease. *Nature Reviews Endocrinology.* 2021;17(7):421-34.
  22. Dutt M, Wehrle CJ, Jialal I. *Physiology, Adrenal Gland.* StatPearls. Treasure Island (FL): StatPearls Publishing
- Copyright © 2021, StatPearls Publishing LLC.; 2021.
23. Carbone E, Borges R, Eiden LE, García AG, Hernández-Cruz A. Chromaffin Cells of the Adrenal Medulla: Physiology, Pharmacology, and Disease. *Comprehensive Physiology.* 2019;9(4):1443-502.
  24. Goldstein DS. Adrenal responses to stress. *Cell Mol Neurobiol.* 2010;30(8):1433-40.
  25. Perlman RL, Chalfie M. Catecholamine release from the adrenal medulla. *Clinics in endocrinology and metabolism.* 1977;6(3):551-76.
  26. Lambert-Langlais S, Pointud J-C, Lefrançois-Martinez A-M, Volat F, Manin M, Coudoré F, et al. Aldo keto reductase 1B7 and prostaglandin F2alpha are regulators of adrenal endocrine functions. *PLoS One.* 2009;4(10):e7309-e.
  27. Dumontet T, Sahut-Barnola I, Septier A, Montanier N, Plotton I, Roucher-Boulez F, et al. Adrenocortical development: Lessons from mouse models. *Annales d'Endocrinologie.* 2018;79(3):95-7.
  28. Xing Y, Lerario AM, Rainey W, Hammer GD. Development of adrenal cortex zonation. *Endocrinology and metabolism clinics of North America.* 2015;44(2):243-74.
  29. Chapman K, Holmes M, Seckl J.  $11\beta$ -hydroxysteroid dehydrogenases: intracellular gatekeepers of tissue glucocorticoid action. *Physiological reviews.* 2013;93(3):1139-206.
  30. Hofland J, de Jong FH. Inhibins and activins: their roles in the adrenal gland and the development of adrenocortical tumors. *Mol Cell Endocrinol.* 2012;359(1-2):92-100.

31. Drelon C, Berthon A, Sahut-Barnola I, Mathieu M, Dumontet T, Rodriguez S, et al. PKA inhibits WNT signalling in adrenal cortex zonation and prevents malignant tumour development. *Nature communications*. 2016;7(1):12751.
32. Sarkar SB, Sarkar S, Ghosh S, Bandyopadhyay S. Addison's disease. *Contemp Clin Dent*. 2012;3(4):484-6.
33. Arlt W, Allolio B. Adrenal insufficiency. *The Lancet*. 2003;361(9372):1881-93.
34. Bornstein SR, Allolio B, Arlt W, Barthel A, Don-Wauchope A, Hammer GD, et al. Diagnosis and Treatment of Primary Adrenal Insufficiency: An Endocrine Society Clinical Practice Guideline. *J Clin Endocrinol Metab*. 2016;101(2):364-89.
35. Rushworth RL, Torpy DJ, Falhammar H. Adrenal crises: perspectives and research directions. *Endocrine*. 2017;55(2):336-45.
36. El-Maouche D, Arlt W, Merke DP. Congenital adrenal hyperplasia. *Lancet (London, England)*. 2017;390(10108):2194-210.
37. .
38. Miller WL. Fetal endocrine therapy for congenital adrenal hyperplasia should not be done. *Best Practice & Research Clinical Endocrinology & Metabolism*. 2015;29(3):469-83.
39. Nieman LK. Cushing's syndrome: update on signs, symptoms and biochemical screening. *European Journal of Endocrinology*. 2015;173(4):M33-M8.
40. Louiset E, Duparc C, Young J, Renouf S, Tetsi Nomigni M, Boutelet I, et al. Intraadrenal corticotropin in bilateral macronodular adrenal hyperplasia. *The New England journal of medicine*. 2013;369(22):2115-25.
41. Ilias I, Torpy DJ, Pacak K, Mullen N, Wesley RA, Nieman LK. Cushing's syndrome due to ectopic corticotropin secretion: twenty years' experience at the National Institutes of Health. *J Clin Endocrinol Metab*. 2005;90(8):4955-62.
42. Buliman A, Tataranu LG, Paun DL, Mirica A, Dumitrache C. Cushing's disease: a multidisciplinary overview of the clinical features, diagnosis, and treatment. *J Med Life*. 2016;9(1):12-8.
43. Zennaro M-C, Boulkroun S, Fernandes-Rosa FL. Pathogenesis and treatment of primary aldosteronism. *Nature Reviews Endocrinology*. 2020;16(10):578-89.
44. Williams TA, Lenders JWM, Mulatero P, Burrello J, Rottenkolber M, Adolf C, et al. Outcomes after adrenalectomy for unilateral primary aldosteronism: an international consensus on outcome measures and analysis of remission rates in an international cohort. *Lancet Diabetes Endocrinol*. 2017;5(9):689-99.
45. Younes A, Elgendy A, Zekri W, Fadel S, Elfandy H, Romeih M, et al. Operative management and outcome in children with pheochromocytoma. *Asian Journal of Surgery*. 2021.
46. Fishbein L, Leshchiner I, Walter V, Danilova L, Robertson AG, Johnson AR, et al. Comprehensive Molecular Characterization of Pheochromocytoma and Paraganglioma. *Cancer Cell*. 2017;31(2):181-93.



47. Favier J, Amar L, Gimenez-Roqueplo AP. Paraganglioma and pheochromocytoma: from genetics to personalized medicine. *Nature reviews Endocrinology*. 2015;11(2):101-11.
  48. Bonnet-Serrano F, Bertherat J. Genetics of tumors of the adrenal cortex. *Endocrine-Related Cancer*. 2018;25(3):R131-R52.
  49. Singh P, Soon PSH, Feige J-J, Chabre O, Zhao JT, Cherradi N, et al. Dysregulation of microRNAs in adrenocortical tumors. *Mol Cell Endocrinol*. 2012;351(1):118-28.
  50. Prilutskiy A, Nosé V. Update on adrenal cortical neoplasia. *Diagnostic Histopathology*. 2021;27(6):240-51.
  51. Jouinot A, Armignacco R, Assié G. Genomics of benign adrenocortical tumors. *The Journal of Steroid Biochemistry and Molecular Biology*. 2019;193:105414.
  52. Goh G, Scholl UI, Healy JM, Choi M, Prasad ML, Nelson-Williams C, et al. Recurrent activating mutation in PRKACA in cortisol-producing adrenal tumors. *Nature Genetics*. 2014;46(6):613-7.
  53. Lacroix A. Heredity and Cortisol Regulation in Bilateral Macronodular Adrenal Hyperplasia. *New England Journal of Medicine*. 2013;369(22):2147-9.
  54. Assié G, Libé R, Espiard S, Rizk-Rabin M, Guimier A, Luscap W, et al. ARMC5 Mutations in Macronodular Adrenal Hyperplasia with Cushing's Syndrome. *New England Journal of Medicine*. 2013;369(22):2105-14.
  55. Allolio B, Fassnacht M. Adrenocortical Carcinoma: Clinical Update. *The Journal of Clinical Endocrinology & Metabolism*. 2006;91(6):2027-37.
  56. Michalkiewicz E, Sandrini R, Figueiredo B, Miranda ECM, Caran E, Oliveira-Filho AG, et al. Clinical and Outcome Characteristics of Children With Adrenocortical Tumors: A Report From the International Pediatric Adrenocortical Tumor Registry. *Journal of Clinical Oncology*. 2004;22(5):838-45.
  57. Dumontet T, Sahut-Barnola I, Septier A, Montanier N, Plotton I, Roucher-Boulez F, et al. PKA signaling drives reticularis differentiation and sexually dimorphic adrenal cortex renewal. *JCI Insight*. 2018;3(2).
  58. Grabek A, Dolfi B, Klein B, Jian-Motamedi F, Chaboissier MC, Schedl A. The Adult Adrenal Cortex Undergoes Rapid Tissue Renewal in a Sex-Specific Manner. *Cell stem cell*. 2019;25(2):290-6.e2.
  59. Torti JF, Correa R. Adrenal Cancer. StatPearls. Treasure Island (FL): StatPearls Publishing
- Copyright © 2021, StatPearls Publishing LLC.; 2021.
60. Zini L, Porpiglia F, Fassnacht M. Contemporary management of adrenocortical carcinoma. *European urology*. 2011;60(5):1055-65.
  61. Wasserman JD, Novokmet A, Eichler-Jonsson C, Ribeiro RC, Rodriguez-Galindo C, Zambetti GP, et al. Prevalence and functional consequence of TP53 mutations in pediatric adrenocortical carcinoma: a children's oncology group study. *Journal of clinical oncology : official journal of the American Society of Clinical Oncology*. 2015;33(6):602-9.
  62. Assié G, Letouzé E, Fassnacht M, Jouinot A, Luscap W, Barreau O, et al. Integrated genomic characterization of adrenocortical carcinoma. *Nature Genetics*. 2014;46(6):607-12.

63. Chompret A, Brugières L, Ronsin M, Gardes M, Dessarps-Freichay F, Abel A, et al. P53 germline mutations in childhood cancers and cancer risk for carrier individuals. *Br J Cancer*. 2000;82(12):1932-7.
64. Herrmann LJM, Heinze B, Fassnacht M, Willenberg HS, Quinkler M, Reisch N, et al. TP53 Germline Mutations in Adult Patients with Adrenocortical Carcinoma. *The Journal of Clinical Endocrinology & Metabolism*. 2012;97(3):E476-E85.
65. Gicquel C, Bertagna X, Schneid H, Francillard-Leblond M, Luton JP, Girard F, et al. Rearrangements at the 11p15 locus and overexpression of insulin-like growth factor-II gene in sporadic adrenocortical tumors. *J Clin Endocrinol Metab*. 1994;78(6):1444-53.
66. Chandrasekharappa SC, Guru SC, Manickam P, Olufemi SE, Collins FS, Emmert-Buck MR, et al. Positional cloning of the gene for multiple endocrine neoplasia-type 1. *Science (New York, NY)*. 1997;276(5311):404-7.
67. Gatta-Cherifi B, Chabre O, Murat A, Niccoli P, Cardot-Bauters C, Rohmer V, et al. Adrenal involvement in MEN1. Analysis of 715 cases from the Groupe d'etude des Tumeurs Endocrines database. *Eur J Endocrinol*. 2012;166(2):269-79.
68. Gaujoux S, Pinson S, Gimenez-Roqueplo AP, Amar L, Ragazzon B, Launay P, et al. Inactivation of the APC gene is constant in adrenocortical tumors from patients with familial adenomatous polyposis but not frequent in sporadic adrenocortical cancers. *Clinical cancer research : an official journal of the American Association for Cancer Research*. 2010;16(21):5133-41.
69. Fassnacht M, Assie G, Baudin E, Eisenhofer G, de la Fouchardiere C, Haak HR, et al. Adrenocortical carcinomas and malignant pheochromocytomas: ESMO-EURACAN Clinical Practice Guidelines for diagnosis, treatment and follow-up. *Annals of oncology : official journal of the European Society for Medical Oncology*. 2020;31(11):1476-90.
70. Fassnacht M, Arlt W, Bancos I, Dralle H, Newell-Price J, Sahdev A, et al. Management of adrenal incidentalomas: European Society of Endocrinology Clinical Practice Guideline in collaboration with the European Network for the Study of Adrenal Tumors. *European Journal of Endocrinology*. 2016;175(2):G1-G34.
71. Bharwani N, Rockall AG, Sahdev A, Gueorguiev M, Drake W, Grossman AB, et al. Adrenocortical carcinoma: the range of appearances on CT and MRI. *AJR American journal of roentgenology*. 2011;196(6):W706-14.
72. Sundin A. Imaging of adrenal masses with emphasis on adrenocortical tumors. *Theranostics*. 2012;2(5):516-22.
73. Weiss LM, Medeiros LJ, Vickery AL, Jr. Pathologic features of prognostic significance in adrenocortical carcinoma. *The American journal of surgical pathology*. 1989;13(3):202-6.
74. Papotti M, Libè R, Duregon E, Volante M, Bertherat J, Tissier F. The Weiss score and beyond--histopathology for adrenocortical carcinoma. *Hormones & cancer*. 2011;2(6):333-40.
75. Terzolo M, Boccuzzi A, Bovio S, Cappia S, De Giuli P, Ali A, et al. Immunohistochemical assessment of Ki-67 in the differential diagnosis of adrenocortical tumors. *Urology*. 2001;57(1):176-82.

76. Beuschlein F, Weigel J, Saeger W, Kroiss M, Wild V, Daffara F, et al. Major prognostic role of Ki67 in localized adrenocortical carcinoma after complete resection. *J Clin Endocrinol Metab.* 2015;100(3):841-9.
77. Fassnacht M, Dekkers OM, Else T, Baudin E, Berruti A, de Krijger RR, et al. European Society of Endocrinology Clinical Practice Guidelines on the management of adrenocortical carcinoma in adults, in collaboration with the European Network for the Study of Adrenal Tumors. *European Journal of Endocrinology.* 2018;179(4):G1-G46.
78. Mizdrak M, Tičinović Kurir T, Božić J. The Role of Biomarkers in Adrenocortical Carcinoma: A Review of Current Evidence and Future Perspectives. *Biomedicines.* 2021;9(2):174.
79. Libé R, Borget I, Ronchi CL, Zaggia B, Kroiss M, Kerkhofs T, et al. Prognostic factors in stage III-IV adrenocortical carcinomas (ACC): an European Network for the Study of Adrenal Tumor (ENSAT) study. *Annals of oncology : official journal of the European Society for Medical Oncology.* 2015;26(10):2119-25.
80. Lorenz K, Langer P, Niederle B, Alesina P, Holzer K, Nies C, et al. Surgical therapy of adrenal tumors: guidelines from the German Association of Endocrine Surgeons (CAEK). *Langenbeck's archives of surgery.* 2019;404(4):385-401.
81. Libé R. Adrenocortical carcinoma (ACC): diagnosis, prognosis, and treatment. *Frontiers in cell and developmental biology.* 2015;3:45.
82. Kiesewetter B, Riss P. Management of adrenocortical carcinoma: are we making progress? *2021;13:17588359211038409.*
83. Nelson AA, Woodard G. Adrenal cortical atrophy and liver damage produced in dogs by feeding 2,2-bis-(parachloro-phenyl)-1,1-dichloroethane. *Federation proceedings.* 1948;7 1 Pt 1:277.
84. Corso CR, Acco A. Pharmacological profile and effects of mitotane in adrenocortical carcinoma. *2021;87(7):2698-710.*
85. Terzolo M, Angeli A, Fassnacht M, Daffara F, Tauchmanova L, Conton PA, et al. Adjuvant mitotane treatment for adrenocortical carcinoma. *The New England journal of medicine.* 2007;356(23):2372-80.
86. Postlewait LM, Ethun CG, Tran TB, Prescott JD, Pawlik TM, Wang TS, et al. Outcomes of Adjuvant Mitotane after Resection of Adrenocortical Carcinoma: A 13-Institution Study by the US Adrenocortical Carcinoma Group. *Journal of the American College of Surgeons.* 2016;222(4):480-90.
87. Terzolo M, Fassnacht M, Perotti P, Libe R, Lacroix A, Kastelan D, et al. Results of the ADIUVO Study, the First Randomized Trial on Adjuvant Mitotane in Adrenocortical Carcinoma Patients. *Journal of the Endocrine Society.* 2021;5(Supplement\_1):A166-A7.
88. Berruti A. Adjuvant Mitotane Treatment (ADIUVO) NCT00777244 2008. Available from: <https://clinicaltrials.gov/ct2/show/NCT00777244>.
89. Terzolo M, Baudin AE, Ardito A, Kroiss M, Leboulleux S, Daffara F, et al. Mitotane levels predict the outcome of patients with adrenocortical carcinoma treated adjuvantly following radical resection. *European Journal of Endocrinology.* 2013;169(3):263-70.

90. Bedrose S, Daher M, Altameemi L, Habra MA. Adjuvant Therapy in Adrenocortical Carcinoma: Reflections and Future Directions. *Cancers*. 2020;12(2).
91. Flynn SD, Murren JR, Kirby WM, Honig J, Kan L, Kinder BK. P-glycoprotein expression and multidrug resistance in adrenocortical carcinoma. *Surgery*. 1992;112(6):981-6.
92. BATES SE, SHIEH C-Y, MICKLEY LA, DICHEK HL, GAZDAR A, LORIAUX DL, et al. Mitotane Enhances Cytotoxicity of Chemotherapy in Cell Lines Expressing a Multidrug Resistance Gene (mdr-1/P-Glycoprotein) which is also Expressed by Adrenocortical Carcinomas. *The Journal of Clinical Endocrinology & Metabolism*. 1991;73(1):18-29.
93. Fassnacht M. Trial in Locally Advanced and Metastatic Adrenocortical Carcinoma Treatment (FIRM-ACT) NCT00094497 ClinicalTrials.gov2004. Available from: <https://clinicaltrials.gov/ct2/show/NCT00094497>.
94. Fassnacht M, Terzolo M, Allolio B, Baudin E, Haak H, Berruti A, et al. Combination chemotherapy in advanced adrenocortical carcinoma. *The New England journal of medicine*. 2012;366(23):2189-97.
95. Fassnacht M, Hahner S, Polat B, Koschker AC, Kenn W, Flentje M, et al. Efficacy of adjuvant radiotherapy of the tumor bed on local recurrence of adrenocortical carcinoma. *J Clin Endocrinol Metab*. 2006;91(11):4501-4.
96. Thomas JJ, Tward JD. Stage Presentation, Care Patterns, Treatment Outcomes, and Impact of Radiotherapy on Overall Survival for Adrenocortical Carcinoma. *Clinical Genitourinary Cancer*. 2021;19(5):417-24.
97. Zhu J, Zheng Z, Shen J, Lian X, Miao Z, Shen J, et al. Efficacy of adjuvant radiotherapy for treatment of adrenocortical carcinoma: a retrospective study and an updated meta-analysis. *Radiation oncology (London, England)*. 2020;15(1):118.
98. Adam P, Hahner S, Hartmann M, Heinrich B, Quinkler M, Willenberg HS, et al. Epidermal growth factor receptor in adrenocortical tumors: analysis of gene sequence, protein expression and correlation with clinical outcome. *Modern Pathology*. 2010;23(12):1596-604.
99. Demeure MJ, Bussey KJ, Kirschner LS. Targeted Therapies for Adrenocortical Carcinoma: IGF and Beyond. *Hormones and Cancer*. 2011;2(6):385-92.
100. Quinkler M, Hahner S, Wortmann S, Johanssen S, Adam P, Ritter C, et al. Treatment of advanced adrenocortical carcinoma with erlotinib plus gemcitabine. *J Clin Endocrinol Metab*. 2008;93(6):2057-62.
101. Bergers G, Hanahan D. Modes of resistance to anti-angiogenic therapy. *Nature reviews Cancer*. 2008;8(8):592-603.
102. Cerquetti L, Bucci B, Raffa S, Amendola D, Maggio R, Lardo P, et al. Effects of Sorafenib, a Tyrosin Kinase Inhibitor, on Adrenocortical Cancer. *Frontiers in endocrinology*. 2021;12:667798.
103. Berruti A, Sperone P, Ferrero A, Germano A, Ardito A, Priola AM, et al. Phase II study of weekly paclitaxel and sorafenib as second/third-line therapy in patients with adrenocortical carcinoma. *Eur J Endocrinol*. 2012;166(3):451-8.

104. Almeida MQ, Fragoso MC, Lotfi CF, Santos MG, Nishi MY, Costa MH, et al. Expression of insulin-like growth factor-II and its receptor in pediatric and adult adrenocortical tumors. *J Clin Endocrinol Metab.* 2008;93(9):3524-31.
105. Fassnacht M, Berruti A, Baudin E, Demeure MJ, Gilbert J, Haak H, et al. Linsitinib (OSI-906) versus placebo for patients with locally advanced or metastatic adrenocortical carcinoma: a double-blind, randomised, phase 3 study. *The Lancet Oncology.* 2015;16(4):426-35.
106. Lerario AM, Worden FP, Ramm CA, Hesseltine EA, Stadler WM, Else T, et al. The combination of insulin-like growth factor receptor 1 (IGF1R) antibody cixutumumab and mitotane as a first-line therapy for patients with recurrent/metastatic adrenocortical carcinoma: a multi-institutional NCI-sponsored trial. *Hormones & cancer.* 2014;5(4):232-9.
107. Fraenkel M, Gueorguiev M, Barak D, Salmon A, Grossman AB, Gross DJ. Everolimus therapy for progressive adrenocortical cancer. *Endocrine.* 2013;44(1):187-92.
108. De Martino MC, van Koetsveld PM, Feelders RA, de Herder WW, Dogan F, Janssen J, et al. IGF and mTOR pathway expression and in vitro effects of linsitinib and mTOR inhibitors in adrenocortical cancer. *Endocrine.* 2019;64(3):673-84.
109. Konda B, Kirschner LS. Novel targeted therapies in adrenocortical carcinoma. *Current opinion in endocrinology, diabetes, and obesity.* 2016;23(3):233-41.
110. Rodon J, Argilés G, Connolly RM, Vaishampayan U, de Jonge M, Garralda E, et al. Phase 1 study of single-agent WNT974, a first-in-class Porcupine inhibitor, in patients with advanced solid tumours. *Br J Cancer.* 2021;125(1):28-37.
111. Yu F, Yu C, Li F, Zuo Y, Wang Y, Yao L, et al. Wnt/ $\beta$ -catenin signaling in cancers and targeted therapies. *Signal Transduction and Targeted Therapy.* 2021;6(1):307.
112. Fischer MM, Cancilla B, Yeung VP, Cattaruzza F, Chartier C, Murriel CL. WNT antagonists exhibit unique combinatorial antitumor activity with taxanes by potentiating mitotic cell death. 2017;3(6):e1700090.
113. Sbiera S, Schull S, Assie G, Voelker H-U, Kraus L, Beyer M, et al. High Diagnostic and Prognostic Value of Steroidogenic Factor-1 Expression in Adrenal Tumors. *The Journal of Clinical Endocrinology & Metabolism.* 2010;95(10):E161-E71.
114. Ehrlund A, Jonsson P, Vedin LL, Williams C, Gustafsson J, Treuter E. Knockdown of SF-1 and RNF31 affects components of steroidogenesis, TGF $\beta$ , and Wnt/ $\beta$ -catenin signaling in adrenocortical carcinoma cells. *PLoS One.* 2012;7(3):e32080.
115. Pegna GJ, Roper N, Kaplan RN, Bergsland E, Kiseljak-Vassiliades K, Habra MA. The Immunotherapy Landscape in Adrenocortical Cancer. 2021;13(11).
116. Habra MA, Stephen B, Campbell M, Hess K, Tapia C, Xu M, et al. Phase II clinical trial of pembrolizumab efficacy and safety in advanced adrenocortical carcinoma. *Journal for immunotherapy of cancer.* 2019;7(1):253.
117. Raj N, Zheng Y, Kelly V, Katz SS, Chou J, Do RKG, et al. PD-1 Blockade in Advanced Adrenocortical Carcinoma. *Journal of clinical oncology : official journal of the American Society of Clinical Oncology.* 2020;38(1):71-80.

118. Le Tourneau C, Hoimes C, Zarwan C, Wong DJ, Bauer S, Claus R, et al. Avelumab in patients with previously treated metastatic adrenocortical carcinoma: phase 1b results from the JAVELIN solid tumor trial. *Journal for immunotherapy of cancer*. 2018;6(1):111.
119. Fiorentini C, Grisanti S, Cosentini D, Abate A, Rossini E, Berruti A, et al. Molecular Drivers of Potential Immunotherapy Failure in Adrenocortical Carcinoma. 2019;2019:6072863.
120. Araujo-Castro M, Pascual-Corrales E. Immunotherapy in Adrenocortical Carcinoma: Predictors of Response, Efficacy, Safety, and Mechanisms of Resistance. 2021;9(3).
121. Zheng S, Cherniack Andrew D, Dewal N, Moffitt Richard A, Danilova L, Murray Bradley A, et al. Comprehensive Pan-Genomic Characterization of Adrenocortical Carcinoma. *Cancer Cell*. 2016;29(5):723-36.
122. McCabe MT, Brandes JC, Vertino PM. Cancer DNA methylation: molecular mechanisms and clinical implications. *Clinical cancer research : an official journal of the American Association for Cancer Research*. 2009;15(12):3927-37.
123. Rechache NS, Wang Y, Stevenson HS, Killian JK, Edelman DC, Merino M, et al. DNA methylation profiling identifies global methylation differences and markers of adrenocortical tumors. *J Clin Endocrinol Metab*. 2012;97(6):E1004-13.
124. Barreau O, Assié G, Wilmot-Roussel H, Ragazzon B, Baudry C, Perlemoine K, et al. Identification of a CpG Island Methylator Phenotype in Adrenocortical Carcinomas. *The Journal of Clinical Endocrinology & Metabolism*. 2013;98(1):E174-E84.
125. Ragazzon B, Assié G, Bertherat J. Transcriptome analysis of adrenocortical cancers: from molecular classification to the identification of new treatments. *Endocrine-Related Cancer*. 2011;18(2):R15-R27.
126. de Fraipont F, El Atifi M, Cherradi N, Le Moigne G, Defaye Gv, Houlgatte Rm, et al. Gene Expression Profiling of Human Adrenocortical Tumors Using Complementary Deoxyribonucleic Acid Microarrays Identifies Several Candidate Genes as Markers of Malignancy. *The Journal of Clinical Endocrinology & Metabolism*. 2005;90(3):1819-29.
127. de Reyniès A, Assié G, Rickman DS, Tissier F, Groussin L, René-Corail F, et al. Gene expression profiling reveals a new classification of adrenocortical tumors and identifies molecular predictors of malignancy and survival. *Journal of clinical oncology : official journal of the American Society of Clinical Oncology*. 2009;27(7):1108-15.
128. Gerstberger S, Hafner M, Tuschl T. A census of human RNA-binding proteins. *Nature Reviews Genetics*. 2014;15(12):829-45.
129. Esteller M. Non-coding RNAs in human disease. *Nature Reviews Genetics*. 2011;12(12):861-74.
130. La Ferlita A, Battaglia R, Andronico F, Caruso S, Cianci A, Purrello M, et al. Non-Coding RNAs in Endometrial Physiopathology. *International Journal of Molecular Sciences*. 2018;19(7):2120.
131. GENCODE. GENCODE. 38 ed2021.
132. Zhang P, Wu W, Chen Q, Chen M. Non-Coding RNAs and their Integrated Networks. *Journal of integrative bioinformatics*. 2019;16(3).

133. Fire A, Xu S, Montgomery MK, Kostas SA, Driver SE, Mello CC. Potent and specific genetic interference by double-stranded RNA in *Caenorhabditis elegans*. *Nature*. 1998;391(6669):806-11.
134. Kim D, Rossi J. RNAi mechanisms and applications. *BioTechniques*. 2008;44(5):613-6.
135. Schwarz DS, Hutvagner G, Du T, Xu Z, Aronin N, Zamore PD. Asymmetry in the Assembly of the RNAi Enzyme Complex. *Cell*. 2003;115(2):199-208.
136. Foster DJ, Barros S, Duncan R, Shaikh S, Cantley W, Dell A, et al. Comprehensive evaluation of canonical versus Dicer-substrate siRNA in vitro and in vivo. *RNA (New York, NY)*. 2012;18(3):557-68.
137. Han H. RNA Interference to Knock Down Gene Expression. *Methods in molecular biology (Clifton, NJ)*. 2018;1706:293-302.
138. Setten RL, Rossi JJ, Han S-p. The current state and future directions of RNAi-based therapeutics. *Nature Reviews Drug Discovery*. 2019;18(6):421-46.
139. Ambros V. The functions of animal microRNAs. *Nature*. 2004;431(7006):350-5.
140. Lee RC, Feinbaum RL, Ambros V. The *C. elegans* heterochronic gene *lin-4* encodes small RNAs with antisense complementarity to *lin-14*. *Cell*. 1993;75(5):843-54.
141. Almeida MI, Reis RM, Calin GA. MicroRNA history: Discovery, recent applications, and next frontiers. *Mutation Research/Fundamental and Molecular Mechanisms of Mutagenesis*. 2011;717(1):1-8.
142. Desvignes T, Batzel P, Berezikov E, Eilbeck K, Eppig JT, McAndrews MS, et al. miRNA Nomenclature: A View Incorporating Genetic Origins, Biosynthetic Pathways, and Sequence Variants. *Trends in genetics : TIG*. 2015;31(11):613-26.
143. Sun Q, Song YJ, Prasanth KV. One locus with two roles: microRNA-independent functions of microRNA-host-gene locus-encoded long noncoding RNAs. *WIREs RNA*. 2021;12(3):e1625.
144. França GS, Vibranovski MD, Galante PA. Host gene constraints and genomic context impact the expression and evolution of human microRNAs. *Nature communications*. 2016;7:11438.
145. Galatenko VV, Galatenko AV, Samatov TR, Turchinovich AA, Shkurnikov MY, Makarova JA, et al. Comprehensive network of miRNA-induced intergenic interactions and a biological role of its core in cancer. *Scientific Reports*. 2018;8(1):2418.
146. Kuhn CD, Joshua-Tor L. Eukaryotic Argonautes come into focus. *Trends in biochemical sciences*. 2013;38(5):263-71.
147. Ha M, Kim VN. Regulation of microRNA biogenesis. *Nature reviews Molecular cell biology*. 2014;15(8):509-24.
148. Yang J-S, Maurin T, Robine N, Rasmussen KD, Jeffrey KL, Chandwani R, et al. Conserved vertebrate *mir-451* provides a platform for Dicer-independent, Ago2-mediated microRNA biogenesis. *Proceedings of the National Academy of Sciences*. 2010;107(34):15163-8.
149. Witkos TM, Koscianska E, Krzyzosiak WJ. Practical Aspects of microRNA Target Prediction. *Current molecular medicine*. 2011;11(2):93-109.

150. Akhtar MM, Micolucci L, Islam MS, Olivieri F, Procopio AD. A Practical Guide to miRNA Target Prediction. *Methods in molecular biology* (Clifton, NJ). 2019;1970:1-13.
151. Quillet A, Saad C, Ferry G, Anouar Y, Vergne N, Lecroq T, et al. Improving Bioinformatics Prediction of microRNA Targets by Ranks Aggregation. *Frontiers in Genetics*. 2020;10(1330).
152. Lee FCY, Ule J. Advances in CLIP Technologies for Studies of Protein-RNA Interactions. *Molecular Cell*. 2018;69(3):354-69.
153. Karginov FV, Conaco C, Xuan Z, Schmidt BH, Parker JS, Mandel G, et al. A biochemical approach to identifying microRNA targets. *Proceedings of the National Academy of Sciences of the United States of America*. 2007;104(49):19291-6.
154. Darnell RB. HITS-CLIP: panoramic views of protein-RNA regulation in living cells. *Wiley interdisciplinary reviews RNA*. 2010;1(2):266-86.
155. Gay LA, Turner PC, Renne R. Contemporary Ribonomics Methods for Viral microRNA Target Analysis. *Non-Coding RNA*. 2018;4(4):31.
156. Helwak A, Kudla G, Dudnakova T, Tollervey D. Mapping the Human miRNA Interactome by CLASH Reveals Frequent Noncanonical Binding. *Cell*. 2013;153(3):654-65.
157. Dash S, Balasubramaniam M, Dash C, Pandhare J. Biotin-based Pulldown Assay to Validate mRNA Targets of Cellular miRNAs. *Journal of visualized experiments : JoVE*. 2018(136).
158. Awan HM, Shah A, Rashid F, Wei S, Chen L, Shan G. Comparing two approaches of miR-34a target identification, biotinylated-miRNA pulldown vs miRNA overexpression. 2018;15(1):55-61.
159. Lal A, Thomas MP, Altschuler G, Navarro F, O'Day E, Li XL, et al. Capture of MicroRNA-Bound mRNAs Identifies the Tumor Suppressor miR-34a as a Regulator of Growth Factor Signaling. *PLOS Genetics*. 2011;7(11):e1002363.
160. Tan Shen M, Kirchner R, Jin J, Hofmann O, McReynolds L, Hide W, et al. Sequencing of Captive Target Transcripts Identifies the Network of Regulated Genes and Functions of Primate-Specific miR-522. *Cell Reports*. 2014;8(4):1225-39.
161. He L, Hannon GJ. MicroRNAs: small RNAs with a big role in gene regulation. *Nature reviews Genetics*. 2004;5(7):522-31.
162. Fabian MR, Sonenberg N. The mechanics of miRNA-mediated gene silencing: a look under the hood of miRISC. *Nature Structural & Molecular Biology*. 2012;19(6):586-93.
163. Jonas S, Izaurralde E. Towards a molecular understanding of microRNA-mediated gene silencing. *Nature reviews Genetics*. 2015;16(7):421-33.
164. Calin GA, Dumitru CD, Shimizu M, Bichi R, Zupo S, Noch E, et al. Frequent deletions and down-regulation of micro-RNA genes miR15 and miR16 at 13q14 in chronic lymphocytic leukemia. *Proceedings of the National Academy of Sciences of the United States of America*. 2002;99(24):15524-9.
165. Reda El Sayed S. MicroRNA Therapeutics in Cancer: Current Advances and Challenges. *Cancers*. 2021;13(11).



166. Calin GA, Croce CM. MicroRNA signatures in human cancers. *Nature Reviews Cancer*. 2006;6(11):857-66.
167. Suzuki HI, Yamagata K, Sugimoto K, Iwamoto T, Kato S, Miyazono K. Modulation of microRNA processing by p53. *Nature*. 2009;460(7254):529-33.
168. Du R, Sun W, Xia L, Zhao A, Yu Y, Zhao L, et al. Hypoxia-induced down-regulation of microRNA-34a promotes EMT by targeting the Notch signaling pathway in tubular epithelial cells. *PLoS One*. 2012;7(2):e30771.
169. Viticchiè G, Lena AM, Latina A, Formosa A, Gregersen LH, Lund AH, et al. MiR-203 controls proliferation, migration and invasive potential of prostate cancer cell lines. *Cell cycle (Georgetown, Tex)*. 2011;10(7):1121-31.
170. Hassan N, Zhao JT, Glover A, Robinson BG, Sidhu SB. Reciprocal interplay of miR-497 and MALAT1 promotes tumorigenesis of adrenocortical cancer. *Endocr Relat Cancer*. 2019;26(7):677-88.
171. Cherradi N. microRNAs as Potential Biomarkers in Adrenocortical Cancer: Progress and Challenges. *Frontiers in endocrinology*. 2015;6:195.
172. Caramuta S, Lee L, Ozata DM, Akçakaya P, Xie H, Höög A, et al. Clinical and functional impact of TARBP2 over-expression in adrenocortical carcinoma. *Endocr Relat Cancer*. 2013;20(4):551-64.
173. Tömböl Z, Szabo PM, Molnar V, Wiener Z, Tölgyesi G, Horanyi J, et al. Integrative molecular bioinformatics study of human adrenocortical tumors: microRNA, tissue-specific target prediction, and pathway analysis. *Endocrine-related cancer*. 2009;16(3):895-906.
174. Soon PSH, Tacon LJ, Gill AJ, Bambach CP, Sywak MS, Campbell PR, et al. miR-195 and miR-483-5p identified as predictors of poor prognosis in adrenocortical cancer. *Clinical Cancer Research*. 2009;15(24):7684-92.
175. Özata DM, Caramuta S, Velázquez-Fernández D, Akçakaya P, Xie H, Höög A, et al. The role of microRNA deregulation in the pathogenesis of adrenocortical carcinoma. *Endocr Relat Cancer*. 2011;18(6):643-55.
176. Patterson EE, Holloway AK, Weng J, Fojo T, Kebebew E. MicroRNA profiling of adrenocortical tumors reveals miR-483 as a marker of malignancy. *Cancer*. 2011;117(8):1630-9.
177. Schmitz KJ, Helwig J, Bertram S, Sheu SY, Suttrop AC, Seggewiß J, et al. Differential expression of microRNA-675, microRNA-139-3p and microRNA-335 in benign and malignant adrenocortical tumours. *Journal of Clinical Pathology*. 2011;64(6):529-35.
178. Chabre O, Libé R, Assie G, Barreau O, Bertherat J, Bertagna X, et al. Serum miR-483-5p and miR-195 are predictive of recurrence risk in adrenocortical cancer patients. *Endocr Relat Cancer*. 2013;20(4):579-94.
179. Duregon E, Rapa I, Votta A, Giorcelli J, Daffara F, Terzolo M, et al. MicroRNA expression patterns in adrenocortical carcinoma variants and clinical pathologic correlations. *Human pathology*. 2014;45(8):1555-62.
180. Feinmesser M, Benbassat C, Meiri E, Benjamin H, Lebanony D, Lebenthal Y, et al. Specific microRNAs differentiate adrenocortical adenomas from carcinomas and correlate with weiss histopathologic system. *Applied immunohistochemistry & molecular morphology*. 2015;23(7):522-31.

181. Koperski Ł, Kotlarek M, Świerniak M, Kolanowska M, Kubiak A, Górnicka B, et al. Next-generation sequencing reveals microRNA markers of adrenocortical tumors malignancy. *Oncotarget*. 2017;8(30):49191.
182. Oreglia M, Sbiera S. Early Postoperative Circulating miR-483-5p Is a Prognosis Marker for Adrenocortical Cancer. *Cancers*. 2020;12(3).
183. Chehade M, Bullock M. Key MicroRNA's and Their Targetome in Adrenocortical Cancer. *Cancers*. 2020;12(8).
184. Veronese A, Visone R, Consiglio J, Acunzo M, Lupini L, Kim T, et al. Mutated beta-catenin evades a microRNA-dependent regulatory loop. *Proceedings of the National Academy of Sciences of the United States of America*. 2011;108(12):4840-5.
185. Wu K, Ma L, Zhu J. miR-483-5p promotes growth, invasion and self-renewal of gastric cancer stem cells by Wnt/ $\beta$ -catenin signaling. *Molecular medicine reports*. 2016;14(4):3421-8.
186. Cheng J, Yang A, Cheng S, Feng L, Wu X, Lu X, et al. Circulating miR-19a-3p and miR-483-5p as Novel Diagnostic Biomarkers for the Early Diagnosis of Gastric Cancer. *Medical science monitor : international medical journal of experimental and clinical research*. 2020;26:e923444.
187. Wu K, Wang J, He J, Chen Q, Yang L. miR-483-3p promotes proliferation and migration of neuroblastoma cells by targeting PUMA. *International journal of clinical and experimental pathology*. 2018;11(2):490-501.
188. Veronese A, Lupini L, Consiglio J, Visone R, Ferracin M, Fornari F, et al. Oncogenic role of miR-483-3p at the IGF2/483 locus. *Cancer research*. 2010;70(8):3140-9.
189. Rattanapan Y, Korkiatsakul V, Kongruang A, Siriboonpiputtana T, Rerkamnuaychoke B, Chareonsirisuthigul T. High Expression of miR-483-5p Predicts Chemotherapy Resistance in Epithelial Ovarian Cancer. *MicroRNA (Sharjah, United Arab Emirates)*. 2021;10(1):51-7.
190. Menbari MN, Rahimi K. miR-483-3p suppresses the proliferation and progression of human triple negative breast cancer cells by targeting the HDAC8 oncogene. *Journal of cellular physiology*. 2020;235(3):2631-42.
191. Mytareli C, Delivanis DA, Athanassouli F, Kalotychoy V, Mantzourani M. The Diagnostic, Prognostic and Therapeutic Role of miRNAs in Adrenocortical Carcinoma: A Systematic Review. *Biomedicines*. 2021;9(11).
192. Agosta C, Laugier J, Guyon L, Denis J, Bertherat J, Libé R, et al. MiR-483-5p and miR-139-5p promote aggressiveness by targeting N-myc downstream-regulated gene family members in adrenocortical cancer. *International journal of cancer*. 2018;143(4):944-57.
193. Ma J, Zhang J, Weng YC, Wang JC. EZH2-Mediated microRNA-139-5p Regulates Epithelial-Mesenchymal Transition and Lymph Node Metastasis of Pancreatic Cancer. *Molecules and cells*. 2018;41(9):868-80.
194. Emmrich S, Engeland F, El-Khatib M, Henke K, Obulkasim A, Schöning J, et al. miR-139-5p controls translation in myeloid leukemia through EIF4G2. *Oncogene*. 2016;35(14):1822-31.
195. Stavast CJ, van Zuijlen I, Karkoulia E, Özçelik A, van Hoven-Beijen A, Leon LG, et al. The tumor suppressor MIR139 is silenced by POLR2M to promote AML oncogenesis. *Leukemia*. 2021.

196. Khalili N, Nouri-Vaskeh M, Hasanpour Segherlou Z, Baghbanzadeh A, Halimi M, Rezaee H, et al. Diagnostic, prognostic, and therapeutic significance of miR-139-5p in cancers. *Life Sciences*. 2020;256:117865.
197. Ji X, Guo H, Yin S, Du H. miR-139-5p functions as a tumor suppressor in cervical cancer by targeting TCF4 and inhibiting Wnt/ $\beta$ -catenin signaling. *OncoTargets and therapy*. 2019;12:7739-48.
198. Zhao Y, Xu J, Le VM, Gong Q, Li S, Gao F, et al. EpCAM Aptamer-Functionalized Cationic Liposome-Based Nanoparticles Loaded with miR-139-5p for Targeted Therapy in Colorectal Cancer. *Molecular Pharmaceutics*. 2019;16(11):4696-710.
199. Berindan-Neagoe I, Monroig Pdel C, Pasculli B, Calin GA. MicroRNAome genome: a treasure for cancer diagnosis and therapy. *CA: a cancer journal for clinicians*. 2014;64(5):311-36.
200. Mattes J, Collison A, Foster PS. Emerging role of microRNAs in disease pathogenesis and strategies for therapeutic modulation. *Current opinion in molecular therapeutics*. 2008;10(2):150-7.
201. Aquino-Jarquín G. Emerging Role of CRISPR/Cas9 Technology for MicroRNAs Editing in Cancer Research. *Cancer research*. 2017;77(24):6812-7.
202. Ebert MS, Sharp PA. MicroRNA sponges: progress and possibilities. *RNA (New York, NY)*. 2010;16(11):2043-50.
203. Simonson B, Das S. MicroRNA therapeutics: the next magic bullet? *Mini reviews in medicinal chemistry*. 2015;15(6):467-74.
204. Ma L, Young J, Prabhala H, Pan E, Mestdagh P, Muth D, et al. miR-9, a MYC/MYCN-activated microRNA, regulates E-cadherin and cancer metastasis. *Nature cell biology*. 2010;12(3):247-56.
205. Yoshino H, Yonemori M, Miyamoto K, Tatarano S, Kofuji S, Nohata N, et al. microRNA-210-3p depletion by CRISPR/Cas9 promoted tumorigenesis through revival of TWIST1 in renal cell carcinoma. *Oncotarget*. 2017;8(13):20881.
206. Johnson CD, Esquela-Kerscher A, Stefani G, Byrom M, Kelnar K, Ovcharenko D, et al. The let-7 MicroRNA Represses Cell Proliferation Pathways in Human Cells. *Cancer research*. 2007;67(16):7713-22.
207. He L, He X, Lowe SW, Hannon GJ. microRNAs join the p53 network—another piece in the tumour-suppression puzzle. *Nature Reviews Cancer*. 2007;7(11):819-22.
208. Glover AR, Zhao JT, Gill AJ, Weiss J, Mugridge N, Kim E, et al. MicroRNA-7 as a tumor suppressor and novel therapeutic for adrenocortical carcinoma. *Oncotarget*. 2015;6(34):36675-88.
209. Kalinowski FC, Giles KM, Candy PA, Ali A, Ganda C, Epis MR, et al. Regulation of epidermal growth factor receptor signaling and erlotinib sensitivity in head and neck cancer cells by miR-7. *PLoS One*. 2012;7(10):e47067.
210. Kwok GT, Zhao JT, Glover AR, Gill AJ, Clifton-Bligh R, Robinson BG, et al. microRNA-431 as a Chemosensitizer and Potentiator of Drug Activity in Adrenocortical Carcinoma. *The Oncologist*. 2019;24(6):e241-e50.

211. Jung S, Nagy Z, Fassnacht M, Zambetti G, Weiss M, Reincke M, et al. Preclinical progress and first translational steps for a liposomal chemotherapy protocol against adrenocortical carcinoma. *Endocrine-Related Cancer*. 2016;23(10):825-37.
212. Chaudhary V, Jangra S, Yadav NR. Nanotechnology based approaches for detection and delivery of microRNA in healthcare and crop protection. *Journal of nanobiotechnology*. 2018;16(1):1-18.
213. Zhang S, Cheng Z, Wang Y, Han T. The Risks of miRNA Therapeutics: In a Drug Target Perspective. *Drug design, development and therapy*. 2021;15:721-33.
214. Danhier F, Feron O, Pr at V. To exploit the tumor microenvironment: Passive and active tumor targeting of nanocarriers for anti-cancer drug delivery. *Journal of Controlled Release*. 2010;148(2):135-46.
215. Shi Y, van der Meel R, Chen X, Lammers T. The EPR effect and beyond: Strategies to improve tumor targeting and cancer nanomedicine treatment efficacy. *Theranostics*. 2020;10(17):7921-4.
216. Bayda S, Adeel M, Tuccinardi T. The History of Nanoscience and Nanotechnology: From Chemical-Physical Applications to Nanomedicine. *Molecules (Basel, Switzerland)*. 2019;25(1).
217. Fitzpatrick JA, Inouye Y, Manley S, Moerner WE. From "There's Plenty of Room at the Bottom" to seeing what is actually there. *Chemphyschem : a European journal of chemical physics and physical chemistry*. 2014;15(4):547-9.
218. Liu Y, Miyoshi H, Nakamura M. Nanomedicine for drug delivery and imaging: A promising avenue for cancer therapy and diagnosis using targeted functional nanoparticles. *International journal of cancer*. 2007;120(12):2527-37.
219. Medina C, Santos-Martinez MJ, Radomski A, Corrigan OI, Radomski MW. Nanoparticles: pharmacological and toxicological significance. *British journal of pharmacology*. 2007;150(5):552-8.
220. Hines RM, Khumnark M, Macphail B, Hines DJ. Administration of Micronized Caffeine Using a Novel Oral Delivery Film Results in Rapid Absorption and Electroencephalogram Suppression. *Frontiers in Pharmacology*. 2019;10(983).
221. Gnach A, Lipinski T, Bednarkiewicz A, Rybka J, Capobianco JA. Upconverting nanoparticles: assessing the toxicity. *Chemical Society Reviews*. 2015;44(6):1561-84.
222. Shapiro RS. COVID-19 vaccines and nanomedicine. *International journal of dermatology*. 2021;60(9):1047-52.
223. Chaudhary N, Weissman D, Whitehead KA. mRNA vaccines for infectious diseases: principles, delivery and clinical translation. *Nature reviews Drug discovery*. 2021;20(11):817-38.
224. Palmer M, Bhakdi S, editors. The Pfizer mRNA vaccine: pharmacokinetics and toxicity 2021.
225. Sung HD, Kim N, Lee Y, Lee EJ. Protein-Based Nanoparticle Vaccines for SARS-CoV-2. *Int J mol Sci*. 2021;22(24).
226. Chauhan N, Jaggi M, Chauhan SC, Yallapu MM. COVID-19: fighting the invisible enemy with microRNAs. *Expert Review of Anti-infective Therapy*. 2021;19(2):137-45.

227. Editorial. Nanomedicine and the COVID-19 vaccines. *Nat Nanotechnol.* 2020;15(12):963.
228. Ganju A, Khan S, Hafeez BB, Behrman SW, Yallapu MM, Chauhan SC, et al. miRNA nanotherapeutics for cancer. *Drug Discov Today.* 2017;22(2):424-32.
229. Beltrán-Gracia E, López-Camacho A, Higuera-Ciapara I, Velázquez-Fernández JB, Vallejo-Cardona AA. Nanomedicine review: clinical developments in liposomal applications. *Cancer Nanotechnology.* 2019;10(1):11.
230. Pugazhendhi A, Edison TNJI, Karuppusamy I, Kathirvel B. Inorganic nanoparticles: A potential cancer therapy for human welfare. *International Journal of Pharmaceutics.* 2018;539(1):104-11.
231. Maier-Hauff K, Ulrich F, Nestler D, Niehoff H, Wust P, Thiesen B, et al. Efficacy and safety of intratumoral thermotherapy using magnetic iron-oxide nanoparticles combined with external beam radiotherapy on patients with recurrent glioblastoma multiforme. *Journal of neuro-oncology.* 2011;103(2):317-24.
232. Sivasankarapillai VS, Jose J, Shanavas MS, Marathakam A, Uddin MS, Mathew B. Silicon Quantum Dots: Promising Theranostic Probes for the Future. *Current drug targets.* 2019;20(12):1255-63.
233. Yüce M, Kurt H. How to make nanobiosensors: surface modification and characterisation of nanomaterials for biosensing applications. *RSC Advances.* 2017;7(78):49386-403.
234. Ding Y, Jiang Z, Saha K, Kim CS, Kim ST, Landis RF, et al. Gold nanoparticles for nucleic acid delivery. *Molecular therapy : the journal of the American Society of Gene Therapy.* 2014;22(6):1075-83.
235. Ekin A, Karatas OF, Culha M, Ozen M. Designing a gold nanoparticle-based nanocarrier for microRNA transfection into the prostate and breast cancer cells. *The journal of gene medicine.* 2014;16(11-12):331-5.
236. Ghosh R, Singh LC, Shohet JM, Gunaratne PH. A gold nanoparticle platform for the delivery of functional microRNAs into cancer cells. *Biomaterials.* 2013;34(3):807-16.
237. Singh A, Sahoo SK. Magnetic nanoparticles: a novel platform for cancer theranostics. *Drug Discovery Today.* 2014;19(4):474-81.
238. Yalcin S. Dextran-coated iron oxide nanoparticle for delivery of miR-29a to breast cancer cell line. *Pharmaceutical Development and Technology.* 2019;24(8):1032-7.
239. Tivnan A, Orr WS, Gubala V, Nooney R, Williams DE, McDonagh C, et al. Inhibition of neuroblastoma tumor growth by targeted delivery of microRNA-34a using anti-disialoganglioside GD2 coated nanoparticles. *PLoS One.* 2012;7(5):e38129.
240. Zielińska A, Carreiró F, Oliveira AM, Neves A, Pires B, Venkatesh DN. Polymeric Nanoparticles: Production, Characterization, Toxicology and Ecotoxicology. *Molecules (Basel, Switzerland).* 2020;25(16).
241. Calzoni E, Cesaretti A. Biocompatible Polymer Nanoparticles for Drug Delivery Applications in Cancer and Neurodegenerative Disorder Therapies. *Journal of functional biomaterials.* 2019;10(1).

242. Yousefpour Marzbali M, Yari Khosroushahi A. Polymeric micelles as mighty nanocarriers for cancer gene therapy: a review. *Cancer Chemotherapy and Pharmacology*. 2017;79(4):637-49.
243. Tiwari S, Gupta M, Vyas SP. Nanocarrier Mediated Cytosolic Delivery of Drug, DNA and Proteins. *Proceedings of the National Academy of Sciences, India Section B: Biological Sciences*. 2012;82(1):127-50.
244. Oerlemans C, Bult W, Bos M, Storm G, Nijsen JFW, Hennink WE. Polymeric Micelles in Anticancer Therapy: Targeting, Imaging and Triggered Release. *Pharmaceutical Research*. 2010;27(12):2569-89.
245. Mittal A, Chitkara D, Behrman SW, Mahato RI. Efficacy of gemcitabine conjugated and miRNA-205 complexed micelles for treatment of advanced pancreatic cancer. *Biomaterials*. 2014;35(25):7077-87.
246. Boussif O, Lezoualc'h F, Zanta MA, Mergny MD, Scherman D, Demeneix B, et al. A versatile vector for gene and oligonucleotide transfer into cells in culture and in vivo: polyethylenimine. *Proceedings of the National Academy of Sciences of the United States of America*. 1995;92(16):7297-301.
247. Cubillos-Ruiz JR, Baird JR, Tesone AJ, Rutkowski MR, Scarlett UK, Camposeco-Jacobs AL, et al. Reprogramming tumor-associated dendritic cells in vivo using miRNA mimetics triggers protective immunity against ovarian cancer. *Cancer research*. 2012;72(7):1683-93.
248. Höbel S, Aigner A. Polyethylenimines for siRNA and miRNA delivery in vivo. *Wiley interdisciplinary reviews Nanomedicine and nanobiotechnology*. 2013;5(5):484-501.
249. Ren Y, Kang CS, Yuan XB, Zhou X, Xu P, Han L, et al. Co-delivery of as-miR-21 and 5-FU by poly(amidoamine) dendrimer attenuates human glioma cell growth in vitro. *Journal of biomaterials science Polymer edition*. 2010;21(3):303-14.
250. Scheideler M, Vidakovic I, Prassl R. Lipid nanocarriers for microRNA delivery. *Chemistry and physics of lipids*. 2020;226:104837.
251. Hong CA, Nam YS. Functional nanostructures for effective delivery of small interfering RNA therapeutics. *Theranostics*. 2014;4(12):1211-32.
252. Cheng X, Lee RJ. The role of helper lipids in lipid nanoparticles (LNPs) designed for oligonucleotide delivery. *Advanced drug delivery reviews*. 2016;99(Pt A):129-37.
253. Bozzuto G, Molinari A. Liposomes as nanomedical devices. *International journal of nanomedicine*. 2015;10:975-99.
254. Yang G, Yin B. Therapeutic effects of long-circulating miR-135a-containing cationic immunoliposomes against gallbladder carcinoma. *Sci Rep*. 2017;7(1):5982.
255. Kaur IP, Bhandari R, Bhandari S, Kakkar V. Potential of solid lipid nanoparticles in brain targeting. *Journal of controlled release : official journal of the Controlled Release Society*. 2008;127(2):97-109.
256. Shi S-j, Han L, Deng L, Zhang Y, Shen H, Gong T, et al. Dual drugs (microRNA-34a and paclitaxel)-loaded functional solid lipid nanoparticles for synergistic cancer cell suppression. *Journal of controlled release : official journal of the Controlled Release Society*. 2014;194:228-37.

257. Carmona-Ribeiro AM. Biomimetic nanoparticles: preparation, characterization and biomedical applications. *International journal of nanomedicine*. 2010;5:249-59.
258. Zhang M, Du Y, Wang S, Chen B. A Review of Biomimetic Nanoparticle Drug Delivery Systems Based on Cell Membranes. *Drug design, development and therapy*. 2020;14:5495-503.
259. Xia Q, Zhang Y, Li Z, Hou X, Feng N. Red blood cell membrane-camouflaged nanoparticles: a novel drug delivery system for antitumor application. *Acta pharmaceutica Sinica B*. 2019;9(4):675-89.
260. Taylor K, Howard CB, Jones ML, Sedliarou I, MacDiarmid J, Brahmbhatt H, et al. Nanocell targeting using engineered bispecific antibodies. *mAbs*. 2015;7(1):53-65.
261. MacDiarmid JA, Mugridge NB, Weiss JC, Phillips L, Burn AL, Paulin RP, et al. Bacterially derived 400 nm particles for encapsulation and cancer cell targeting of chemotherapeutics. *Cancer Cell*. 2007;11(5):431-45.
262. MacDiarmid JA, Madrid-Weiss J, Amaro-Mugridge NB, Phillips L, Brahmbhatt H. Bacterially-derived nanocells for tumor-targeted delivery of chemotherapeutics and cell cycle inhibitors. *Cell cycle (Georgetown, Tex)*. 2007;6(17):2099-105.
263. van Zandwijk N, Pavlakis N, Kao SC, Linton A, Boyer MJ, Clarke S, et al. Safety and activity of microRNA-loaded minicells in patients with recurrent malignant pleural mesothelioma: a first-in-man, phase 1, open-label, dose-escalation study. *The Lancet Oncology*. 2017;18(10):1386-96.
264. Zhou W, Zhou Y, Chen X, Ning T, Chen H, Guo Q, et al. Pancreatic cancer-targeting exosomes for enhancing immunotherapy and reprogramming tumor microenvironment. *Biomaterials*. 2021;268:120546.
265. Luan X, Sansanaphongpricha K, Myers I, Chen H, Yuan H, Sun D. Engineering exosomes as refined biological nanoplatfoms for drug delivery. *Acta pharmacologica Sinica*. 2017;38(6):754-63.
266. Vázquez-Ríos AJ, Molina-Crespo Á, Bouzo BL, López-López R, Moreno-Bueno G, de la Fuente M. Exosome-mimetic nanoplatfoms for targeted cancer drug delivery. 2019;17(1):85.
267. Sancho-Albero M, Navascués N, Mendoza G, Sebastián V, Arruebo M. Exosome origin determines cell targeting and the transfer of therapeutic nanoparticles towards target cells. *Journal of nanobiotechnology*. 2019;17(1):16.
268. Longmire M, Choyke PL, Kobayashi H. Clearance properties of nano-sized particles and molecules as imaging agents: considerations and caveats. *Nanomedicine (London, England)*. 2008;3(5):703-17.
269. Blanco E, Shen H, Ferrari M. Principles of nanoparticle design for overcoming biological barriers to drug delivery. *Nature biotechnology*. 2015;33(9):941-51.
270. Moghimi SM, Hunter AC, Murray JC. Long-circulating and target-specific nanoparticles: theory to practice. *Pharmacological reviews*. 2001;53(2):283-318.
271. Parodi A, Quattrocchi N, van de Ven AL, Chiappini C, Evangelopoulos M, Martinez JO, et al. Synthetic nanoparticles functionalized with biomimetic leukocyte membranes possess cell-like functions. *Nature Nanotechnology*. 2013;8(1):61-8.

272. Bertrand N, Wu J, Xu X, Kamaly N, Farokhzad OC. Cancer nanotechnology: the impact of passive and active targeting in the era of modern cancer biology. *Advanced drug delivery reviews*. 2014;66:2-25.
273. Matsumura Y, Maeda H. A new concept for macromolecular therapeutics in cancer chemotherapy: mechanism of tumoritropic accumulation of proteins and the antitumor agent smancs. *Cancer research*. 1986;46(12 Pt 1):6387-92.
274. Sindhvani S, Syed AM, Ngai J, Kingston BR, Maiorino L, Rothschild J, et al. The entry of nanoparticles into solid tumours. *Nature Materials*. 2020;19(5):566-75.
275. Carmeliet P. Mechanisms of angiogenesis and arteriogenesis. *Nature medicine*. 2000;6(4):389-95.
276. Lugano R, Ramachandran M, Dimberg A. Tumor angiogenesis: causes, consequences, challenges and opportunities. *Cellular and molecular life sciences : CMLS*. 2020;77(9):1745-70.
277. Jain RK, Stylianopoulos T. Delivering nanomedicine to solid tumors. *Nature Reviews Clinical Oncology*. 2010;7(11):653-64.
278. Wu J. The Enhanced Permeability and Retention (EPR) Effect: The Significance of the Concept and Methods to Enhance Its Application. *Journal of Personalized Medicine*. 2021;11(8):771.
279. Haute DV, Berlin JM. Challenges in realizing selectivity for nanoparticle biodistribution and clearance: lessons from gold nanoparticles. *Therapeutic delivery*. 2017;8(9):763-74.
280. Jeong EJ, Choi M, Lee J, Rhim T, Lee KY. The spacer arm length in cell-penetrating peptides influences chitosan/siRNA nanoparticle delivery for pulmonary inflammation treatment. *Nanoscale*. 2015;7(47):20095-104.
281. Acharya S, Dilnawaz F, Sahoo SK. Targeted epidermal growth factor receptor nanoparticle bioconjugates for breast cancer therapy. *Biomaterials*. 2009;30(29):5737-50.
282. Neves AR, van der Putten L, Queiroz JF, Pinheiro M, Reis S. Transferrin-functionalized lipid nanoparticles for curcumin brain delivery. *Journal of biotechnology*. 2021;331:108-17.
283. Huang X, Schwind S, Yu B, Santhanam R, Wang H, Hoellerbauer P, et al. Targeted Delivery of microRNA-29b by Transferrin-Conjugated Anionic Lipopolyplex Nanoparticles: A Novel Therapeutic Strategy in Acute Myeloid Leukemia. *Clinical Cancer Research*. 2013;19(9):2355-67.
284. Orellana EA, Tenneti S. FolamiRs: Ligand-targeted, vehicle-free delivery of microRNAs for the treatment of cancer. *Science translational medicine*. 2017;9(401).
285. Riaz MK, Riaz MA, Zhang X, Lin C, Wong KH, Chen X, et al. Surface Functionalization and Targeting Strategies of Liposomes in Solid Tumor Therapy: A Review. *Int J Mol Sci*. 2018;19(1).
286. Peng J, Wang R, Sun W, Huang M, Wang R, Li Y, et al. Delivery of miR-320a-3p by gold nanoparticles combined with photothermal therapy for directly targeting Sp1 in lung cancer. *Biomaterials Science*. 2021;9(19):6528-41.
287. Carmeliet P. VEGF as a key mediator of angiogenesis in cancer. *Oncology*. 2005;69 Suppl 3:4-10.



288. Voltan AR, Alarcon KM, Fusco-Almeida AM, Soares CP, Mendes-Giannini MJS, Chorilli M. Highlights in Endocytosis of Nanostructured Systems. *Current medicinal chemistry*. 2017;24(18):1909-29.
289. Sousa de Almeida M, Susnik E, Drasler B, Taladriz-Blanco P, Petri-Fink A, Rothen-Rutishauser B. Understanding nanoparticle endocytosis to improve targeting strategies in nanomedicine. *Chem Soc Rev*. 2021;50(9):5397-434.
290. Ou H, Cheng T, Zhang Y, Liu J, Ding Y, Zhen J, et al. Surface-adaptive zwitterionic nanoparticles for prolonged blood circulation time and enhanced cellular uptake in tumor cells. *Acta Biomaterialia*. 2018;65:339-48.
291. Behzadi S, Serpooshan V, Tao W, Hamaly MA, Alkawareek MY, Dreaden EC, et al. Cellular uptake of nanoparticles: journey inside the cell. *Chemical Society Reviews*. 2017;46(14):4218-44.
292. Moore NM, Sheppard CL, Barbour TR, Sakiyama-Elbert SE. The effect of endosomal escape peptides on in vitro gene delivery of polyethylene glycol-based vehicles. *The journal of gene medicine*. 2008;10(10):1134-49.
293. Jones CH, Chen C-K, Ravikrishnan A, Rane S, Pfeifer BA. Overcoming nonviral gene delivery barriers: perspective and future. *Molecular pharmaceutics*. 2013;10(11):4082-98.
294. Gilleron J, Querbes W, Zeigerer A, Borodovsky A, Marsico G, Schubert U, et al. Image-based analysis of lipid nanoparticle-mediated siRNA delivery, intracellular trafficking and endosomal escape. *Nature biotechnology*. 2013;31(7):638-46.
295. Torchilin V. NEXT STEP IN DRUG DELIVERY: GETTING TO INDIVIDUAL ORGANELLES. *Drug delivery and translational research*. 2012;2(6):415-7.
296. Tammam SN, Azzazy HME, Lamprecht A. The effect of nanoparticle size and NLS density on nuclear targeting in cancer and normal cells; impaired nuclear import and aberrant nanoparticle intracellular trafficking in glioma. *Journal of Controlled Release*. 2017;253:30-6.
297. Mullard A. 2017 FDA drug approvals. *Nature Reviews Drug Discovery*. 2018;17(2):81-6.
298. Mullard A. 2019 FDA drug approvals. *Nature reviews Drug discovery*. 2020;19(2):79-84.
299. Goutayer M, Dufort S, Josserand V, Royère A, Heinrich E, Vinet F, et al. Tumor targeting of functionalized lipid nanoparticles: Assessment by in vivo fluorescence imaging. *European Journal of Pharmaceutics and Biopharmaceutics*. 2010;75(2):137-47.
300. Courant T, Bayon E, Reynaud-Dougier HL, Villiers C, Menneteau M, Marche PN, et al. Tailoring nanostructured lipid carriers for the delivery of protein antigens: Physicochemical properties versus immunogenicity studies. *Biomaterials*. 2017;136:29-42.
301. Texier I, Goutayer M, Da Silva A, Guyon L, Djaker N, Josserand V, et al. Cyanine-loaded lipid nanoparticles for improved in vivo fluorescence imaging. *Journal of biomedical optics*. 2009;14(5):054005.
302. Mérian J, Boisgard R, Bayle PA, Bardet M, Tavitian B, Texier I. Comparative biodistribution in mice of cyanine dyes loaded in lipid nanoparticles. *European journal of pharmaceutics and biopharmaceutics : official journal of Arbeitsgemeinschaft fur Pharmazeutische Verfahrenstechnik eV*. 2015;93:1-10.

303. Navarro FP, Berger M, Guillermet S, Josserand V, Guyon L, Neumann E, et al. Lipid nanoparticle vectorization of indocyanine green improves fluorescence imaging for tumor diagnosis and lymph node resection. *Journal of biomedical nanotechnology*. 2012;8(5):730-41.
304. Hirsjärvi S, Dufort S, Gravier J, Texier I, Yan Q, Bibette J, et al. Influence of size, surface coating and fine chemical composition on the in vitro reactivity and in vivo biodistribution of lipid nanocapsules versus lipid nanoemulsions in cancer models. *Nanomedicine*. 2013;9(3):375-87.
305. Dey AK, Nougarede A, Clément F, Fournier C, Jouvin-Marche E, Escudé M, et al. Tuning the Immunostimulation Properties of Cationic Lipid Nanocarriers for Nucleic Acid Delivery. *Frontiers in Immunology*. 2021;12.
306. Bayon E, Morlieras J, Dereuddre-Bosquet N, Gonon A, Gosse L, Courant T, et al. Overcoming immunogenicity issues of HIV p24 antigen by the use of innovative nanostructured lipid carriers as delivery systems: evidences in mice and non-human primates. *npj Vaccines*. 2018;3(1):46.
307. Delmas T, Couffin AC, Bayle PA, de Crécy F, Neumann E, Vinet F, et al. Preparation and characterization of highly stable lipid nanoparticles with amorphous core of tuneable viscosity. *Journal of colloid and interface science*. 2011;360(2):471-81.
308. Bruniaux J GX, Navarro YGF, Sulpice E, Texier-Nogues I, inventor Formulation for the Delivery of Nucleotide Sequences That Can Modulate Endogenous Interfering Rna Mechanisms. France patent WO2014032953A1. 2014.
309. Cimino R, Bhangu SK, Baral A. Ultrasound-Assisted Microencapsulation of Soybean Oil and Vitamin D Using Bare Glycogen Nanoparticles. *Molecules (Basel, Switzerland)*. 2021;26(17).
310. Beare-Rogers JL, Dieffenbacher A, Holm JV. Lexicon of lipid nutrition (IUPAC Technical Report). *Pure and Applied Chemistry*. 2001;73(4):685-744.
311. Clayton KN, Salameh JW, Wereley ST, Kinzer-Ursem TL. Physical characterization of nanoparticle size and surface modification using particle scattering diffusometry. *Biomicrofluidics*. 2016;10(5):054107.
312. Jores K, Mehnert W, Mäder K. Physicochemical investigations on solid lipid nanoparticles and on oil-loaded solid lipid nanoparticles: a nuclear magnetic resonance and electron spin resonance study. *Pharm Res*. 2003;20(8):1274-83.
313. Fatehah MO, Aziz HA, Stoll S. Nanoparticle Properties, Behavior, Fate in Aquatic Systems and Characterization Methods. *Journal of Colloid Science and Biotechnology*. 2014;3:111-40.
314. Liu H, Wu D. In vivo Near-infrared Fluorescence Tumor Imaging Using DiR-loaded Nanocarriers. *Current drug delivery*. 2016;13(1):40-8.
315. Sasatsu M, Onishi H, Machida Y. In vitro and in vivo characterization of nanoparticles made of MeO-PEG amine/PLA block copolymer and PLA. *International Journal of Pharmaceutics*. 2006;317(2):167-74.
316. Gravier J, Navarro Y Garcia F, Delmas T, Mittler F, Couffin A-C, Vinet F, et al. Lipidots: competitive organic alternative to quantum dots for in vivo fluorescence imaging. *Journal of biomedical optics*. 2011;16(9):096013.

317. Resnier P, LeQuinio P, Lautram N, André E, Gaillard C, Bastiat G, et al. Efficient in vitro gene therapy with PEG siRNA lipid nanocapsules for passive targeting strategy in melanoma. *Biotechnology journal*. 2014;9(11):1389-401.
318. Moghimi SM, Hunter AC, Andresen TL. Factors controlling nanoparticle pharmacokinetics: an integrated analysis and perspective. *Annual review of pharmacology and toxicology*. 2012;52:481-503.
319. Matuszak J, Baumgartner J, Zaloga J, Juenet M, Silva AEd, Franke D, et al. Nanoparticles for intravascular applications: physicochemical characterization and cytotoxicity testing. *Nanomedicine*. 2016;11(6):597-616.
320. Jacquart A, Keramidis M, Vollaie J, Boisgard R, Pottier G, Rustique E, et al. LipImage™ 815: novel dye-loaded lipid nanoparticles for long-term and sensitive *in vivo* near-infrared fluorescence imaging. *Journal of biomedical optics*. 2013;18(10):101311.
321. Mérian J, Boisgard R, Declèves X, Thezé B, Texier I, Tavitian B. Synthetic Lipid Nanoparticles Targeting Steroid Organs. *Journal of Nuclear Medicine*. 2013;54(11):1996-2003.
322. Bibette J. BR, Boisseau P., Coll J.L., Couffin A.C., Delmas T., Dufort S., Fraichard A., Gravier J., Heinrich E., Mérian J., Navarro F., Tavitian B., Texier I., Thomann J.S.,. Lipid nanoparticles: tumor-targeting nanocargos for drug and contrast agent delivery. *TechConnect Briefs*. 2011;3, *Nanotechnology 2011: Bio Sensors, Instruments, Medical, Environment and Energy*.
323. Navarro FP, Creusat G, Frochot C, Moussaron A, Verhille M, Vanderesse R, et al. Preparation and characterization of mTHPC-loaded solid lipid nanoparticles for photodynamic therapy. *Journal of Photochemistry and Photobiology B: Biology*. 2014;130:161-9.
324. Clément F, Nougarede A, Combe S, Kermarrec F, Dey AK, Obeid P, et al. Therapeutic siRNAs Targeting the JAK/STAT Signalling Pathway in Inflammatory Bowel Diseases. *Journal of Crohn's and Colitis*. 2021.

## RÉSUMÉ DÉTAILLÉ EN FRANCAIS

---



## Introduction:

Le carcinome corticosurrénalien (CCS) est une tumeur endocrine rare qui se développe dans le cortex de la glande surrénale, avec une incidence annuelle de 0,5 à 2 cas par million, représentant 0,2% des décès liés au cancer. Les circonstances de découverte du CCS sont soit des symptômes motivant une imagerie surrénalienne (hypersécrétion hormonale), soit un incidentalome surrénalien, découvert fortuitement lors d'une imagerie abdominale. Près de la moitié des patients sont asymptomatiques, ce qui entraîne un diagnostic tardif, souvent à un stade déjà métastatique. Plusieurs anomalies génétiques identifiées dans le contexte de syndromes (syndrome de Li-Fraumeni, syndrome de Beckwith-Wiedemann) semblent prédisposer au CCS, notamment chez les enfants. À ce jour, la résection chirurgicale est le traitement de référence pour les tumeurs de stade précoce, tandis que la chimiothérapie est adoptée pour les cas avancés. Les thérapies ciblées n'ont pas montré de réponse significative aux traitements testés. Dans ce contexte, la prise en charge clinique du CCS nécessite des approches multidisciplinaires afin de proposer des stratégies thérapeutiques adaptées.

Des analyses multi-omiques ont mis en évidence une série de gènes mutés ou dérégulés, potentiellement impliqués dans la tumorigenèse surrénalienne. Parmi eux, IGF2 est surexprimé dans 90 % des CCS et son niveau d'expression est indicatif d'une malignité ; IGF2 soutient la prolifération tumorale de manière paracrine en se liant à son récepteur IGF1R. La voie de signalisation Wnt/ $\beta$ -caténine est constitutivement active chez 39 % des patients. Des mutations supplémentaires inactivant le gène TP53 ainsi que des gènes de remodelage de la chromatine comme MEN1 et DAXX ont été identifiées. Outre les mutations génétiques, des pertes d'hétérozygotie, des anomalies de la méthylation ainsi que des modifications importantes du profil d'expression des microARN (miRs) ont été rapportées. En effet, l'étude du miRnome du CCS a révélé un panel de miRs différenciellement exprimés en comparaison aux tumeurs bénignes (adénomes) ou aux tissus sains. Notre équipe a notamment montré que miR-139-5p et miR-483-5p sont surexprimés dans les tumeurs agressives et sont associés à un mauvais pronostic.

Les miRs sont des petits ARN non-codants d'une vingtaine de nucléotides qui répriment l'expression des gènes au niveau post-transcriptionnel via un appariement imparfait avec la région 3'-non-traduite (3'UTR) de l'ARNm cible. La biogenèse des miRs implique plusieurs

clivages et transformations d'un précurseur structuré en tige-boucle ou miR primaire (pri-miARN), en miR mature. L'action du miR sur sa cible met en jeu des complexes protéiques, comprenant notamment le complexe RISC (RNA-Induced Silencing Complex) avec la protéine Argonaute 2. En raison du faible degré de complémentarité nécessaire à son activité de répression de l'ARNm cible, un miR peut réguler plusieurs gènes à la fois et ainsi interférer avec différentes étapes du développement cancéreux tels que l'initiation, la progression et le développement de métastases. Il est clairement établi que des déséquilibres de l'expression des miRs dans les tumeurs contribuent à la cancérogenèse. En général, les miRs intégrés dans les loci amplifiés dans le cancer agissent comme des oncogènes (ou oncomiRs) tandis que les miRs localisés dans des régions géniques délétées fonctionnent comme suppresseurs de tumeurs. De plus, des altérations épigénétiques ainsi que des défauts de la machinerie de biosynthèse des miRs affectent fortement leur expression.

Sur la base de ces découvertes, l'inhibition de miRs oncogènes ou la restitution de miRs suppresseurs de tumeurs ont été proposées comme des stratégies thérapeutiques pertinentes pour le cancer. Cependant, le défi majeur de ces approches reste l'adressage spécifique et sécurisé de ces traitements au foyer tumoral pour éviter les effets secondaires. En effet, les miRs synthétiques (mimics) ou les oligonucléotides inhibiteurs de miRs (antimiRs) ont une demi-vie courte et sont immédiatement dégradés dans les fluides biologiques par les nucléases. L'amélioration de leur stabilité, ainsi que la mise au point de systèmes d'administration sûrs et efficaces sont des étapes clés pour mener les thérapies à base de miRs vers le succès. Ainsi, plusieurs stratégies ont été conçues, y compris des modifications chimiques et structurales des acides nucléiques. De plus, la vectorisation de miRs thérapeutiques par des nanoparticules (NP) fonctionnalisées a permis leur protection contre la dégradation, s'affranchissant ainsi de la réponse immunitaire et augmentant leur temps de circulation. Avec l'essor des nanotechnologies, les biomatériaux utilisés sont parfaitement modulables pour envisager des applications thérapeutiques basées sur la capacité des NP à franchir les barrières biologiques et à s'accumuler spécifiquement dans les tumeurs. Les NP ont montré leur pertinence en oncologie de précision pour le diagnostic, l'imagerie et l'administration de médicaments. Certaines NP comme les liposomes et les micelles polymériques sont déjà en clinique, notamment pour les traitements conventionnels du cancer tels que la chimiothérapie, la radiothérapie et l'immunothérapie, mais dans une

moindre mesure pour la thérapie génique basée sur l'interférence par ARN. Les configurations des biomatériaux au sein des NP affectent fortement leurs propriétés de stabilité, d'efficacité d'encapsulation de molécules thérapeutiques et de ciblage. Les NP sont constituées de biomatériaux organiques ou inorganiques, qui sont conçus pour répondre aux besoins cliniques. Alors que les NP inorganiques rassemblent les NP métalliques à propriétés magnétiques, les NP organiques regroupent d'une part les polymères (micelles, dendrimères...), et d'autre part les NP lipidiques (LNP) tel que les liposomes et les NP structurées autour d'un cœur lipidique solide. Si le choix du cœur d'une NP est essentiel pour le conditionnement et la libération des médicaments, le contrôle de sa surface est tout aussi critique. C'est en fait la couche externe de la NP qui va permettre son interaction avec son environnement, permettant ainsi son acheminement vers le site souhaité. De ce fait, il est possible de moduler les propriétés de surface des NP afin d'améliorer leur comportement biologique. Au vu de leur diversité, les NP sont désormais impliquées dans une pléthore d'applications, dont la thérapie génique.

Le laboratoire LETI/DTBS du CEA a développé et breveté des nanoparticules lipidiques biocompatibles et biodégradables : les Lipidots® (LNP) dont les composants sont approuvés par la FDA. Les Lipidots ont démontré une stabilité colloïdale et photochimique à long terme, avec une cytotoxicité limitée. Leur capacité à intégrer des fluorophores leur confère des propriétés comparables aux quantum dots. De plus, guidés par l'effet EPR (Enhanced Permeability and Retention), les LNP peuvent se faufiler via les fenestrations de l'endothélium tumoral pour s'accumuler au niveau des sites tumoraux. De manière intéressante, les LNP présentent un tropisme puissant pour le cortex surrénal, suggérant qu'ils peuvent servir de vecteurs pour cibler ce tissu et adresser des molécules thérapeutiques au CCS. La charge d'acides nucléiques est réalisable grâce à leurs interactions électrostatiques avec les lipides cationiques incorporés dans la monocouche de phospholipides. Un rapport N/P (N pour amine, P pour phosphate) tenant compte des charges positives portées par les fonctions amines des lipides cationiques et des charges négatives portées par les groupements phosphate de la séquence d'acide nucléique, est ensuite utilisé pour calculer le taux de chargement des acides nucléiques sur les LNP. Etant donné l'efficacité démontrée des LNP dans la vectorisation de siARN et la similitude structurale entre les siARN et les miRs, l'application des LNP pourrait s'étendre vers la délivrance de miRs thérapeutiques.



Compte tenu de la biodistribution préférentielle des LNP dans les tissus producteurs d'hormones stéroïdes comme le cortex surrénal, ce travail visait à évaluer miR-139-5p et miR-483-5p comme cibles thérapeutiques dans le CCS par nanovectorisation de leurs antimiRs respectifs via les LNP.

### **Les objectifs de la thèse ont été les suivants :**

- 1) Établir in vitro la preuve de concept que miR-483-5p et miR-139-5p sont des cibles thérapeutiques pertinentes pour le CCS. Cette étude a été réalisée à l'aide d'antimiRs non vectorisés dans la lignée de carcinome corticosurrénalien humain NCI H295R.
- (2) Caractériser le comportement des Lipidots® in vitro dans des NCI H295R en culture, en termes de toxicité et d'absorption cellulaire.
- (3) Générer des nanoparticules associant les antimiR-483-5p et antimiR-139-5p aux Lipidots® puis analyser leurs effets fonctionnels dans les cellules NCI H295R.
- (4) Évaluer l'efficacité thérapeutique de ces nanoparticules par injection systémique chez des souris immunodéficientes porteuses de tumeurs de CCS sous-cutanées.

### **Résultats:**

Afin de déterminer le rôle de miR-139-5p et de miR-483-5p dans l'agressivité du CCS, les cellules NCI H295R ont été transfectées de façon transitoire avec des antimiRs contrôle, antimiR-139-5p, antimiR-483-5p ou une combinaison des deux antimiRs (Mix AntimiRs). Nous avons montré que l'inhibition de ces deux miRs restaure l'expression de deux gènes cibles identifiés précédemment par notre équipe (NDRG2 et NDRG4). L'analyse du protéome du CCS par des approches de puces à anticorps a révélé que l'inhibition simultanée de miR-139-5p et miR-483-5p dans la lignée NCI H295R diminue l'expression de protéines associées au cancer, tel que EGFR, la Survivin, la Vimentin, SPARC, la Cathepsin D, l'Osteopontin, et MMP2. De même, les niveaux de phosphorylation de plusieurs kinases, y compris Akt, et les MAP kinases JNK, ERK et p38 ont été diminués lorsque miR-139-5p et miR-483-5p sont réprimés. La voie de signalisation Wnt/ $\beta$ -caténine est également atténuée dans ces mêmes conditions. Bien que ces analyses regroupent les cibles directes et indirectes des deux miRs, la contribution de ces protéines à la signalisation oncogénique est clairement démontrée. Par ailleurs, des cibles potentielles directes de chaque miR ont été identifiées dans des expériences de pulldown,

dont des gènes en lien avec la fonction stéroïdogène de la glande surrénale. Des investigations plus poussées in vitro ont révélé que l'inhibition de miR-139-5p réduit la sécrétion hormonale (cortisol) des cellules NCI H295R, en adéquation avec les études menées par notre équipe sur des cohortes de patients. L'ensemble de ces résultats montrent que la suppression de l'expression de miR-139-5p et miR-483-5p inhibe des voies de signalisation pro-tumorales dans le CCS. Par conséquent, adresser des inhibiteurs de ces miRs à l'aide d'un système de délivrance sécurisé apparaît comme une approche thérapeutique pertinente.

Nous avons donc généré des LNP complexées à un mélange d'antimiR-139-5p et antimiR-483-5p, selon un rapport N/P 16. Nous avons caractérisé ces nanoformulations in vitro puis mis en évidence l'internalisation de ces complexes par les cellules NCI H295R en culture et démontré leur efficacité dans l'inhibition simultanée de l'expression de miR-483-5p et miR-139-5p endogènes. Les antimiRs délivrés par les LNP ont donc conservé leur capacité d'inhibition spécifique des miRs. Une inhibition de la migration et de l'invasion cellulaires observée précédemment avec les antimiR-139-5p et antimiR-483-5p nus a été confirmée avec ces nouvelles nanoformulations.

Enfin, nous avons montré que l'injection systémique des antimiRs-LNP chez la souris immunodéficiente *scid/CB17* induit une accumulation préférentielle des nanoparticules dans les surrénales et les ovaires sans toxicité apparente. Nous avons rapporté dans des expériences de xélogreffe sous-cutanée de cellules NCI H295R que l'administration d'antimiR-483-5p-LNP ou de la combinaison antimiR-139-5p/antimiR-483-5p-LNP inhibe significativement la croissance tumorale. Cependant, bien qu'une co-localisation des antimiRs et des LNP ait été observée in vivo, nous n'avons pas pu la corrélérer à une inhibition des miRs dans les tissus tumoraux. En effet, aucun changement significatif dans miR-139-5p n'a été détecté par PCR quantitative, en raison de la grande variabilité entre individus du même groupe de traitement. Une tendance à la réduction de l'expression tumorale de miR-483-5p a néanmoins été observée chez les animaux traités avec l'antimiR correspondant. De façon intéressante, l'analyse par immunohistochimie des tumeurs traitées par les antimiR-483-5p-LNP a révélé une diminution de l'expression de Ki67, un marqueur pronostique majeur du CCS.

## Conclusion et perspectives:

Le CCS est une tumeur maligne rare associée à un pronostic sombre et des besoins médicaux non satisfaits. Dans ce travail, nous nous sommes concentrés sur deux miRs surexprimés dans le CCS, miR-483-5p et miR-139-5p, que nous proposons comme cibles thérapeutiques pour ce cancer. Nous avons validé leur fonction en tant qu'oncomiRs médiateurs de l'agressivité du CCS et montré leur pertinence comme candidats à un ciblage thérapeutique. Outre la répression de certaines voies de signalisation pro-tumorales via l'inactivation de kinases, nous avons observé que l'expression de plusieurs gènes clés de l'invasion et de la transition épithélio-mésenchymateuse est diminuée après inhibition de miR-139-5p et miR-483-5p. Nos analyses moléculaires démontrent que les antimiRs modifient simultanément diverses voies liées au cancer et ont donc le potentiel d'exercer des effets thérapeutiques synergiques.

Cette capacité des miRs à exercer une «régulation fine» de plusieurs voies de signalisation nous a amenés à tester les antimiRs dans un contexte thérapeutique en les délivrant via les nanoparticules lipidiques ou Lipidots (LNP) cationiques, d'abord in vitro puis in vivo. Les analyses en diffusion dynamique de la lumière (DLS) des complexes LNP-AntimiRs ont révélé une charge globale fortement positive à N/P 16, ce qui suggère la possibilité de piéger davantage d'antimiRs pour atteindre la saturation des nanoparticules. Ainsi, nous identifions les LNP comme réservoirs importants pour la vectorisation des miRs. Nous avons ensuite administré les complexes AntimiRs-LNP par voie systémique à des souris porteuses de CCS. Nous avons démontré pour la première fois que le tropisme pour les glandes surrénales observé initialement in vivo avec les LNP neutres, est maintenu avec les LNP cationiques. La fluorescence ex vivo des principaux organes a non seulement confirmé ce schéma de biodistribution dans les tissus stéroïdogènes mais a aussi révélé l'accumulation des AntimiRs-LNP dans les tumeurs. Ce tropisme naturel des LNP pour les organes avides de lipides est probablement dû à une activité « lipoprotein-like » de ces nanoparticules dans des tissus très riches en récepteurs pour les lipoprotéines de types LDL ou HDL. L'accumulation des LNP dans les tumeurs peut être attribuée à la combinaison de ce tropisme et de l'effet EPR favorisé par le réseau vasculaire tumoral. Par ailleurs, les composants des LNP étant naturellement métabolisés dans le foie, ceci explique les signaux Dil occasionnels collectés dans cet organe. D'autre part, nous avons observé une croissance et un poids tumoraux significativement réduits après injection intraveineuse de nos nouvelles formulations, notamment celles

contenant AntimiR-483-5p. Cependant, nos tests in vitro n'ont montré aucun impact de miR-139-5p et miR-483-5p sur la prolifération des cellules NCI H295R. Cette discordance suggère un rôle potentiel du microenvironnement tumoral, qui n'est pas observable in vitro sur des cultures cellulaires de cellules cancéreuses. Des analyses complémentaires sont requises pour mieux caractériser les événements impliqués dans ce retard de croissance tumorale.

En conclusion, ce travail décrit la première utilisation des Lipidots pour vectoriser des miRs à visée thérapeutique et suggère que le ciblage des miRs est une stratégie pertinente pour le traitement du CCS. Bien que les mécanismes moléculaires mis en jeu par miR-139-5p et miR-483-5p dans le CCS ne soient pas encore élucidés dans le détail, nos données ouvrent des perspectives prometteuses pour orienter le développement de thérapies innovantes pour le carcinome corticosurrénalien. De plus, ces approches de nanomédecine pourraient être étendues à des cancers plus fréquents impliquant une dérégulation des miRs.